FRATAXIN (FXN) BASED REGULATION OF THE IRON-SULFUR CLUSTER ASSEMBLY COMPLEX

A Dissertation

by

JENNIFER DIANE RABB

Submitted to the Office of Graduate Studies of
Texas A&M University
in partial fulfillment of the requirements for the degree of

DOCTOR OF PHILOSOPHY

May 2012

Major Subject: Chemistry

FRATAXIN (FXN) BASED REGULATION OF THE IRON-SULFUR CLUSTER ASSEMBLY COMPLEX

A Dissertation

by

JENNIFER DIANE RABB

Submitted to the Office of Graduate Studies of
Texas A&M University
in partial fulfillment of the requirements for the degree of

DOCTOR OF PHILOSOPHY

Approved by:

Chair of Committee,	David P. Barondeau
Committee Members,	Tadhg P. Begley
	Deborah Bell-Pedersen
	Frank M. Raushel
Head of Department,	David H. Russell

May 2012

Major Subject: Chemistry

ABSTRACT

Frataxin (FXN) Based Regulation of the Iron-Sulfur Cluster Assembly Complex. (May 2012)

Jennifer Diane Rabb, B.S., Central Michigan University

Chair of Advisory Committee: Dr. David P. Barondeau

Iron-sulfur clusters are protein cofactors that are critical for all life forms. Elaborate multi-component systems have evolved for the biosynthesis of these cofactors to protect organisms from the toxic effects of free iron and sulfide ions. In eukaryotes, the Fe-S cluster assembly machinery operates in the matrix space of the mitochondria and contains a myriad of proteins that mediate sulfur, iron, and electron transfer to assemble Fe-S clusters on the scaffold protein ISCU2 and then distribute these clusters to target proteins. Our lab has recently described stable 3, and 4-protein complexes composed of the cysteine desulfurase NFS1, the co-chaperone ISD11, and ISCU2 (SDU), and NFS1, ISD11, ISCU2, and FXN (SDUF) subunits. In the latter, SDUF, FXN functions as an allosteric activator switching this assembly complex on for Fe-S cluster biosynthesis. Insufficient expression of the mitochondrial protein FXN leads to a progressive neurodegenerative disease, Friedreich's Ataxia (FRDA). In ~2% of patients, FRDA is caused by one of 15 known missense mutations on one allele accompanied by the GAA repeat on the other leading to a complicated phenotype that includes loss of Fe-

S clusters. Here we present *in vitro* evidence that FRDA FXN variants are deficient in their ability to bind the SDU complex, their ability to stimulate the sulfur transfer reaction from NFS1 to ISCU2, and in their ability to stimulate the rate of cluster assembly on ISCU2. Here, *in vitro* evidence is presented that FXN accelerates the sulfur transfer reaction from NFS1 to ISCU2. Additionally, we present kinetic evidence that identifies the most buried cysteine residue, C104 on ISCU2 as the sulfur acceptor residue suggesting, FXN stabilizes a conformational change to facilitate sulfur delivery. Subsequent mutational studies suggest FXN binding to SDU results in a helix to coil transition in ISCU2 exposing C104 to accept the persulfide sulfur and thereby accelerating the rate of sulfur transfer. We further provide the first biochemical evidence that the persulfide transferred to ISCU2 from NFS1 is viable in Fe-S cluster formation. In contrast to human FXN, the *Escherichia coli* FXN homolog CyaY has been reported to inhibit Fe-S cluster biosynthesis. To resolve this discrepancy, a series of inter-species enzyme kinetic experiments were performed. Surprisingly, our results reveal that activation or inhibition by the frataxin homolog is determined by which cysteine desulfurase is present and not by the identity of the frataxin homolog. These data are consistent with a model in which the frataxin-less Fe-S assembly complex exists as a mixture of functional and nonfunctional states, which are stabilized by binding of frataxin homologs. Intriguingly, this appears to be an unusual example in which modifications to an enzyme during evolution inverts or reverses the mode of control imparted by a regulatory molecule.

DEDICATION

Many fine people have surrounded me throughout my life: excellent teachers, enlightened professors, wonderful peers, and an extremely loving family. Thank you to each of you. I know I am very fortunate and I deeply appreciate each of you.

I have also worked very hard; lots of long hours meant time away from home and time away from my husband. And although I wouldn't change anything I want to take this moment to mention that throughout my education and all of the long hours, my husband not only stood next to me, but he supported me, stayed patient with me and continues to love me. I dedicate my dissertation to you, Dustin. I couldn't have done this without you.

ACKNOWLEDGEMENTS

First and foremost, I would like to acknowledge my advisor Dr. David Barondeau who was abundantly helpful and offered invaluable assistance, support, inspiration, and guidance. I would also like to thank my committee members; Dr. Tadhg Begley, Dr. Deborah Bell-Pedersen, and Dr. Frank Raushel for their help, support, and guidance through my career at Texas A&M.

I would like to thank Chris Putnam and the Barondeau group members for their helpful discussions and suggestions in my research endeavors. Specifically, I would like to acknowledge Chi-Lin Tsai for training me and building the Fe-S cluster assembly project. Additionally, I need to thank Nicholas Fox for his help on the radiolabeled sulfur transfer experiments and my undergraduate Andrew Winn.

Portions of this research were carried out at the Stanford Synchrotron Radiation Laboratory, a national user facility operated by Stanford University on behalf of the U.S. Department of Energy, Office of Basic Energy Sciences. The SSRL Structural Molecular Biology Program is supported by the Department of Energy, Office of Biological and Environmental Research, and by the National Institutes of Health, National Center for Research Resources, Biomedical Technology Program, and the National Institute of General Medical Sciences. Use of the Advanced Photon Source was supported by the U. S. Department of Energy, Office of Science, Office of Basic Energy Sciences, under Contract No. DE-AC02-06CH11357. The Advanced Light Source is supported by the

Director, Office of Science, Office of Basic Energy Sciences, of the U.S. Department of Energy under Contract No. DE-AC02-05CH11231.

NOMENCLATURE

A. vinelandii	*Azotobacter vinelandii*
A. aeolicus	*Aquifex aeolicus*
DTT	Dithiothreitol
E. coli	*Escherichia coli*
EDTA	Ethylenediaminetetraacetic acid
FRDA	Friedreich's Ataxia
FXN	Frataxin (also referred to as Fxn, Yfh1 (yeast frataxin), and CyaY (*E. coli* frataxin))
HEPES	N-2-hydroxyethylpiperazine-N'-2-ethanesulfonic acid
IPTG	Isopropyl β–D-thiogalactopyranoside
ISCU2	Human scaffold protein (also referred to as Isu2 (human) and IscU (*E. coli* scaffold protein))
MES	2-(N-morpholino)-ethanesulfonic acid
NFS1	Human cysteine desulfurase enzyme (also referred to as IscS (*E. coli* cysteine desulfurase))
PAGE	Polyacrylamide gel electrophoresis
PEG	Poly(ethylene glycol)
PLP	Pyridoxal-5'-phosphate
SD	Human NFS1-ISD11 protein complex
SDU	Human NFS1-ISD11-ISCU2 protein complex
SDUF	Human NFS1-ISD11-ISCU2-FXN protein complex

S_{ec}	*E. coli* IscS
U_{ec}	*E. coli* IscU
C_{ec}	*E. coli* CyaY
$S_{ec}U_{ec}$	*E coli* IscS-IscU protein complex
$S_{ec}U_{ec}C_{ec}$	*E. coli* IscS-IscU-CyaY protein complex
Tris	Tris(hydroxymethyl) aminomethane
T. maritima	*Thermotoga maritima*

TABLE OF CONTENTS

Page

LIST OF FIGURES

LIST OF TABLES

CHAPTER 1

INTRODUCTION

Wächtershäuser proposed that iron-sulfur (Fe-S) complexes, which are structurally and functionally versatile catalysts, may have played a critical role in the origin of life on early earth [1]. Today, all living organisms utilize the diverse biochemical properties of protein-bound Fe-S clusters in important cellular processes. These Fe-S cofactors are central players in metabolism, respiration, gene regulation, DNA repair and replication, and RNA modification owing to their wide range of reduction potentials, flexible geometries, and ability to access various redox states. The ability to delocalize electron density over both Fe and S atoms and exist with multiple stable oxidation states makes [Fe-S] clusters ideal for their primary electron transfer role in biology [2-4]. While these Fe-S cofactors are typically coordinated by cysteine thiolate ligands, aspartate, histidine, serine, or backbone amide ligations are also known [2]. In addition to electron transfer, the structure and reactivity properties of protein-bound Fe-S clusters lead to their involvement in substrate binding and activation, coupled electron/proton transfer, radical generation and stabilization, protein stabilization, regulation of gene expression or enzyme activity, disulfide reduction, DNA repair, sulfur donation, and as a sensor for iron, superoxide, and dioxygen [5-12].

This dissertation follows the style of *Biochemistry*.

These diverse biological functions require protein scaffolds that can accommodate Fe-S clusters in solvent accessible or completely buried orientations [13].

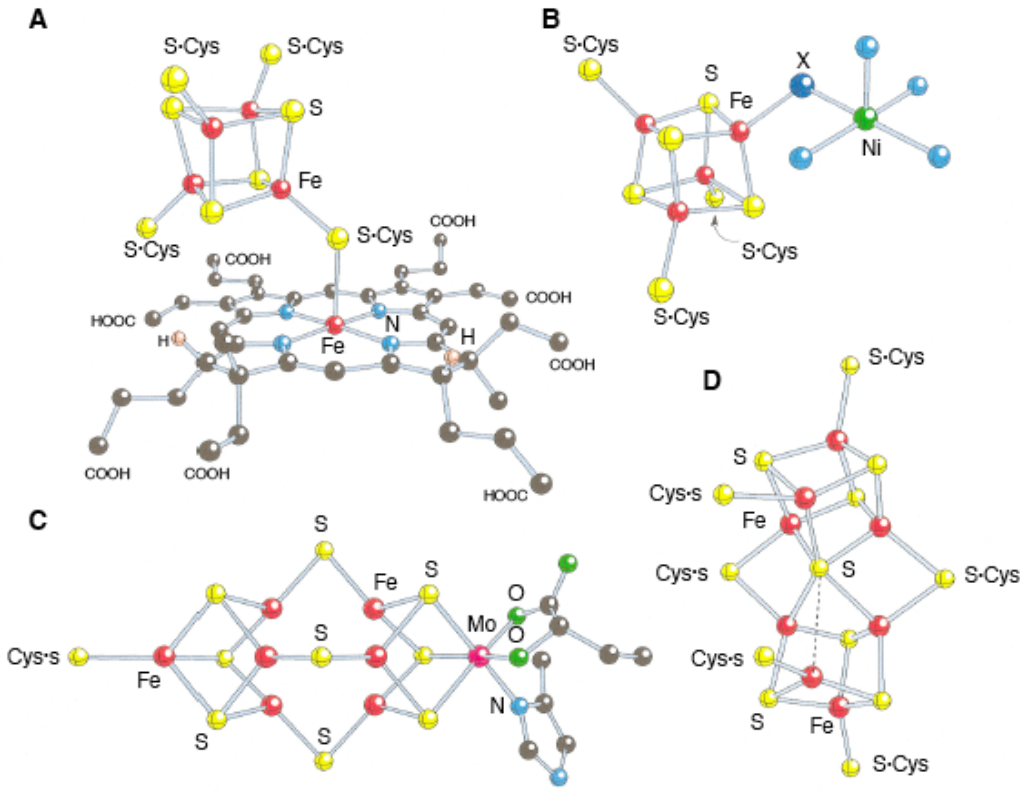

Figure 1-1. Complex [Fe-S]-coupled active sites. (A) *Escherichia coli* sulfite reductase, (B) carbon monoxide dehydrogenase, (C) nitrogenase, and (D) P cluster of nitrogenase. Reprinted with permission from *Science*, 277 (5326): 653-659. Copyright 1997 American Association for the Advancement of Science.

The most common Fe-S cofactors are rhombic [2Fe-2S] and cubic [4Fe-4S] clusters, but

other forms such as [3Fe-4S] and [8Fe-7S] clusters have also been characterized. Fe-S clusters are also found in complex [Fe-S]-coupled active sites, such as in sulfite reductase [14], carbon monoxide dehydrogenase [15], and nitrogenase [16, 17] (Figure 1-1). Investigating the mechanism of Fe-S cluster biosynthesis provides both challenges and opportunities. Challenges include a significant uncatalyzed Fe-S assembly reaction that complicates kinetic measurements by the biosynthetic process. At the same time, almost no mechanistic details are available for any Fe-S assembly process. While these clusters are simple inorganic compounds consisting of ferrous iron, ferric iron, and inorganic sulfide anions, their biosynthesis is surprisingly complex. Elaborate multi-component systems have evolved to protect organisms from the toxic effects of free iron and sulfide ions while promoting the efficient biosynthesis of these cofactors for apo target proteins. Defects in this Fe-S biosynthesis machinery result in compromised iron metabolism, and lead to mitochondrial dysfunction and human disease [18].

In 1989, Dennis Dean's group pioneered the investigation of Fe-S cluster biosynthesis by identifying proteins that comprise the nitrogen fixation pathway (NIF), which is essential for generating the Fe-S clusters of nitrogenase. This NIF pathway is one of three prokaryotic biosynthetic systems for the assembly of Fe-S clusters that have been identified (Figure 1-2). The Dean group also discovered a second, more universal set of assembly proteins in *A. vinelandii*, which is now known as the iron-sulfur cluster assembly pathway (ISC) [19, 20]. In 2002, Tokumoto's group discovered a third Fe-S assembly system, which is known as the sulfur mobilization pathway (SUF) [21]. Many of the prokaryotic organisms contain two of the three Fe-S biosynthesis pathways: one

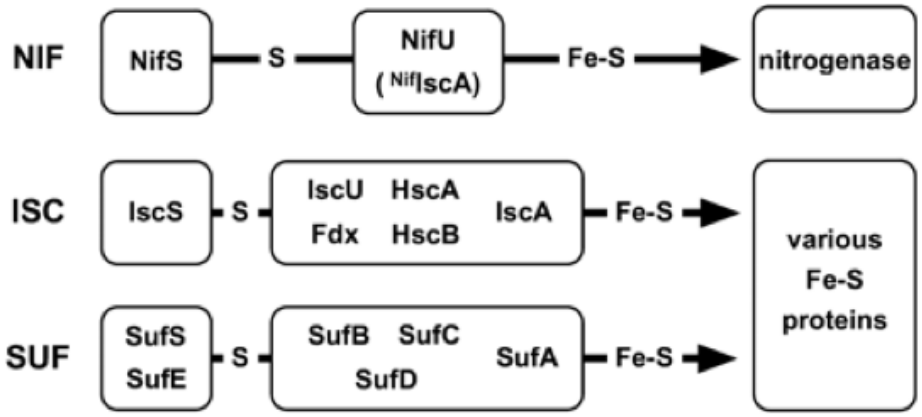

Figure 1-2. Comparison of the three identified prokaryotic systems for Fe-S cluster biosynthesis. Each system utilizes a cysteine desulfurase enzyme (NifS, IscS, or SufS) and the remaining components involved in generating a cluster are shown. The NIF system assembles Fe-S clusters for the nitrogenase Fe protein and MoFe protein. The ISC and SUF systems have redundant roles in *E. coli* building clusters for a wide range of proteins. Reprinted with permission from *J. Biochem*, 136 (2): 199-209. Copyright 2004 Oxford University Press.

that is used for "house keeping" and another "specialized" machinery [22-24]. For example, *A. vinelandii* contains a generalized iron-sulfur cluster assembly pathway (ISC) and a specialized nitrogen fixation machinery (NIF) to form the Fe-S clusters of nitrogenase [19, 20]. In contrast, *E. coli* contains an ISC system that operates under most conditions and a SUF system that functions under iron limiting or oxidative stress conditions [25]. More specifically, the SUF system, which is evidently less susceptible to sub-micromolar levels of hydrogen peroxide than the ISC system [26], is activated during oxidative stress to augment Fe-S cluster assembly by an upregulated ISC system [25].

Iron-sulfur clusters are notoriously susceptible to oxidative-stress induced degradation. A cell is in a state of oxidative stress when intracellular concentrations of O_2^- and H_2O_2 overcome the available antioxidant defenses [26-28]. The major source of reactive oxygen species is the mitochondrial respiratory chain which converts 1-2% of the total consumed molecular oxygen into reactive oxygen species [28]. Initial generation of superoxide is often through molecular oxygen based oxidation of electron transfer reagents [27], such as Fe-S clusters in the respiratory chain of Complex I and III [29]. Compared to the cytosol and nucleus, the mitochondrial matrix contains 5-10 fold higher concentrations of O_2^- [28]. Hydrogen peroxide, a product of superoxide dismutation, has been shown to oxidize [4Fe-4S] clusters in dehydratase enzymes with a rate constant of 10^2-10^3 M^{-1} sec^{-1} and participate in Fenton chemistry to generate hydroxyl radicals capable of oxidizing organic molecules at diffusion-limited rates [26, 27]. Hydrogen peroxide is particularly detrimental to Fe-S cluster biosynthetic pathways because it can oxidize iron, which is prone to precipitation, oxidize cysteine residues to generate sulfenic and sulfinic acid species, and disrupt sulfur transfer reactions, as the persulfide sulfur is also sensitive to hydrogen peroxide [23, 27]. In humans, oxidative stress has been linked to neurodegenerative diseases, type II diabetes, cancer, ischemia, and chronic inflammatory processes [28]. Unlike prokaryotic organisms, however, the human mitochondria lack the back-up oxidative stress tolerant SUF system and rely exclusively on a system composed of proteins that have high similarity to the bacterial ISC system.

There are three evolutionary well-conserved concepts for Fe-S cluster biosynthesis: the conversion of cysteine to alanine and formation of elemental sulfur that is accomplished by a PLP-dependent cysteine desulfurase [30] (Figure 1-3), assembly of iron and sulfide on a scaffold protein to build the Fe-S cluster, and insertion of the intact cluster into an apo target (Figure 1-4). In addition to the cysteine desulfurase and

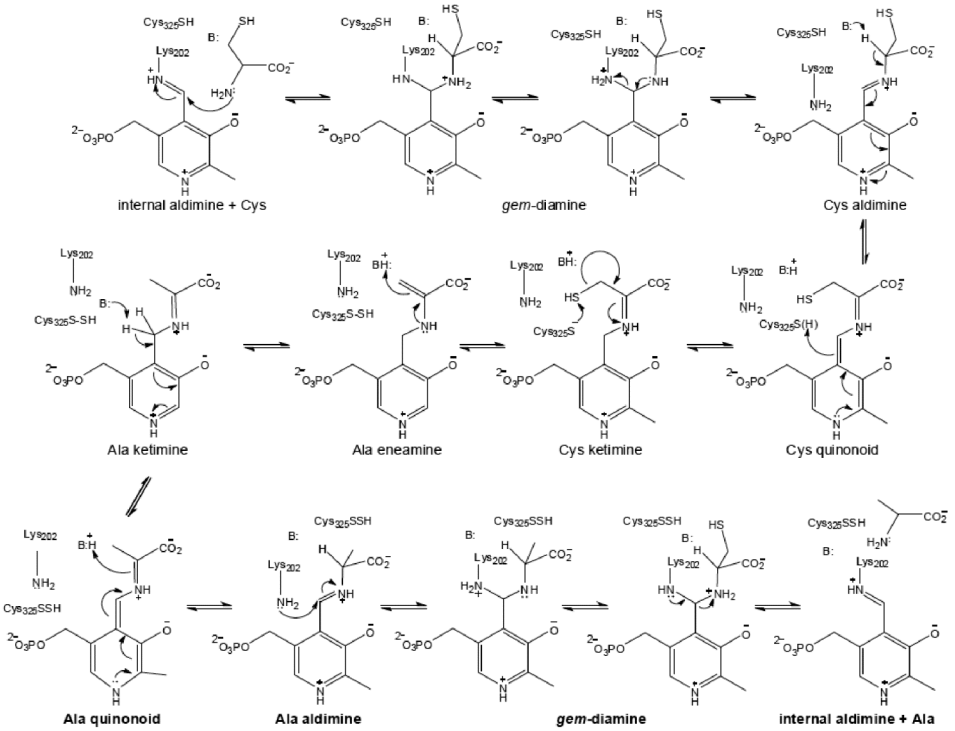

Figure 1-3. Mechanism of the PLP catalyzed conversion of cysteine to alanine with concomitant formation of a persulfide on the catalytic cysteine of the cysteine desulfurase enzyme. Adapted from Zheng *et. al.*, Biochemistry 1994 33, 4714-4720.

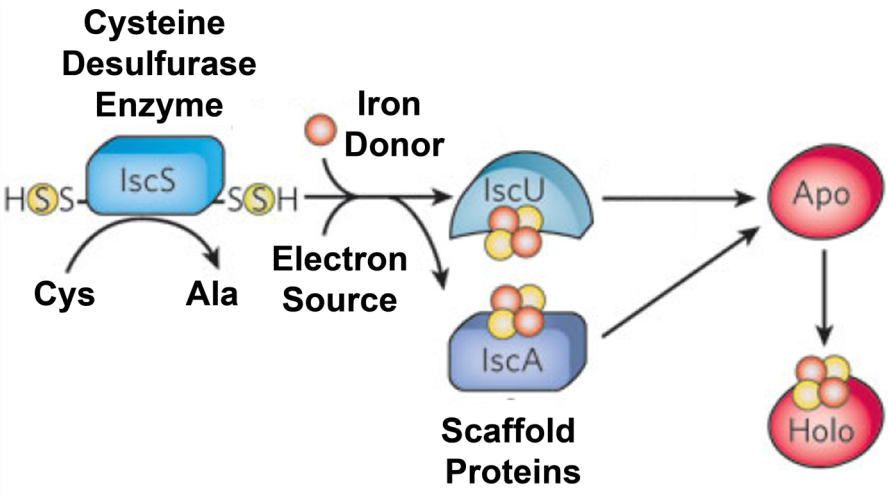

Figure 1-4. Concepts for Fe-S cluster biosyntheisis. A cysteine desulfurase enzyme is used to catalyze the PLP dependent conversion of cysteine to alanine and sulfur that will be combined with iron and electrons to build a Fe-S cluster on a scaffold protein. This intermediate cluster built on the scaffold protein will be donated to an apo target protein. Reprinted with permission from *Nature*, 460 (7257): 831-838. Copyright 2009 Nature Publishing Group.

scaffold protein, the ISC system contains more than a dozen proteins that participate in the generation and transfer of a Fe-S cluster [8, 18, 31]. These proteins include an NADH-dependent ferredoxin reductase (FdxR), an electron donor ferredoxin (Fdx), a monothiol glutaredoxin Grx5, and a proposed iron donor frataxin (FXN). Hsp70 and Hsp20 chaperones facilitate cluster transfer from the Fe-S assembly scaffold to the target apo protein and require an ATP exchange protein in some organisms. Additionally, less well-defined proteins such as IscA and Nfu have been suggested to act as alternate scaffold proteins [32].

Organisms have generated tightly regulated mechanisms to control both the reactivity of iron and sulfur, in an activated persulfide form, and the flux of these substrates through Fe-S cluster biosynthetic pathways. *In vitro*, Fe-S cluster proteins can be spontaneously reconstituted by the addition of ferrous iron and sulfide. *In vivo*, however, free iron and sulfide are both toxic, and regulatory features are required to control the reactivity, minimize release to solution, and aid in the efficient distribution of iron and sulfur to other biochemical pathways. For example, cysteine desulfurase enzymes such as *E. coli* IscS are involved in multiple pathways and use a persulfide species to deliver sulfur to proteins such as IscU, ThiI, TusA, and MoaD/MoeB [33]. As well, iron limitation is a common environmental stress due to its low solubility and its use in both hemes and Fe-S clusters [23]. Regulation at the level of gene expression is accomplished by proteins such as the *E. coli* IscR transcriptional regulator, which synchronizes the expression of the Fe-S cluster assembly machinery with the demand for

Fe-S cluster proteins [34, 35]. RhyB is a 90 nucleotide non-coding RNA responsible for the degradation of target mRNA's that encode iron-utilizing and iron-storage proteins in times of iron limitation [23]. Additionally, the human apo-Irp1 protein responds to iron-deplete conditions in the cytosol by binding mRNA and repressing genes involved in heme biosynthesis and iron storage [36]. Regulation at the level of allostery is exhibited both by the cysteine desulfurase enzyme and the Hsp70 chaperone. For example, the intrinsic ATPase activity of an Hsp70 chaperone can be stimulated up to ~1000 times in the presence of both substrate and co-chaperone Hsp20 [37]. In this case, allostery prevents futile ATP cycling of the Hsp70 in the absence of substrate [37]. Although the proteins involved in the biosynthesis of Fe-S clusters in humans have been identified, little is known about the regulation of cluster assembly and distribution. It is clear, however, that several levels of regulation must exist as a breakdown in the pathway can lead to toxic conditions.

THE ROLE OF FRATAXIN

Several human diseases have been linked to defects in the Fe-S cluster biosynthetic machinery including cardiomyopathy, sideroblastic anemia, and Friedreich's ataxia (FRDA). FRDA is an autosomal recessive neurodegenerative disease and is the most common form of hereditary ataxia having an estimated prevalence of 1 in 50,000 people [38, 39]. 96 percent of patients who have FRDA carry an expanded GAA repeat (66-1700 repeats) on the first intron of their frataxin (FXN) gene [38, 39]. The remaining 4 percent of patients with FRDA are heterozygous, having a mutation on one allele of their FXN gene and an expanded GAA repeat on the other allele [39]. Approximately 2% of the known FXN mutations found in FRDA patients are point mutations and are mostly located on the conserved β–sheet region of the FXN protein (Figure 1-5) [38]. FRDA is a progressive disease and the first symptom is often difficulty in walking. FRDA somatic instability occurs after early embryonic development and advances throughout life [40]. The outcome is progressive spinocerebellar neurodegeneration, causing symptoms of gait and limb ataxia (loss of coordination), dysathria (motor speech disorder characterized by poor articulation), muscle weakness, sensory loss, cardiomyopathy, and diabetes [41]. For FRDA patients harboring point mutations, often the phenotype of disease is more severe and often early onset [38].

While the frataxin protein has been intensively studied its biological role remains controversial. Loss of FXN results in mitochondrial iron accumulation [42, 43], loss of iron-sulfur dependent enzyme activity [44], reduced oxidative phosphorylation [45], and

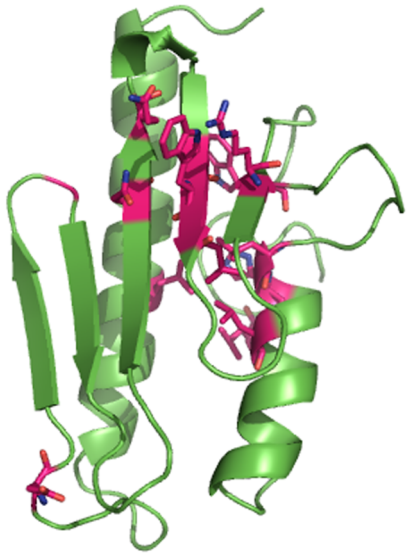

Figure 1-5. Frataxin residues (pink) affected by point mutations in FRDA patients. PDB 3S4M.

increased susceptibility to oxidative stress [46]. Based on this complicated phenotype, or on the properties of the isolated protein, frataxin has been proposed to function as: (A) an iron storage protein similar to ferritin [47-51]; (B) as an oligomer with ferroxidase activity removing oxidative stress [52]; (C) an iron chaperone in Fe-S cluster [53-57] and heme [58] biosynthesis; (D) as a metabolic switch between Fe-S cluster and heme biosynthesis [59]; (E) as an iron sensor [60], and also in general iron homeostasis [45, 61-64] (Figure 1-6)

The iron storage (Figure 1-6A) and reactive oxygen species control (Figure 1-6B) roles proposed for FXN rely on an alternate functional form and oligomeric state. The

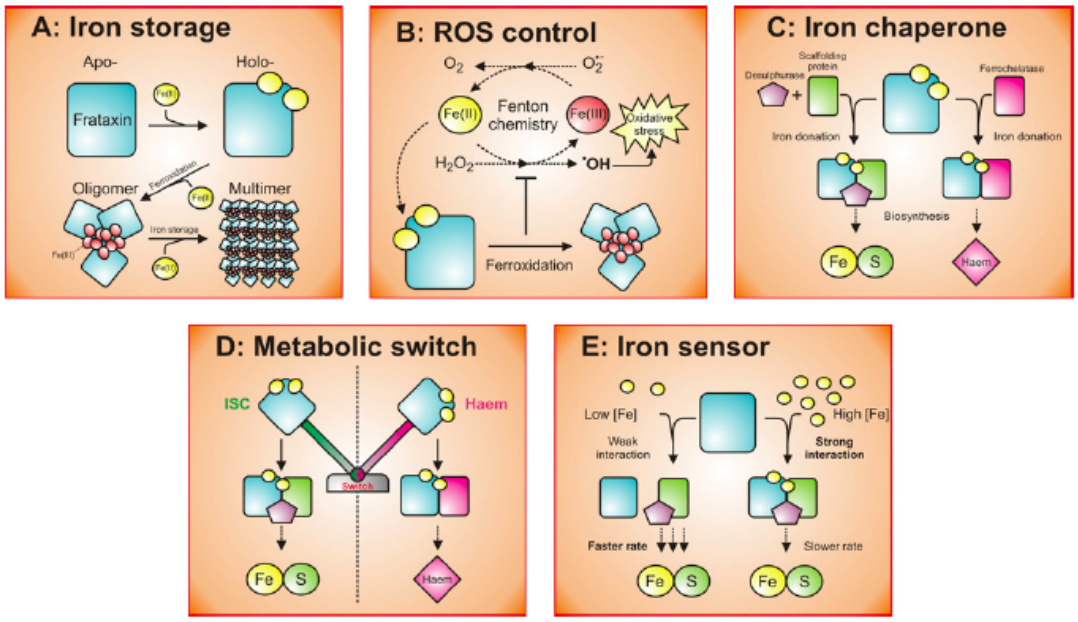

Figure 1-6. Proposed roles for frataxin function. Reprinted with permission from Darius J. R. Lane and Des R. Richardson (2010) Frataxin, a molecule of mystery: trading stability for function in its iron-binding site *Biochem. J.,* 426(2) e1-e3. Copyright the Biochemical Society.

mitochondrial incorporation of FXN (210 amino acids) requires a two-step maturation process in which the mitochondrial processing peptidase (MPP) first cleaves the mitochondrial targeting sequence to generate FXN^{56-210}, followed by a second cleavage reaction to form the FXN^{81-210} mature form. The Isaya group proposed a model in which FXN exists in two functional forms that are both capable of stimulating Fe-S cluster formation on ISCU2 and are relevant in FRDA pathophysiology: a ~14 kDa (FXN^{81-210}) species that is considered the functional form by most investigators, and a ~17 kDa form

(FXN^{56-210}) that requires its residues 56-81 to assemble into large oligomers [65]. Electron Microscopy (EM) and EXAFS studies both support the iron storage role of FXN showing the protein assembles into a large ferritin-like oligomer that can store more than 2000 iron atoms [50, 51, 66]. As well, both the bacterial and yeast strains of FXN can be stimulated to oligomerize in the presence of ferrous iron and oxygen [67, 68]. Data opposing the functional oligomeric form of FXN in yeast is provided by the Aloria *et al*., who generated a FXN oligomerization deficient yeast strain that did not have any growth defects or apparent phenotype [69] and by Seguin *et al*., who showed that increased levels of yeast FXN *in vivo* did not correlate with a change in the distribution of soluble iron [70].

The iron chaperone role of FXN (Figure 1-6C) is supported by the semi-conserved nature of the acidic patch of solvent-exposed aspartate and glutamate residues that binds iron with micromolar affinity [53, 71-73]. Mutation of residues in this acidic patch result in impaired iron binding *in vitro* and decreased Fe-S cluster biosynthesis *in vivo* when 2-4 of the acidic residues are replaced with alanine or lysine [71, 74]. In addition, the observations that FXN knockouts result in defects in Fe-S cluster proteins and mitochondrial iron accumulation, the fact that FXN interacts with cluster assembly proteins IscU and IscS, and *in vitro* studies that demonstrate iron transfer from FXN to the scaffold protein all support an iron donor role for FXN [53, 54, 56, 75, 76]. The metabolic switch role of FXN (Figure 1-6D) is supported by down-regulation of FXN protein levels in response to increased levels of protoporphyrin IX and a corresponding increase in mitochondrial heme iron loading [59]. Finally, the Pastore group provided *in*

vitro evidence that the bacterial homolog CyaY functions as a negative regulator or inhibitor for Fe-S cluster synthesis and suggest the physiological role is an iron sensor (Figure 1-6E: see below for more details) that turns off Fe-S cluster assembly under high iron conditions [60].

Another approach to understand frataxin is to evaluate how FRDA missense mutations are functionally compromised. As W155 is the only completely conserved residue on the FXN protein, most previous studies have focused on this residue. Specifically, W155 has been shown to be an oxidative hotspot susceptible to hydroxyl radicals and nitration using chemical modification experiments and may suggest a role for FXN in oxidative stress protection [77]. As well, mutation of W155 to alanine has been shown to decrease FXN interaction with the yeast scaffold protein in pull-down experiments [78]. Additionally, the N146K clinical frataxin mutant in yeast leads to decreased interaction with the yeast scaffold protein suggesting roles of the solvent exposed residues on the β–sheet region of the FXN in protein-protein interactions [79]. Previous studies implicate missense mutations W155R, I154F, D122Y, and G130V (human numbering) in decreasing the protein stability of FXN [77, 80]. NMR studies of the *S. cerevisiae* FXN homolog Yfh1 [81] along with pull-down studies for frataxin variants [82-85] indicate residues on the β-sheet such as V144, N146, Q148, Q153, W155, and R165 (human numbering) contribute to FXN binding interactions with other Fe-S assembly proteins. Lastly, Foury's group has shown that Q153A, I154F, W155A, W155F, and R165C mutations in yeast frataxin lead to decreased aconitase activity in isolated mitochondria [78].

ESCHERICHIA COLI (E. COLI) ISC MACHINERY

In *E. coli*, there are nine proteins involved in the ISC biosynthetic machinery and eight of these proteins are found in the same gene cluster [23]. This gene cluster encodes IscR, the cysteine desulfurase (IscS), the scaffold protein (IscU), IscA, HscA, HscB, Ferredoxin, and IscX [23]. The *E. coli* cysteine desulfurase enzyme crystal structure has been determined to a resolution of 2.1 Å and shows the PLP cofactor at the base of an active site pocket. The catalytic Cys328 is located greater than 17 Å away from the PLP cofactor on a disordered loop. Mobility of this loop might be required for function as a significant conformational change is required for nucleophilic attack by Cys328 on the cysteine substrate adduct with PLP [86]. In 2010, Cygler's group published a 3.0 Å crystal structure of the IscS-IscU complex (Figure 1-7A). In the crystal structure, the catalytic cysteine loop is not visible due to its conformational flexibility. However, the distance between the catalytic cysteine residue and the conserved cysteine residues of IscU could be estimated to be between 12 and 18 Å (Figure 1-7B). This suggests that the cysteine loop samples a distance of ~30 Å during catalysis. IscA has been suggested to function as an [Fe-S] cluster carrier or scaffold protein and that the HscA/HscB are a specialized chaperone/co-chaperone pair that is involved in delivery of the Fe-S cluster built on IscU to an apo target protein. Ferredoxin is an electron donor, and IscX is a gene of unknown function.

As mentioned earlier, IscR is a transcriptional regulator responsible for governing the expression of the *IscRSUA* operon in response to hydrogen peroxide, iron starvation, and the availability of Fe-S clusters [35]. IscR shares 47% sequence identity

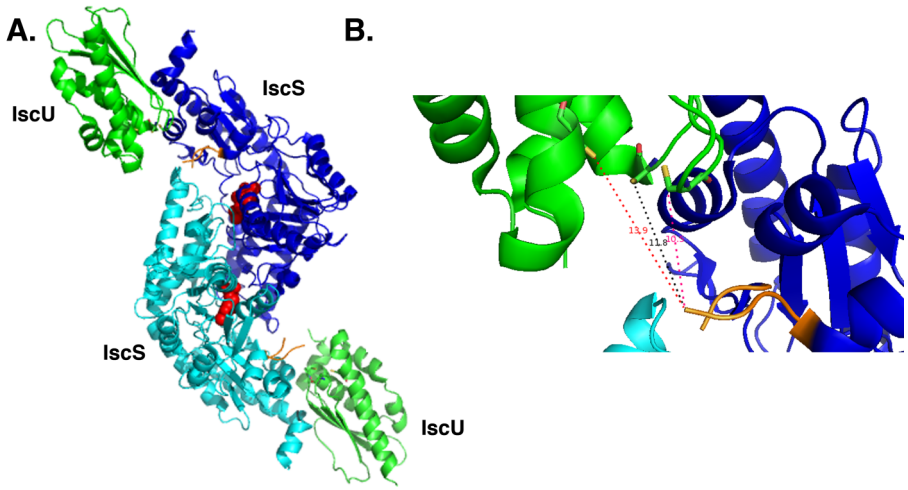

Figure 1-7. Crystal structure of the *E. coli* IscS-IscU complex (PDB: 3LVL). (A) The IscS-IscU is a heterodimeric complex. IscS components are cyan and blue while IscU components are green. PLP cofactors are shown in red and the disordered catalytic cysteine desulfurase missing C328 is highlighted in orange. (B) Measured distances between the disordered catalytic cysteine desulfurase loop and the conserved cysteine residues on IscU are shown.

with the MarA transcriptional regulator with an additional stretch of amino acids responsible for coordination of a [2Fe-2S] cluster [87, 88]. IscR possesses a winged helix-turn-helix DNA binding motif and has been shown to bind the *IscRSUA* promoter and repress transcription of the operon (Figure 1-8) [23]. As deletion of IscS or HscA result in increased transcription from the *isc* promoter, the prevailing model is that holo IscR represses the *isc* locus [88]. When the amount of assembled [Fe-S] clusters is low or oxygen is present, IscR loses its Fe-S cluster and dissociates from the promoter region allowing transcription of the operon [23]. The last protein thought to be involved in this machinery is CyaY. While not located in the same gene locus, CyaY is a frataxin-like

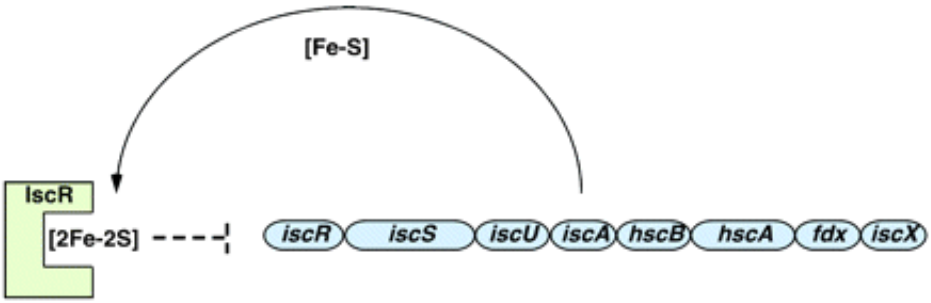

Figure 1-8. The eight genes of the *E. coli* ISC operon are under transcriptional control of IscR. The [2Fe-2S] cluster bound IscR will repress transcription of *isc* genes. Reprinted with permission from *Microbiology and Molecular Biology Reviews*, 72 (1): 110-125. Copyright 2008 American Society for Microbiology.

protein and has thus been implicated as an iron donor [53, 54, 56, 75, 76], an inhibitor of [Fe-S] cluster assembly [60], and as a ferritin-like iron storage protein [47-51].

The cellular function of CyaY in the biosynthesis of Fe-S clusters remains controversial. CyaY has been implicated in Fe-S cluster biosynthesis based on its ability to form interactions with the core components of the machinery, IscU and IscS [75, 89]. However, in contrast to FXN, CyaY has been shown to decrease the *in vitro* rate of formation of [2Fe-2S] and [4Fe-4S] clusters monitored by CD, UV-visible, and Mössbauer spectroscopy [90, 91]. In the presence of CyaY, the formation of [2Fe-2S]

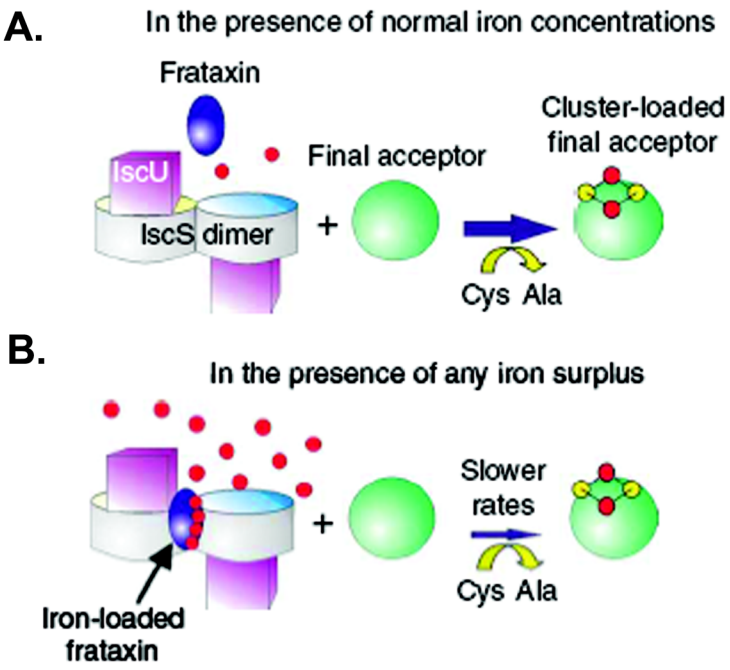

Figure 1-9. Model for CyaY based inhibition of Fe-S cluster assembly in *E. coli*. (A) In the presence of normal iron conditions, the IscS-IscU complex will assemble Fe-S clusters and deliver them to apo-acceptor proteins. (B) In the presence of an iron surplus (large amount of iron relative to apo-target proteins) the affinity of CyaY for the IscS-IscU complex is increased and the rate of Fe-S cluster formation is decreased. Reprinted with permission from *Nat. Struct. Mol. Biol.* 16 (4): 390-396. Copyright 2009 Nature Publishing Group.

clusters decreased 80% relative to a control sample containing only IscS and IscU, and this inhibitory effect was more pronounced at higher iron concentrations [90]. The

Pastore group called CyaY a gatekeeper for Fe-S cluster biosynthesis and proposed a model in which normal iron levels resulted in weak CyaY binding and an active IscS-IscU complex (Figure 1-9A), whereas increased iron levels promoted CyaY binding and inhibition of Fe-S cluster assembly (Figure 1-9B) [90]. The exact mode of Fe-S cluster inhibition by CyaY is still unclear. The addition of CyaY slightly decreases the cysteinedesulfurase activity [91], but experiments to confirm a sulfur transfer defect from IscS to IscU have not been performed. Part of the difficulty in assigning an *in vivo* function to CyaY is the lack of phenotype: deletion or overexpression of CyaY does not affect cellular growth, iron content, or survival after exposure to H_2O_2 [92, 93]. These types of studies are complicated by the presence of both the ISC and SUF Fe-S assembly systems in *E. coli*. However, if the physiological role of CyaY were to inhibit Fe-S cluster formation by the ISC system, then one would expect overexpression of CyaY in the absence of the SUF system to give a loss of Fe-S cluster phenotype.

HUMAN ISC MACHINERY

In eukaryotes, the Fe-S cluster assembly machinery operates in the matrix space of the mitochondria and contains a myriad of proteins that mediate sulfur, iron, and electron transfer to assemble Fe-S clusters on the scaffold protein ISCU2 and then insert these clusters into target proteins (Figure 1-10). The human cysteine desulfurase enzyme

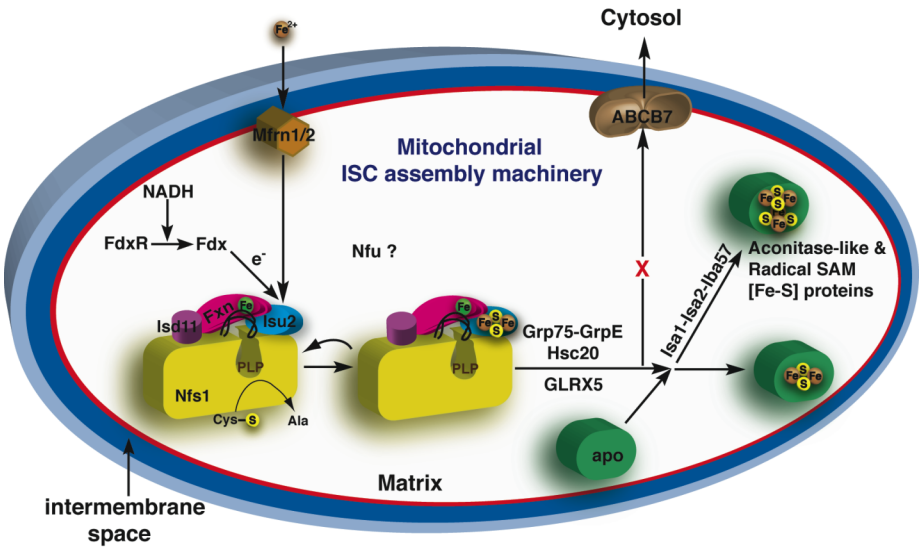

Figure 1-10. Human mitochondrial Fe-S cluster assembly machinery.

NFS1 is a 94 kDa homodimeric protein that aggregates in the absence of its 11 kDa protein partner ISD11 [94, 95]. The ISD11 gene is found in plants, fungi, and animal

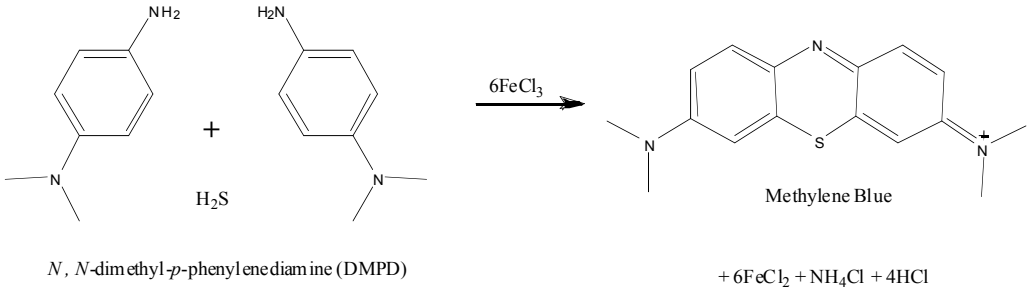

Figure 1-11. Sulfide production assay. After reductive cleavage of a persulfide from NFS1 or ISCU2, hydrogen sulfide reacts with N, N-dimethyl-p-phenylyenediamine (DMPD) and ferric iron to make methylene blue that can be monitored at 670 nm.

genomes but is absent in prokaryotes. The human ISCU2 scaffold protein shares 72% sequence identity with *E. coli* IscU and 55% sequence identity with *S. cerevisiae* Isu1. Recently, stable 2, 3, and 4-protein complexes composed of NFS1 and ISD11 (SD), NFS1, ISD11, and ISCU2 (SDU), and NFS1, ISD11, ISCU2, and FXN (SDUF) subunits have been reconstituted and functionally characterized [96]. Michaelis-Menten kinetics for the cysteine desulfurase reaction of the SD, SDU, and SDUF protein complexes were measured with an assay that determines PLP-dependent cysteine turnover as a function of sulfide production [96]. In this assay, cysteine is converted into alanine and a persulfide intermediate, which can be reductively cleaved with DTT and then released as sulfide into solution [96]. The sulfide was reacted with *N,N*-dimethyl-*p*-phenylenediamine and $FeCl_3$ to produced methylene blue and then quantitated using the absorbance at 670 nm (Figure 1-11) [96]. The SD protein complex exhibited a

Michaelis constant of 0.34 mM for cysteine and a k_{cat} of 1.9 min^{-1}, while the SDU complex showed a Michaelis constant of 0.59 mM for cysteine and a k_{cat} of 0.89 min^{-1} [96]. In the SDUF complex, FXN functions as an allosteric activator decreasing the K_M for cysteine 50-fold and increasing the k_{cat} 6-fold thereby switching this assembly complex on for Fe-S cluster biosynthesis (Figure 1-12) [96].

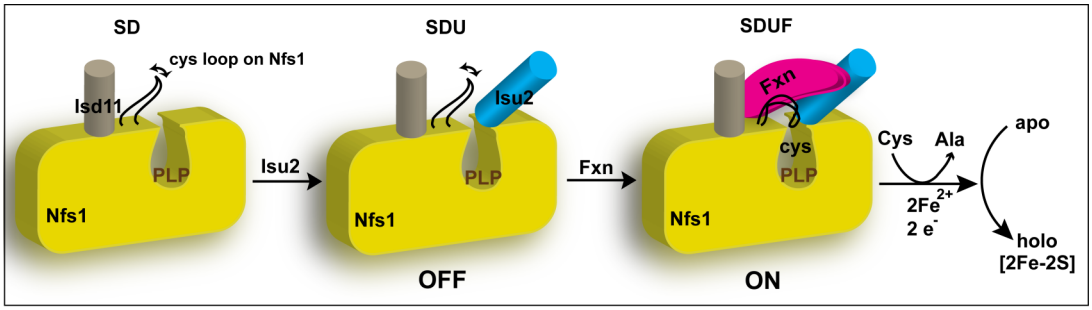

Figure 1-12. Frataxin is an allosteric activator for human Fe-S cluster biosyntheses. Frataxin binding to the SDU complex enhances substrate binding and accelerates the rate of persulfide bond formation on NFS1. Frataxin binding may also increase the rate of persulfide transfer to ISCU2. Reprinted with permission from *Biochemistry*, 2010, 49 (43), pp 9132–9139. Copyright 2010 American Chemical Society.

The Hsp70 chaperone utilized in mitochondrial Fe-S cluster biosynthesis has been implicated in Parkinson's disease, Alzheimer's disease, and cancer. The Hsp70 family of chaperones is highly conserved between prokaryotes and eukaryotes and is involved in protein folding, stress response, cellular trafficking, and translocation of

proteins across membranes [37]. These chaperones are characterized by an approximate 45 kDa N-terminal nucleotide binding domain that has ATPase activity and a smaller 25 kDa C-terminal domain involved in substrate binding [37]. The ATPase activity of the N-terminal domain is generally on the order of 0.1 min^{-1} and can be stimulated by co-chaperone and/or substrate binding [37]. Unlike in the *E. coli* and yeast systems where there is a specialized Hsp70 chaperone involved in Fe-S cluster biosynthesis, the Hsp70 in human mitochondria has several Hsp20 protein partners and is thus involved in a wide range of biosynthetic pathways. The human Hsc20 J-protein is classified as a DnaJ type III protein as it has a specialized N-terminal J-domain that is essential for interaction with its designated Hsp70 [97]. Type III J-proteins are not chaperones alone and generally interact with a single substrate or a limited selection [97]. Hsc20 shares 34% sequence identity with the *E. coli* co-chaperone HscB [97]. The defining difference is these co-chaperones localizes to the N-terminal region where Hsc20 has an extra domain harboring two CXXC motifs that can coordinate a zinc ion (Figure 1-13) [97, 98]. The metal binding domain of Hsc20 has similarities to both rubredoxin and zinc finger domains and is found in higher eukaryotes, plants, parasites, and a few bacterial species that have unusually high iron requirements for their metabolic pathways [98]. The presence of this N-terminal domain has been speculated to bind iron and be involved in one electron redox chemistry, act as an electron source for the reductive coupling of [2Fe-2S] clusters to make [4Fe-4S] clusters, or mediate specific interactions with transport proteins [98]. The appearance of this additional domain in higher eukaryotes is correlated with the lack of a specific Hsp70 chaperone in ISC biogenesis and thus may

serve to mediate a more stringent interaction with the chaperone [97]. Under conditions of oxidative stress, si-RNA based knockdown of Hsc20 results in impaired repair and regeneration of Fe-S cluster containing proteins [97]. Paraquat treatment of HeLa cells results in a 62% reduction of Hsc20 protein levels after 72 hours while the Hsc20 transcript levels remain relatively unchanged [97]. The decreased Hsc20 protein levels suggest post-transcriptional regulation of Hsc20 as a function of oxidative stress by degradation or decreased stability of the protein [97]. In contrast, over-expression of Hsc20 protects cells from oxidative stress and may be explained by excess recruitment of the Hsp70 into Fe-S cluster biosynthesis and faster regeneration of Fe-S cluster containing proteins [97].

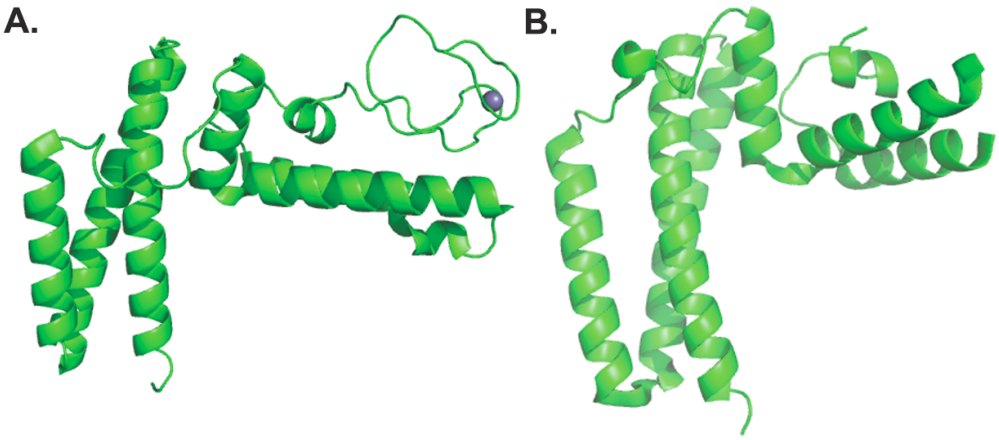

Figure 1-13. Comparison of (A) the crystal structure of human HSC20 (3BVO) and (B) the crystal structure of HscB from *E. coli* (1FPO). The human co-chaperone protein has an additional N-terminal extension that harbors two CXXC motifs shown to coordinate a zinc ion in the crystal structure. The human co-chaperone shares 34% sequence identity with its bacterial homolog.

PROPOSED MECHANISMS FOR FE-S CLUSTER ASSEMBLY

Despite the wealth of information available on the proteins involved in building Fe-S clusters, few details are known about the mechanism of cluster formation on the scaffold protein. For the SUF system, two possible Fe-S cluster assembly mechanisms have been proposed [75, 99, 100]. The first proposed mechanism is called the iron-first model (Figure 1-14A) and is supported by ~3 μM binding constants for ferrous and ferric iron to the *Thermotoga maritima* IscU [101]. The iron-first mechanism requires that the first step of [2Fe-2S] cluster formation is ligation of two ferrous atoms to cysteine residues contributed by two subunits of a SufA dimer (homologous to ISCU2), after iron binds, sulfur is transferred from the cysteine desulfurase in the form of S^0. A [2Fe-2S] cluster requires the addition of 4 electrons to reduce the sulfane sulfur atoms; 2 of which are contributed from the ferrous iron atoms and 2 of which come from an external source. Contrastingly, the sulfur-first mechanism (Figure 1-14B) is initiated by a cysteine residue of the SufA dimer nucleophilically attacking the persulfidic species generated on the catalytic loop of the cysteine desulfurase. Ferrous iron binding follows transpersulfuration of the SufA dimer and cluster is formed by sequential 2-electron reduction of each sulfane sulfur atom. Incubation of the prokaryotic IscS with IscU in the absence of DTT results in a persulfide-bound or polysulfide-bound IscU and provides experimental evidence for the sulfur first mechanism [102, 103]. Accordingly, sulfurated SufA can be combined with ^{57}Fe and DTT to yield both [2Fe-2S] and [4Fe-4S] clusters [104]. Unfortunately as the *E. coli* scaffold, the human scaffold, or the *A. vinelandii* scaffold have never been shown to bind ferrous iron with cysteine ligation,

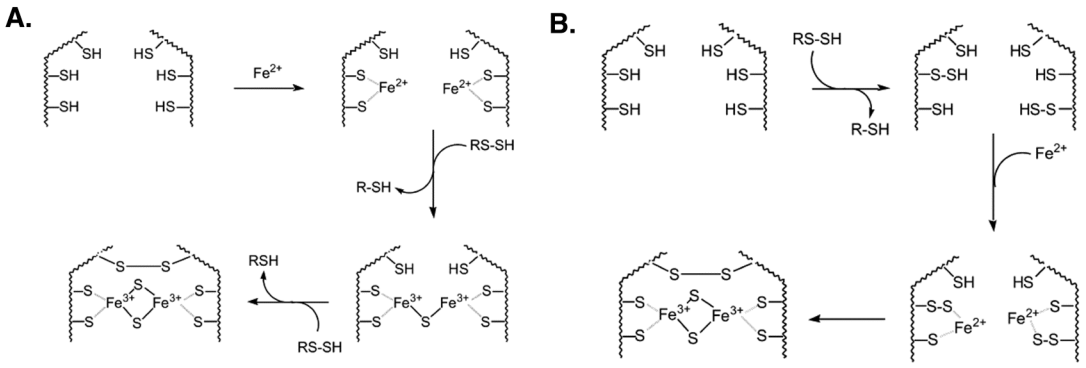

Figure 1-14. Proposed mechanisms for the assembly of Fe-S clusters. (A) Iron-first model for Fe-S cluster assembly and (B) Sulfur-first model for Fe-S cluster assembly. Reprinted with permission from *J. Biol, Inorg. Chem.*, 276 (25): 22604-22607. Copyright 2005 Springer/Heidelberg.

and neither the persulfide-bound or polysulfide-bound forms of IscU have been shown to be viable in cluster formation [103], the Fe-S cluster assembly mechanism has yet to be resolved. Additional controversy arrives for the sulfur-first mechanism, over whether a particular cysteine, and, if so, which cysteine accepts the sulfur atom donated by the cysteine desulfurase for Fe-S cluster biosynthesis.

The human ISCU2 contains three conserved cysteine residues: C35, C61, and C104 that could ligate a Fe-S cluster. The fourth cluster ligand is unknown but has been suggested to be H103 [105, 106], C96 [107], or an ISCU2 ligand formed from ISCU2 dimerization [108]. Each of these three conserved cysteine residues on the scaffold protein have been implicated in acting as the sulfur acceptor residue during the sulfur transfer reaction. In 2002, C63 (C61 in human numbering) on the *E. coli* scaffold

protein was shown to stimulate the cysteine desulfurase activity of IscS and additionally found to form a disulfide bridge with the catalytic cysteine residue of IscS [109]. In 2005, Johnson's group used electrospray-ionization mass spectrometry to show that the *Azotobacter vinelandii* cysteine desulfurase could deliver a persulfide or polysulfide species to each of three alanine substituted forms of the scaffold protein and then further showed a covalent disulfide bridge could form between C37 (C35 in human numbering) and the catalytic cysteine of the enzyme [110]. In 2011, Vickery's group identified an essential role for C106 (C104 in human numbering) on the *E. coli* scaffold protein in accepting the persulfide sulfur from the cysteine desulfurase enzyme [111]. The equivalent sulfur transfer experiments have not yet been performed on a eukaryotic system and have not yet been performed in the context of a complex.

CHAPTER II

FRIEDREICH'S ATAXIA VARIANTS I154F AND W155R DIMINISH FRATAXIN-BASED ACTIVATION OF THE HUMAN IRON-SULFUR CLUSTER ASSEMBLY COMPLEX*

INTRODUCTION

Friedreich's ataxia (FRDA) is an autosomal recessive neurodegenerative disease caused by reduced amounts of the protein frataxin (Fxn) [39]. The loss of Fxn results in a complex phenotype that includes increased iron in the mitochondria, deficiencies in Fe-S cluster enzymes, and enhanced sensitivity to oxidative stress [112]. FRDA patients typically present symptoms during adolescence such as progressive limb and gait ataxia and often die prematurely from cardiomyopathy. There is currently no cure. The majority (>95%) of FRDA patients are homozygous for an unstable GAA trinucleotide repeat expansion in the first intron of the *FXN* gene [113]. The number of repeats range from 7 to 40 [1]for normal individuals and from 66 to >1700 for FRDA patients [113, 114]. Importantly, larger numbers of GAA repeats correlate with lower Fxn expression and an earlier age of disease onset [115, 116]. A small fraction of FRDA patients are

compound heterozygotes with an expanded GAA repeat affecting one allele and a missense or nonsense mutation affecting the other allele [117]. For compound heterozygote patients, the Fxn protein levels do not necessarily correspond to the age of onset [113, 118].

Most researchers agree that Fxn has a critical role in iron-sulfur (Fe-S) cluster assembly [56, 57]. Eukaryotic Fe-S cluster biosynthesis occurs in the matrix space of the mitochondria and involves at least a dozen proteins [119]. $[2Fe\text{-}2S]^{2+/1+}$ clusters and, possibly, $[4Fe\text{-}4S]^{2+/1+}$ clusters are assembled on the monomeric Isu2 scaffold [120]. Nfs1, which forms a functional complex with Isd11 [121-123], catalyzes the PLP-dependent breakdown of cysteine to alanine and produces a transient persulfide species on a mobile loop [8, 124]. The sulfur from this persulfide species is then transferred to Isu2 and becomes the inorganic sulfide of the Fe-S clusters. After iron incorporation and Fe-S cluster synthesis, chaperones interact with the scaffold protein and assist in delivering intact Fe-S clusters to their apo targets [97, 125, 126]. Many potential roles for Fxn in this process have been suggested, which is complicated by the presence of multiple Fxn proteolytic products [127-133]. The 14 kDa monomeric form (referred to as Fxn in this manuscript) includes residues 81-210 and is commonly thought to function as an iron chaperone in Fe-S cluster biosynthesis [134]. Both *in vivo* and *in vitro* data

support pairwise physical interactions between eukaryotic Nfs1, Isd11, Isu1/2, and Fxn [53, 54, 76, 84, 85, 121, 122]. Recently, biochemical evidence was provided for Nfs1, Isd11, and Isu2 (SDU) and Nfs1, Isd11, Isu2, and Fxn (SDUF) Fe-S cluster assembly complexes [82, 96]. This work also identified Fxn as an allosteric activator of Fe-S cluster assembly that increases the catalytic efficiency (k_{cat}/K_M) for the cysteine desulfurase component of SDUF and the rate of Fe-S cluster biosynthesis [96].

The *FXN* missense mutations present in compound heterozygous patients likely cause at least partial defects in Fxn function that may provide additional insight into the role of Fxn in Fe-S cluster biosynthesis. Therefore, the human FRDA mutations I154F and W155R and related Fxn variants were investigated using our recently developed biochemical assays for Fxn combined with determination of X-ray crystal structures. The data indicated that these mutations and variants have defects in binding and activating the SDU complex. The relative effects of the I154F and W155R mutations *in vitro* correlate with the reported age of onset in patients. In addition, structure-function properties for the W155A, W155R and W155F variants contribute to a model for how Fxn facilitiates direct sulfur transfer from Nfs1 to Isu2 for Fe-S cluster assembly.

EXPERIMENTAL PROCEDURES

Protein Preparation. The QuikChange method (Stratagene) was used to introduce point mutants (I154F, W155A, W155R, and W155F) into a pET11a plasmid containing human Fxn (Δ1-55) [96], and the mutation sites were confirmed by DNA sequencing. Plasmids containing the Fxn variants were individually transformed into *E. coli* strain BL21(DE3), and the cells were grown at 16 ^{o}C. Protein expression was induced at an OD_{600} of 0.6 with 0.5 mM IPTG. Cells were harvested 16 hours later and purified as previously described for native Fxn [96]. The Fxn variants spontaneously truncate to a form that includes residues 82-210, similar to native Fxn. The protein expression and purification of native Fxn, Isu2, and the Nfs1/Isd11 (SD) complex were performed as previously described [96]. Protein concentrations for I154F, W155A, W155R, and W155F were estimated by their absorbance at 280 nm using extinction coefficients of 26030, 21430, 20340, and 21430 $M^{-1}cm^{-1}$, respectively.

Cysteine Desulfurase Activity Measurements. Reaction mixtures (800 μL) containing SD (0.5 μM), Isu2 (1.5 μM), PLP (10 μM), DTT (2 mM), $Fe(NH_4)_2(SO_4)_2$ (5 μM), Fxn variants (1.5 μM), 50 mM Tris pH 8.0, and 250 mM NaCl were incubated in an anaerobic glovebox (10~14 ^{o}C) for 30 minutes [96, 135, 136]. The cysteine desulfurase reactions were initiated by addition of 100 μM L-cysteine at 37 °C. Sulfide production was typically linear for the first 30 minutes and an incubation time of 10 minutes was chosen to generate sufficient product for detection. Assays were quenched by addition of 100 μl of 20 mM *N,N*-dimethyl-*p*-phenylenediamine in 7.2 N HCl and 100 μl of 30 mM $FeCl_3$ in 1.2 N HCl, which also initiated the conversion of sulfide to

methylene blue. After a 20 minute incubation at 37 ^{o}C, the absorption at 670 nm due to methylene blue formation was measured and compared with a Na_2S standard curve to quantitate sulfide production. Units are defined as μmol sulfide/μmol SD per minute at 37 ^{o}C. The rates for the cysteine desulfurase reaction were also examined in the presence of 10 equivalents of $Fe(NH_4)_2(SO_4)_2$ and with increasing amounts of Fxn to determine the number of equivalents, or the saturating amount, that are required to maximize the cysteine desulfurase activity. Batch one of Nfs1/Isd11 (cysteine desulfurase activity of 8.3 min^{-1}) was used for the initial Michaelis-Menten kinetics for all of the variants and the determination of the binding constants for the native Fxn, I154F and W155R variants. A second batch of SD with lower activity (4.8 min^{-1}) was used for determining the binding constants of the W155A and W155F Fxn variants.

An alternate cysteine desulfurase activity assay that monitored cysteine in solution (38) was used to verify the rate enhancement upon addition of Fxn variants. In this assay, reaction components were prepared at the same concentrations of the methylene blue assay (above), but at a final reaction volume of 50 μL. After incubation in the anaerobic glovebox for 30 min, the cysteine desulfurase reaction was initiated with the addition of 100 μM L-cysteine at 37^{o}C and quenched after 20 min using 50 μL of acetic acid. Next, 50 μL of acid ninhydrin reagent 2 (stock solution was made by dissolving 25 mg of ninhydrin in 600 μL of acetic acid and 400 μL of HCl) was added to the reaction mixtures, the samples were boiled for 10 min, rapidly cooled on ice, and diluted to 1 mL in 95% ethanol. The amount of cysteine reacted was quantitated using

an extinction coefficient of 27.5 mM^{-1} cm^{-1} at 560 nm (38) and compared to a sample that lacked enzyme.

Fe-S Cluster Formation on Isu2. Assay mixtures contained 8 μM SD, 24 μM Isu2, 24 μM Fxn variants, 5 mM DTT, 200 μM $Fe(NH_4)_2(SO_4)_2$, 100 μM L-cysteine, 50 mM Tris pH 8.0, and 250 mM NaCl in a total volume of 0.2 mL. Isu2 was incubated with 5 mM DTT in 50 mM Tris pH 8, 250 mM NaCl in an anaerobic glovebox for 1 hour prior to mixing with the remaining assay components in an anaerobic cuvette. The reaction was initiated by injecting L-cysteine to a final concentration of 100 μM with a gas-tight syringe. Fe-S cluster formation was monitored at 456 nm at room temperature and then the first 600 seconds were fit as first-order kinetics using KaleidaGraph (Synergy Software). The rate was converted to the activity of Isu2 using an extinction coefficient of 9.8 $mM^{-1}cm^{-1}$ at 456 nm, previously determined for a $[2Fe\text{-}2S]^{2+}$ cluster bound to the human scaffold protein [137]. Units are defined as μmol of $[2Fe\text{-}2S]^{2+}$ cluster / μmol SDU complex per minute at 25 ^{o}C.

Michaelis-Menten Kinetics for Fxn Variants in SDUF Complex. The saturating amounts of the different Fxn variants were separately added to a standard reaction mixture (0.5 μM SD, 1.5 μM Isu2, 10 μM PLP, 2 mM DTT, 5 μM $Fe(NH_4)_2(SO_4)_2$, 50 mM Tris pH 8.0, and 250 mM NaCl) and incubated anaerobically for 30 minutes. The cysteine desulfurase activities were measured after initiating the reaction with the substrate L-cysteine (0.01 to 1 mM). Reaction rates as a function of cysteine concentration were fit to the Michaelis-Menten equation using Kaleidagraph. The k_{cat}

was also measured as a function of FXN concentration and used to determine the FXN binding constant for the SDU complex.

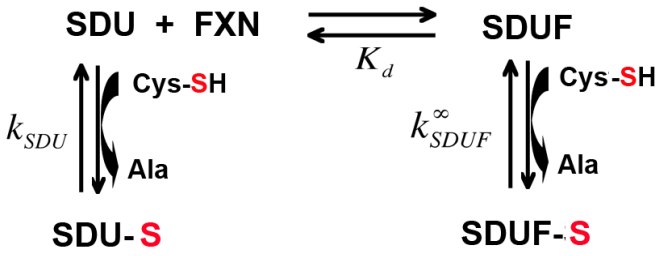

Scheme 2-1.

Using scheme 2-1, a kinetic equation was derived to define the K_d based on the concentrations of SDU, FXN, and SDUF (equation 2-1), where $[SDU]_{total}$ describes the total amount of enzyme partitioned between SDU and SDUF forms of the enzyme.

$$K_d = \frac{([FXN]_{total} - [SDUF])([SDU]_{total} - [SDUF])}{[SDUF]} \qquad (2\text{-}1)$$

Multiplying both sides of equation 2-1 by [SDUF] results in equation 2-2:

$$K_d[SDUF] - (([FXN] - [SDUF])([SDU]_{total} - [SDUF])) = 0 \qquad (2\text{-}2)$$

which can be rearranged to yield equation 2-3:

$$-[SDUF]^2 + ([SDU]_{total} + [FXN] + K_d)[SDUF] - (([SDU]_{total})(FXN)) = 0 \quad (2\text{-}3)$$

Equation 2-3, a quadratic equation, can be solved in terms of [SDUF] to yield equation 2-4:

$$[SDUF] = \frac{b - \sqrt{b^2 - 4ac}}{2}$$
$$a = 1$$
$$b = [SDU]_{total} + [FXN]_{total} + K_d \quad (2\text{-}4)$$
$$c = [SDU]_{total}[FXN]_{total}$$

From scheme 2-1, the measured k_{obs} can be expressed as equation 2-5:

$$k_{obs}([SDUF] + [SDU]) = k_{SDU}[SDU] + k^{\infty}_{SDUF}[SDUF] \quad (2\text{-}5)$$

where k_{SDU} is the k_{cat} in the absence of Fxn, and $k_{SDUF}{}^{\infty}$ is the k_{cat} with saturated amounts of FXN. Solving equation 2-5 for k_{obs} yields equation 2-6:

$$k_{obs} = \frac{k_{SDU}([SDU]_{total} - [SDUF]) + k^{\infty}_{SDUF}[SDUF]}{[SDU]_{total}} \quad (2\text{-}6)$$

which can be expressed alternatively using equation 2-7:

$$[SDU]_{total} = [SDU] + [SDUF] \qquad (2\text{-}7)$$

as equation 2-8:

$$k_{obs} = \frac{k_{SDU}([SDU]_{total} - [SDUF]) + k^{\infty}_{SDUF}[SDUF]}{[SDU]_{total}} \qquad (2\text{-}8)$$

In equation 2-8, [SDUF] is calculated as shown by equation 2-4 and a plot of k_{obs} versus FXN concentration allows K_d determination.

Protein Crystallization, Data Collection, and Refinement. Protein crystallization trials were initiated with hanging-drop vapor diffusion methods by mixing 2 μL of protein and 2 μL of reservoir solution, followed by incubation at 22 ^{o}C. Native Fxn at 15 mg/mL in a 50 mM HEPES pH 7.5 buffer that included 50 mM NaCl was crystallized after a one month incubation with 30% 2-methyl-2,4-pentanediol, 0.1 M sodium citrate pH 5.6, and 0.2 M ammonium acetate. The crystals were flash frozen without additional cryoprotection. The W155R variant was concentrated to 25 mg/mL in a 25 mM HEPES pH 7.5 buffer and then crystallized after a three-day incubation with 16% PEG monomethyl ether 2000 and 0.1 M MES pH 6.0. Single crystals were transferred to a cryoprotection solution that included the reservoir solution plus 16% ethylene glycol for ~1 minute and flash frozen in liquid nitrogen. Initial crystallization conditions for the W155A variant at 10 mg/mL in a 50 mM Tris pH 7.5 buffer included 2.0 M ammonium

sulfate, 0.2 M potassium sodium tartrate tetrahydrate, and 0.1 M sodium citrate tribasic dihydrate pH 5.0. These initial crystals were used for microseeding experiments using the same reservoir solution except the ammonium sulfate concentration was lowered to 1.8 M. Crystals of the W155F variant at 10 mg/mL in a 50 mM Tris pH 7.5 buffer were generated after incubation for a few months with a reservoir solution of 0.2 M sodium acetate trihydrate, 0.1 M Tris hydrochloride pH 8.5, and 30% PEG 4000. Single crystals of the W155A and W155F variants were transferred to a cryoprotection solution that included their respective reservoir solutions plus 20% glycerol for ~0.5 minutes and flash frozen in liquid nitrogen. X-ray diffraction data for native Fxn, W155R, and W155F crystals were collected at SSRL beamline 7-1 (ADSC Quantum-315R CCD detector), whereas diffraction data for the W155A variant was collected at APS beamline 23-ID-D (MAR 300 CCD detector). The images were integrated and scaled with iMosflm [139] and Scala of the CCP4 suite [140]. Phases were determined by molecular replacement with Phaser [141], using a previously refined structure of human Fxn [142] as a search model (PDB code: 1EKG). Difference electron density and omit maps were manually fit with the XtalView package [143], and refined in Refmac5 [144] with all of the diffraction data, except for 5% used for R_{free} calculations [145]. PDB codes are 3S4M for native Fxn, 3S5E for W155R, 3S5D for W155A, and 3S5F for W155F.

RESULTS

Diminished Allosteric Activation for Fxn Variants. Previously, human Fxn was shown to bind to the Nfs1, Isd11, Isu2 (SDU) complex and to stimulate sulfide production and Fe-S cluster biosynthesis [96]. Here we tested the ability of purified recombinant I154F and W155R FRDA mutants as well as the related W155A and W155F variants to activate SDU. These biochemical assays were performed using 3 equivalents of each Fxn variant, a cysteine concentration of 0.1 mM, which was chosen to mimic physiological conditions [146], and 10 equivalents of ferrous iron, which further stimulates the rate of sulfide production for the SDUF complex [96].

Table 2-1: The Rate of Fe-S cluster formation and Binding and Rate Constants for Nfs1 Activity with Fxn Variants

Complex	Nfs1 activity (min^{-1})	Fe-S cluster formation (min^{-1})	Fxn K_d (μM)	k_{cat} (min^{-1})	K_M^{Cys} (mM)	k_{cat}/K_M ($M^{-1}s^{-1}$)	Age of onset[1]	Fxn expression[1]
SDU + Fxn[2]	8.25 ± 0.90	12.3 ± 0.4	0.07 ± 0.04	8.5 ± 0.3	0.014 ± 0.002	9800 ± 1700	NA	100
SDU + I154F	4.14 ± 0.20	7.6 ± 0.5	0.40 ± 0.08	6.6 ± 0.4	0.025 ± 0.004	4400 ± 800	16	18
SDU + W155R	0.60 ± 0.07	0.9 ± 0.1	5.49 ± 1.30	1.8 ± 0.1	0.013 ± 0.003	2300 ± 500	4	18
SDU + W155A	0.83 ± 0.28	2.0 ± 0.1	5.85 ± 1.56	3.9 ± 0.2	0.012 ± 0.003	5600 ± 1600	NA	NA
SDU + W155F	2.09 ± 0.51	3.4 ± 0.1	1.52 ± 0.27	4.5 ± 0.1	0.018 ± 0.003	4100 ± 800	NA	NA
SDU[2]	0.65 ± 0.02	0.7 ± 0.1	NA	0.89 ± 0.04	0.59 ± 0.05	25 ± 3	NA	NA

[1]From reference [118]. [2]Kinetic data from reference [96].

Each of the mutants exhibited a lower level of activation than native Fxn (Fxn > I154F > W155F > W155A > W155R), with the W155R mutation being most similar to a SDU sample that lacked Fxn (Fig. 2-1A and Table 2-1). A separate control assay to determine the cysteine concentration at different time points confirmed the Fxn-based activation (Fig. 2-1B). In this assay, cysteine is reacted with ninhydrin and the adduct is quantitated spectrophotometrically.

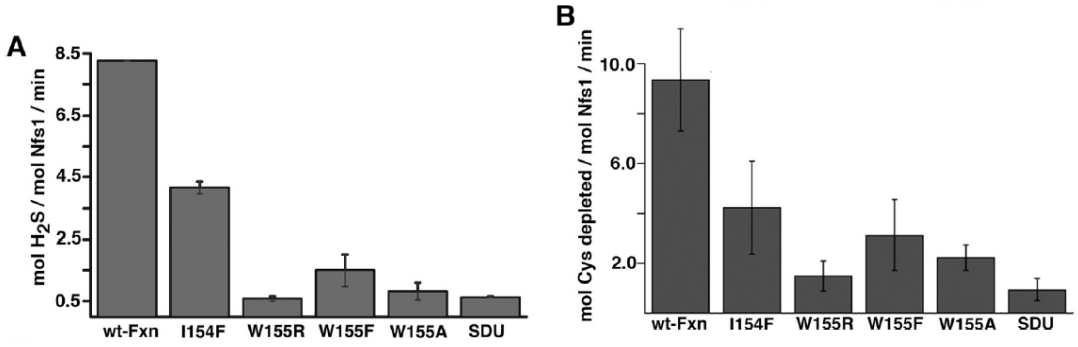

Figure 2-1. Fxn variants show diminished ability to activate cysteine desulfurase activities for the Fe-S assembly complex. Cysteine desulfurase activity was determined spectrophotometrically in the presence of 1 equiv of the Nfs1/Isd11 complex, 3 equiv of each Fxn variant, 3 equiv of Isu2, and 10 equiv of ferrous iron. (A) Activity was determined by converting generated sulfide to methylene blue. (B) Activity was determined by reacting cysteine in solution with ninhydrin. Error bars are for at least three independent measurements.

Diminished Fe-S Cluster Biosynthesis for Fxn Variants. Next, the rate of Fe-S cluster assembly on Isu2 was determined for each Fxn variant by monitoring increases in absorbance at 456 nm [137, 147]. The SDUF complex with native Fxn exhibited an

activity of 12.3 μmol [2Fe-2S] / μmol SDU per minute (Fig. 2-2), which is similar to the 6 μmol [2Fe-2S] / μmol min^{-1} reported previously using the *Thermotoga maritima* NifS enzyme as the sulfur source and slightly different experimental conditions [137]. All Fxn variants displayed lower Fe-S cluster assembly activities than native Fxn, with the W155R variant similar to a sample that lacked Fxn (Fig. 2-2 and Table 2-1). Control assays with 100 μM sulfide rather than cysteine exhibited significantly slower rates than any of the other samples indicating that efficient Fe-S formation was not mediated by sulfide in solution (Fig. 2-2). Overall, the relative activities for the different Fxn variants in the Fe-S cluster biosynthetic assay mirrored their ability to activate the cysteine desulfurase component of the assembly complex (Table 2-1).

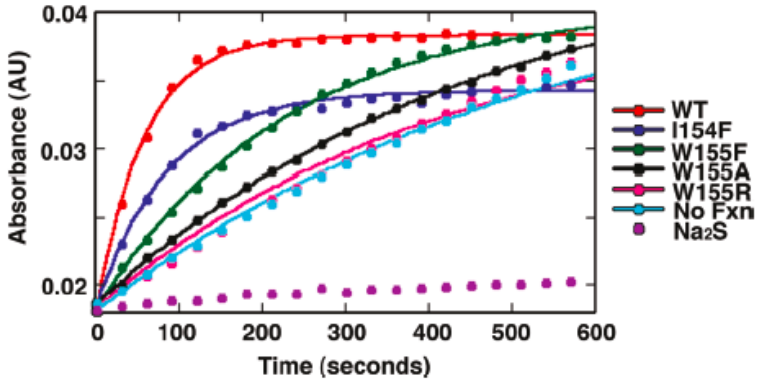

Figure 2-2. Fxn variants exhibit diminished Fe-S cluster assembly activity. Fe-S cluster formation was monitored by an increase in absorbance at 456 nm as a function of time (first 600 s displayed). Assays included Nfs1/Isd11 with 3 equiv of Isu2 and 3 equiv of Fxn variants. The lines through the data are the fits using first-order kinetics. Control samples without Fxn and with Na_2S rather than cysteine are included.

Binding Constants for Fxn Variants. The activation defects of the Fxn variants could be due to defects in variant binding to SDU. We therefore determined binding constants for the Fxn variants by measuring the rates of sulfide production as a function of L-cysteine at different concentrations of added Fxn. The resulting k_{cat} values were plotted against the Fxn concentration and the data were fit as a type II allosteric activator to equation [1] (Fig. 2-3). A K_d of 0.07 μM was determined for native Fxn binding to

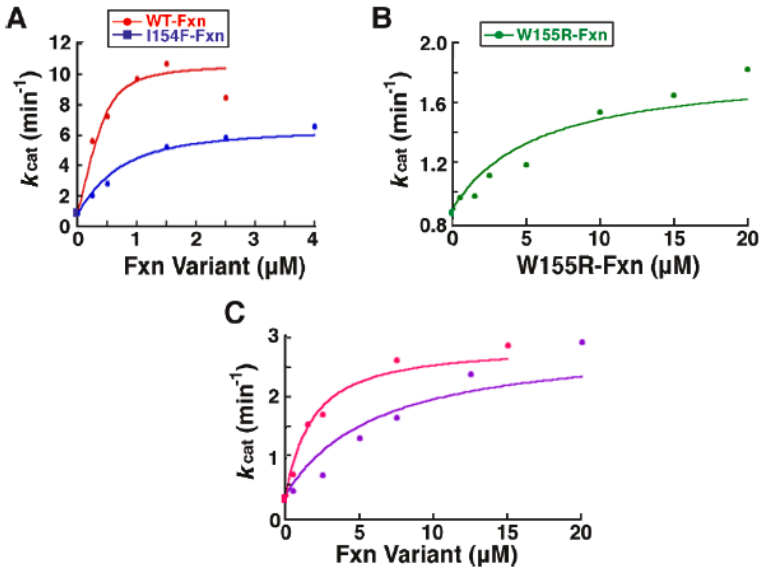

Figure 2-3. Determination of binding constants for Fxn variants. The k_{cat} was determined at different Fxn concentrations. The lines through the data are the fits as a type II allosteric activator to eq 1. The R^2 values are 0.92, 0.98, 0.90, 0.94, and 0.99 for the Fxn, I154F, W155R, W155A, and W155F variants, respectively.

SDU, which was similar to the 0.4 μM binding constant reported for the association of the Fxn homolog CyaY to the IscS/IscU complex [89]; the prokaryotic IscU/IscS complex is analogous to the eukaryotic SDU complex. Each Fxn variant exhibited weaker binding to the SDU complex than native Fxn by a factor of 3 (I154F), 8 (W155F), 28 (W155A), and 30 (W155R) (Fig. 2-3 and Table 2-1).

Kinetic Parameters for Fxn Variants. The Michaelis-Menten kinetic parameters for the cysteine desulfurase reaction were determined for the SDUF complex with the different Fxn variants. To compensate for weaker binding of the different Fxn mutants, cysteine desulfurase activities were measured as a function of added Fxn. The cysteine desulfurase activity maximized, or saturated, after the addition of 3 equivalents of Fxn, 8 equivalents of I154F, 30 equivalents of W155F, 40 equivalents of W155A, and 40 equivalents of W155R (data not shown). Saturating amounts of the different Fxn variants were then added to the SDU complex and the rates of the cysteine desulfurase reaction were measured as a function of the L-cysteine concentration. The four Fxn variants exhibited lower k_{cat} values, but similar K_M values compared to native Fxn (Table 2-1). The most significant change was observed for the W155R variant, which lowered the k_{cat}/K_M by a factor of four.

Crystal Structures of Fxn Variants. High-resolution crystal structures were determined for native Fxn, plus the W155R, W155A, and W155F variants to understand the structural basis for the altered functional properties (Table 2-2). The 1.30 Å resolution native human Fxn structure contains N- and C-terminal α-helices that pack against an antiparallel β-sheet (Fig. 2-4A), as previously described [142, 148]. Overall,

Table 2-2. X-Ray Data Collection and Refinement Statistics

Fxn Variants	WT	W155A	W155R	W155F
Data Collection	SSRL BL7-1	APS BL23-ID-D	SSRL BL7-1	SSRL BL7-1
Wavelength (Å)	0.97945	1.03315	0.97945	0.97945
Space Group	$P2_12_12_1$	C2	$P2_12_12_1$	$P2_1$
Unit cell (Å and °)	42.9, 44.8, 69.0 90^o, 90^o, 90^o	87.5, 32.3, 44.8 90^o, 91.4^o, 90^o	38.9, 49.2, 67.1 90^o, 90^o, 90^o	47.7, 53.1, 48.5 90°, 112.3°, 90°
Resolution (Å)	44.86-1.30	44.797-1.50	39.68-1.31	34.27-1.50
Outer shell (Å)	1.37-1.30	1.58-1.50	1.38-1.31	1.58-1.50
Observations	258690	147672	476216	237470
Unique Observations	33576	20101	31647	35399
Redundancy	7.7	7.3	15.0	6.7
Completeness (%)*	100.0 (100.0)	99.3 (98.6)	99.8 (99.7)	97.7 (97.2)
Mean I/(σI)*	14 (2.6)	12.0 (6.6)	22.2 (5.6)	13.8 (2.2)
R_{sym} (%)*†	8.2 (62.4)	13.8 (48.3)	6.4 (41.3)	7.2 (88.4)
Refinement				
Residues not in model	82-88, 210	82-89	82-87, 209-210	82-84, 210
Solvent atoms	201	101	169	138
Ligand		SO_4	Mg	Mg
R_{work}/R_{free} (%)‡	15.3/18.7	16.9/19.2	15.1/19.7	16.4/21.3
r.m.s.d. bond lengths (Å)	0.032	0.029	0.023	0.023
r.m.s.d. bond angles (°)	2.7	2.6	1.8	1.9
Average B-factor ($Å^2$)				
Protein	16.8	9.9	13.2	22.2
Water	60	34.6	60	40
Ramachandran (%)				
Most favored	93.4	91.5	93.4	94.8
Additional allowed	6.6	8.5	6.6	5.2
Generous	0	0	0	0
Disallowed	0	0	0	0
PDB code	3S4M	3S5D	3S5E	3S5F

*Values in parentheses are the statistics for the highest resolution shell of data

†$R_{sym} = S \mid I_{hkl} - \langle I \rangle \mid / S \langle I \rangle$, where $\langle I \rangle$ is the average individual measurement of I_{hkl}.

‡$R_{work} = (S \mid F_{obs} - F_{calc} \mid) / S \mid F_{obs} \mid$, where F_{obs} and F_{calc} are the observed and calculated structure factors, respectively. R_{free} is calculated the same as R_{work}, but from the data (5%) that were excluded from the refinement.

the structures of the W155A, W155R, and W155F variants displayed very similar backbone conformations with each exhibiting a Cα RMSD of < 0.5 Å compared to native Fxn. The primary structural differences were due to side-chain conformational changes near the mutation sites.

In the native human Fxn structure, electron density maps revealed that the W155 side chain is constrained by a hydrogen bond between the indole ring nitrogen and the side-chain oxygen of Q153 as well as van der Waals interactions with the side chains of R165 and Q148 (Fig. 2-4B). Q153 also forms a hydrogen bond to D167. The position of R165 is reinforced in the crystal structure by a hydrogen bond to residue E101 of a symmetry molecule in the $P2_12_12_1$ space group. Residue Q148 is the first residue in a class I-αRS α-turn [149] that connects β-strands 3 and 4, and its side-chain oxygen forms a hydrogen bond to the nitrogenf the N151 side-chain. Residues I154 and L156 are oriented in the opposite direction on β-strand 4 compared to W155, and make up part of the hydrophobic core of Fxn. Notably, there is a water-filled pocket on the Fxn surface near W155 that is on the opposite face of β-strand 4 from L156 (Figure 2-4B).

The W155A variant, which crystallized in the C2 space group, resulted in minor side chain rearrangements for residues N151 and R165 to form hydrogen bonds with Q153 (Fig. 2-4C). These new hydrogen bonds replaced the hydrogen bond to Q153 that was eliminated due to the loss of the indole ring. Residue Q153 maintained the native Fxn conformation and hydrogen bond to the D167 side-chain. A rearrangement of the N151 side-chain to interact with Q153 resulted in loss of the hydrogen bond between the N151 and Q148 side-chains observed in the native Fxn structure (Fig. 2-4D). Instead,

the Q148 side-chain underwent a slight rearrangement to form a hydrogen bond to the backbone amide of residue 152 (Fig. 2-4C).

The FRDA mutation W155R crystallized in the $P2_12_12_1$ space group and exhibited a significant side-chain reorganization compared to native Fxn (Fig. 2-4D). A minor rearrangement for the side-chains of residues Q148 and N151 resulted in formation of hydrogen bonds with D115 of a symmetry molecule, whereas a conformational change for residue R165 resulted in formation of a salt bridge with E108 of a symmetry molecule (Fig. 2-4E). The FRDA mutant underwent a side-chain rotation for residue 155 to fill a cavity on the surface of Fxn (Fig. 2-4F) and formed hydrogen bonds to N146 and to E108 of a symmetry molecule. A ~1.5 Å translation of the Q148-N151 α-loop between the third and fourth β-strand was also observed (Fig. 2-4D).

The W155F variant crystallized in the $P2_1$ space group with two Fxn molecules in the asymmetric unit. The W155F structure revealed rearrangements to form a hydrogen bond between residues Q153 and N151 (Fig. 2-4G). The electron density for N151 indicated multiple side-chain conformations. A conformational change for residue R165 resulted in the formation of a hydrogen bond to the D139 carbonyl oxygen of an adjacent Fxn molecule (not shown). The W155F side-chain exhibited a rotated conformer compared to native Fxn and the phenylalanine filled the same cavity as the W155R side-chain (Fig. 2-4D and 2-4F). In addition, residue V144 underwent a rearrangement to better pack against the W155F side-chain. Together, these crystal structures showed minor rearrangements outside of the mutation site (Fig. 2-4D) and

provided hints to the correlation between structural changes and the altered Fxn binding affinity and ability to function as an allosteric activator.

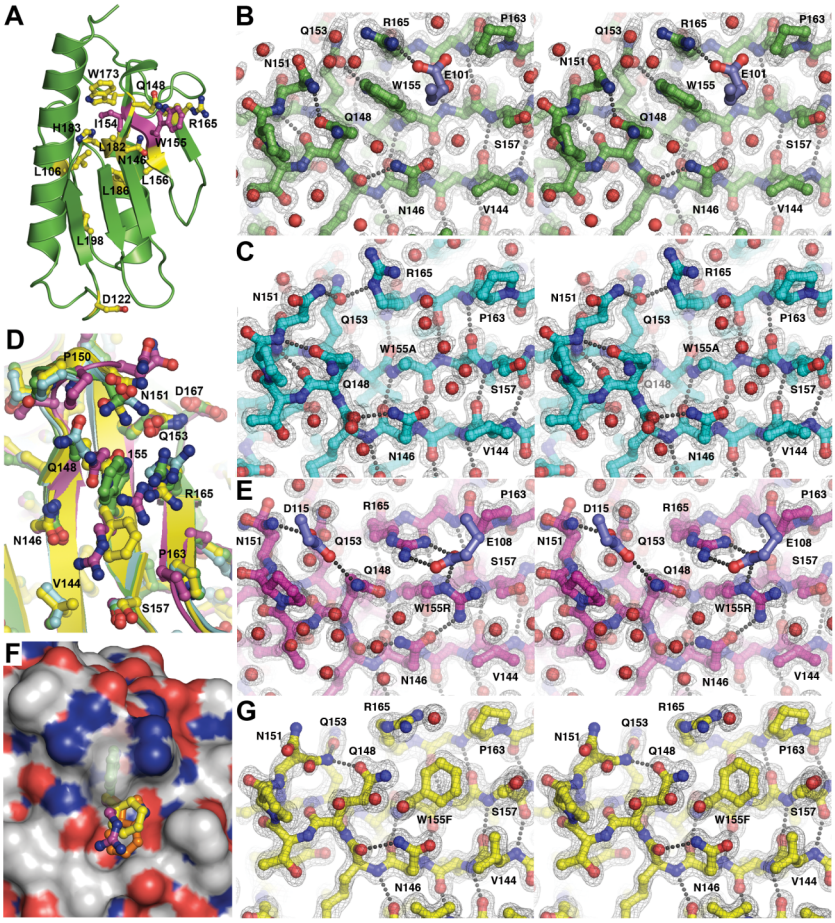

Figure 2-4. Crystallographic structures of Fxn and the W155A, W155R, and W155F variants. (A) FRDA missense mutations (yellow) mapped onto the structure of Fxn. The I154F and W155R mutants are shown in magenta. Stereo images with $2F_o$ - F_c electron density contoured at 1 sigma for (B) Fxn (green), (C) W155A (cyan), (E) W155R (magenta), and (G) W155F (yellow) structures. Symmetry molecules are shown without electron density in lavender. Panel D displays an overlay of native Fxn (green), W155A (cyan), W155R (magenta), and W155F (yellow) structures. Panel F displays a molecular surface of native Fxn along with the side chain for the W155R (magenta), W155F (yellow), and a modeled conformer of W155 (orange). Residue W155 is shown with a semitransparent molecular surface.

DISCUSSION

FXN missense mutations present in compound heterozygous patients were investigated to provide additional insight into the role of Fxn in Fe-S cluster biosynthesis, as these missense mutations likely cause at least partial defects in Fxn function. Here the results showed that the FRDA missense mutations I154F and W155R and the related W155 variants W155A and W155F are impaired allosteric activators both for sulfide formation and for Fe-S cluster biosynthesis by the SDU complex. For the clinical mutations, W155R was much more defective *in vitro* than I154F. The clinical phenotype for patients with the I154F missense mutation and a GAA expansion are indistinguishable from individuals that are homozygous for the GAA repeat expansion [116, 117, 150]. In contrast, individuals with the W155R missense mutation and a GAA expansion exhibit early onset FRDA pathogenesis [113, 151]. Thus, the level of severity of the defects *in vitro* correlates with the clinical phenotypes.

In patients, several lines of evidence suggest that the I154F and W155R missense mutations could be compromised due to low *in vivo* protein levels similar to the effect of GAA repeat expansion [118, 152]: the I154F and W155R mutations *in vitro* have decreased thermodynamic stability and a tendency to precipitate upon iron binding [148, 153, 154]; the I154F mutation may [130] or may not [155] have slower *in vivo* maturation kinetics; and residues I154 and W155 are near K147, which is important for the ubiquitin-based degradation of Fxn [156].

Regardless of any defects in protein concentrations, previous *in vivo* data as well as *in vitro* data presented here suggest that the I154F and W155R additionally possess

biochemical defects. The I154F mutation rescues the lethality of *FXN*$^{-/-}$ mice, but also resulted in a FRDA-like phenotype that included loss of iron-sulfur cluster enzyme activity [157]. The *Saccaharomyces cerevisiae yfh1* alleles *W131A*, *W131F*, and *I130A* (equivalent to human *FXN* variants *W155A*, *W155F*, and *I154A*) also cause cellular growth defects on high-iron media and diminish aconitase activity similar to a deletion of *YFH1* that could be rescued by overexpression of *yfh1-W131F*, but not *yfh1-W131A* or *yfh1-I130A* [78]. The Fxn variants tested here all had equivalent defects in the cysteine desulfurase (Fig. 2-1) and Fe-S cluster assembly (Fig. 2-2) assays relative to native Fxn, ranging from ~2-fold for I154F to ~14-fold for W155R (Table 2-1). As these *in vitro* assays cannot distinguish between mutants that do not bind SDU from those that bind but cannot activate, the relative binding constants of the Fxn variants were determined (the I154F, W155F, W155A, and W155R variants bind 6-, 22-, 84-, and 78-fold weaker than native Fxn, respectively; Table 2-1). Weaker binding is consistent with previous pull down assays that reveal I154F and W155R Fxn variants have diminished binding to Isd11 [85], that the I154F mutant, but not the W155A or W155R variants, is capable of interacting with Nfs1 and IscU [82], and *S. cerevisiae* studies that indicate W131F, but not W131A, is able to interact with Isu1 [78]. In addition, the recombinant Fxn variants exhibited modest 2- to 4-fold decreases in k_{cat}/K_M for cysteine turnover by the SDUF complex (Table 2-1). Weaker or non-productive binding by these mutants would exacerbate any effects of lower protein levels.

The Fxn binding constant and protein concentration in the mitochondria appear appropriately matched for a Fxn role in regulating Fe-S cluster biosynthesis. Although

Fxn levels in human lymphocytes [158, 159], and buccal cells or whole blood [118] are known (in pg Fxn/μg total protein), the concentration of Fxn in mitochondria from any human cell type, to the best of our knowledge, has not been reported. The concentration of Fxn has been estimated in yeast mitochondria to be 0.3 μM [160], based on global expression studies while the concentration of Nfs1 has been estimated to be 0.09 μM [161]. Assuming these concentration estimates are also accurate for human mitochondria, using equation 2-9, then the fraction of Fxn bound in the SDUF complex with a K_d of 0.07 μM (Table 1) would be 78%. The concentration

$$\%SDUF = \frac{[SDUF]}{[SDU]+[SDUF]} = \frac{[SDUF]}{[SDU]_{total}} \times 100\% \qquad 2\text{-}9$$

of Fxn for FRDA patients was determined to be 4-29% [162], 29% [163], 21% [118], 27% [159], and 36% [152] of control Fxn levels. Lowering the Fxn level, for example, to ~25% of the normal Fxn concentration would decrease the activated SDUF fraction from 78% to 38%. Thus, the measured binding constant for native Fxn and the estimated level of Fxn in the mitochondria could explain the loss of Fe-S cluster activity for individuals with the GAA repeat expansion.

Interestingly, our results indicate that the cysteine desulfurase and Fe-S cluster activities appear to be correlated for the Fxn variants. One explanation for this correlation is that the different Fxn variants affect the rate of persulfide cleavage from

Nfs1 and the released sulfide combines with iron (in solution or on Isu2) to form Fe-S clusters (Fig. 2-5A; reactions A1, A2, and A3). Two pieces of data argue against this model. First, a control reaction (Fig. 2-2) using 100 μM sulfide rather than 100 μM cysteine exhibited no significant increase in absorbance in the time frame of the Fe-S assembly assay, inconsistent with scheme A (see reaction A3). Second, the Fe-S assembly activities (determined at 25 °C) are faster than the cysteine desulfurase activities (measured at 37 °C) (Table 2-1). In scheme A, the rate of sulfide production (reaction A2) is required to be faster than that for Fe-S cluster formation (reaction A3). Together this data indicates the correlation for the cysteine desulfurase and Fe-S assembly activities is not due to differences in the ability of Fxn variants to facilitate DTT-induced release of sulfide from Nfs1.

An alternate explanation for this activity correlation is that Fxn induces rapid internal sulfur transfer from Nfs1 to Isu2. In this scheme (Fig. 2-5B), cysteine is converted to alanine by the SDU complex (reaction B1) and the resulting persulfide species on Nfs1 can be cleaved by DTT to produce sulfide (reaction B2). In the presence of Fxn, sulfur is transferred from the mobile loop on Nfs1 to generate a persulfide species on Isu2 (reaction B3). This persulfide species on Isu2 can then be reductively cleaved by DTT (reaction B4) or used for Fe-S cluster assembly (reaction B5). The Fxn-induced rate enhancement for the cysteine desulfurase reaction can be explained if DTT cleavage of the persulfide on Isu2 (reaction B4) is faster than on Nfs1 (reaction B2), and Fxn induces the sulfur transfer from Nfs1 to Isu2 (reaction B3). Moreover, the activity correlation for the Fxn variants could be explained by a common

Fxn-induced sulfur transfer step (reaction B3) that depends on both Fxn binding and an Fxn-induced conformational change. In scheme 5B, internal sulfur transfer from Nfs1 to Isu2, and not DTT-induced sulfur cleavage, is the prerequisite for Fe-S cluster assembly and the rate of Fe-S cluster formation (reaction B5) must be faster than sulfide release from Isu2 (reaction B4); otherwise the added DTT in the Fe-S cluster assay would cleave the persulfide prior to Fe-S cluster formation. We therefore hypothesize that Fxn binding induces or stabilizes a conformational change that facilitates rapid sulfur transfer from Nfs1 to Isu2 for Fe-S cluster formation.

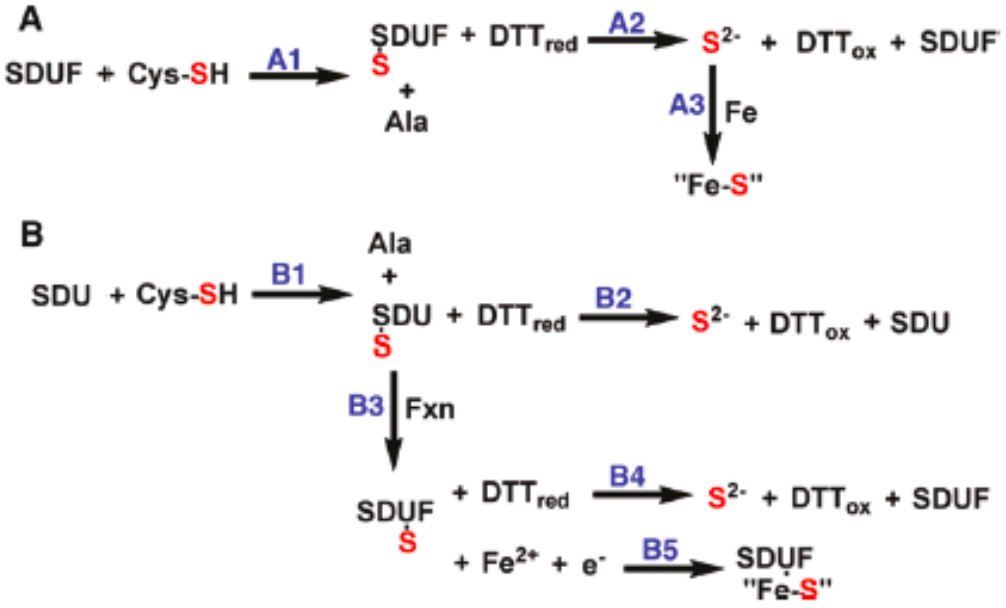

Figure 2-5. Alternate schemes for in vitro sulfide production and Fe-S cluster assembly by the human assembly system. See text for details.

There is currently limited structural data for how Fxn interacts with the other components of the human Fe-S assembly complex. Here a comparison of native Fxn and W155A (Fig. 2-4B, 2-4C and 2-4D) variants revealed very minor structural differences, yet these variants have a 28-fold difference in binding affinity (Table 2-1). Tryptophan residues often participate in protein-protein interfaces through hydrophobic, π-π, and cation-π interactions [164, 165]. W155 is stacked in a positively charged pocket on the surface of Fxn between R165 and Q148 (Fig. 2-4B and 2-4F). The W155A substitution diminishes a W155-dependent protrusion on the surface of Fxn (Fig. 2-4C) that could be part of the Fxn binding interface with the SDU complex. Alternately, W155 could undergo a conformational change, which would have minor steric clashes for an energetically favorable rotomer (Fig. 2-4F; orange), and fill a pocket on the surface of the protein that is on the opposite face of the β-sheet from L144 (Fig. 2-4B), which is occupied by the side-chain of residue 155 in the W155R (Fig. 2-4E) and W155F (Fig 2-4G) structures. This induced-fit model (Fig. 2-6) might provide a protein partner with opportunities for hydrophobic and π-stacking interactions with the indole ring of W155 that are not available in the native structure of Fxn. We hypothesize that the aromatic ring for W155 (and W155F) occupies this surface pocket on Fxn and interacts with a residue of SDU through π-π or cation-π interactions. In our working model, thisinteraction is important for both Fxn binding to the SDU complex and also in favoring a conformation in Isu2 that positions a cysteine residue appropriately for sulfur transfer from Nfs1. The positively charged pocket between Fxn residues R165 and Q148 could form a separate interaction site in the Fe-S assembly complex. This

scenario would explain the relative binding affinities of the W155 variants (Fxn > W155F > W155R, W155A), but requires additional mutational or structural data to confirm this model. This hypothesis is also consistent with NMR studies of the Yfh1 homolog that suggests the Isu1 scaffold protein interacts primarily with residues of the N-terminal α-helix and the first three β-strands [81]. Notably, the equivalent of Fxn W155R for the *E. coli* system, CyaY W61R, also compromises protein function, despite the fact that CyaY is proposed to function as a suppressor rather than an activator of Fe-S cluster biosynthesis [60]. Together these results highlight the importance of W155 in the SDU-Fxn interface and the differing roles of Fxn-like regulators in prokaryotes and eukaryotes that requires further investigation.

In summary, we provide evidence that Fxn functions as a positive allosteric activator that may regulate human Fe-S cluster biosynthesis. The measured Fxn binding constant is similar to the estimated concentration of Fxn in mitochondria [160], which allows changes in Fxn levels to readily switch the Fe-S assembly complex on or off. The greater than three fold variation in protein levels for normal individuals [158] is also consistent with a regulatory role for Fxn. In addition, the lower levels of Fxn in FRDA patients would greatly decrease the amount of activated Fe-S assembly complex and explain the observed loss of activity for Fe-S containing enzymes. *In vitro* assays for the recombinant W155R and I154F variants revealed the loss of binding affinity and ability to function as an activator that explains the more severe disease pathogenesis for W155R compared to I154F. Our data is consistent with a model in which Fxn functions in facilitating sulfur transfer from Nfs1 to Isu2 for cluster assembly. Future studies will be

aimed at understanding the molecular basis for this Fxn-induced sulfur transfer from Nfs1 to Isu2, and providing additional mechanistic details for Fe-S cluster biosynthesis.

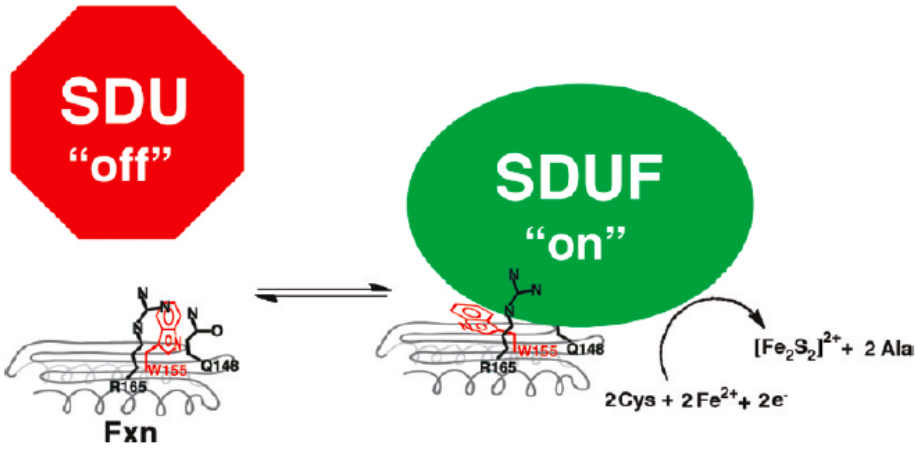

Figure 2-6. Cartoon of induced-fit model for Fxn binding and activating the SDU complex.

CHAPTER III

STRUCTURE-FUNCTION ANALYSIS OF FRIEDREICH'S ATAXIA MUTANTS REVEALS DETERMINANTS OF FXN BINDING AND ACTIVATION OF THE IRON-SULFUR CLUSTER ASSEMBLY COMPLEX*

INTRODUCTION

Friedreich's ataxia (FRDA) is a currently incurable autosomal recessive neurodegenerative disease caused by reduced amounts of the protein frataxin (FXN) [150]. The majority (>95%) of FRD[2]A patients are homozygous for an unstable GAA trinucleotide repeat expansion in the first intron of the *FXN* gene [113]. The number of repeats range from 7 to 40 for normal individuals and from 66 to >1700 for FRDA patients [113, 114], with larger numbers of GAA repeats correlating with lower FXN expression and an earlier age of disease onset [115, 116]. A small fraction of FRDA patients are compound heterozygotes with an expanded GAA repeat affecting one allele and a missense or nonsense mutation affecting the other allele [117]. The loss of FXN results in a complex phenotype that includes increased iron in the mitochondria, deficiencies in Fe-S cluster enzymes, and enhanced sensitivity to oxidative stress [112].

The diminished *in vivo* activity for Fe-S proteins suggests that FXN may have a role in iron-sulfur (Fe-S) cluster assembly [56, 57].

Human Fe-S cluster biosynthesis occurs in the matrix space of the mitochondria and is catalyzed by a four-component core complex composed of NFS1, ISD11, ISCU2, and FXN [96], which is also known as the SDUF complex. The cysteine desulfurase NFS1, which forms a functional complex with ISD11 [121-123], catalyzes the PLP-dependent breakdown of cysteine to alanine and produces a transient persulfide species [2, 124]. The terminal sulfur of this species is transferred to the scaffold protein ISCU2 to build [2Fe-2S] and, possibly, [4Fe-4S] cluster intermediates [120, 147]. Chaperones interact with the scaffold protein and assist in delivering intact Fe-S clusters to their apo targets [97, 125, 126]. Many functions have been proposed for frataxin [166] in Fe-S cluster biosynthesis including a role as an iron chaperone [53, 167] and a role, either positive [96] or negative [60], in regulating cluster assembly.

Molecular level details are lacking for protein-protein interactions between human FXN and the other components of the SDUF Fe-S assembly complex. Recently, a crystal structure was determined for a protein complex between the cysteine desulfurase IscS and scaffold protein IscU for a prokaryotic system [33], and SAXS data suggest a potential binding site for the FXN homolog CyaY on this IscS-IscU complex [33, 89]. The structures of human NFS1, ISD11, and ISCU2 have not been determined. The FXN structure (Fig. 3-1A) has N- and C-terminal α-helices that pack against an antiparallel β-sheet [142, 148, 168].

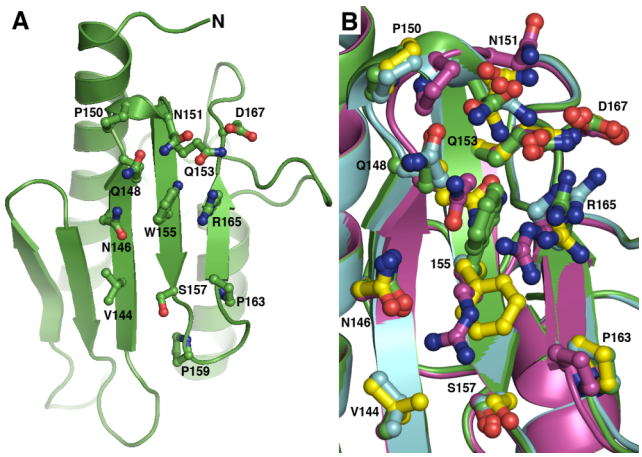

Figure 3-1. Native frataxin structure and overlay with W155R, W155A, and W155F variants. (A) Overall structural fold of FXN with surface exposed residues. (B) Overlay of native FXN (green), W155R (magenta), W155A (cyan), and W155F (yellow) structures.

NMR studies of the *S. cerevisiae* FXN homolog Yfh1 [81] along with pull-down studies for frataxin variants [82-85] indicate residues on the β-sheet such as V144, N146, Q148, Q153, W155, and R165 (human numbering) contribute to FXN binding interactions with other Fe-S assembly proteins. Interestingly, many of these residues are also identified as FRDA missense mutations, including the N146K, Q148R, W155R, and R165C variants [113]. Previous structure-function studies of FXN variants led to a model in which residue W155 undergoes a conformational change to occupy a surface cavity, similar to the position of residue 155 in the W155R and W155F structures (Fig. 3-1B), to interact with and activate the SDU complex for sulfur transfer and Fe-S cluster biosynthesis [169].

Here FRDA clinical variants N146K, Q148R, and R165C, along with related N146A, Q148G, and Q153A variants were constructed to evaluate the FXN binding model [169] and also examine how FRDA missense variants are functionally compromised. The determination of binding constants, functional properties in cysteine desulfurase and Fe-S cluster assembly assays, and crystal structures of five of the variants reveal structure-function correlations and details for how these residues contribute to binding and to the allosteric activation [96] of the human Fe-S assembly complex.

EXPERIMENTAL PROCEDURES

Protein Preparation. The QuikChange method (Stratagene) was used to introduce point mutants (N146A, N146K, Q148G, Q148R, Q153A, and R165C) into a pET11a plasmid containing a codon optimized human *FXN* gene lacking the first 55 amino acids (FXN Δ1-55) [96], and the mutant genes were confirmed by DNA sequencing. The plasmids containing mutant *FXN* genes were individually transformed into *E. coli* strain BL21(DE3) cells and grown at 37 ^{o}C. When the cells reached an OD_{600} of ~0.6, the temperature was reduced to 16 ^{o}C and protein expression was induced with 0.5 mM isopropyl β-D-1-thiogalactopyranoside (IPTG). Cells were harvested 16 hours later and lysed by sonication (Branson Sonifier 450) in 50 mM Tris pH = 7.5. The supernatant was loaded onto an anion exchange column (26/20 POROS 50HQ, Applied Biosystems) and eluted with a linear gradient from 0 to 800 mM NaCl in 50 mM Tris pH 7.5. FXN-containing fractions were collected and further purified on a Sephacryl S100 (26/60, GE Healthcare) size exclusion column equilibrated in 50 mM HEPES, pH 7.5, 150 mM NaCl. The ISCU2 and the NFS1/ISD11 complex were purified as previously described [96]. Protein concentrations for the FXN variants were estimated by their absorbance at 280 nm using an extinction coefficient of 26030 $M^{-1}cm^{-1}$ [170]. Protein concentrations for NFS1/ISD11 and ISCU2 were estimated using extinction coefficients of 42670 and 8250 $M^{-1}cm^{-1}$ [170], respectively.

Cysteine Desulfurase Activity Measurements. Reactions were performed as previously described in a total volume of 800 μL [135, 136, 171]. Briefly, reaction mixtures containing 0.5 μM NFS1/ISD11 (SD), 1.5 μM ISCU2, and 1.5 μM FXN (or

FXN point mutant) were incubated with 10 μM pyridoxal-5'-phosphate (PLP), 2 mM dithiothreitol (DTT), 5 μM $Fe(NH_4)_2(SO_4)_2$, 50 mM Tris pH 8.0, and 250 mM NaCl for 30 minutes in an anaerobic (10~14 ^oC) glovebox [171]. The cysteine desulfurase reaction was initiated with 100 μM L-cysteine at 37 °C and quenched by the addition of 100 μl of 20 mM *N,N*-dimethyl-*p*-phenylenediamine in 7.2 N HCl and 100 μl of 30 mM $FeCl_3$ in 1.2 N HCl. Methylene blue formation was measured at 670 nm after a 20-minute incubation of the quenched reactions at 37 ^oC, and compared to a Na_2S standard curve to quantitate sulfide production. Units are defined as μmol sulfide/μmol SD per minute at 37 ^oC. The rates for the cysteine desulfurase reaction were also examined with increasing amounts of FXN (or FXN variant) to determine the number of equivalents, or the saturating amount, required to maximize the cysteine desulfurase activity.

Fe-S Cluster Formation. Fe-S cluster biosynthetic assays were performed as previously described in a total volume of 200 μL [171]. Assay mixtures containing 24 μM ISCU2 were incubated with 5 mM DTT in 50 mM Tris pH = 8.0 and 250 mM NaCl in an anaerobic glovebox for 1 hour prior to addition of 8 μM SD, 24 μM FXN (or FXN variants), and 200 μM $Fe(NH_4)_2(SO_4)_2$. The reaction was initiated at room temperature with 100 μM cysteine injected from a gas-tight syringe and monitored at 456 nm. The time-dependent increase in absorbance at 456 nm was fit over the first 1000 seconds to first order kinetics using KaleidaGraph (Synergy Software) and the rate was converted to the amount of [2Fe-2S] formed using an extinction coefficient of 9.8 mM^{-1} cm^{-1} [137]. Units are defined as the μmol [2Fe-2S] cluster formed per μmol of SDU complex per minute at 25°C.

Michaelis-Menten Kinetics for Frataxin Variants in SDUF Complex. The saturating amounts of the different FXN variants were added to a standard reaction mixture (0.5 µM SD, 1.5 µM ISCU2, 10 µM PLP, 2 mM DTT, 5 µM $Fe(NH_4)_2(SO_4)_2$, 50 mM Tris pH 8.0, and 250 mM NaCl) and incubated for 30 minutes in an anaerobic glovebox. Cysteine desulfurase activity measurements were initiated with the addition of L-cysteine (0.01 to 1 mM), and the rates were fit to the Michaelis-Menten equation using KaleidaGraph. Reaction rates as a function of cysteine concentration were fit to the Michaelis-Menten equation using Kaleidagraph. The k_{cat} was also measured as a function of FXN concentration and used to determine the FXN binding constant for the SDU complex.

[1]

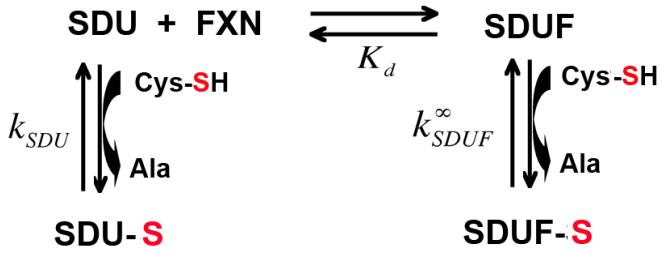

Scheme 3-1.

Using scheme 3-1, a kinetic equation was derived to define the K_d based on the concentrations of SDU, FXN, and SDUF (equation 3-1), where $[SDU]_{total}$ describes the total amount of enzyme partitioned between SDU and SDUF forms of the enzyme.

$$K_d = \frac{([FXN]_{total} - [SDUF])([SDU]_{total} - [SDUF])}{[SDUF]} \quad (3\text{-}1)$$

Multiplying both sides of equation 3-1 by [SDUF] results in equation 3-2:

$$K_d[SDUF] - (([FXN] - [SDUF])([SDU]_{total} - [SDUF])) = 0 \quad (3\text{-}2)$$

which can be rearranged to yield equation 3-3:

$$\begin{aligned} &-[SDUF]^2 + ([SDU]_{total} + [FXN] + K_d)[SDUF] \\ &-(([SDU]_{total})(FXN)) = 0 \end{aligned} \quad (3\text{-}3)$$

Equation 3-3, a quadratic equation, can be solved in terms of [SDUF] to yield equation 3-4:

$$\begin{aligned} [SDUF] &= \frac{b - \sqrt{b^2 - 4ac}}{2} \\ a &= 1 \\ b &= [SDU]_{total} + [FXN]_{total} + K_d \\ c &= [SDU]_{total}[FXN]_{total} \end{aligned} \quad (3\text{-}4)$$

From scheme 3-1, the measured k_{obs} can be expressed as equation 3-5:

$$k_{obs}([SDUF] + [SDU]) = k_{SDU}[SDU] + k^{\infty}_{SDUF}[SDUF] \quad (3\text{-}5)$$

where k_{SDU} is the k_{cat} in the absence of Fxn, and k_{SDUF}^{∞} is the k_{cat} with saturated amounts of FXN. Solving equation 3-5 for k_{obs} yields equation 3-6:

$$k_{obs} = \frac{k_{SDU}([SDU]_{total} - [SDUF]) + k_{SDUF}^{\infty}[SDUF]}{[SDU]_{total}} \qquad (3\text{-}6)$$

which can be expressed alternatively using equation 3-7:

$$[SDU]_{total} = [SDU] + [SDUF] \qquad (3\text{-}7)$$

as equation 3-8:

$$k_{obs} = \frac{k_{SDU}([SDU]_{total} - [SDUF]) + k_{SDUF}^{\infty}[SDUF]}{[SDU]_{total}} \qquad (3\text{-}8)$$

In equation 3-8, [SDUF] is calculated as shown by equation 3-4 and a plot of k_{obs} versus FXN concentration allows K_d determination.

Protein Crystallization, Data Collection, and Refinement. Protein crystallization trials for FXN variants at 10 mg/mL in 50 mM Tris pH = 7.5 were initiated with hanging-drop vapor diffusion methods by mixing 2 μL of protein and 2 μL of reservoir solution, followed by incubation at 22 °C. The N146K variant crystallized in 28% PEG monomethyl ether 2000 and 100 mM Tris pH = 7.0. Initial crystallization conditions for the Q148G and R165C variants included 2.0 M ammonium sulfate and 0.1 M sodium citrate pH = 5.5. These initial crystals were used for microseeding with the same

reservoir solution except the ammonium sulfate concentration was decreased to 1.9 M. Q148R crystallized in 20% PEG 3000 with 0.1 M sodium citrate pH = 5.5. Q153A crystallized in 2.0 M ammonium sulfate, 0.1 M sodium citrate tribasic dihydrate pH = 5.6, and 0.2 M potassium sodium tartrate tetrahydrate. Single crystals for the N146K, Q148G, Q148R, and Q153A variants were transferred to a cryoprotection solution that contained their respective reservoir solutions plus 20% ethylene glycol for ~0.5 minutes and flash frozen in liquid nitrogen. The same procedure was used for crystals for the R165C variant except 20% glycerol was substituted for the ethylene glycol. X-ray diffraction data were collected at SSRL beamline 7-1 (ADSC Quantum-315R CCD detector) for crystals of the Q148R and Q153A variants, SSRL beamline 11-1 (MAR 325 CCD detector) for a Q148G crystal, APS beamline 23-ID-D (MAR 300 CCD detector) for a N146K crystal, and ALS beamline 4.2.2 (NOIR-1 CCD detector) for a R165C crystal. The images were integrated and scaled with iMosflm [139] and Scala of the CCP4 suite [140] . Phases for the variants were determined by molecular replacement using Phaser [141] with a previously refined structure of FXN [142] as a search model (PDB code: 1EKG). Difference electron density and omit maps were manually fit with the XtalView package [143] and refined in Refmac5 [144] with all of the data except the 5% used for R_{free} calculations [145]. PDB codes are 3T3J for N146K, 3T3T for Q148G, 3T3K for Q148R, 3T3L for Q153A, and 3T3X for R165C.

RESULTS

Diminished Activity for Fe-S Assembly Complex Substituted with Frataxin Variants. The N146K, Q148R, and R165C FRDA mutants and related N146A, Q148G, and Q153A FXN variants were heterologously expressed in *E. coli* and purified to >95% homogeneity. These Δ1-55 FXN variants spontaneously truncated N-terminal residues 56-81 [133] to generate the mature form of FXN (residues 82-210; Figure 3-2), and exhibited monomeric behavior on size-exclusion chromatography (data not shown).

Figure 3-2. Sodium dodecyl sulfate−polyacrylamide gel electrophoresis gel that shows the recombinant FXN variants underwent spontaneous cleavage during purification.

The six variants were tested for their ability to stimulate cysteine desulfurase and Fe-S assembly activities of the reconstituted Fe-S assembly complex composed of NFS1, ISD11, and ISCU2 (SDU). Equivalent amounts of the FXN variants were included in these assays to estimate the *in vivo* functional consequences of the point mutants (assuming similar protein levels), whereas 100 μM L-cysteine was used to mimic cellular substrate concentrations [171]. All six FXN variants exhibited decreased activity compared to native FXN (Fig. 3-3) and followed the trend FXN > N146A > Q148G > Q148R ~ R165C ~ N146K > Q153A > SDU (Table 3-1).

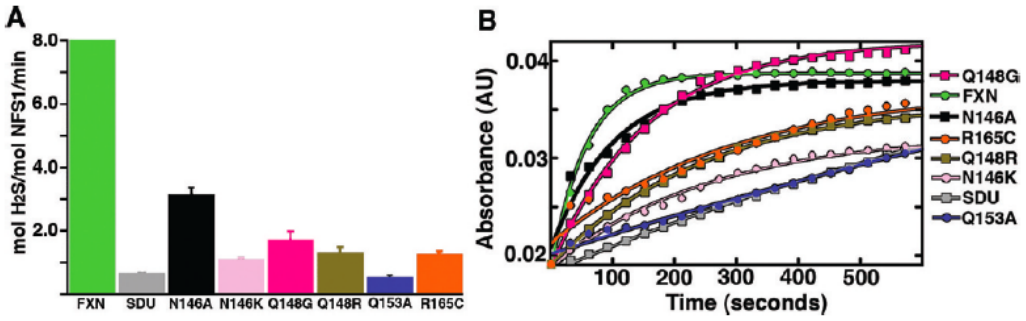

Figure 3-3. Frataxin variants are less able to activate cysteine desulfurase activity and Fe−S cluster biosynthesis. (A) Sulfide production was assessed in the presence of 1 equiv of the NFS1−ISD11 complex, 3 equiv of each FXN variant, 3 equiv of ISCU2, and 10 equiv of ferrous iron. Error bars are for three independent measurements. (B) Fe−S cluster formation was monitored by an increase in absorbance at 456 nm as a function of time. Assays included the NFS1−ISD11 complex with 3 equiv of ISCU2 and 3 equiv of FXN variants. The lines through the data are the fits using first-order kinetics.

These activities are significantly higher than previous control assays with 100 μM sulfide rather than cysteine [169], which indicated that efficient Fe-S formation was not mediated by sulfide in solution. Notably, the relative activities of the FRDA variants N146K, Q148R, and R165C were similar in the cysteine desulfurase and Fe-S assembly assays.

Table 3-1 Summary of Activity, Binding, and Kinetic Parameters for FXN Variants

Complex	FXN Class[1]	NFS1 activity (U/min^{-1})	Fe-S formation (U/min^{-1})	FXN K_d (μM)	k_{cat} (min^{-1})	K_M^{Cys} (mM)	k_{cat}/K_M ($M^{-1}s^{-1}$)
SDU + FXN		8.25 ± 0.90	12.3 ± 0.4	0.07 ± 0.04	8.5 ± 0.3	0.014 ± 0.002	9800 ± 1700
SDU + N146A	IV	3.13 ± 0.24	10.1± 1.1	1.14 ± 0.26	5.8 ± 0.2	0.021 ± 0.004	4700 ± 1000
SDU + N146K	II	1.08 ± 0.08	2.8 ± 0.3	5.96 ± 1.60	4.0 ± 0.1	0.019 ± 0.004	3500 ± 700
SDU + Q148G	IV	1.71 ± 0.27	4.7 ± 0.1	1.93 ± 0.30	4.0 ± 0.1	0.009 ± 0.002	7000 ± 1600
SDU + Q148R	III	1.29 ± 0.20	2.9 ± 0.2	0.72 ± 0.15	2.0 ± 0.1	0.019 ± 0.004	1800 ± 300
SDU + Q153A	I	0.52 ± 0.08	0.8 ± 0.2	7.22 ± 2.70	2.4 ± 0.1	0.014 ± 0.003	2900 ± 600
SDU + R165C	II	1.26 ± 0.10	4.1 ± 0.9	10.12 ± 2.60	8.1 ± 0.1	0.012 ± 0.001	11000 ± 1400
SDU + I154F	IV	4.14 ± 0.20	7.6 ± 0.5	0.40 ± 0.08	6.6 ± 0.4	0.025 ± 0.004	4400 ± 800
SDU + W155R	I	0.60 ± 0.07	0.9 ± 0.1	5.49 ± 1.30	1.8 ± 0.1	0.013 ± 0.003	2300 ± 500
SDU + W155A	II	0.83 ± 0.28	2.0 ± 0.1	5.85 ± 1.56	3.9 ± 0.2	0.012 ± 0.003	5600 ± 1600
SDU + W155F	IV	2.09 ± 0.51	3.4 ± 0.1	1.52 ± 0.27	4.5 ± 0.1	0.018 ± 0.003	4100 ± 800
SDU		0.65 ± 0.02	0.7 ± 0.1	NA	0.89 ± 0.04	0.59 ± 0.05	25 ± 3

[1]FXN classes are defined in the Discussion.

Binding Affinity of Frataxin Variants to the SDU Complex. Next, binding constants for the variants were determined to explore if the lower activation levels were due to weaker binding of the FXN variants to the SDU complex. The rates of sulfide production were determined as a function of L-cysteine at different concentrations of added FXN, as previously described for the I154F and W155 variants [169]. The resulting *kcat* values were plotted against the FXN concentration and the data were fit as a type II allosteric activator to equation [1] (Fig. 3-4). Previously, a *K*d of 0.07 μM was determined for native FXN binding to the SDU complex [169]. Here binding constants range from 0.72 μM to 10.12 μM for the six FXN variants (Table 3-1). The weaker binding for the N146K compared to the N146A variant is consistent with previous pull-down experiments [82]. Interestingly, the Q148R and R165C variants, which have similar ability to activate the Fe-S assembly complex under standard conditions (Fig.3-3), exhibited the tightest and weakest binding of the six variants, respectively.

Kinetic Parameters for Assembly Complexes Substituted with Frataxin Variants. The Michaelis-Menten kinetic parameters for the cysteine desulfurase reaction were determined for the SDUF complex with the different FXN variants under conditions in which each FXN variant was saturating to compensate for weaker binding. Cysteine desulfurase activity was measured as a function of added FXN variant to determine the amount required to saturate FXN binding to the SDU complex. The activity maximized by the addition of 3 equiv of wild-type FXN, 10 equiv of Q148R, 30 equiv of N146A, 50 equiv of Q148G and N146K, 90 equiv of R165C, or 100 equiv of Q153A (data not shown). Saturating amounts of the different FXN variants were then added to the SDU

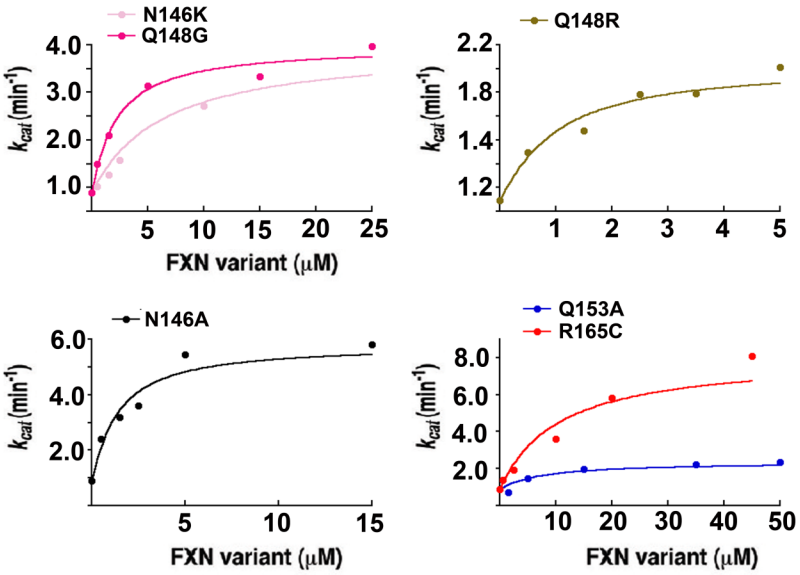

Figure 3-4. Determination of binding constants for FXN variants. k_{cat} was determined at different FXN concentrations. The lines through the data are the fits as a type II allosteric activator to eq 1. The R^2 values are 0.94, 0.98, 0.95, 0.95, 0.90, and 0.94 for the N146K, Q148G, Q148R, N146A, Q153A, and R165C variants, respectively.

complex and the rates of the cysteine desulfurase reaction were measured as a function of the L-cysteine concentration. The R165C variant, which is the weakest binding of the six variants, exhibited activation of the SDU complex (under saturating FXN conditions) that was equivalent to native FXN (Table 3-1). In contrast, the tightest binding variant, Q148R, exhibited the lowest k_{cat}/K_M, which is lower than native FXN by a factor of ~5.

Crystal Structures for Frataxin Variants. High-resolution crystal structures (Table 3-2) were determined for the N146K, Q148G, Q148R, Q153A, and R165C

variants to understand the structural basis for altered functional properties (Table 3-1). Previously, residue W155 was shown to contribute to binding interactions with partner proteins and also be important for frataxin function in Fe-S cluster biosynthesis [82, 83, 85, 169]. The orientation of the W155 side chain is constrained by a hydrogen bond between the indole ring nitrogen and the side-chain oxygen of Q153, as well as van der Waals interactions with the side chains of N146, Q148, and R165 (Fig. 3-1A). In addition, the N146 side-chain nitrogen atom forms a hydrogen bond to the backbone carbonyl of K147; Q148, whose side-chain oxygen forms a hydrogen bond to N151, is the first residue in a α-turn between β-strands 3 and 4; and R165 exhibits no intramolecular hydrogen bonds to other FXN residues, but is appropriately positioned to form a cation-π interaction with W155.

The N146K FRDA missense mutant crystallized in the $P2_1$ space group, the crystals diffracted to 1.70 Å resolution (Table 3-2), and the refined structure exhibited similar backbone (Cα RMSD 0.30 Å) and side-chain conformations to native FXN. In the N146K structure (Fig. 3-5A), the W155 side chain stacked between the Q148 and R165 side chains, similar to native FXN, and exhibited a similar hydrogen bond pattern to FXN (Fig. 3-5B). Changes due to the N146K mutation include the loss of a hydrogen bond between the side-chain of residue 146 and the carbonyl oxygen of K147 and localized alteration in the electrostatic and molecular surface of FXN.

The Q148R FRDA missense mutation crystallized in the $P2_12_12_1$ space group (Table 2), and the 1.24 Å electron density maps (Fig. 3-5C) revealed very minor structural rearrangements relative to native FXN (Cα RMSD 0.44 Å). The position of

Table 3-2: X-ray Data Collection and Refinement Statistics

FXN Variants	N146K	Q148G	Q148R	Q153A	R165C
Data Collection	APS 23-ID-D	SSRL BL11-1	SSRL BL7-1	SSRL BL7-1	ALS BL4-2-2
Wavelength (Å)	1.0331	1.0971	0.9794	0.9794	1.0000
Space Group	$P2_1$	$P2_1$	$P2_12_12_1$	C2	C2
Unit cell (Å and °)	30.47, 45.82, 38.9 β = 97.36°	46.41, 68.56, 89.97 β = 93.23°	42.53, 45.31, 69.12	87.44, 32.46, 45.17 β = 91.87°	86.02, 32,12, 92.08 β = 91.16°
Molecules/ASU	1	4	1	1	2
Resolution (Å)	30.33-1.70	26.19-1.38	28.29-1.24	25.37-1.15	19.5-1.57
Outer shell (Å)	1.79-1.70	1.45-1.38	1.31-1.24	1.21-1.15	4.96-1.57
Observations	84900	787564	517442	318181	128770
Unique Observations	11654	111516	38275	45196	35106
Redundancy	7.3	7.1	13.5	7.0	3.7
Completeness (%)*	98.9 (100)	96.7 (94.7)	99.6 (99.2)	99.4 (99.7)	98.8 (98.0)
Mean I/(σI)*	20.2 (10.1)	14.5 (2.3)	27.2 (9.4)	19.0 (4.5)	11.5 (4.3)
R_{sym} (%)*†	5.9 (13.9)	7.0 (84.7)	5.6 (28.5)	6.0 (40.1)	6.2 (33.1)
Refinement					
Residues not in model	82-85	82-88	82-88	82-89	82-89
Solvent atoms	66	352	127	95	133
R_{work}/R_{free} (%)‡	21.4/24.5	19.9/22.7	18.3/19.7	16.7/17.9	21.6/25.2
r.m.s.d. bond lengths (Å)	0.008	0.032	0.030	0.030	0.025
r.m.s.d. bond angles (°)	1.2	2.5	2.2	2.4	2.3
Ramachandran (%)					
Most favored	96.2	94.7	95.3	94.3	92.0
Additional allowed	3.8	5.3	4.7	5.7	8.0
Generous	0	0	0	0	0
Disallowed	0	0	0	0	0
PDB code	3T3J	3T3T	3T3K	3T3L	3T3X

*Values in parentheses are the statistics for the highest resolution shell of data

†$R_{sym} = S \mid I_{hkl} - \langle I \rangle \mid / S \langle I \rangle$, where $\langle I \rangle$ is the average individual measurement of I_{hkl}.

‡$R_{work} = (S \mid F_{obs} - F_{calc} \mid) / S \mid F_{obs} \mid$, where F_{obs} and F_{calc} are the observed and calculated structure factors, respectively. R_{free} is calculated the same as R_{work}, but from the data (5%) that were excluded from the refinement.

W155, R165, and the backbone conformation of the α-turn initiated by residue 148 were not altered by the Q148R substitution (Fig. 3-5D). The electron density revealed that residue Q148R, which provided part of the pocket for W155 in the native FXN structure (Fig. 3-1A), was in position to provide cation-π stabilization for the W155 side chain. In addition, residue N151 rearranged to form a hydrogen bond with the Q153, rather than Q148, side-chain. Although the N146K and Q148R variants incorporate a positively charged residue, the structures reveal minor overall changes to the binding surface of FXN.

The Q148 residue was also mutated to a glycine and the purified Q148G protein crystallized in the $P2_1$ space group with four molecules in the asymmetric unit (Table 3-2). The 1.38 Å resolution electron density maps (Fig. 3-5E) revealed a rearrangement of the α-turn (between β-strands 3 and 4) that positioned P150 to pack against a rotated W155 side-chain. Overlaying the four independent molecules in the asymmetric unit revealed one conformation for W155, but two conformations for N146 and R165 (Fig. 3-5F). The electron density for two of the four Q148G molecules in the asymmetric unit indicated R165 occupies two alternate side-chain conformations, with one of these conformers positioned to hydrogen bond to the N151 and Q153 side-chains (Fig. 3-5E). Minor rearrangements were also observed for residues S157 and P163.

The Q153 side-chain, which formed a hydrogen bond to W155 in the native FXN structure (Fig. 3-1A), was mutated to an alanine and the recombinant protein crystallized in the C2 space group (Table 3-2). The 1.15 Å resolution electron density maps (Fig. 3-5G) revealed substantial rearrangements near the mutation site. Residue N151

underwent a conformational change to replace the hydrogen bond to W155 lost by the Q153A substitution (Fig. 3-5H). The R165 side-chain exhibited two conformations, which would be sterically forbidden in the native FXN structure, to form hydrogen bonds with the backbone carbonyl of N151 and to the side-chain of D167. This new position for R165 allowed a rearrangement of the W155 side-chain.

The FRDA missense mutation R165C crystallized in the C2 space group with two molecules in the asymmetric unit (Table 3-2). The 1.57 Å resolution electron density maps revealed one molecule was significantly better ordered and was modeled with the R165C side-chain in three distinct conformations, two conformations for the N146 side-chain, and multiple positions for the W155 indole ring (Fig. 3-5I). Additional electron density near one of the alternate conformations of W155 was due to a symmetry molecule (not shown). A third conformation for the W155 side-chain was found in the other molecule in the asymmetric unit that was oriented similar to that of native FXN (Fig. 3-5J). Together these crystal structures coupled to kinetic analysis help define the determinants for FXN binding and function as an allosteric activator for the SDU complex.

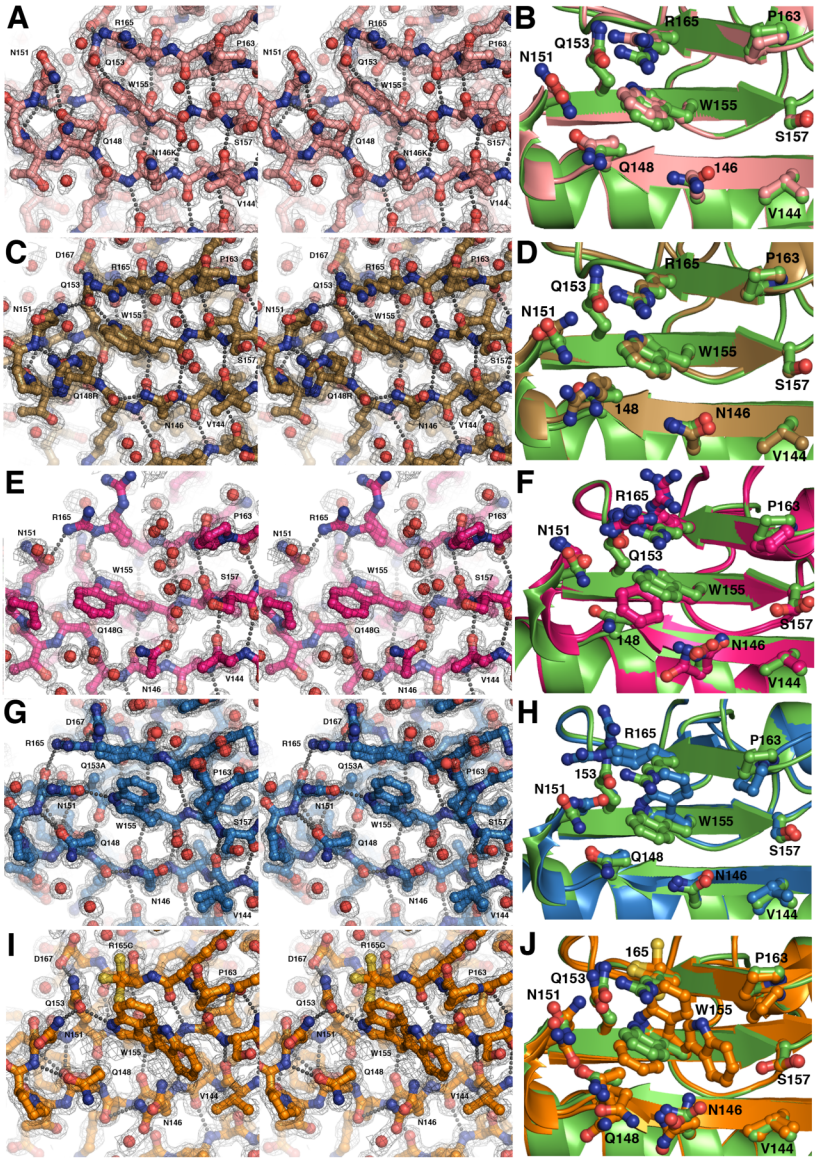

Figure 3-5. Crystal structures of the N146K, Q148R, Q148G, Q153A, and R165C variants. Stereo images with 2*Fo* − *Fc* electron density contoured at 1σ for (A) N146K, (C) Q148R, (E) Q148G, G (Q153A), and (I) R165C structures. Panels B, D, H show overlays of N146K (salmon), Q148R (sand), and Q153A (blue) with native FXN (green), respectively. Panels F and J show overlays of the four independent molecules of Q148G (hot pink) and two independent molecules of R165C (orange) overlaid with native FXN (green), respectively.

DISCUSSION

Previously, FXN missense I154F and W155R mutations present in compound heterozygous patients were shown to exhibit binding and activation defects in cysteine desulfurase and Fe-S cluster biosynthesis assays [169]. The magnitude of these defects appeared to correlate with the clinical phenotype and suggested that biochemical characterization of FRDA mutants may provide mechanistic insight and details into how FXN variants are functionally compromised. Based on these results, a model was proposed in which FXN residue W155 undergoes a conformational change to fill an empty pocket (between W155 and S157; see Fig. 3-1A) on the surface of the protein and position W155 for binding and activation of the SDU complex [169]. Here additional FRDA missense mutations N146K, Q148R, and R165C, along with related N146A, Q148G, and Q153A variants were evaluated to further understand biochemical defects in FRDA missense mutations and test this initial binding and activation model. Interestingly, the three FRDA missense mutants exhibited similar deficiencies in cysteine desulfurase and Fe-S cluster formation activities (Table 3-1), but the causes of these activation defects were dramatically different. The R165C variant exhibited a higher k_{cat}/K_M than native FXN but weak binding to the SDU complex, whereas the Q148R variant exhibited a much lower k_{cat}/K_M and only a modest binding deficiency. Crystal structures for five of these FXN variants were determined to provide insight into how these mutations result in changes in binding and activation of the SDU complex.

Biochemical data for the FRDA missense and related FXN variants presented here and in a previous manuscript [169] suggest four general classes of FXN variants,

each of which contains FRDA missense mutations. Class I variants (Q153A and W155R) displayed weak binding (at least 78-fold more weakly than FXN) and substantially reduced activation of the cysteine desulfurase activity (k_{cat} less than 30% of FXN). Class II variants (R165C, N146K, and W155A) displayed weak binding but possessed catalysis that was only mildly reduced (k_{cat} more than 45% of FXN). Class III variants (Q148R) had only modest defects in binding (10-fold weaker than FXN) but substantially reduced catalysis (k_{cat} less than 25% of FXN). Class IV variants (W155F, N146A, Q148G, and I154F) had only modest defects in both binding and activation of the SDU complex.

The crystal structures for the Class I and II variants that bound at least 78-fold more weakly to the SDU complex (Fig. 3-6A; R165C < Q153A < W155R < N146K < W155A) suggested that two factors contributed to the binding defects. First, the weakest binding variant, R165C, lacks the guanidinium group of the R165 side-chain, the Q153A variant exhibits two conformation for R165 that are distinct from that of native FXN and are stabilized by hydrogen bond interactions with D167 and N151, and the W155A variant underwent a rearrangement of the R165 side-chain to hydrogen bond to Q153 (Fig. 3-6A). In these mutants, the guanidinium group of the R165 side-chain is not available or less able to interact with partner proteins. Second, the W155R and N146K structures (Fig. 3-6A) revealed the presence of positively charged residues that are adjacent to a surface pocket near S157 that may lower the FXN binding affinity to SDU. In contrast, the available crystal structures of the Class III and IV variants that bind only 6-28 fold more weakly than wild-type (Q148G < W155F < N146A < Q148R < I154F)

revealed that the R165 side chain was positioned similar to native FXN and that these variants lacked a positively charged residue near the surface pocket (Fig. 3-6B). Together, these structure-function correlations suggest that FXN binding to the SDU complex is stabilized by the native FXN conformation of R165, whereas a positive charge near a surface pocket destabilizes the complex.

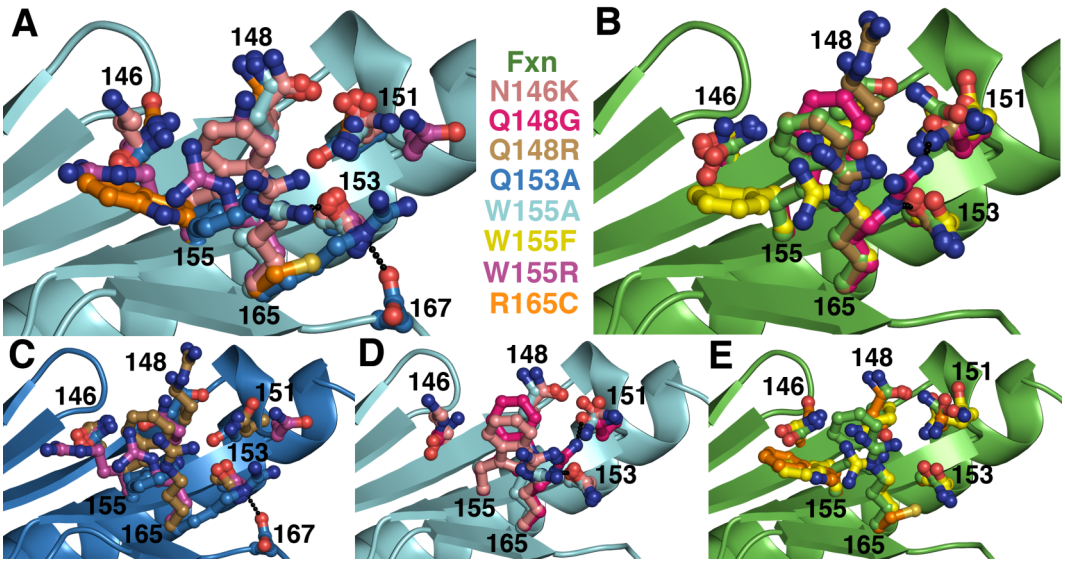

Figure 3-6. Grouping of FXN variant structures by their ability to bind and activate the SDU complex. Structural overlay for (A) class I (Q153A and W155R) and II (R165C, N146K, and W155A) variants that bind the SDU complex at least 78-fold more weakly than FXN, (B) class III (Q148R) and IV (W155F and Q148G) variants that bind the SDU complex 10-22 -fold more weakly than FXN, (C) class I (Q153A and W155R) and class III (Q148R) variants that have k_{cat} values that are <30% of that of FXN, (D) class II (N146K and W155A) and IV (Q148G) variants that have k_{cat} values that are between 45 and 50% of that of FXN, and (E) class II (R165C) and IV (W155F) variants that exhibit *k*cat values that are >50% of that of FXN. The color scheme is as follows: green for FXN, salmon for N146K, hot pink for Q148G, sand for Q148R, sky blue for Q153A, cyan for W155A, yellow for W155F, magenta for W155R, and orange for R165C.

Structure-function properties were also examined for the different FXN variants to understand the determinants for stimulating the cysteine desulfurase reaction of the SDU complex. Crystal structures of Class I and III variants, which possess substantially reduced activation of the cysteine desulfurase reaction (W155R < Q148R < Q153A; Fig 3-6C), revealed that these variants may lose the ability of residue 155 to occupy the surface pocket and activate the SDU complex. The W155R variant substitutes the tryptophan with a positively charged residue; the Q148R mutant stabilized W155 in the native conformation through a cation-π interaction, and the Q153A variant stabilized an alternate conformation of the W155 side chain (Fig. 3-6C). The crystal structures of Class II and IV variants, which possess only moderately reduced activation, reveal that the relative effects of the variants W155A < N146K < Q148G < W155F < N146A < I154F < R165C, can be also linked to their effects on W155 and adjacent residues. The Class II and IV variants with weaker activation (k_{cat} between 45-50% of FXN) include the W155A variant, which lacks the indole ring of residue 155, the N146K variant, which incorporates a positive charge near the proposed W155 interaction site, and Q148G that stabilizes an alternate conformation for the W155 side chain (Fig. 3-6D). The Class II and IV variants with the highest k_{cat} (W155F and R165C) placed an aromatic ring in the surface cavity (Fig. 3-6E). Together this data is consistent with a model for efficient catalysis being mediated when W155 occupies a pocket on the surface of FXN for interactions with partner proteins, possibly through π-π or cation-π interactions, that are inhibited by positive charge.

A general correlation was observed for a log-log plot of the binding constants for the different FXN variants (K_d) and the k_{cat} values for the cysteine desulfurase reaction (Fig. 3-7). Such a correlation has been observed for other systems [172-174], and suggests these FXN variants are altering molecular interactions important for binding to the SDU complex that are also important for stimulating the cysteine desulfurase activity. The variants above the line have larger binding than activation deficiencies, whereas those below the line exhibit larger activation than binding defects. A binding defect outlier, R165C, has 149-fold weaker binding to the SDU complex, yet exhibits a similar k_{cat} compared to native FXN. We hypothesize these properties of R165C are due to the loss of the guanidinium group of the R165 side-chain, which primarily contributes to binding, and the positioning of W155 in a pocket for interactions with SDU (Fig. 3-7E). An activation defect outlier, Q148R, exhibits a modest decrease in binding affinity, but is one of the most compromised variants in its ability to stimulate the cysteine desulfurase activity of the SDU complex. We hypothesize that these properties of Q148R are due to the near native conformation of R165, which contributes to the binding affinity, and the introduced Q148R positive charge, which provides cation-π interactions to lock W155 in the native FXN conformation and inhibit the proposed conformational change that places the indole ring in a surface pocket for interactions with the SDU complex.

The three FRDA missense mutations R165C, N146K, and Q148R investigated here were equally compromised in the *in vitro* cysteine desulfurase and Fe-S cluster assembly assays. Initially, one might predict that the clinical consequences of these

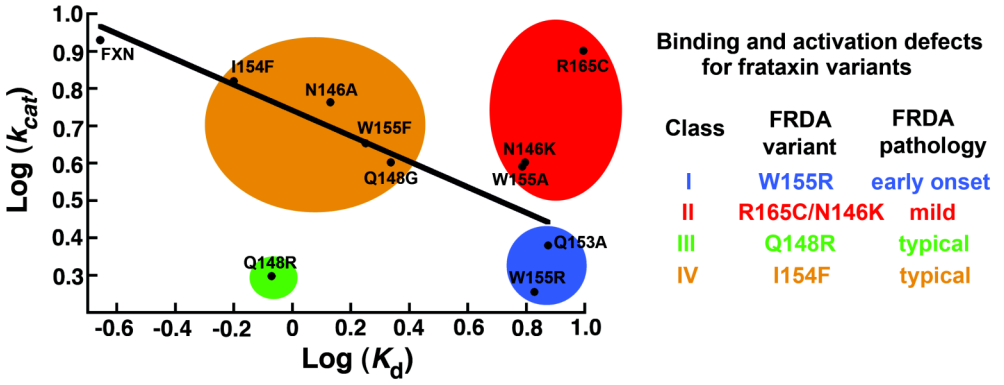

Figure 3-7. Correlation between the binding constant and the *k*cat of the cysteine desulfurase reaction for the SDUF complex with different FXN variants. The different classes of variants are highlighted in blue (class I), red (class II), green (class III), and orange (class IV).

variants would then be similar. However, the situation is more complicated in FRDA patients with missense mutations, as these patients express both a native FXN from a GAA expanded allele along with the mutant FXN from the missense allele. These two forms of FXN would compete for binding to the SDU complex *in vivo*. The 3-5 fold loss in catalytic efficiency observed for many of the FRDA missense mutants (Table 3-1) is on the order of the 3-5 fold loss in FXN levels that appears to be sufficient to develop a FRDA phenotype for patients with two GAA repeat alleles [118, 152, 159, 162, 163]. Therefore, Class III FXN missense mutants such as Q148R that have a ~5-fold loss in catalytic efficiency but binds relatively well might be expected to be more detrimental than Class II missense mutants such as R165C or N146K that bind weakly

but have mild, if any, catalytic deficiencies. Consistent with this idea, patients with the Class III mutation Q148R exhibit typical FRDA pathogenesis, while patients with Class II mutants R165C and N146K mutations have unusually mild disease progression [113]. Notably, the Class I mutant W155R, which is characterized by both weak binding and low activity, is classified as an early onset FRDA missense mutant, whereas the Class IV missense mutant I154F with modest binding and activation defects has typical disease progression [113].

In summary, the results presented here allow an initial classification of FRDA and related FXN variants based on their ability to bind to the SDU complex and stimulate the cysteine desulfurase reaction. The biochemical properties for these different classes of FXN variants may help explain the clinical outcomes for FRDA missense mutations that range from early onset to atypically mild [113]. From a mechanistic perspective, it is difficult to understand how FXN functions as an activator without molecular level structural data for the SDUF complex. Here we start to define the contributions of individual FXN residues in the binding and activation of the SDU complex that may lead to the design of biomimetics that can therapeutically replace FXN function. Future experiments will be aimed at testing and refining this model for FXN activation by defining the role of specific residues in the SDU complex that are important for sulfur transfer from NFS1 to ISCU2 and Fe-S cluster assembly.

CHAPTER IV

FRATAXIN DEPENDENT SULFUR TRANSFER MECHANISM FOR THE HUMAN FE-S CLUSTER BIOSYNTHETIC COMPLEX

INTRODUCTION

Sulfur is a critical element for all life forms and is found in a variety of protein cofactors including molybdopterins, lipoic acid, thiamin, biotin, and iron-sulfur clusters. Even though these cofactors are functionally well understood, mechanistic details are just emerging for how sulfur is incorporated into these biomolecules [175, 176]. A common early step for these pathways is the cysteine desulfurase catalyzed degradation of cysteine to alanine and the generation of a protein-bound persulfide species. This activated sulfur is reductively cleaved by distinct acceptor proteins for the biosynthesis of sulfur-containing cofactors and modification of tRNA [175]. Redox agents such as cysteine and DTT (*in vitro*) can also release the terminal sulfur of the persulfide in a rate-limiting step that produces hydrogen sulfide [30, 177].

Bacteria, archaea, and eukaryotic organelles use one or more of the ISC, NIF, or SUF systems for the biosynthesis of Fe-S clusters. Although still debated, many researchers favor a "sulfur-first" mechanism in which sulfur is transferred from a persulfide species on a cysteine desulfurase to a cysteine residue on an acceptor protein. Indeed, radiolabeling and mass spectrometry experiments have been used to track interprotein persulfide-base sulfur transfer from a cysteine desulfurase to an acceptor protein for bacterial ISC [102, 103, 110] and SUF systems [104, 178-181]. In one of the

better studied systems, the ISC assembly system of *Escherichia coli (E. coli)*, the cysteine desulfurase IscS uses a PLP cofactor to assist in cleaving the sulfur-carbon bond of L-cysteine, generates a persulfide intermediate on residue C328, and then transfers the terminal sulfur of this persulfide species to the scaffold protein IscU for synthesis of Fe-S clusters [182-184]. A recent IscS-IscU crystal structure revealed that residue C328, which is located on a highly flexible loop, appears to sample a distance of ~30 Å by interacting with both the IscS substrate-PLP adduct and also conserved cysteine residues on IscU [33]. The IscU cysteine residues C37 and C63 are positioned on loops at the IscS-IscU interface and proposed to function in a sulfur acceptor role for Fe-S cluster biosynthesis [33]. In contrast, C106 is somewhat buried on the C-terminal helix of IscU (Figure 4-1). Although the functional significance for sulfur transfer is unclear, disulfide crosslinks between IscS C328 and IscU residues C37 [185] and C63 [109] confirm that these IscU residues can interact with the flexible loop of IscS.

Mass spectrometry and kinetic experiments have been performed to understand which residue on the Fe-S assembly scaffold protein functions as the sulfur acceptor. Mass spectrometry data for the *A. vinelandii* system indicates that variants of all three IscU conserved cysteines can function as sulfur acceptors and form persulfide or polysulfide species on the scaffold protein [185]. Kinetic data for the *E. coli* ISC system revealed that C37S and C106S, but not C63S, IscU variants are able to stimulate IscS activity [109], leading to the conclusion that C63 may assist in the rate-limiting cleavage of the C328 persulfide species on IscS. In contrast, recent ferredoxin reconstitution experiments suggest IscU residue C106 rather than C37 or C63 participates in sulfur

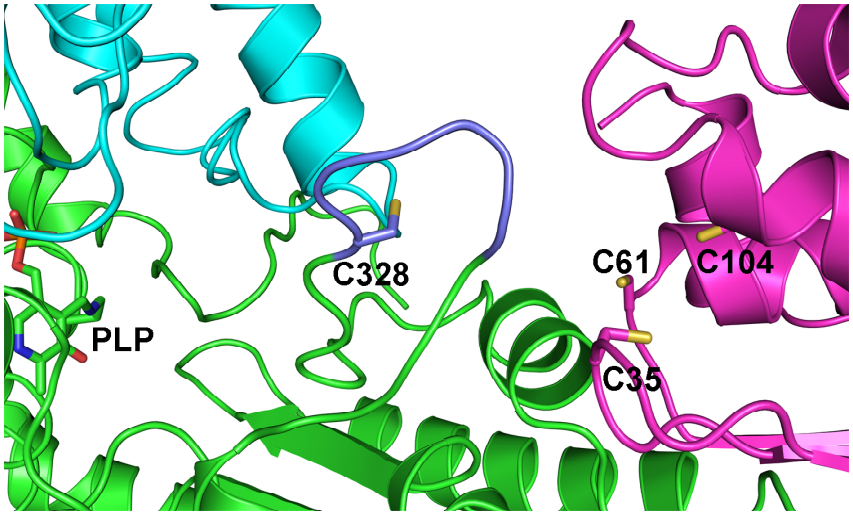

Figure 4-1. *E. coli* IscS-IscU complex structure (PDB 3LVL)

transfer from IscS to IscU [186], and additional kinetic experiments fail to observe IscU-based stimulation of IscS activity ([187] Chapter VIII). In the *Enterococcus faecalis* SUF system, the scaffold protein SufU stimulates the cysteine desulfurase activity of SufS and mass spectrometry experiments identify a persulfide species on C128 implicating this residue (equivalent of *E. coli* C106) as the sulfur acceptor [181]. In contrast, in the *Bacillus subtilis* SUF system the scaffold protein SufU, but not the C41, C65, or C128 mutants, stimulates SufS activity and the C41A variant can inhibit the native SufU-based activation of SufS [188]. These inconsistent results and different conclusions may be due to experimental challenges that include the chemical reactivity

of the persulfide moiety, loss of IscS binding affinity for IscU variants, and the large thermodynamic driving force associated with Fe-S cluster formation.

In eukaryotes, recent evidence suggests Fe-S cluster biosynthesis is catalyzed by an assembly complex that exists in at least two forms: a mostly inactive complex of NFS1, ISD11, ISCU2 (SDU) and an activated complex with NFS1, ISD11, ISCU2, and frataxin (SDUF) subunits [82, 96]. In humans, the 94 kDa homodimeric cysteine desulfurase NFS1 (homolog of IscS) provides sulfur for Fe-S cluster biosynthesis [30, 124]. ISD11 is a eukaryotic-specific protein that interacts and stabilizes NFS1 [121-123]. Cluster assembly is templated by the scaffold protein ISCU2 (homolog of IscU), whereas frataxin (FXN) stimulates both the cysteine desulfurase and Fe-S cluster assembly reactions [96]. Few details are known about the eukaryotic hand-off mechanism from NFS1 to ISCU2 and the role of FXN in this process. Here we present enzyme kinetic and radiolabeling experiments that support a model in which FXN stabilizes a conformation for sulfur transfer from NFS1 to a particular cysteine on ISCU2 as an early step in Fe-S cluster biosynthesis.

EXPERIMENTAL PROCEDURES

Protein Expression and Purification. Eight human ISCU2 cysteine variants (C96S, C35A, C35S, C61A, C61S, C104A, C104S, and C35A/C61A) were created by QuikChange site-directed mutagenesis (Stratagene) using a pET11a-ISCU2 plasmid template, and the mutation sites were confirmed by DNA sequencing (Gene Technologies Lab at TAMU). The resulting ISCU2 variant pET11a plasmids were transformed into BL21(DE3) cells and grown at 16 ^{o}C until reaching an OD_{600} of 0.6. Protein expression was then induced with 0.5 mM IPTG and the cells were harvested 16 hrs later. The ISCU2 variants along with human NFS1/ISD11 and FXN were purified as previously described [96] with the exception of adding 10% glycerol to the buffers for C61A and C35A/C61A.

ISCU2 *Variant Binding to and Stimulation of Fe-S Assembly Complex.* Sulfide production was measured using a previously described methylene blue formation assay [96]. For the titration of ISCU2 variants, the reaction mixtures were initiated with 100 μM cysteine and included 0.5 μM SD, 2 mM DTT, 10 μM PLP, 50 mM Tris pH 8.0, 250 mM NaCl. The number of equivalents for the ISCU2 variants (calculated based on the SD concentration) that saturated the cysteine desulfurase activities was then determined to be 3 (native ISCU2, C35A, and C104A), 30 (C96S), 20 (C35S), 80 (C61A and C61S), 10 (C104S), and 200 (C35A/C61A). Once the saturating amounts of the ISCU2 variants had been determined, additional titrations were performed to determine the amount of FXN needed to maximize the activity of the SDU complexes. The number of

equivalents of FXN was determined to be 3 (native ISCU2), 5 (C96S), 80 (C35A and C35S), 200 (C61A and C61S), 30 (C104A), 50 (C104S), and 400 (C35A/C61A).

Determination of kinetic parameters for *ISCU2 variants.* Reaction mixtures included 0.5 μM SD, 2 mM DTT, 10 μM PLP, 50 mM Tris (pH 8.0), 250 mM NaCl, and the saturating amount of ISCU2 variant and FXN (determined above) in the presence or absence of 5 μM $Fe(NH_4)_2(SO_4)_2$. The samples were incubated in the glove box for 30 minutes prior to initiation with cysteine. The cysteine concentration ranges used were 12.5-400 μM for native, C35A, C35S C61A, C61S, and C96S variants, 12.5-1000 μM for C104A, C104S, C35A/C61A, and C35A/C61A/C104A. Reaction rates as a function of cysteine concentration were fit to the Michaelis-Menten equation using KaleidaGraph (Synergy Software).

Cysteine Desulfurase Activities with ISCU2 *Variants at a Physiological Cysteine Concentration (0.1 mM)*. The cysteine desulfurase activity was determined at 0.1 mM cysteine concentration with 0.5 μM SD, 2 mM DTT, 10 μM PLP, 50 mM Tris pH 8.0, 250 mM NaCl, and saturated amounts of ISCU2. Three independent measurements were conducted and averaged. Similar experiments were also performed with saturating FXN in the absence or presence of 5 μM $Fe(NH_4)_2(SO_4)_2$.

Fe-S Cluster Formation. Assay mixtures contained 8 μM of SD, 5 mM DTT, 200 μM $Fe(NH_4)_2(SO_4)_2$, 100 μM L-cysteine, 50 mM Tris pH 8.0, and 250 mM NaCl in a total volume of 0.2 mL. In addition, the saturating amounts of C35A, C61A, C104A, or C96S and FXN were added to the assay mixture. Two additional cluster formation reactions were assayed containing SD with saturating amounts of ISCU2 or C96S

without addition of FXN. The scaffold protein was incubated for 1 hour with 5 mM DTT in an anaerobic glovebox prior to addition of the remaining components in an anaerobic cuvette. The reaction was initiated by injecting L-cysteine to a final concentration of 100 μM with a gas-tight syringe. Fe-S cluster formation was monitored at 456 nm at room temperature for 3000 seconds and then fit as first order kinetics using Kaleidagraph.

SDS-PAGE Analysis of Sulfur Transfer. Reaction mixtures (30 μL) included 3 μM SD, 50 mM Tris (pH 8.0), 250 mM NaCl, and the saturating amount of ISCU2 variant and FXN (determined above). The samples were incubated in the glovebox for 10 minutes prior to the addition of 5 Ci/mmol ^{35}S-Cysteine (American Radiolabeled Chemicals Inc.) to a final concentration of 100 μM. After a 2-minute incubation at 37^{o}C, reactions were terminated by centrifugation through a Micro Bio-Spin P-6 gel filtration column (Bio-Rad). The spin column flow through was combined with SDS-PAGE sample loading buffer and then loaded on a 12% SDS-PAGE gel. The gel was dried onto chromatography paper in a gel drying oven at 60^{o}C under vacuum before a 12 hour exposure to a phosphor screen. ^{35}S label incorporation was visualized using a Phosphorimager (Typhoon Trio, GE Healthcare) and analyzed with ImageQuant software.

RESULTS

Conserved Cysteines on ISCU2 Contribute to SDUF complex Formation. Previously, the FXN-dependent stimulation in cysteine desulfurase activity for the human NFS1-ISD11-ISCU2 (SDU) complex was hypothesized to result from sulfur transfer from NFS1 to ISCU2 (Figure 4-2; reaction 2) and more rapid DTT-dependent reductive cleavage of a persulfide on ISCU2 (Figure 4-2; reaction 3) than on NFS1 (Figure 4-2; reaction 1). This model predicts mutation of the sulfur acceptor on ISCU2 will eliminate the FXN-based stimulation. To test this hypothesis, ISCU2 mutations of the three conserved cysteines (C35, C61, and C104) to both alanine and serine, the non-conserved cysteine (C96) to serine, and a double mutant C35A/C61A were constructed.

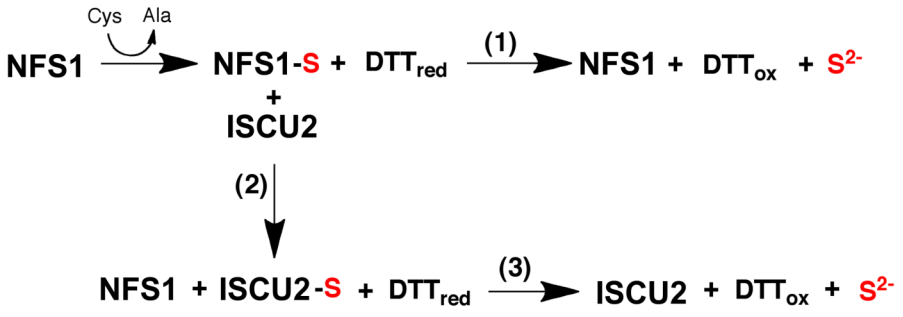

Figure 4-2: Proposed sulfur transfer mechanism from NFS1 to ISCU2 in the presence of FXN.

First, SD titrations with ISCU2 variants were performed to determine reaction stoichiometries and account for weaker binding of ISCU2 variants to the SD complex. The sulfide production of the SD complex was monitored as a function of increasing amounts of the ISCU2 variants until the activity plateaued. This saturation behavior was interpreted as binding phenomenon in which the addition of ISCU2 generates the Fe-S assembly competent SDU complex, and that the ISCU2 variants have distinct binding affinities and ability to change the activity of the complex. Native ISCU2 and the C96S variant (data not shown) required 3 and 30 equivalents respectively to saturate the cysteine desulfurase activity while the addition of the C104A and C104S variants had little effect on the activity of the NFS1-ISD11 (SD) complex. The C35A variant saturated after 5 equivalents, whereas the C35S variant required 15 equivalents. The C61A and C61S variants saturated at 80 equivalents and the double mutant C35A/C61A required 200 equivalents to saturate the cysteine desulfurase activity. Together this data indicates that mutation of any of the cysteines on ISCU2 resulted in weaker binding, and that residue C61 has the largest role in SDU complex formation.

Each of these SDU complexes, using the defined stoichiometry (above), was then titrated with FXN and the rate of sulfide production was measured. Saturation of the cysteine desulfurase activity signaled formation of the SDUF protein complex. As previously described, the native SDU complex required 3 equivalents of FXN to saturate the rate of sulfide production [96]. In contrast, more FXN was required to saturate the cysteine desulfurase activity for the SDU_{C96S} (5 equiv), SDU_{C35A} and SDU_{C35S} (80 equiv), SDU_{C61A} and SDU_{C61S} (200 equiv), SDU_{C104} (30 equiv), SDU_{C104S} (50 equiv),

and $SDU_{C35A/C61A}$ (400 equiv) variants. The conserved cysteines on ISCU2 not only contribute to binding the SD complex, but also appear to contribute to FXN binding to the resulting SDU complexes.

Sulfur Transfer from NFS1 to ISCU2 Residue C104. Here the cysteine desulfurase activities for the 8 ISCU2 variants were determined in the presence of FXN. Saturating amounts of ISCU2 and FXN (see above) relative to SD were used in these assays to remove complications from weaker binding of ISCU2 variants to the SDUF complex. The C35A and C35S ISCU2 mutants exhibited similar FXN-dependent stimulation of cysteine desulfurase activity using a physiological cysteine concentration of 100 μM (Figure 4-3A). Examination of the Michaelis-Menten kinetics revealed a k_{cat} of 11.1 min^{-1} for the C35A variant and 9.4 min^{-1} for the C35S variant, which are essentially identical to the 10.7 min^{-1} rate of native ISCU2 (Table 4-1). The C61A and C61S ISCU2 mutants exhibited a k_{cat} of 9.6 min^{-1}, whereas the C61S variant exhibited a k_{cat} of 5.9 min^{-1} (Table 4-1). In contrast, the C104A and C104S ISCU2 variant complexes exhibited activity at about 8 and 25%, respectively, of the native SDUF complex (Figure 4-3A). Interestingly, unlike the other cysteine ISCU2 variants, the C104 variants did not exhibit a ferrous iron based stimulation of the cysteine desulfurase activity (Figure 4-3A).

The slower kinetics of the C104 variants suggests that this residue may be involved in the sulfur transfer reaction. One possibility is that C104 is the sulfur acceptor on ISCU2 (Figure 4-2; reaction 2). A second possibility is that one of the other ISCU2 conserved cysteines is the initial sulfur acceptor and, after internal or intraprotein

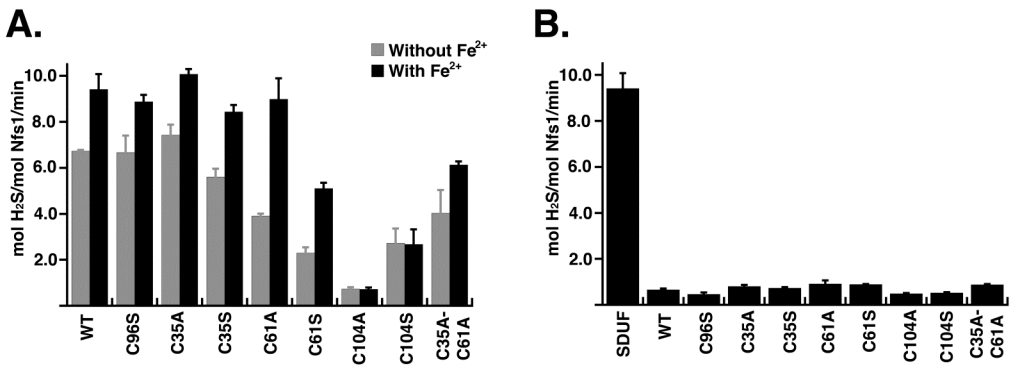

Figure 4-3. ISCU2 variants effect on the cysteine desulfurase activity of the SDU and SDUF protein complexes. (A) Sulfide production was assessed in the presence of NFS1-IDS11 with saturating amounts of FXN and ISCU2 variant in the presence and absence of 10 equiv of Fe^{2+}. (B) Sulfide production was assessed in the presence of NFS1-ISD11 with saturating amounts of ISCU2 variant and compared to the wt-SDUF protein complex. Error bars in A and B are for three independent measurements.

sulfur transfer, a persulfide on C104 is generated and then released by DTT. To evaluate this second possibility, the double mutant C35A/C61A was constructed and its kinetics were examined. The double mutant exhibited a k_{cat} that is 60% of the activity of native ISCU2 in a standard assay and a catalytic efficiency of 10,600 $M^{-1}s^{-1}$ (Figure 4-2A and Table 4-1). As a control, the fourth non-conserved cysteine (C96) in human ISCU2 was mutated to a serine and this variant was shown to have similar activity as native ISCU2 and the C35A and C61A variants (Figure 4-3A). Together, the kinetics results were consistent with the C104 residue on ISCU2 serving as the primary sulfur acceptor from NFS1 for Fe-S cluster assembly.

FXN Facilitates Sulfur Transfer From NFS1 to ISCU2. Here the cysteine desulfurase activities for the different ISCU2 variants were determined in the absence of FXN. Again, saturating amounts of the ISCU2 variants were added to the SD complex and sulfide production was quantitated in the presence of 100 μM cysteine. The mutants all exhibited 10-15% of the sulfide production activity of the SDUF complex (Figure 4-3B). Importantly, the ISCU2 dependent differences in sulfide production were no longer apparent in the absence of FXN.

Table 4-1. Kinetic Parameters for ISCU2 Cysteine Variants

Complex	k_{cat} (min^{-1})	K_M $^{L\text{-}cys}$ (mM)	k_{cat}/K_M (M^{-1} s^{-1})
SD with ISCU2	0.8 ± 0.1	0.052 ± 0.014	260 ± 70
SD with ISCU2, FXN, and Fe^{2+}	10.7 ± 0.8	0.019 ± 0.006	9200 ± 3000
SD with ISCU2, FXN	7.8 ± 0.4	0.015 ± 0.005	8500 ± 3100
SD with C35A-ISCU2, FXN, and Fe^{2+}	11.1 ± 0.6	0.018 ± 0.005	10000 ± 2600
SD with C35A-ISCU2, FXN	8.7 ± 0.5	0.024 ± 0.005	6100 ± 1400
SD with C35S-ISCU2, FXN, and Fe^{2+}	9.4 ± 0.5	0.020 ± 0.005	7700 ± 2200
SD with C35S-ISCU2, FXN	5.9 ± 0.3	0.014 ± 0.003	7200 ± 1700
SD with C61A-ISCU2, FXN, and Fe^{2+}	9.6 ± 0.5	0.017 ± 0.004	9300 ± 2300
SD with C61A-ISCU2, FXN	4.2 ± 0.1	0.010 ± 0.001	6700 ± 930
SD with C61S-ISCU2, FXN, and Fe^{2+}	5.9 ± 0.2	0.012 ± 0.003	8300 ± 1800
SD with C61S-ISCU2, FXN	3.0 ± 0.2	0.018 ± 0.005	2800 ± 670
SD with C104A-ISCU2, FXN and Fe^{2+}	0.9 ± 0.1	0.023 ± 0.001	640 ± 200
SD with C104A-ISCU2, FXN	1.0 ± 0.1	0.033 ± 0.001	500 ± 170
SD with C104S-ISCU2, FXN and Fe^{2+}	2.7 ± 0.1	0.016 ± 0.004	2800 ± 670
SD with C104S-ISCU2, FXN	3.2 ± 0.1	0.014 ± 0.002	4000 ± 680
SD with C35A,C61A-ISCU2, FXN and Fe^{2+}	6.4 ± 0.2	0.010 ± 0.002	10600 ± 2300
SD with C35A,C61A-ISCU2, FXN	4.5 ± 0.3	0.021 ± 0.007	3600 ± 1200
SD with C96S-ISCU2, FXN, and Fe^{2+}	9.9 ± 0.9	0.021 ± 0.008	8000 ± 3200
SD with C96S-ISCU2, FXN	8.2 ± 0.3	0.018 ± 0.004	7700 ± 1600

Radiolabel Sulfur Tracking for ISCU2 Variants. Here interprotein 35-S transfer experiments were performed to further understand the sulfur transfer mechanism. These experiments were performed under conditions similar to the Michaelis-Menten kinetics except for the addition of ^{35}S- L-cysteine substrate and the absence of DTT. After a 2-minute incubation, excess label was removed with a desalting column and then the individual SDUF components were separated with non-reducing SDS-PAGE and visualized with a phosphorimager (Figure 4-4). A covalent 35-S adduct, presumably a

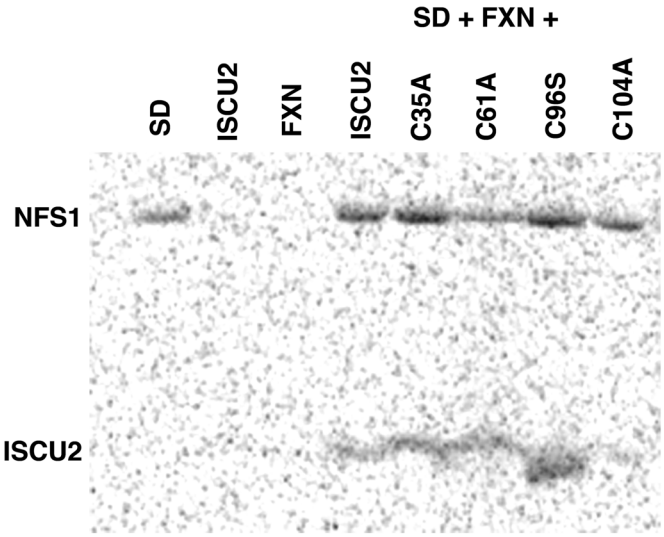

Figure 4-4: SDS-PAGE analysis of sulfur transfer from NFS1 to ISCU2. Phosphor image obtained after a 12 hour exposure of the SDS-PAGE gel. Lanes 1,2, and 3 are SD, ISCU2, or FXN incubated for 2 minutes in the presence of ^{35}S-Cysteine. Lanes 4,5,6,7, and 8 are SD incubated with saturating amount of ISCU2 variant and FXN in the presence of ^{35}S-Cysteine for 2 minutes.

persulfide species, was observed for NFS1 in each reaction. The label was also visible for the native ISCU2 and for the C35A, C61A, and on C96S variants (Figure 4-4). The absence of label incorporation for the C104A variant is consistent with C104 being required for sulfur transfer from NFS1 to ISCU2.

Fe-S Cluster Formation on ISCU2. Here Fe-S cluster formation on wt-ISCU2 and ISCU2 variants was monitored by an increase in the absorbance at 456 nm to determine which cysteine residues are critical for building and ligating a cluster. First, a mutation of the non-conserved cysteine, C96S, was tested and found to have Fe-S cluster assembly activities similar to the native SDU and SDUF complexes (Figure 4-5A), indicating that this residue is not essential for cluster ligation or the mechanism of cluster formation. Unlike mutation of C96, Fe-S cluster formation for SDUF complexes with the C35A, C61A, and C104A ISCU2 variants resulted in rates of cluster formation that were similar to or lower than that of the wild-type SDU complex (Figure 4-5B). The requirement of all three conserved, but not C96, in Fe-S cluster assembly appears to be inconsistent with previous conclusions for the human system [107], and recent results for the *E. coli* system in which Fe-S clusters were still formed for IscU variants with each of the three conserved cysteines mutated [111].

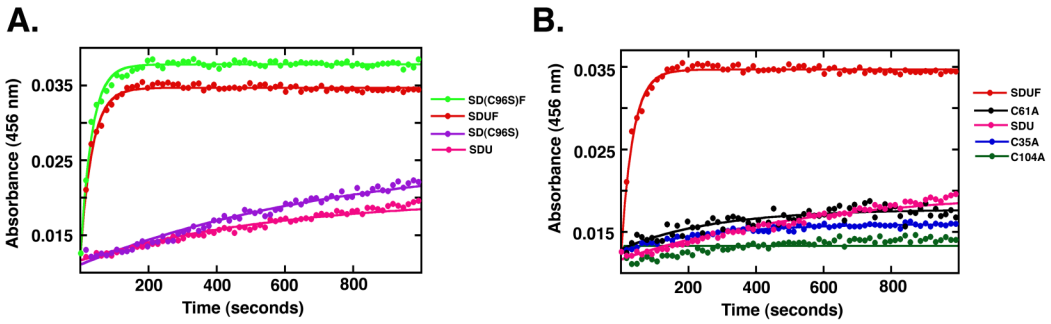

Figure 4-5. Fe-S cluster formation was monitored at 456 nm as a function of time. (A) Assays contained NFS1-ISD11 protein complex with 3 equiv of ISCU2 and 3 equiv of FXN (red), with 3 equiv of ISCU2 (pink), with 30 equiv of C96S-ISCU2 and 5 equiv of FXN (green), and with 30 equiv of C96S-ISCU2 (purple). (B) Assay mixtures contained NFS1-ISD11 and saturating amounts of ISCU2 variants and FXN. The lines through the data are the fits using first order kinetics.

DISCUSSION

Despite the importance of Fe-S clusters, few details are known about their assembly mechanisms. Sulfur is mobilized by a cysteine desulfurase from a cysteine substrate in the form of a reactive persulfide intermediate that can be transferred to a scaffold protein for cluster assembly. In prokaryotes, sulfur transfer from IscS to IscU has been suggested as the first step in Fe–S cluster biosynthesis [182]. However, there is controversy over whether a particular cysteine, and, if so, which cysteine accepts the sulfur atom donated by the cysteine desulfurase for Fe-S cluster biosynthesis [185]. Experiments aimed at identification of the sulfur acceptor on ISCU2 are complicated by the reactivity of the persulfide moiety formed on NFS1 and on ISCU2. As well, the thermodynamic driving force for cluster formation due to the reactivity of free iron and sulfide in solution complicate studies aimed at the identification of residues involved in cluster ligation. Lastly, as stable protein complexes have been described in both the *E. coli* [33, 89] and human ISC systems [82, 96], the disregard for use of the proper reaction stoichiometries has led to further complications and misleading results.

Previously, the rate of sulfide production from NFS1 was shown to be stimulated by the presence of ISCU2 and FXN [96]. The objectives of these experiments were to address the controversy over the sulfur accepting residue on ISCU2 and in doing so gain a better understanding of the FXN based rate enhancement previously hypothesized to follow scheme 1 [189] (Figure 4-2). In the absence of FXN, we hypothesize that internal sulfur transfer from NFS1 to ISCU2 either does not occur or occurs at a minimal rate compared to DTT-dependent sulfide release from the NFS1 persulfide loop (Figure 4-2;

reaction [1]). In the presence of FXN, we hypothesize that internal transfer from NFS1 to ISCU2 (Figure 4-2; reaction [2]) is favored and that the sulfide is released from a persulfide species on ISCU2 at a faster rate than from NFS1 (Figure 4-2; reaction [3] > [1]). This scheme explains the overall rate enhancement for sulfide production by FXN and predicts that if the sulfur acceptor on ISCU2 were removed the rate enhancement by FXN would be lost.

To address this scheme for the FXN based rate enhancement, the three conserved cysteine residues (C35, C61, and C104) on human ISCU2 were mutated to either alanine or serine and kinetically characterized. First, titrations of ISCU2 variants, followed by FXN titrations were conducted to determine the conditions necessary to generate an SDUF complex. The titration results show C61-ISCU2 variants required 80 equivalents to saturate the NFS1 activity, which implies C61 is critical for ISCU2 interaction with NFS1. Using saturating amounts of the C61-ISCU2 variant and FXN, the resulting cysteine desulfurase activity is similar to the wt-SDUF complex suggesting mutation of C61 does not impair the sulfur transfer mechanism. C35 and C104 showed higher affinity for binding the SD protein complex and C35-ISCU2 mutants maintained near wild-type activity levels in the presence of FXN. Contrastingly, C104-ISCU2 mutants abolish FXN and ferrous iron based stimulation of the cysteine desulfurase activity. Kinetic analysis of the C35A-C61A ISCU2 variant revealed a catalytic efficiency similar to the wt-SDUF complex suggesting C104 is a key residue for the sulfur transfer. In the absence of FXN, wt-ISCU2 and variants show similar levels of sulfide production suggesting that sulfur transfer from NFS1 to ISCU2 no longer occurs or the rate of sulfur

transfer is too low for the assay to be sensitive to the cysteine variant differences. Further validation for C104 as the sulfur acceptor residue was demonstrated by use of a radio-labeled cysteine substrate with the wt-SDUF and ISCU2 variant complexes in which label transfer from NFS1 to ISCU2 was observed in the wt, C35A, C61A, and C96S variant complexes and not in the C104A complex.

Previously, C96 has been implicated along with C35, C61, and C104 in being important for cluster ligation in the human ISCU2 protein [107]. Interestingly, prokaryotic IscU and NifU proteins lack the corresponding C96 residue and would hence possess alternative cluster ligands or utilize scaffold protein dimerization to bind a cluster [107]. Here each residue was tested in its ability to build a cluster using the SDUF variant complexes and measuring the rate of cluster reconstitution at 456 nm over time. For the first time, the human C96S-ISCU2 variant was shown to build a cluster using the human SD and FXN proteins with a rate for Fe-S cluster assembly that was comparable to the wt-SDUF complex indicating C96 is not essential for the rate of cluster reconstitution or the amount of cluster formed. This is in contrast to Cowan's results that relied on overexpression and purification of the C96A-D37A ISCU2 double mutant from *E. coli* [107]. The resultant protein was colorless and lacked the characteristic Fe-S cluster UV-visible absorbance bands seen when the more stable cluster binding D37A ISCU2 variant is expressed and purified the same way [107]. Each of the remaining variant complexes tested showed significantly decreased ability to assemble Fe-S clusters relative to the wt-SDUF complex. Contrastingly, CD spectroscopy results from the Vickery lab on *E. coli* IscU showed that each

corresponding IscU variant could be chemically reconstituted to bind a cluster with different coordination environments [111]. Correspondingly however, while the C37 and C63 (equivalent to human residues C35 and C61) IscU variants were able to reconstitute apo-ferredoxin when incubated with IscS, cysteine, and iron, C106 (equivalent to human residue C104) was completely inactive suggesting C106 plays a role in the sulfur delivery step from IscS [111]. Discrepancies in the ability of the variants to efficiently assemble Fe-S clusters may be due to the *E. coli* scaffold protein being more conformationally flexible and able to employ different metal binding ligands than human ISCU2. Alternatively, the Fe-S cluster initially built on the scaffold protein may be unstable due to alteration of the native cluster environment; in the presence of ferredoxin there is a stable acceptor and in the absence the cluster falls out of the scaffold. Regardless of the differences observed in the C35A and C61A variants, it appears that both the *E. coli* and human scaffold proteins utilize C104 in the sulfur transfer reaction.

The crystal structure of the trimeric *A. aeolicus* IscU shows two IscU conformations, the Fe–S cluster bound conformation (subunit B) and apo form (subunits A and C) [190]. The differences in these two conformations are a helix to coil transition in which the C-terminal region (residues 103–109), housing residues K103 (equivalent of human K101), H106 (equivalent of human H103), and C107 (equivalent of human C104) has become partially unwound. Structural alignment of *A. aeolicus* apo-IscU subunit A and *E. coli* apo-IscU shows that C104 (human ISCU2 residue number)

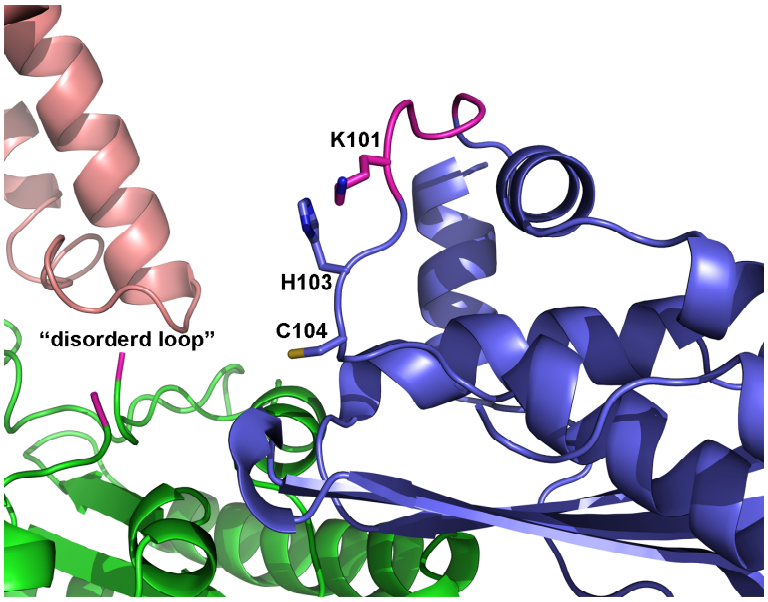

Figure 4-6: Model of helix to coil transition. *A. aeolicus* IscU subunit A (PDB 2Z7E) with *E. coli* IscS.

becomes exposed in this helix-to-coil switch (Figure 4-6) from its original buried conformation about 18 Å away from catalytic cysteine loop on IscS. Two distinct conformations of IscU that interconvert on the millisecond time scale in solution were also proposed by Markley's group [191]. Accordingly, Markley's group has further defined these two interconverting states as structured and disordered conformational states for the *E. coli* IscU in which the disordered conformational state preferentially binds the cysteine desulfurase for Fe-S cluster assembly [192]. Taken together, we propose a working model to explain the sulfur transfer mechanism from NFS1 to ISCU2

in the presence of FXN. First, cysteine substrate binds to the PLP cofactor in the active site of NFS1. Second, the substrate is converted to alanine generating a persulfide on C328 of NFS1. Third, FXN binds SDU, and induces or stabilizes the helix-to-coil transition of ISCU2, exposing C104 to accept the persulfide sulfur from NFS1. The persulfide- bound C104 on ISCU2 can either be cleaved by DTT or used for Fe–S cluster assembly. Taken together, these results suggest C104 is the initial and primary sulfur-accepting residue on ISCU2.

CHAPTER V

AN ISCU2 POINT MUTATION NEGATES THE NEED FOR FXN ACTIVATION

INTRODUCTION

Frataxin (FXN) is a conserved mitochondrial protein that interacts with the core components of the Fe-S cluster biosynthetic machinery to form a multi-subunit complex [79, 82, 96]. The Fe-S assembly complex exists in two forms: a low activity form composed of the cysteine desulfurase enzyme NFS1, the protein-partner ISD11, and the scaffold protein ISCU2, which is named SDU, and a high activity form that also includes FXN and is named SDUF [96]. Deficiency in the frataxin protein results in a complicated phenotype that includes mitochondrial iron accumulation, a decrease in both heme and Fe-S cluster biosynthesis, and additionally, is associated with the neurodegenerative disease Friedreich's ataxia (FRDA) [162, 193]. Previous *in vitro* research suggests that FXN together with ferrous iron acts as an allosteric activator and increases the rate of Fe-S cluster assembly nearly 25 fold upon binding to the SDU complex [96]. This FXN binding event is propagated as a 50 fold decrease in the K_M for cysteine, a 6 fold increase in the k_{cat} for cysteine turnover, and is enhanced by the addition of ferrous iron [96]. In the absence of FXN, the SDU complex is still able to synthesize Fe-S clusters albeit at a much slower rate [96]; *in vivo*, the allosteric activator role of FXN may serve to control the rate of Fe-S cluster biosynthesis in response to environmental stimuli.

Recently, a single amino acid substitution; M106I (human numbering) on ISCU2 has been shown to negate many of the deleterious effects of frataxin depletion in yeast cells [194]. Specifically, frataxin depleted yeast cells carrying the ISCU2 mutant had improved iron homeostasis, restoration of cytochrome and heme biosynthesis, and improved Fe-S cluster enzyme activities [194]. This suppressor mutation of ISCU2 that bypasses frataxin deficiency is located on a surfaced exposed C-terminal alpha helix close to the chaperone binding LPPVK motif and two amino acids away from C104, which we have shown (Chapter IV) to be involved in sulfur transfer from NFS1 to ISCU2 and is likely involved in Fe-S cluster ligation (Figure 5-1). Interestingly, the M106I mutation or a branched chain amino acid such as valine, isoleucine, or leucine is found not only in the *E. coli* scaffold protein but also in prokaryotes such as *Rickettsia typhi*, *Shigella dysenteriae*, *Neisseria meningitides*, and *Azotobacter vinelandii* [194]. As mutation to valine also restored growth of frataxin deletion strains in yeast cells, it appears that hydrophobicity in this region is important for the suppression effect and was hypothesized to either improve interactions of the scaffold protein with chaperones for cluster delivery or enhance recruitment or interactions with an iron donor for cluster assembly [194].

However, the mechanism by which the M106I ISCU2 mutant bypasses frataxin deletion remains unknown and it is unclear whether the mutant ISCU2 directly affects Fe-S cluster assembly. Here, the M106I variant was generated in the human ISCU2 construct and kinetically evaluated using *in vitro* cysteine desulfurase and Fe-S cluster assembly assays. Surprisingly, the SDU_{M106I} complex exhibited a 12 fold higher k_{cat}/K_M

than the wild-type SDU complex. These findings suggest that the M106I point mutation favors a conformation of ISCU2 that is inherently more active in accepting the persulfide sulfur from NFS1 during the sulfur transfer reaction, thereby bypassing the need for allosteric activation of this process by frataxin.

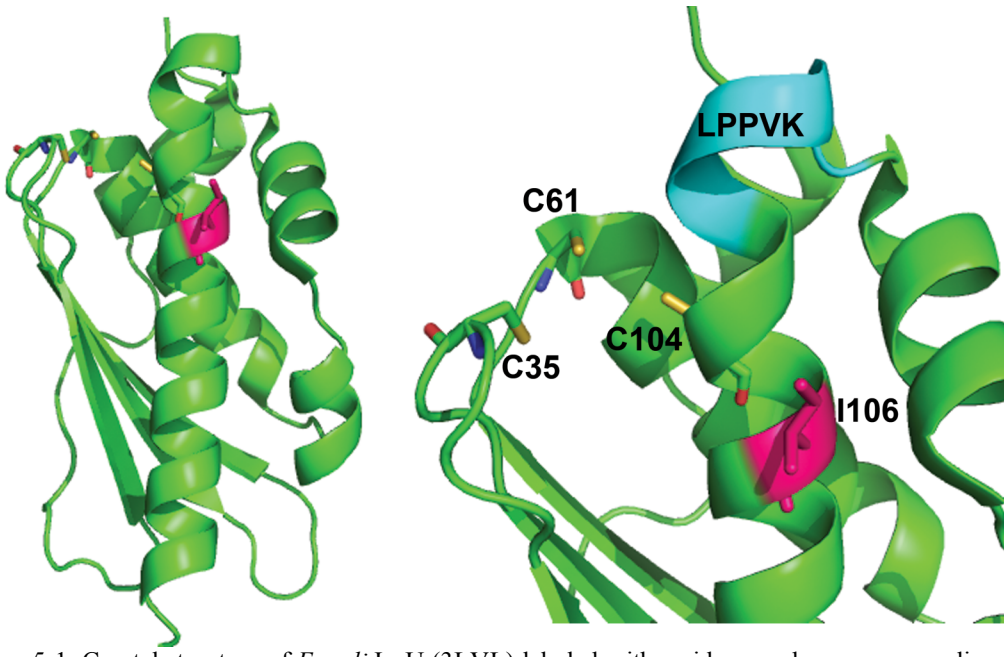

Figure 5-1. Crystal structure of *E. coli* IscU (3LVL) labeled with residue numbers corresponding to human ISCU2. Overall structure of IscU (left) with I106 highlighted in pink and three conserved cysteine residues implicated in cluster binding shown as stick residues. Close up of IscU cysteine residues and I106 (right) with chaperone binding residues LPPVK highlighted in cyan.

EXPERIMENTAL PROCEDURES

Protein preparation. The QuikChange method (Stratagene) was used to introduce the M106I point mutant into a pET11a plasmid containing human ISCU2, and the mutation site was confirmed by DNA sequencing. The confirmed mutant plasmid was transformed into *E. coli* BL21 (DE3) cells and grown to an OD_{600} of 0.6. Protein expression was induced with 0.5 mM IPTG for 16 hours at 16°C and the M106I variant was purified as described for native ISCU2 [96].

Cysteine Desulfurase Activity Measurements. The rate of sulfide production for the NFS1, ISD11, ISCU2, and FXN (SDUF) complex was measured using a previously described methylene blue formation assay [39, 96]. For the titration of ISCU2 variants, the reaction mixtures were initiated with 100 μM cysteine and included 0.5 μM SD, 2 mM DTT, 10 μM PLP, 50 mM Tris pH 8.0, and 250 mM NaCl. 160 equiv of the M106I ISCU2 variant (calculated based on the NFS1-ISD11 (SD) concentration) were required to saturate the cysteine desulfurase activity. Additional titrations of the saturated SDU_{M106I} complex revealed that 50 equiv of FXN were then required to maximize the cysteine desulfurase activity.

Michaelis Menten Kinetics for M106I ISCU2 Variant. Assay mixtures contained 0.5 μM SD, 2 mM DTT, 50 mM Tris pH 8.0, and 250 mM NaCl in a total volume of 0.8 mL. For wt-SDU and SDUF protein complexes, assays additionally contained 1.5 μM ISCU2 with or without 1.5 μM FXN, and in the presence or absence of 5 μM $Fe(NH_4)_2(SO_4)_2$. Michaelis Menten kinetics for the M106I ISCU2 variant were also performed under saturating conditions by including 160 equiv M106I ISCU2, and 160

equiv M106I ISCU2 with 50 equiv of FXN in the presence or absence of 5 μM $Fe(NH_4)_2(SO_4)_2$. Prior to the addition of 12.5 – 1 mM L-cysteine, samples were incubated for 30 minutes in the glovebox. Reaction rates as a function of cysteine concentration were fit to the Michaelis-Menten equation using KaleidaGraph (Synergy Software).

Fe-S Cluster Assembly on ISCU2. Assay mixtures contained 8 μM SD, 5 mM DTT, 200 μM $Fe(NH_4)_2(SO_4)_2$, 50 mM Tris pH 8.0, and 250 mM NaCl in a total volume of 0.2 mL. For wild type SDU and SDUF protein complexes, assays additionally contained 24 μM ISCU2 or 24 μM ISCU2 and 24 μM FXN. Fe-S cluster assay mixtures for the M106I variant additionally contained 1280 μM M106I (160 equiv), or 1280 μM M106I and 400 μM FXN (50 equiv). The reaction was initiated by injecting L-cysteine to a final concentration of 100 μM with a gas-tight syringe. Fe-S cluster formation was monitored at 456 nm at 10ºC for 3000 seconds and then fit as first order kinetics using Kaleidagraph. The rate was converted to activity using an extinction coefficient of 5.8 $mM^{-1}cm^{-1}$ previously determined for a presumed $[2Fe\text{-}2S]^{2+}$ cluster bound to the scaffold protein. Units are defined as the micromoles of [2Fe-2S] cluster formed per micromole of SDU complex per minute at 10 °C.

SDS-PAGE Analysis of Sulfur Transfer. Reaction mixtures (30 μL) included 3 μM SD, 50 mM Tris (pH 8.0), 250 mM NaCl and increasing amounts of M106I ISCU2. Additional reaction mixtures included SD, ISCU2, FXN, SDU, and SDUF controls in which 1 equiv of SD was combined with either 3 equiv of ISCU2 and/or 3 equiv of FXN. As well, an M106I sample was included which contained 480 μM M106I (160X to SD concentration used) and a sample that contained SD with 160 equiv of M106I and 50 equiv of FXN. The samples were incubated in the glovebox for 10 minutes prior to the addition of 5 Ci/mmol ^{35}S-Cysteine (American Radiolabeled Chemicals Inc.) to a final concentration of 100 μM. After a 2-minute incubation at 37^{o}C, reactions were terminated by centrifugation through a Micro Bio-Spin P-6 gel filtration column (Bio-Rad). The spin column flow through was combined with SDS-PAGE sample loading buffer and then loaded on a 12% SDS-PAGE gel. The gel was dried onto chromatography paper in a gel drying oven at 60^{o}C under vacuum before a 12 hour exposure to a phosphor screen. ^{35}S label incorporation was visualized using a Phosphorimager (Typhoon Trio, GE Healthcare) and analyzed with ImageQuant software. Label incorporation on ISCU2 and the M106 variant were quantitated using ImageJ software.

RESULTS

Protein complex stoichiometries for activity measurements. Here the cysteine desulfurase activity of the SD complex was measured as a function of added M106I variant (Figure 5-2A). Previous experiments revealed that adding 3 equiv of ISCU2 minimized the cysteine desulfurase activity of the NFS1-ISD11 (SD) complex, likely through formation of a NFS1-ISD11-ISCU2 (SDU) species [96]. Further titration of FXN to the SDU complex revealed that 3 equivalents of FXN were required to maximally stimulate the cysteine desulfurase reaction [96]. These experiments revealed that FXN functions as an allosteric activator and triggers the first sulfur transfer step in cluster formation [96]. Unlike the wild-type ISCU2, which maximally decreased the cysteine desulfurase activity of NFS1 at 3 equivalents, titration of M106I ISCU2 to SD resulted in progressively higher cysteine desulfurase rates, which maximized with the addition of 160 equivalents of M106I ISCU2 (Figure 5-2A and Figure 5-3).

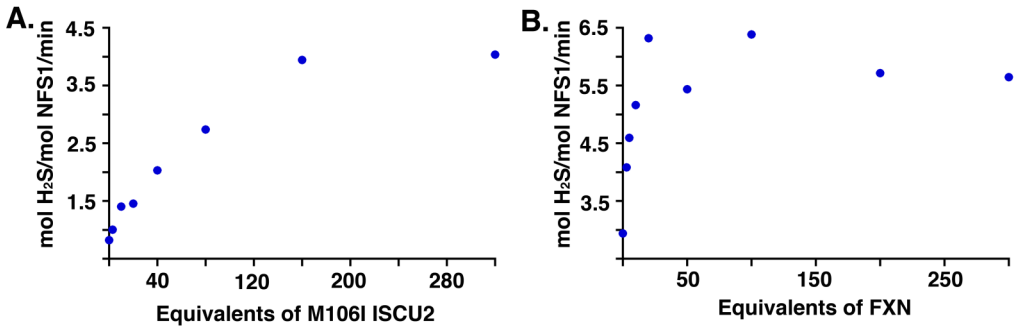

Figure 5-2. Cysteine desulfurase activity measurements as a function of added (A) $ISCU2_{M106I}$ to SD and (B) FXN to SD + 160 equivalents of $ISCU2_{M106I}$.

This maximized rate of the cysteine desulfurase could be further stimulated with the sequential addition of up to 50 equivalents of FXN (Figure 5-2B and Figure 5-3) and then further increased with the addition of Fe^{2+} (Figure 5-3).

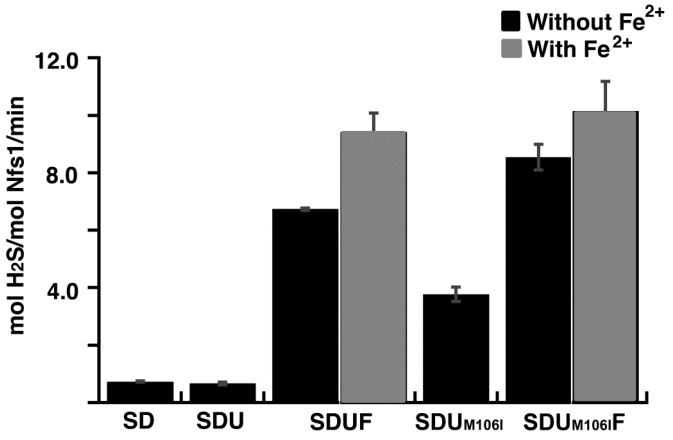

Figure 5-3. $ISCU2_{M106I}$ stimulates the cysteine desulfurase activity of NFS1. Rate of NFS1 sulfide production was determined in the presence of 3 equivalents of ISCU2, 3 equivalents of ISCU2 and FXN with and without ferrous iron, 160 equivalents of $ISCU2_{M106I}$, and 160 equivalents of $ISCU2_{M106I}$ and 50 equivalents of FXN with and without ferrous iron.

Increased Cysteine Desulfurase Activity of the SDU_{M1006I} Complex. Previously, the binding of native FXN to the SDU complex was shown to activate the cysteine desulfurase activity of NFS1 elevating the catalytic efficiency from 25 to 7900 M^{-1} sec^{-1},

this rate could be further enhanced to 10500 M^{-1} sec^{-1} with the addition of Fe^{2+}[96]. These studies indicated that FXN likely causes a conformational change that favors sulfur transfer from NFS1 to ISCU2, and thereby increases the rate of cysteine turnover [96]. Here, the Michaelis-Menten kinetics were determined for SD with 160 equivalents of M106I, and SD with 160 equivalents of M106I and 50 equivalents of FXN in the presence and absence of 10 equivalents of ferrous iron (Table 5-1 and Figure 5-4). As controls, the SDU and SDUF protein complex Michaelis-Menten kinetics were also measured (Table 5-1). Surprisingly, the SDU_{M106I} complex exhibited an enhanced k_{cat} (~5 fold) and a catalytic efficiency (~12 fold) compared to the native SDU complex. The measured catalytic efficiency of the $SDU_{M106}F$ complex with Fe^{2+} was comparable to the native SDUF complex.

Table 5-1. Kinetic Parameters for $ISCU2_{M106I}$ Variant Complexes

Complex	k_{cat} (min^{-1})	K_M^{Cys} (mM)	k_{cat}/K_M ($M^{-1}s^{-1}$)
SDU	0.8 ± 0.1	0.052 ± 0.014	260 ± 70
SDUF	7.8 ± 0.4	0.015 ± 0.005	8500 ± 3100
SDUF + Fe^{2+}	10.7 ± 0.8	0.019 ± 0.006	9200 ± 3000
SDU_{M106I}	4.4 ± 0.1	0.023 ± 0.003	3100 ± 340
$SDU_{M106I}F$	9.5 ± 0.5	0.022 ± 0.005	7100 ± 1800
$SDU_{M106I}F$ + Fe^{2+}	10.2 ± 0.5	0.016 ± 0.004	10900 ± 2700

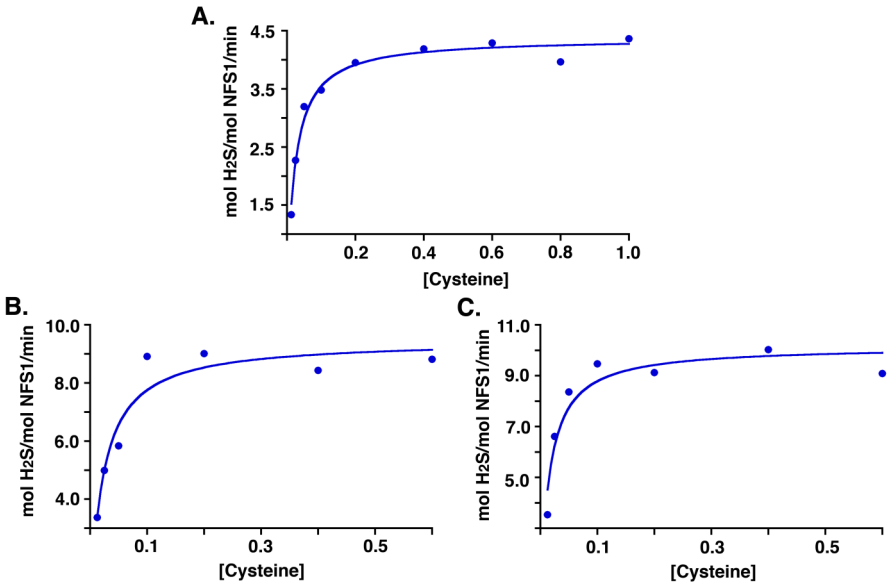

Figure 5-4. Cysteine desulfurase activity of NFS1 with (A) 160 equivalents of $ISCU2_{M106I}$, (B) 160 equivalents of $ISCU2_{M106I}$ and 50 equivalents of FXN, and (C) 160 equivalents of $ISCU2_{M106I}$, 50 equivalents of FXN, and ferrous iron. The lines through the data are the fits to the Michaelis Menten equation; R^2 values = 0.98, 0.92, and 0.91 for (A), (B), and (C) respectively.

Increased Rate of Fe-S Cluster Assembly with the M106I Variant. Next, the ability of the M106I variant to replace native ISCU2 in Fe-S cluster assembly assay was assessed by monitoring the increase in absorbance at 456 nm for both the native SDU and the SDU_{M106I} complexes as a function of time (Figure 5-5). The rate of cluster formation on the M106I variant was nearly 3 times faster than the rate of cluster formation on native ISCU2 (Table 5-2). The rate enhancement upon FXN binding for the SDU_{M106I} complex was significantly lower (~2 fold) than that of the native SDU complex (~7 fold) (Table 5-2).

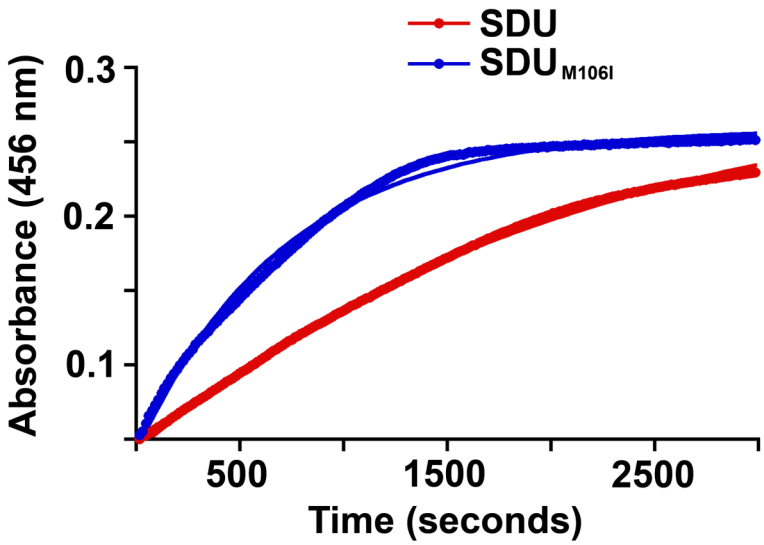

Figure 5-5. Comparison of the Fe-S cluster assembly between the native SDU complex and the SDU_{M106I} complex. Fe-S cluster formation was monitored by an increase in absorbance at 456 nm as a function of time at 10ºC. Reaction mixtures contained the NFS1-ISD11 complex with 3 equivalents of ISCU2 or 160 equivalents of $ISCU2_{M106I}$. The lines through the data are the fits using first-order kinetics.

Table 5-2. Fe-S Cluster Assembly Rates for $ISCU2_{M106I}$ Variant Complexes

Complex	Fe-S Cluster Formation (Units/min)
SDU	0.6 ± 0.1
SDU_{M106I}	1.7 ± 0.1
SDUF	4.0 ± 0.2
SDU_{M106I} F	5.7 ± 0.9

Increased sulfur incorporation of the M106I Variant. Here sulfur transfer from NFS1 to the M106I variant was investigated using a ^{35}S- L-cysteine substrate. Label incorporation was visualized using a phosphorimager and non-reducing SDS-PAGE to separate the individual reaction components (Figure 5-6A). As the M106I variant binds weaker to the SD protein complex than native ISCU2, the level of label incorporation on M106I when 1, 3, or 5 equivalents were added to SD was between 37-42% that seen on native ISCU2 (Figure 5-6B). At 10 equivalents, however, the level of label incorporated on M106I-ISCU2 surpassed that of native ISCU2 and continued to increase with increasing amounts of M106I (Figure 5-6B). At 160 equivalents of M106I, the label incorporation was ~3 times higher than that seen on native ISCU2 (Figure 5-6B).

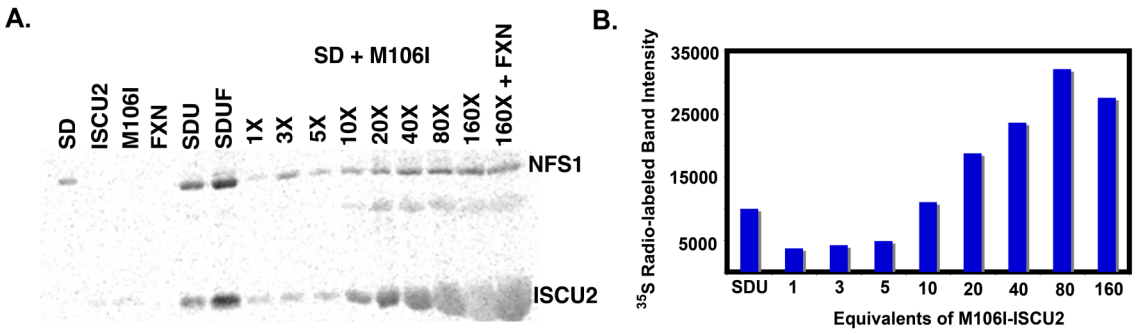

Figure 5-6. SDS-PAGE analysis of sulfur transfer from NFS1 to $ISCU2_{M106I}$. (A) Phosphor image obtained after a 12 hour exposure of the SDS-PAGE gel. Lanes 1, 2, 3, and 4 are SD, ISCU2, $ISCU2_{M106I}$, or FXN incubated for 2 minutes in the presence of ^{35}S-Cysteine. Lanes 5 and 6 are SDU and SDUF complexes, lanes 7-14 are SD incubated with increasing amounts of $ISCU2_{M106I}$ and ^{35}S-Cysteine, and lane 15 is SD incubated with 160 equivalents of $ISCU2_{M106I}$, 50 equivalents of FXN, and ^{35}S-Cysteine. (B) Using ImageJ Software, the ISCU2 band intensity from A was measured and plotted as a series of peaks, these peak areas are plotted in B as a function of $ISCU2_{M106I}$ equivalents and are compared to the peak area of the native SDU complex.

DISCUSSION

Previously, the equivalent of the M106I variant of human ISCU2 was identified as a suppressor mutant of a frataxin (Yfh1) depleted yeast strain [194]. The single point mutation introduced into the yeast scaffold protein decreased mitochondrial iron accumulation relative to the FXN knockout and restored Fe-S cluster assembly [194]. On the basis of these results, three models were proposed to describe this frataxin bypass mechanism; alteration of secondary structure exposing a cysteine to better facilitate sulfur transfer, better recruitment of an iron donor, or enhancement of chaperone interaction thereby facilitating cluster transfer to apo target proteins [194].

Here the M106I point mutation was introduced into the human ISCU2 protein and evaluated relative to native ISCU2 in both cysteine desulfurase and Fe-S cluster assembly assays. Interestingly, a titration of the ISCU2 variant to the SD complex revealed 160 equivalents were required to maximally saturate the cysteine desulfurase activity compared to 3 equivalents of native ISCU2. This difference suggests that the M106 point mutation imposes structural rearrangements that decrease the binding affinity of ISCU2 for the SD protein complex. However, at saturating levels, the SDU_{M106I} complex has a ~12 fold higher catalytic efficiency and a ~3 fold higher rate of Fe-S cluster assembly relative to the native SDU complex. These results can explain the *in vivo* results in which aconitase activity in the frataxin depleted yeast cells was 8% of the wild-type strain and could be increased to 38.9% by introduction of the M106I (human numbering) scaffold protein [194]. Additionally, the weak binding in our *in vitro* assay can be reconciled with the *in vivo* results as increased protein levels of the

yeast scaffold protein have been reported in frataxin mutant strains [195] and M106I (human numbering) was also expressed at a higher level in the frataxin depleted yeast cells [194].

Interestingly, our results indicate that the suppressor mutant bypasses frataxin at the level of the cysteine desulfurase reaction and thus likely acts by facilitating the sulfur transfer reaction from NFS1 to ISCU2. As Markley's group has previously identified two distinct conformations of the *E. coli* scaffold protein using NMR that interconvert on the millisecond time scale [196], one explanation for the increased catalytic efficiency is that the M106I variant shifts the equilibrium of this interconversion favoring the form that accepts the persulfide sulfur from NFS1. This result is also consistent with our model for the FXN-dependent sulfur transfer mechanism (Chapter IV). In this model, frataxin binding stabilizes a coiled conformation of ISCU2 exposing C104 to accept the persulfide sulfur from NFS1 and thereby accelerates the rate of the sulfur transfer reaction. Two distinct conformations for the *A. aeolicus* IscU were shown in the trimeric IscU crystal structure in which the helix housing residue C104 (human numbering) in the Fe-S cluster bound subunit has become partially unwound in the apo subunits [106]. One explanation for the decreased need for FXN activation in the M106I variant is the lower helix forming propensity for isoleucine compared to methionine [197]. However, mutation of residue 106 to helix breaking residues proline or glycine [197] did not restore growth in the frataxin depleted yeast strains [194] and suggest complete disruption of the helix results in protein misfolding, impedes a step in the

cluster assembly reaction, or slows the downstream transfer of the cluster to an apo target.

Substitution of hydrophobic residue (Ile, Val, or Leu) at M106 are found in gram negative bacteria, nitrogen fixing bacteria, and primitive intracellular pathogens [194]. Similarly, the Dancis group showed the M106V (human numbering) mutation also bypassed frataxin depletion in yeast cells while no data was reported for the M106L variant [194]. The *E. coli* cysteine desulfurase, IscS, has a reported k_{cat} of 8.5 min^{-1} (~5 times faster than the human SD complex) and a K_M for cysteine 0f 2.7 μM [183], accordingly, we have measured the catalytic efficiency of *E. coli* IscS to be 7300 M^{-1} sec^{-1} and that of the *E. coli* IscS-IscU complex to be 4100 M^{-1} sec^{-1} (Chapter VIII). While the idea is compelling that the increased activity seen for the SDU_{M106I} complex is due to the prokaryotic residue replacement, we have previously provided data that substitution of the *E. coli* scaffold protein into the human system did not result in similar activity (Chapter VIII). We hypothesize that additional secondary substitutions in prokaryotes, such as L102I counteracts the M106I mutation (Figure 5-7).

The FXN bypass mechanism presented here implies a drug or small molecule that stabilizes the coiled ISCU2 conformation may provide a therapeutic strategy to overcome the deleterious effects of FXN depletion in FRDA patients. In doing so, the human SDU complex would be turned "on" and more closely resemble the *E. coli* IscS-IscU complex. This inversion in activity seen through evolution implies that an additional level of regulation is imposed on human Fe-S cluster assembly relative to the prokaryotic systems and may be involved in the relay of environmental stimuli to the

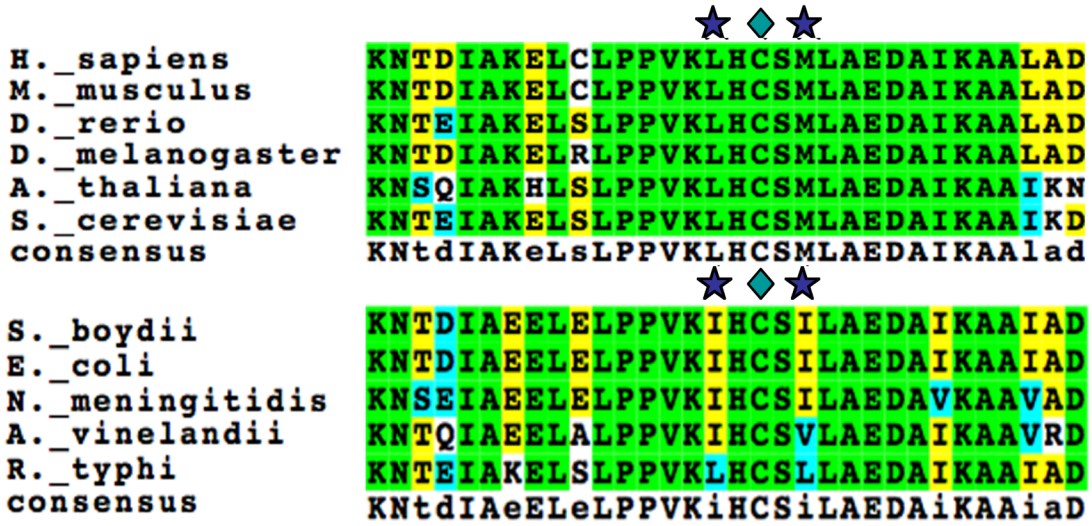

Figure 5-7. Sequence alignment of eukaryotic scaffold proteins (top panel) and of prokaryotic scaffold proteins (bottom panel). C104 is denoted with a green diamond and has been implicated as the sulfur accepting residue in human ISCU2, additionally, human residues L102 and M106 are denoted by blue stars. In prokaryotic systems residue 106 is found as isoleucine, valine, or leucine. Human residue L102 is often replaced with isoleucine in prokaryotic systems. Sequences aligned are as follow *Homo sapiens*, *Mus musculus*, *Danio rerio*, *Drosophila melanogaster*, *Arabidopsis thaliana*, *Saccharomyces cerevisiae*, *Shigella boydii*, *Escherichia coli*, *Neisseria meningitidis*, *Azotobacter vinelandii*, and *Rickettsia typhi*.

assembly complex. Interestingly, this inversion of function is correlated with the loss of a "specialized" Fe-S cluster assembly machinery; for example, the SUF system in *E. coli* functions under iron limiting or oxidative stress conditions [25] and is evidently less susceptible to sub-micromolar levels of hydrogen peroxide than the ISC system [26]. Such environmental cues in the human system could be relayed to the assembly complex through FXN; oxidative stress has previously been shown to modify FXN (and likely

decrease activation of the SDUF complex) [77] and oxidizing conditions have been shown to decrease SDUF complex formation and FXN based activation [96]. In these cases, it appears that FXN functions not only as an activator but also as a pace-keeper for Fe-S cluster assembly in response to environmental cues. Therefore, if FXN is involved in regulating the level of Fe-S cluster biosynthesis, therapeutic strategies that focus on bypassing the need for FXN activation of the SDU complex would also bypass a mechanism that evolution has put in place to control both the activity and the environmental responsiveness of the Fe-S assembly complex.

In summary, the results presented here determine that the frataxin bypass mechanism exhibited by the M106I-ISCU2 suppressor mutant in yeast occurs at the level of the sulfur transfer reaction from NFS1 to ISCU2. The M106I mutation likely stabilizes a conformation of ISCU2 that is favored when FXN binds to the SDU complex thereby bypassing the FXN requirement and stimulating the rate of the sulfur transfer reaction (Figure 5-8). Future experiments will be aimed at refining our model for the FXN based activation of the SDU complex: testing how the M106I variant stabilizes the preferred sulfur transfer conformation of ISCU2 and how the SDU, SDUF, and SDU_{M106I} complexes facilitate Fe-S cluster transfer reactions to apo-acceptor proteins.

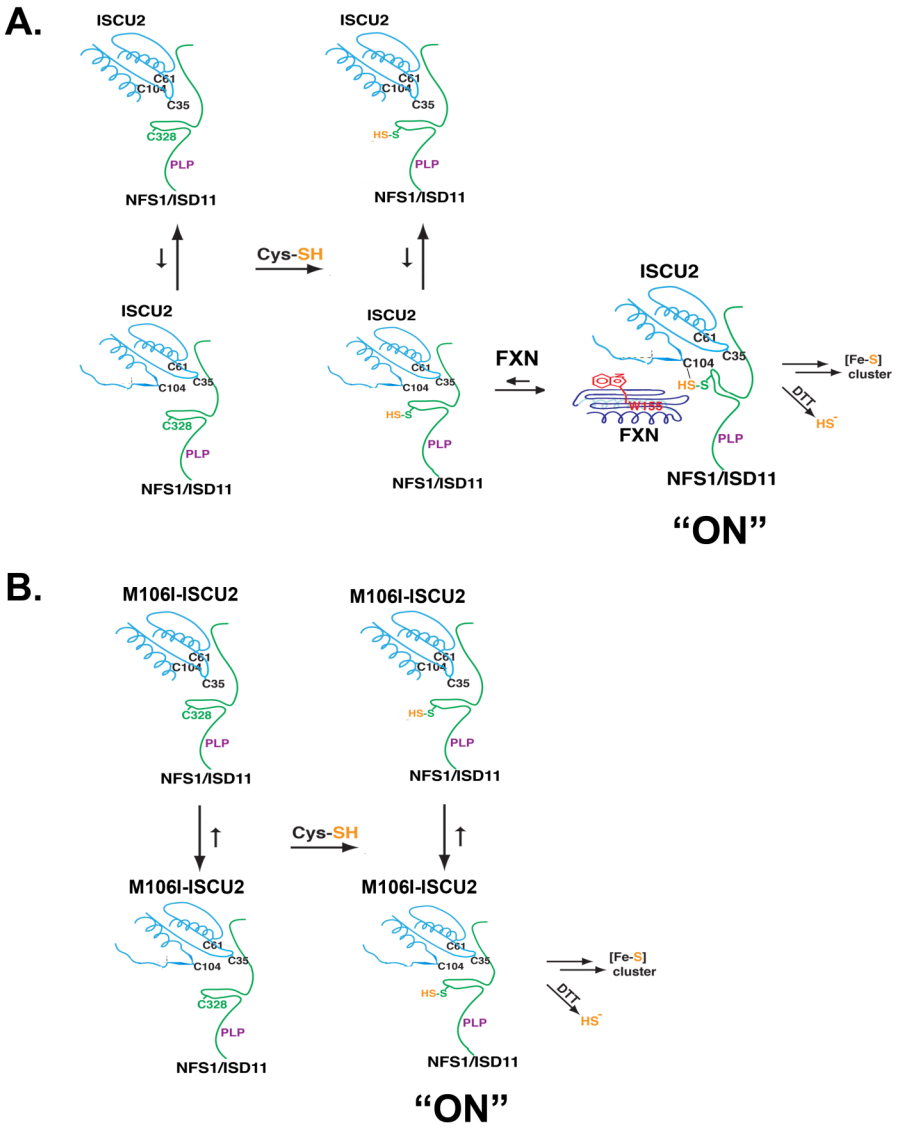

Figure 5-8. The M106I variant bypasses the need for FXN activation. (A) In the absence of FXN, the SDU complex exists in 2 states with the helical state being favored. Frataxin binding stabilizes the coiled conformation of ISCU2 exposing C104 to accept the persulfide sulfur from NFS1 and thereby accelerates the rate of the sulfur transfer reaction and Fe-S cluster assembly. (B) The M106I mutation stabilizes the preferred sulfur transfer conformation of ISCU2 and bypasses the need for FXN activation.

CHAPTER VI

HISTIDINE 103 ON ISCU2 IS IMPORTANT FOR FRATAXIN INTERACTION WITH THE SDU COMPLEX

INTRODUCTION

The human ISCU2 protein serves as a scaffold for the assembly of Fe-S clusters prior to their delivery to biological targets and both the structure and function have been remarkably conserved throughout evolution. The three highly conserved cysteine residues (C35, C61, and C104 in human numbering) are universally agreed to be critical for Fe-S cluster biosynthesis (Figure 6-1). These cysteines have been proposed to be Fe-S ligands along with either H103 [105, 106], C96 [107], or conserved cysteines from a second ISCU2 molecule in a dimeric assembly [108, 111]. The Vickery group showed that the *E. coli* H105A (equivalent of human ISCU2 H103) and native IscU have highly similar Fe-S dependent CD spectral properties, which suggests that H105 is not required for ligation of a chemically reconstituted Fe-S cluster [111]. Notably, residue H103 is conserved in organisms with a frataxin and is replaced with a positively charged lysine in gram positive and thermophilic bacteria, which do not appear to have a frataxin homolog.

Frataxin (FXN) is a conserved mitochondrial protein that interacts with the core components of the Fe-S cluster biosynthetic machinery and forms a multi-subunit complex, SDUF, composed of the cysteine desulfurase protein NFS1, NFS1's protein partner ISD11, and the scaffold protein ISCU2 [79, 82, 96]. Previous data indicated that

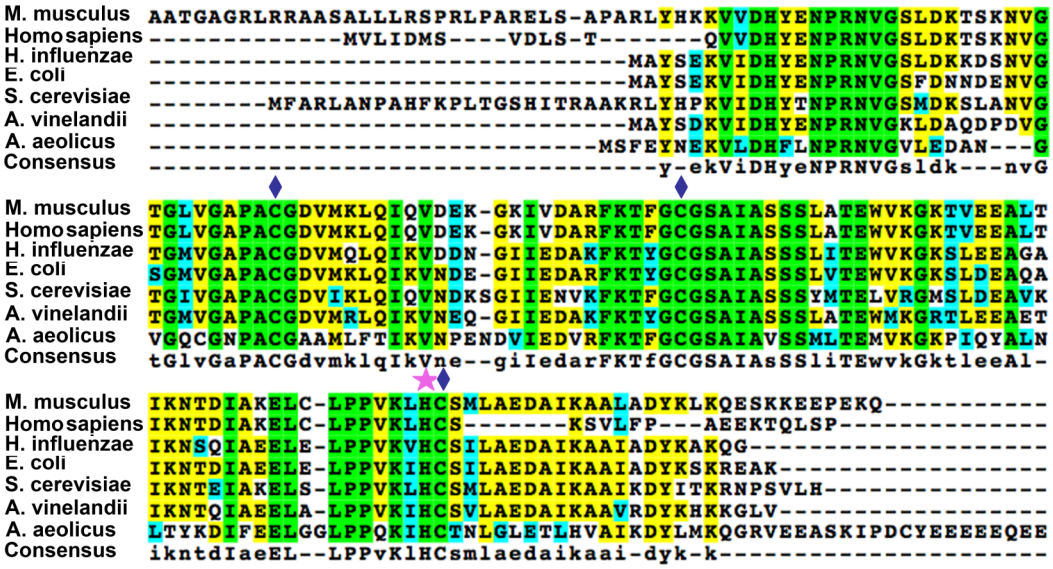

Figure 6-1. Sequence alignment of ISCU2 proteins from *M. musculus, Homo sapiens, H. influenzae, E. coli, S. cerevisiae, A. vinelandii, and A. aeolicus*. The three conserved cysteine residues (C35, C61, and C104 in human numbering) are denoted with a blue diamond and H103 residue is indicated with a pink star. H103 is 2 residues away from K101 of the LPPVK chaperone interaction motif.

FXN binding to the SDU complex dramatically changed the catalytic efficiency (k_{cat} /K_M) of the cysteine desulfurase from 25 to 7900 $M^{-1}sec^{-1}$ and resulted in a 25-fold increase in the rate of Fe-S cluster biosynthesis [96]. Subsequent studies investigating the impact of substituting Friedreich's ataxia (FRDA) clinical variants for the native FXN on the rates of the cysteine desulfurase and Fe-S cluster assembly reactions revealed that these variants were compromised in their binding affinity for the SDU complex and also in their abilities to facilitate sulfur transfer from NFS1 to ISCU2 [189, 198]. Additionally, structural studies of the clinical variants suggested rotation of the

only completely conserved FXN residue W155 into a solvent filled cavity on the surface of the protein correlated with the ability of FXN to function as an allosteric activator for the SDU complex (Figure 6-2A) [189, 198]. In the native FXN crystal structure, W155 is stacked above the positive charge contributed by residue R165 (Figure 6-2A) [198]. Consistent with this hypothesis, the crystal structure of the FRDA clinical R165C FXN variant revealed W155 in the proposed rotated conformation (Figure 6-2A) and while the mutant bound the SDU complex ~150 times weaker than native FXN, the k_{cat}/K_M for the cysteine desulfurase was nearly equivalent to that of the wild-type SDUF complex [198].

We previously hypothesized that an important component for FXN interactions with the SDU complex is the rotated W155 conformation, which allows hydrophobic or π-stacking interactions of the W155 indole ring of W155 that are not possible in the native conformation of FXN [189, 198]. We identified ISCU2 residue H103 as a candidate for interactions with this rotated conformation of FXN due to its conservation and its proximity to residue C104 that is implicated as the primary sulfur acceptor residue (Chapter IV) during catalysis (Figure 6-2B). H103 might interact with FXN either through π-stacking interactions with the indole ring of W155 or by replacing lost interactions due to rotation of W155, thereby inserting itself into the native W155 position and forming cation-π interactions with FXN residue R165. Here, we show that mutation of ISCU2 H103 to alanine or lysine diminishes FXN binding affinity for the SDU complex ~225 and ~425 fold respectively. Remarkably, a compensating mutation for the H103K-ISCU2 variant was created by mutation of FXN residue R165 to

histidine, which may remove the incompatible positive charge and provide a cation-π interaction in the $SDU_{H103K}F_{R165H}$ complex.

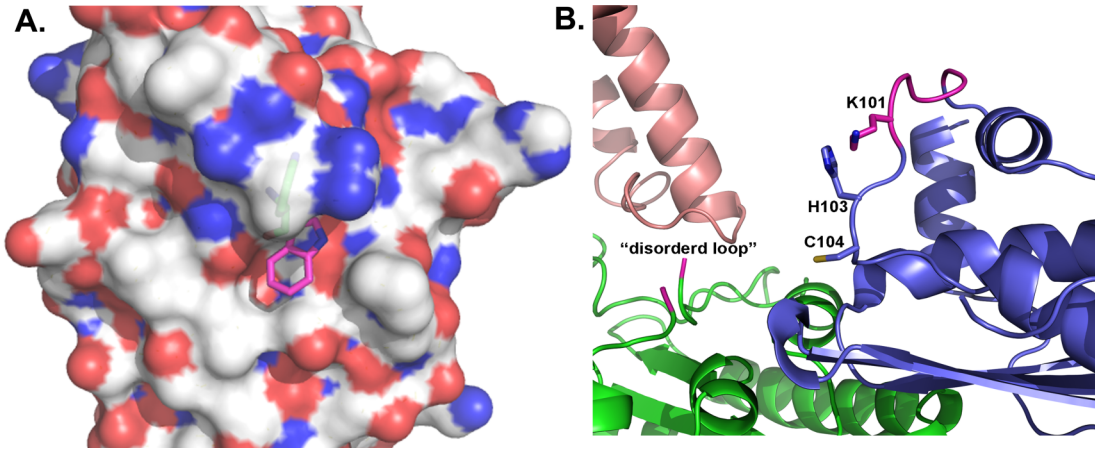

Figure 6-2. Model for proposed interactions between FXN and the SDU Complex. (A) Native FXN crystal structure (3S4M) overlaid with W155 (pink) from the R165C-FXN crystal structure (3T3X) rotated into the solvent exposed region on the surface of FXN. W155 in the wt-FXN crystal structure is shown in green stacked between the positive charges contributed by R165 and Q148. (B) Model of the SDU protein complex with ISCU2 in the coiled conformation (3LVL and 2Z7E). H103 and C104 residues on ISCU2 are shown in blue sticks and the LPPVK motif is highlighted in pink. Our model suggests that the H103 ISCU2 residue will replace lost interactions of W155 with R165 and Q148 upon rotation into the solvent filled pocket on the surface of FXN or form π-stacking interactions with the indole ring of W155.

EXPERIMENTAL PROCEDURES

Protein preparation. The QuikChange method (Stratagene) was used to introduce point mutants (H103A and H103K) into a pET11a vector containing the human ISCU2 gene or the point mutant (R165H) into a pET11a vector containing human FXN (Δ1-55). After DNA sequencing confirmed the mutation sites, H103A ISCU2, H103K ISCU2, and R165H FXN were individually transformed into *E. coli* strain BL21 (DE3) cells and grown at 37°C until an OD_{600} of 0.6. Expression was induced with 0.5 mM IPTG and left at 16°C for 16 hours. Both ISCU2 variants and R165H FXN were purified as previously described for wild-type ISCU2 and FXN [96].

Cysteine Desulfurase Activity of ISCU2 Variants. A previously described assay to detect methylene blue formation was employed to determine the rate of sulfide production of the SDU complex as a function of added ISCU2 variant (34). For the titration reactions, assay mixtures contained 0.5 μM SD, 2 mM DTT, 10 μM PLP, 50 mM Tris pH 8.0, and 250 mM NaCl. The number of equivalents that saturated the cysteine desulfurase activity of SD was found to be 10 for H103A ISCU2 and 3 for H103K ISCU2. Further titrations were performed to determine the saturating amount of FXN required to maximize the activity of the SDU_{H103A} complex and the SDU_{H103K} complex. Titration experiments indicated 300 and 600 equiv of FXN were required to maximize the cysteine desulfurase activity of the SDU_{H103A} and SDU_{H103K} complexes respectively.

Cysteine Desulfurase Activity of R165H FXN. The methylene blue assay was used to evaluate the rate of sulfide production for the SDU and SDU_{H103K} complexes as a

function of added FXN variant R165H. The standard assay mixture composed of 0.5 μM SD, 2 mM DTT, 10 μM PLP, 50 mM Tris pH 8.0, 250 mM NaCl, and 5 μM $Fe(NH_4)_2(SO_4)_2$ was incubated for 30 minutes in the glovebox prior to the addition of 100 μM cysteine. Assay mixtures additionally contained either 1.5 μM wild-type ISCU2 or 1.5 μM ISCU2 variant H103K. Titration experiments indicated 80 and 10 equiv of the R165H FXN variant were required to maximize the cysteine desulfurase activity of the SDU and SDU_{H103K} complexes, respectively.

Michaelis Menten Kinetics. The standard assay mixture [96] that contained 0.5 μM SD was combined with 1.5 μM ISCU2 and 1.5 μM FXN (SDUF), or 5 μM H103A-ISCU2 and 150 μM FXN, or 1.5 μM H103K-ISCU2 and 300 μM FXN, or 1.5 μM ISCU2 and 40 μM R165H Fxn, or 1.5 μM H103K-ISCU2 and 5 μM R165H FXN. Reaction rates as a function of cysteine concentration (12.5-1.0 mM) were fit to the Michaelis-Menten equation using KaleidaGraph (Synergy Software).

Binding Constant Measurements. Binding constants for wild-type FXN to the to the SDU_{H103A} and SDU_{H103K} and for R165H FXN to SDU and SDU_{H103K} complexes were determined as previously described [189, 198]. Reaction rates as a function of cysteine concentration were fit to the Michaelis-Menten equation using Kaleidagraph. The k_{cat} was also measured as a function of FXN concentration and used to determine the FXN binding constant for the SDU complex. In short, a kinetic equation was derived to define the K_d based on the concentrations of SDU, FXN, and SDUF (equation 6-1), where $[SDU]_{total}$ represents the total amount of enzyme partitioned between SDU and

SDUF forms of the enzyme.

$$K_d = \frac{([FXN]_{total} - [SDUF])([SDU]_{total} - [SDUF])}{[SDUF]} \qquad (6\text{-}1)$$

Multiplying both sides of equation 6-1 by [SDUF] results in equation 6-2:

$$K_d[SDUF] - (([FXN] - [SDUF])([SDU]_{total} - [SDUF])) = 0 \qquad (6\text{-}2)$$

which can be rearranged to yield equation 6-3:

$$\begin{aligned} &-[SDUF]^2 + ([SDU]_{total} + [FXN] + K_d)[SDUF] \\ &-(([SDU]_{total})(FXN)) = 0 \end{aligned} \qquad (6\text{-}3)$$

Equation 6-3, a quadratic equation, can be solved in terms of [SDUF] to yield equation 6-4:

$$\begin{aligned} [SDUF] &= \frac{b - \sqrt{b^2 - 4ac}}{2} \\ a &= 1 \\ b &= [SDU]_{total} + [FXN]_{total} + K_d \\ c &= [SDU]_{total}[FXN]_{total} \end{aligned} \qquad (6\text{-}4)$$

The measured k_{obs} can be expressed as equation 6-5:

$$k_{obs}([SDUF]+[SDU]) = k_{SDU}[SDU] + k_{SDUF}^{\infty}[SDUF] \qquad (6\text{-}5)$$

where k_{SDU} is the k_{cat} in the absence of Fxn, and k_{SDUF}^{∞} is the k_{cat} with saturated amounts of FXN. Solving equation 6-5 for k_{obs} yields equation 6-6:

$$k_{obs} = \frac{k_{SDU}([SDU]_{total} - [SDUF]) + k_{SDUF}^{\infty}[SDUF]}{[SDU]_{total}} \qquad (6\text{-}6)$$

which can be expressed alternatively using equation 6-7:

$$[SDU]_{total} = [SDU] + [SDUF] \qquad (6\text{-}7)$$

as equation 6-8:

$$k_{obs} = \frac{k_{SDU}([SDU]_{total} - [SDUF]) + k_{SDUF}^{\infty}[SDUF]}{[SDU]_{total}} \qquad (6\text{-}8)$$

In equation 6-8, [SDUF] is calculated as shown by equation 6-4 and a plot of k_{obs} versus FXN concentration allows K_d determination.

RESULTS

Protein complex stoichiometries for activity measurements. Here, the cysteine desulfurase activity of the NFS1-ISD11 (SD) was measured as a function of added native ISCU2, plus H103A and H103K variants. The cysteine desulfurase activity of SD was minimized with the addition of 3 equivalents of ISCU2 (Figure 6-3A), consistent with published results [96]. Unlike native ISCU2, the cysteine desulfurase activity

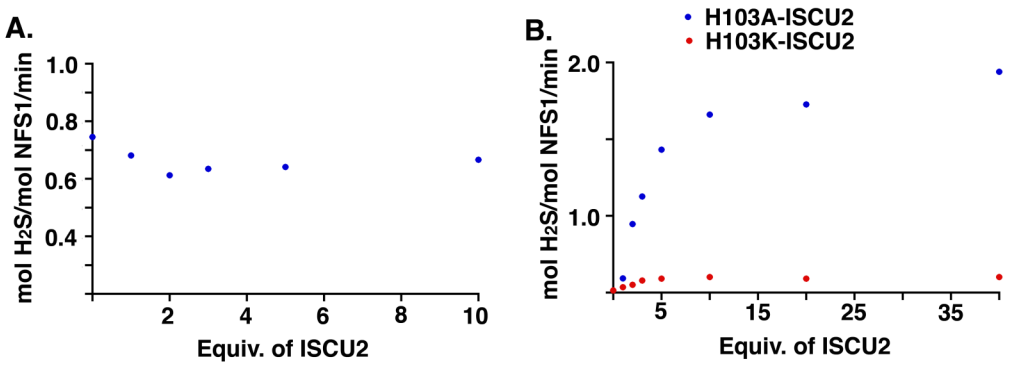

Figure 6-3. Titration of ISCU2 and ISCU2 variants to SD. (A.) Cysteine desulfurase activity of SD as a function of added ISCU2. (B.) Cysteine desulfurase activity as a function of added H103A-ISCU2 (blue) and H103K-ISCU2 (red).

increased as a function of added H103 ISCU2 variants and maximized with the addition of 10 equivalents of H103A and 3 equivalents of H103K (Figure 6-3B). Previous data indicated 3 equivalents of FXN were required to achieve maximal stimulation of the

cysteine desulfurase activity. This was previously interpreted as favoring formation of the SDUF complex and a conformation that facilitates sulfur transfer from NFS1 to ISCU2 (Figure 6-4A) [96]. FXN titrations of SDU_{H103A} and SDU_{H103K} complexes revealed 300 and 600 equiv respectively were necessary to achieve maximum stimulation (Figure 6-4B and Figure 6-4C).

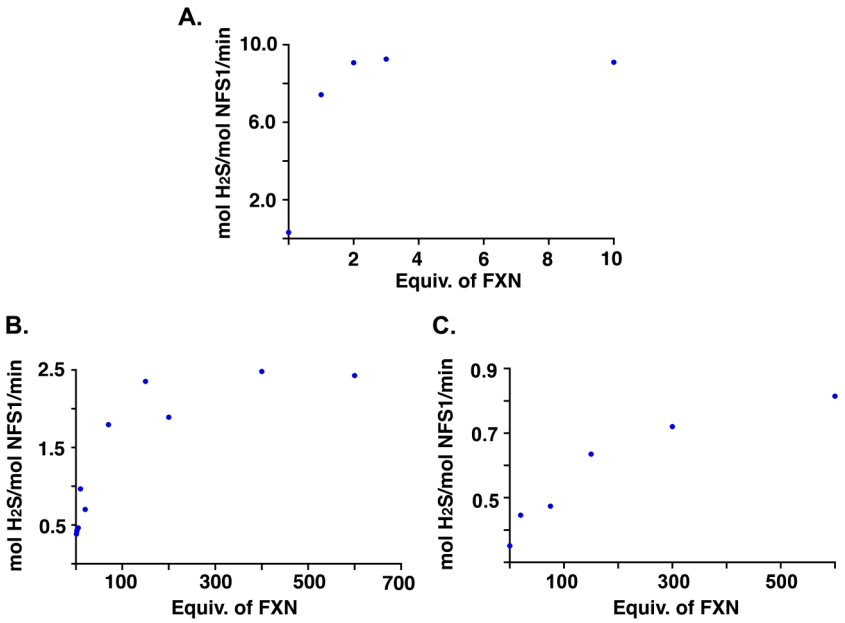

Figure 6-4. Titration of FXN to SDU, SD(H103A-ISCU2), and SD(H103K-ISCU2) complexes. (A.) Cysteine desulfurase activity of SDU as a function of added FXN. (B.) Cysteine desulfurase activity of SD(H103A-ISCU2) as a function of added FXN. (C.) Cysteine desulfurase activity of SD(H103K-ISCU2) as a function of added FXN.

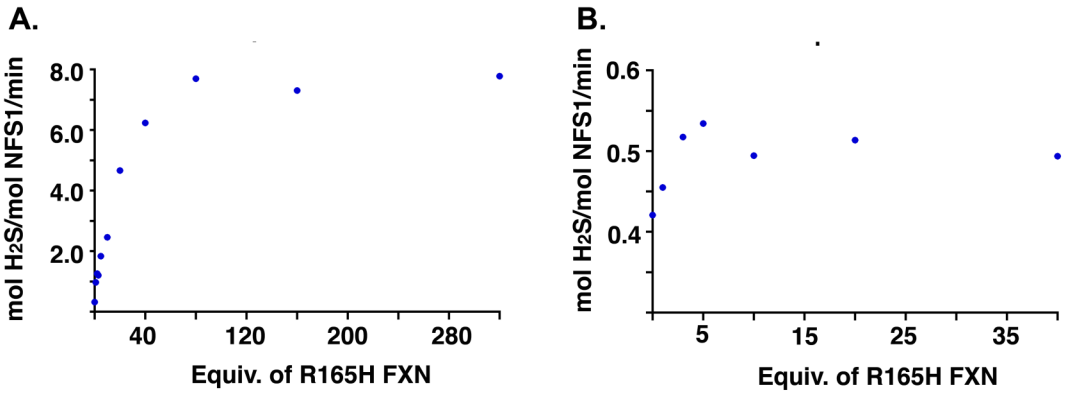

Figure 6-5. Titration of R165H FXN to SDU and SD(H103K-ISCU2) complexes. (A.) Cysteine desulfurase activity of SDU as a function of added R165H FXN. (B.) Cysteine desulfurase activity of SD(H103K-ISCU2) as a function of added R165H FXN.

Table 6-1. Kinetic Parameters for H103 ISCU2 and/or R165H FXN Variant Complexes

Complex	k_{cat} (min^{-1})	K_M^{Cys} (mM)	k_{cat}/K_M ($M^{-1}s^{-1}$)
SDU	0.8 ± 0.1	0.052 ± 0.014	260 ± 70
SDUF	10.7 ± 0.8	0.019 ± 0.006	9200 ± 3000
SD + H103A ISCU2 + FXN	4.2 ± 0.2	0.011 ± 0.002	6200 ± 1300
SD + H103K ISCU2 + FXN	0.9 ± 0.1	0.008 ± 0.002	1800 ± 500
SD + H103K ISCU2 + R165H FXN	0.9 ± 0.1	0.030 ± 0.010	510 ± 170
SDU + R165H FXN	6.8 ± 0.3	0.009 ± 0.003	12100 ± 3500

Additional titrations revealed that 80 (Figure 6-5A) and 10 (Figure 6-5B) equiv of R165H FXN were required to maximally stimulate the cysteine desulfurase activity of the native SDU and variant SDU_{H103K} complexes respectively.*Kinetic Parameters for Assembly Complexes Substituted with H103-ISCU2 Variants and/or R165H FXN.* Next, the Michaelis Menten kinetic parameters were determined for the native SDU, SDUF, $SDU_{H103A}F$, $SDU_{H103K}F$, $SDU_{H103K}F_{R165H}$, and $SDUF_{R165H}$ complex under saturating stoichiometry conditions (see above) that compensates for weaker binding (Table 6-1). The replacement of H103 with alanine on ISCU2 decreased the k_{cat}/K_M ~1.5 fold whereas replacement of H103 with lysine decreased the k_{cat}/K_M ~ 5 fold. The use of R165H FXN instead of native FXN did not relieve the depressed k_{cat}/K_M measured for the complex with the H103K ISCU2 variant, while the native SDU complex with R165H FXN resulted in a slightly elevated k_{cat}/K_M of 12100 ± 3500.

Binding Constant Determination for FXN and R165H FXN Binding to Native SDU and SD-H103 ISCU2 Variant Complexes.

We hypothesize that H103 on ISCU2 interacts with FXN by inserting between FXN residues R165 and Q148 in the SDUF complex. To test this hypothesis, binding of FXN variants to SDU complexes with different ISCU2 variants were determined by fitting k_{cat} at different concentrations of added FXN, as previously described for FRDA FXN variants [198]. Native FXN binds to the SDU complex with a binding constant (K_d) of 0.07 μM [159]. Similarly, we determined the FXN binding affinity to decreased ~225-425 fold with measured values of 15.7 ± 4.2 μM and 29.8 ± 10.9 μM for the SDU_{H103A} and SDU_{H103K} complexes respectively (Table 6-2 and Figure 6-6A and 6-6B). Next, the FXN variant R165H binding affinity to the native SDU and variant SDU_{H103K} complexes were determined (Figure 6-6C and Figure 6-6D). The R165H FXN variant bound weaker to the native SDU complex, exhibiting a K_d of 3.7 ± 0.7 (Table 6-2). In contrast, the R165H FXN variant bound 70 times tighter to the SDU_{H103K} complex than native FXN with a measured K_d of 0.42 ± 0.17 μM (Table 6-2).

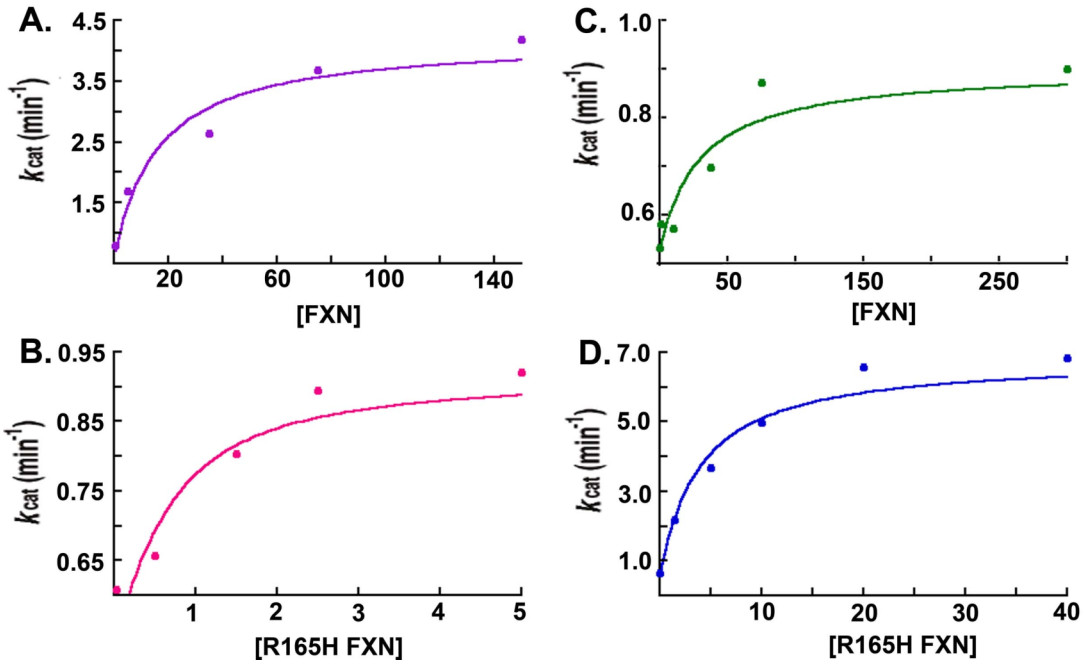

Figure 6-6. Determination of binding constants for FXN and R165H FXN. k_{cat} was determined at different FXN concentrations The lines through the data are the fits as a type II allosteric activator to eq 1. (A) FXN binding to SD + H103A ISCU2 (R^2 value = 0.94), (B) FXN binding to SD + H103K ISCU2 (R^2 value = 0.89), (C) R165H FXN binding to SD + H103K ISCU2 (R^2 value = 0.89), and (D) R165H FXN binding to SDU (R^2 value = 0.97).

Table 6-2. Binding Constants for FXN and R165H FXN to SDU Complexes

Complex	FXN K_d (μM)
SDU + FXN	0.07 ± 0.04
SD + H103A ISCU2 + FXN	15.7 ± 4.2
SD + H103K ISCU2 + FXN	29.8 ± 10.9
SD + H103K ISCU2 + R165H FXN	0.42 ± 0.17
SDU + R165H FXN	3.7 ± 0.7

DISCUSSION

The FXN protein fold encompasses parallel N- and C-terminal α-helices and a flat β-sheet platform. A majority of the FRDA FXN point mutations occur on the β-sheet, and these residues area also implicated in forming interactions with protein components of the SDU complex [78, 79, 81, 82, 85, 113]. W155, which is the only completely conserved residue in FXN, is located in a positively charged region of the β-sheet structure and is sandwiched between residues R165 and Q148 [189, 198]. Previous structural studies on FXN FRDA variants W155F, W155R, and R165C revealed an energetically favorable rotamer in which residue 155 underwent a conformational change to fill a pocket on the surface of the protein [189, 198]. This conformational change would introduce opportunities for protein-protein contacts mediated by the W155 indole ring via hydrophobic, π-π, or cation-π interactions [189, 198].

FXN residue R165 is an important contributor to FXN binding as its mutation to cysteine results in a ~150 fold decrease in binding affinity [198]. Arginine is one of the most common protein-protein interface residues due to its capacity to form hydrogen bonds, favorably contribute to the hydrophobic effect, and its ability to participate in cation-π interactions [199]. Cation-π interactions are calculated to be more stable than salt-bridge interactions and also not attenuated by the influence of water [199, 200]. Arginine cation-π interactions are estimated to contribute 3.3 kcal/mol of free energy in favor of forming protein complexes and are thought to impose specificity in protein-protein association [199, 200].

Here we investigated a well-conserved ISCU2 protein residue H103 to

understand its role in complex formation. A titration of H103A and H103K ISCU2 variants to SD revealed that either 10 or 3 equivalents of ISCU2 respectively were required to maximally stimulate the cysteine desulfurase reaction and thus replacement of H103 with either alanine or lysine did not appear to greatly affect the binding affinity of ISCU2 for the SD protein complex. Unlike with the native SDU complex that has slightly decreased cysteine desulfurase activity relative to SD, the H103 variant complexes have increased activity. In the cysteine desulfurase assay, DTT is used to cleave persulfidic species and release sulfide into solution, this free sulfide is detected after its reaction with DPD and $FeCl_3$ and therefore any residue replacement that increases the accessibility of DTT to the persulfide will result in an increase in the cysteine desulfurase rate and may explain the observed results. A second titration of FXN to the SDU_{H103} variant complexes revealed that 300 and 600 equivalents of FXN respectively were required to maximally stimulate the rate of the cysteine desulfurase reaction; these values are 100-200 fold higher than that required for the native SDU complex and suggest substantial perturbation of the native FXN interaction. Subsequent measurements of FXN binding constants to the H103 variant SDU complexes revealed substantial changes in affinity indicating H103 is involved in mediating FXN interactions. Specifically mutation of H103 to alanine resulted in a 224-fold decrease in FXN affinity for the SDU complex, which suggested either a non-polar substitution, or loss of the imidiazole side chain resulted in the decreased affinity. Next, H103 was mutated to lysine to test if H103 was interacting with FXN residue R165 through cation-π interactions; this replacement resulted in an even more unfavorable FXN binding

environment with a 426-fold decrease in FXN binding affinity. Interestingly, the replacement of residue H103 with lysine appears in gram- positive and thermophilic bacteria and based on sequence alignments, these organisms don't appear to have a FXN homolog [105, 201]. As well, gram-positive bacteria possess only a SUF system for the biogenesis of Fe-S clusters [202]. This may explain the decreased ability of FXN to stimulate the cysteine desulfurase activity of SDU_{H103K} as it is not found in organisms that have this ISCU2 point mutation whereas FXN stimulates both the native SDU and SDU_{H103A} complex activities.

Mutation of the ISCU2 H103 residue to lysine was accompanied by a significant decrease in FXN binding affinity presumably due to the positive charge of lysine being incompatible with the positively charged pocket produced with rotation of FXN residue W155. To test this theory, the R165H point mutation was introduced into FXN to remove the positive charge contributed by R165 and create a possible cation-π interaction between FXN R165H and the H103K ISCU2 variant (Figure 6-7). Lysine residues account for 20 percent of cation-π interactions found in homodimers and protein complex interfaces which is less often than arginine due to its exclusion from protein complex interfaces [199]. The R165H-FXN variant bound the SDU_{H103K} complex 70 times tighter than native FXN. The drastic change in binding affinity of the R165H FXN variant for the SDU_{H103K} complex revealed a favorable binding interaction had been created although the low activity of $SDU_{H103K}F$ complex was not rescued. Previous data from the Cowan lab showed the *in vitro* reconstitution of a human ISCU2 double mutant H103A/D39A in the presence of *T. maritima* NifS, cysteine, frataxin, and

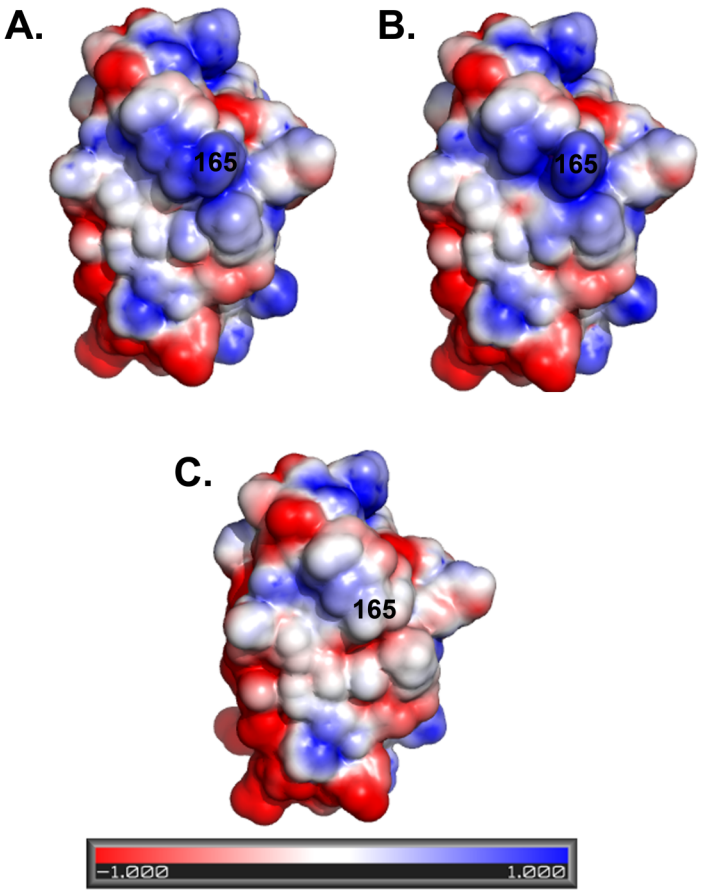

Figure 6-7. Elecrostatic potential surfaces of (A) wt-FXN, (B) wt-FXN with rotated W155, and (C) R165H FXN as calculated by PBEQ Solver, CHARMM-GUI.

ferrous iron was ~17 times slower than that of the D39A mutant (a mutant previously shown to more stably bind a 2Fe-2S cluster [120]), and accordingly, the reconstitution of H103D/D39A ISCU2 mutant was only slightly slower than D39A [105]. This data was accompanied by FXN binding constants of 10.4 ± 0.3 μM and 4.7 ± 0. 9 μM for the

H103A/D39A and H103D/D39A mutant respectively [105]. The binding constant of FXN to the H103A/D39A mutant is comparable to our measured FXN binding constant to the SD(H103A-ISCU2) complex of 15.7 ± 4.2 μM and the tighter binding of the H103D/D39A ISCU2 mutant fits our model as aspartate would be expected form a more favorable interaction with residues R165 of FXN than lysine or alanine.

We have previously identified residue C104 on ISCU2 as the primary sulfur acceptor residue from NFS1, C104 is on a surface exposed C-terminal alpha helix close to the chaperone binding LPPVK motif and one amino acid away from H103. Based on the results presented here, we propose a model for the FXN based activation of the SDU complex cysteine desulfurase activity (Figure 6-8). NMR data from the Markley lab suggests two distinct conformations of the *E. coli* scaffold protein that interconvert on the millisecond time scale; we suggest these two states correspond to one in which the C-terminal helix housing C104 is helical and one that is coiled. In order for C104 to accept the persulfide sulfur from NFS1, ISCU2 must be in the coiled conformation. When FXN binds to the SDU complex, it stabilizes the coiled ISCU2 conformation and stimulates the rate of the cysteine desulfurase by exposing C104 to participate in the sulfur transfer reaction. FXN binding is accomplished by rotation of W155 out of the positively charged pocket formed and corresponding insertion of H103 from ISCU2 to replace the lost cation-π interactions (Figure 6-8). Future experiments will be aimed at further defining the different conformational states of ISCU2 and continuing to identify and characterize residues on both FXN and ISCU2 involved in binding and activation of the cysteine desulfurase and Fe-S cluster assembly reactions.

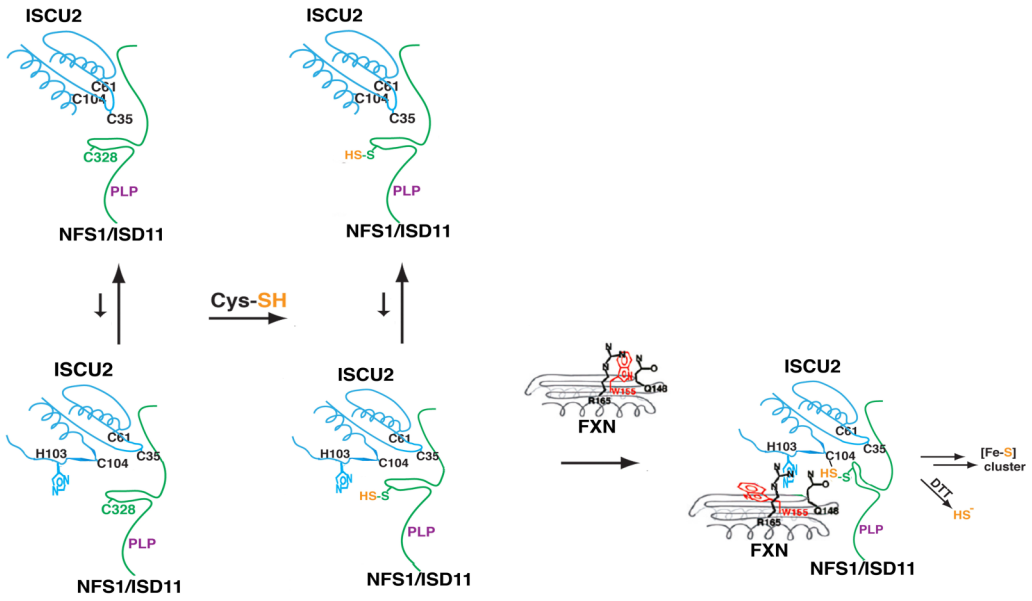

Figure 6-8. Proposed model for the activation of the SDU complex by FXN. FXN binding to the SDU complex is accompanied by rotation of W155 into a solvent filled region on the surface of FXN and concomitant insertion of ISCU2 H103 into the native W155 position. FXN binding stabilizes the coiled conformation of ISCU2 exposing C104 to accept the persulfide sulfur from NFS1 thereby stimulating the rate of the cysteine desulfurase.

CHAPTER VII

DIRECT EVIDENCE THAT THE FRIEDREICH'S ATAXIA PROTEIN FRATAXIN MEDIATES SULFUR TRANSFER IN THE HUMAN FE-S CLUSTER ASSEMBLY COMPLEX

INTRODUCTION

Reduced levels of the human mitochondrial protein frataxin (FXN) leads to decreased levels of Fe-S cluster containing proteins [44], increased iron levels in the mitochondria [42, 43], and increased susceptibility to oxidative stress [46]. Additionally, reduced levels of FXN are associated with an autosomal recessive neurodegenerative disease Friedreich's ataxia (FRDA) [113, 162]. While the majority of FRDA patients are homozygous for a GAA repeat found on the first intron of the *FXN* gene, approximately 2% of patients are heterozygous with a GAA repeat on one allele and one of 15 known missense mutations on the other allele [113, 162]. Importantly, the GAA trinucleotide repeat leads to an abnormal conformation of the DNA and correspondingly lower levels of expressed FXN protein [113]. Many roles for FXN have been suggested to account for the phenotype in FRDA patients; FXN has been proposed to function in iron storage [47-51], in oxidative stress control [52], as an iron chaperone for both heme [58] and iron sulfur cluster biosynthesis [53-57], as a switch diverting iron between metabolic pathways [59], and lastly as an iron sensor [60].

Recent *in vitro* biochemical experiments support a functional role of human FXN as an allosteric activator of the multi-subunit Fe-S cluster biosynthetic complex, SDU,

composed of the cysteine desulfurase protein NFS1, the co-chaperone ISD11, and the scaffold protein ISCU2 [96]. FXN binding to the complex is correlated with an increase of the catalytic efficiency (k_{cat}/K_M) of the cysteine desulfurase and a corresponding increase in the rate of Fe-S cluster assembly on ISCU2 [96]. Subsequent studies on FXN variants identified in FRDA patients revealed compromised biochemical functions; that included decreased binding affinity for the SDU complex and decreased ability of FRDA variants to stimulate the rates of both the cysteine desulfurase and Fe-S cluster formation reactions [189, 198]. Mutational and radiolabeling studies (Chapter IV) together with published biochemical [96, 189, 198] suggest this activity stimulation results from FXN binding to the SDU complex and facilitating sulfur transfer from NFS1 to ISCU2. However, it has not been established that this incorporated sulfur is viable in forming a Fe-S cluster, which is critical for understanding the mechanism of Fe-S assembly.

The mechanism of Fe-S cluster formation still remains unknown and controversial and is best studied in bacterial systems. Two possible Fe-S cluster assembly mechanisms have been proposed; the first proposed mechanism is called the iron-first model and requires that ferrous iron binding to the cluster forming residues is the first step in the biosynthetic process and is followed by sulfane sulfur transfer from the cysteine desulfurase and the subsequent 4 electron reduction of the sulfane sulfur atoms; 2 of which are contributed from the ferrous iron atoms and 2 of which come from an external source [99]. The second proposed mechanism is the sulfur–first mechanism and requires that the first step in cluster assembly is sulfur transfer from NFS1 to the

cluster forming residues on ISCU2 and this is followed by ferrous iron binding and sequential 2-electron reduction of each sulfane sulfur atom [99]. Current data available in support of the Fe-first mechanism for cluster formation on the scaffold protein is μM binding constants for ferrous and ferric iron to the *Thermotoga maritima* IscU [101]. Conversely, incubation of the prokaryotic IscS with IscU in the absence of DTT results in a persulfide-bound or polysulfide-bound IscU and provides experimental evidence for the sulfur first mechanism [103, 183]. Additionally, SufSE incubation with SufA and cysteine results in sulfurated SufA that can be combined with ^{57}Fe, and DTT to yield both [4Fe-4S] and [2Fe-2S] clusters determined by Mössbauer [104]. Unfortunately as the *E. coli* scaffold or the *A. vinelandii* scaffold have never been shown to bind ferrous iron and neither the persulfide-bound or polysulfide-bound forms of IscU have been shown to be viable in cluster formation [103], the Fe-S cluster assembly mechanism has yet to be resolved.

Here, the ability of frataxin and frataxin variants to affect the sulfur transfer reaction from NFS1 to ISCU2 was directly investigated. Additionally, the mechanism of cluster formation on ISCU was probed using a radio-labeled substrate and tracing its progress from NFS1 to ISCU2 and finally to ferredoxin (FDX). These studies provide direct evidence that frataxin binds to the SDU complex and facilitates the sulfur transfer reaction thereby increasing the rate of cluster assembly on ISCU2. Furthermore, these studies show the persulfide formed on ISCU2 in the sulfur transfer reaction is viable and eventually ends up in an Fe-S cluster on an apo-target protein in a mechanism that isconsistent with the proposed sulfur-first mechanism.

EXPERIMENTAL PROCEDURES

Protein Preparation. FRDA variants, FXN, SD complex, and ISCU2 were purified as previously described [96]. FRDA variants, FXN, and ISCU2 were transformed into BL21 (DE3) cells and at grown at 37 ^{o}C. When the cells reached an OD_{600} of ~0.6, the temperature was reduced to 16 ^{o}C and protein expression was induced with 0.5 mM IPTG. FRDA variants and FXN were further purifed by anion exchange and gel filtration columns. ISCU2 was further purifed by anion exchange (protein was in the flow through fractions), cation exchange, and gel filtration columns. Human NFS1 (Δ1-55) and ISD11 were coexpressed in *E. coli* strain BL21 (DE3). After a 16-hour protein expression at 16^{o}C and cell lysis by french press, nickel, cation, and S300 gel filtration columns were used to anaerobically purify the SD protein complex. Ferredoxin was purified as previously described by Kakuta *et a*l.; human ferredoxin was transformed into *E. coli* BL21 (DE3) cells and grown at 37ºC until an OD_{600} of 0.6. Expression was induced with 0.4 mM IPTG, 1 mM cysteine, and 0.1 mg/mL ferric ammonium citrate for 16 hours at 37ºC. After lysis by sonication, the supernatant was loaded onto an anion exchange column (26/20 POROS 50HQ, Applied Biosystems) and eluted with a linear gradient from 0 to 1000 mM NaCl in 50 mM Tris pH 7.5. Fractions containing ferredoxin were further purifed on a Sephacryl S100 (26/60, GE Healthcare) size exclusion column equilibrated in 50 mM Tris, pH 7.4, 50 mM NaCl.

Apo-Ferredoxin Preparation. Apo-ferredoxin was prepared as previously described; protein was precipitated with 10% trichloroacetic acid and incubated on ice for 10 minutes with 10 mM DTT [203]. After incubation, the sample was centrifuged

for 10 minutes at 10,000 rpm and 4°C [203]. Following centrifugation, the supernatant was discarded and the pellet was rinsed twice with water and then re-suspended anaerobically in 50 mM Tris pH=8.0, 250 mM NaCl [203].

SDS-PAGE Analysis of Sulfur Transfer. Reaction mixtures (30 μL) included 3 μM SD, 50 mM Tris (pH 8.0) and 250 mM NaCl. For the FRDA variant gel, reaction mixtures additionally included 9 μM ISCU2 and 9 μM FXN or FRDA variant. For the gel comparing sulfur transfer in the SDU and SDUF protein complexes, reaction mixtures additionally included 9-120 μM ISCU2 with or without 9 μM FXN. For each gel, the samples were incubated in the glovebox for 30 minutes prior to the addition of 5 Ci/mmol ^{35}S-Cysteine (American Radiolabeled Chemicals Inc.) to a final concentration of 100 μM. After a 2-minute incubation at 37°C, reactions were terminated by centrifugation through a Micro Bio-Spin P-6 gel filtration column (Bio-Rad). The spin column flow through was combined with non-reducing SDS-PAGE sample loading buffer and then loaded on a 14% SDS-PAGE gel. The gel was dried onto chromatography paper in a gel drying oven at 60°C under vacuum before a 12 hour exposure to a phosphor screen. ^{35}S-label incorporation was visualized using a Phosphorimager (Typhoon Trio, GE Healthcare) and analyzed with ImageQuant software. ImageJ software was used to quantitate the amount of label incorporation on ISCU2.

Isolation of ^{35}S-persulfide bound SDUF Complex. Reaction mixtures (400 μL) contained 80 μM SD, 240 μM ISCU2, 240 μM FXN, 50 mM Tris pH=8.0, and 250 mM NaCl. The reaction was initiated with the addition of 20 Ci/mmol ^{35}S-Cysteine

(American Radiolabeled Chemicals Inc.) and incubated for 40 minutes at 10 ^{o}C. The sample was loaded on a 1 mL HisTrap HP column (GE Healthcare) equilibrated in 50 mM Tris pH=7.5, 200 mM NaCl, 5 mM Imidiazole and eluted with a linear gradient from 5 to 500 mM Imidiazole. To evaluate ^{35}S-persulfide incorporation, 30 µL of each fraction from the 1 mL HisTrap HP column was centrifuged through a Micro Bio-Spin P-6 gel filtration column (Bio-Rad) and combined with 8 µL SDS-gel loading dye in the absence of reducing agent. Samples were applied to a 14% SDS-PAGE gel that was dried, exposed, and imaged the same way as described above. Fractions that showed labeled NFS1 and ISCU2 were combined and concentrated to 70 µL (20 µL of the concentrated labeled SDUF complex was removed and used on a 6.5% Native gel).

Isolation of Fe-S Cluster Bound SDUF Complex. The remaining 50 µL of radio-labeled SDUF complex was incubated with 600 µM $Fe(NH_4)_2(SO_4)_2$, 160 µM L-cysteine, and 1 mM DTT for 1 hour. After incubation, the reaction was buffer exchanged into 50 mM Tris pH=8.0, 250 mM NaCl using a Micro Bio-Spin P-6 gel filtration column and loaded onto the 1 mL HisTrap HP column. Cluster-bound SDUF complex was eluted with a linear gradient from 5 to 500 mM Imidiazole and monitored with a 405 nm filter. The fractions corresponding to the cluster bound SDUF complex were collected and concentrated to 50 µL (20 µL of the concentrated cluster bound SDUF complex was removed and used on a 6.5% Native gel).

Analysis of Cluster Transfer to Ferredoxin. The remaining 30 µL of cluster bound SDUF complex was incubated with 200 µM apo-ferredoxin for 1 hour and then buffer exchanged into 50 mM Tris pH=8.0, 250 mM NaCl using a Micro Bio-Spin P-6 gel filtration column and loaded onto the 1 mL HisTrap HP column. Cluster incorporation in ferredoxin was monitored using a 405 nm filter and the flow-through fractions corresponding to ferredoxin were collected and concentrated to 20 µL before loading 2 samples onto a 6.5% Native gel.

Native-PAGE Analysis of ^{35}S Incorporation into Cluster-Bound SDUF Complex and Ferredoxin. 6.5% Native PAGE gels contained standards for SD, ISCU2, FXN, FDX, and the SDU complex, the standard SD concentration was 30 µM and ISCU2, FXN, and FDX were included at 120 µM in a final volume of 15 µL. The Native-PAGE gels were run for 120 minutes on ice and samples contained non-reducing gel loading buffer. The above samples (^{35}S-SDUF complex, Fe-S cluster bound SDUF complex, and Fe-S cluster bound Fdx) were analyzed for radio-label incorporation as described above.

RESULTS

Direct Evidence that FXN Accelerates the Rate of Sulfur Transfer to ISCU2. Here, sulfur transfer from NFS1 to ISCU2 was investigated using a ^{35}S- L-cysteine substrate in the presence and absence of FXN, label incorporation was visualized using a phosphorimager and non-reducing SDS-PAGE to separate the individual reaction components (Figure 7-1). For the titration of ISCU2 to SD, the level of radio-label incorporated on ISCU2 was consistently 2 -3 times higher in the presence of FXN.

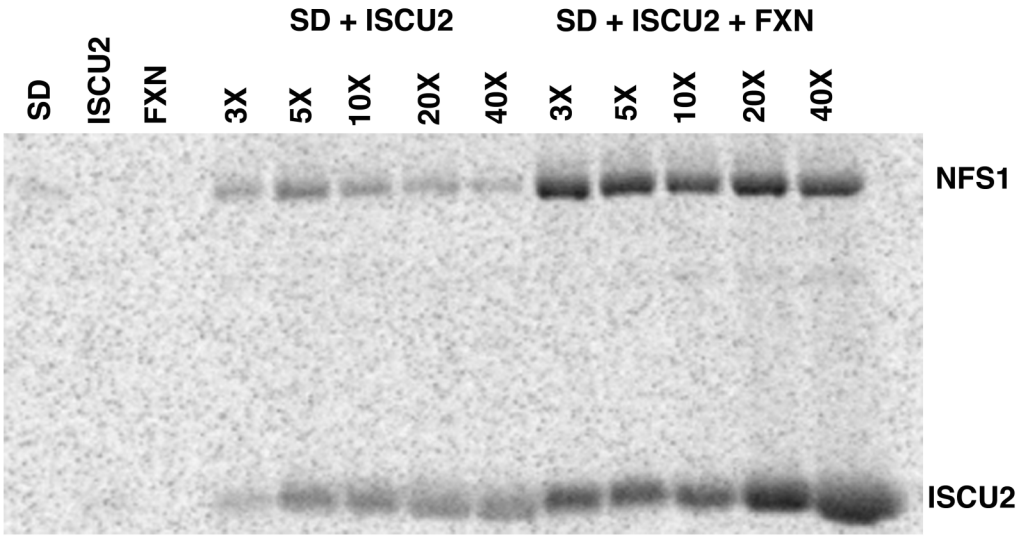

Figure 7-1. FXN accelerates the rate of sulfur transfer. SDS-PAGE analysis of sulfur transfer from NFS1 to ISCU2 in the presence and absence of FXN. Phosphor image obtained after a 12 hour exposure of the SDS-PAGE gel. Lanes 1,2, and 3 are SD, ISCU2, and FXN incubated for 2 minutes in the presence of ^{35}S-Cysteine. Lanes 4-8 are SD incubated with increasing amounts of ISCU2 (3-40 equivalents) and ^{35}S-Cysteine, lanes 9-13 are SD incubated with increasing amounts of ISCU2 (3-40 equivalents), 3 equivalents of FXN, and ^{35}S-Cysteine.

Direct Evidence that FRDA Variants Decrease the Rate of Sulfur Transfer to ISCU2. To address if FRDA variants were compromised in facilitating the sulfur transfer reaction directly, the level of ^{35}S-label incorporation on ISCU2 was compared using SD with 3 equivalents of native FXN or 3 equivalents of FRDA clinical mutants (Figure 7-2). Each of the reactions that included an FRDA variant instead of native FXN showed lower levels of label incorporation on NFS1 and ISCU2.

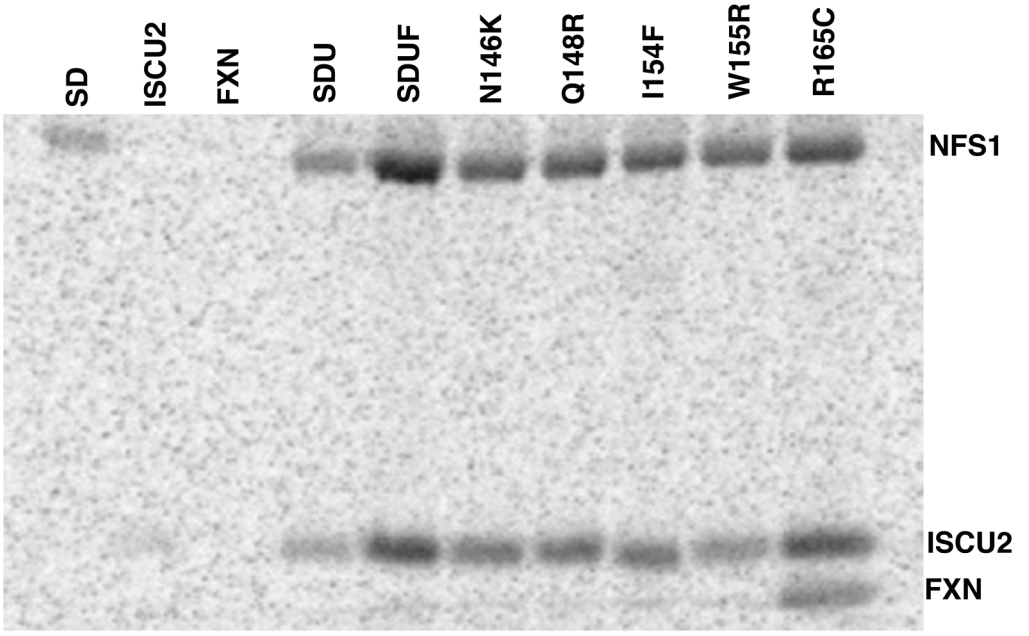

Figure 7-2. FRDA variants decrease the rate of sulfur transfer from NFS1 to ISCU2. SDS-PAGE analysis of sulfur transfer from NFS1 to ISCU2 in the presence of clinical FRDA variants. Phosphor image obtained after a 12 hour exposure of the SDS-PAGE gel. Lanes 1,2, and 3 are SD, ISCU2, and FXN incubated for 2 minutes in the presence of ^{35}S-Cysteine. Lanes 4 and 5 are SD incubated with 3 equivalents of ISCU2 with and without FXN and ^{35}S-Cysteine. Lanes 6-11 are SD incubated with 3 equivalents of ISCU2 and 3 equivalents of N146K, Q148R, I154F, W155R, R165C FXN, and ^{35}S-Cysteine.

Direct Evidence that the "Sulfur-first" mechanism is viable. Here, sulfur transfer from NFS1 to ISCU2 and subsequent incorporation into an Fe-S cluster was investigated using the radio-labeled cysteine substrate and tracking its progression from NFS1 to ISCU2 and finally to FDX. Initially, SD was combined with 3 equivalents of ISCU2, 3 equivalents of FXN, and ^{35}S- L-cysteine. The ^{35}S-labeled SDUF complex was isolated away from excess protein and substrate utilizing a nickel column and the N-terminal 6X-His tag on NFS1 (Figure 7-3A). Protein complex components and label incorporation

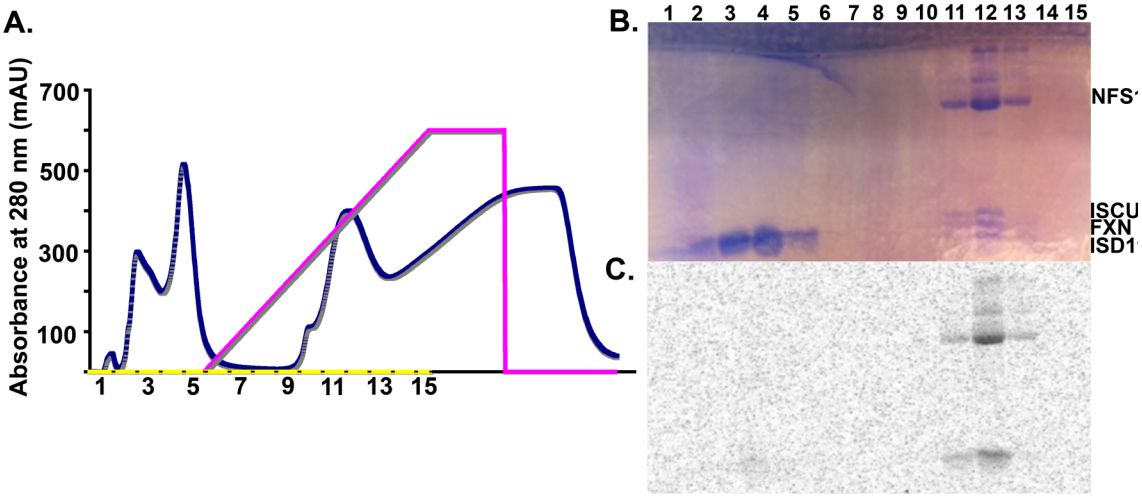

Figure 7-3. Isolation of the ^{35}S-persulfide bound SDUF complex from a 1 mL Nickel column. (A). Chromatogram generated from loading the reaction mixture containing 80 µM SD, 240 µM ISCU2, 240 µM FXN, and 20 Ci/mmol ^{35}S-Cysteine on the 1 mL Nickel column. The absorbance at 280 nm is shown in blue and the 5-500 mM imidiazole gradient used to elute the SDUF complex from the column is shown in pink. The fractions collected are numbered 1-15 and correspond to the lanes labeled on the coomassie stained non-reducing SDS-PAGE gel shown in (B). (C) Phosphor image obtained after a 12-hour exposure of the SDS-PAGE gel shown in B. Fractions corresponding to lanes 11,12, and 13 were collected and concentrated to build a Fe-S cluster bound SDUF complex.

on ISCU2 and NFS1 was verified using a non-reducing SDS-PAGE gel and a phosphorimager to visualize ^{35}S-label incorporation (Figure 7-3B and Figure 7-3C). In order to generate the Fe-S cluster bound SDUF species, the ^{35}S-labeled SDUF complex was incubated with ferrous iron, L-cysteine, and DTT. After incubation, the SDUF complex was separated from the remaining substrates again utilizing a nickel column

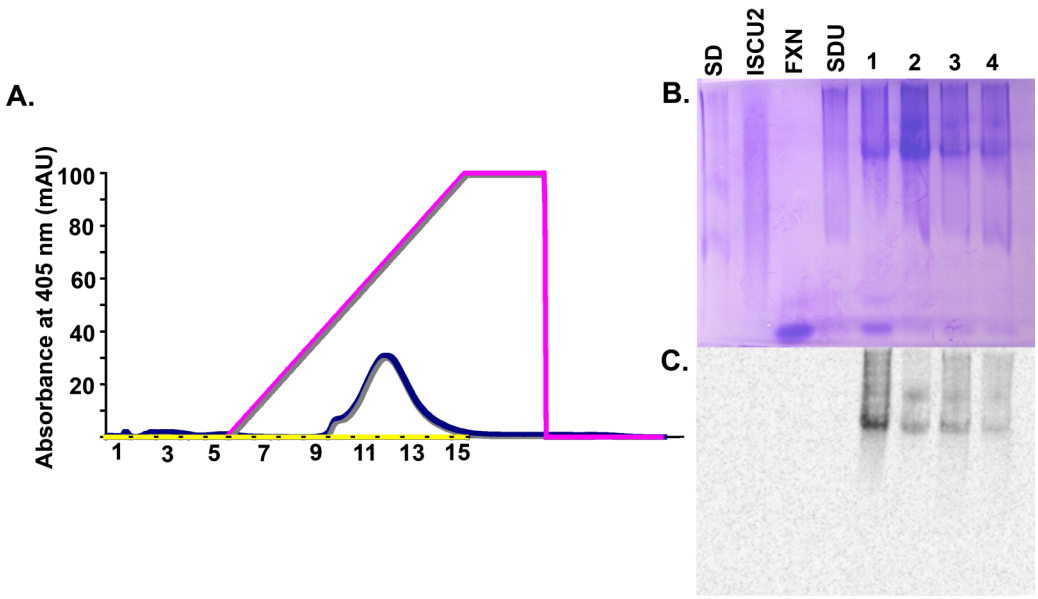

Figure 7-4. Isolation of the Fe-S bound SDUF complex from a 1 mL Nickel column. (A). Chromatogram generated from loading the reaction mixture containing ^{35}S-persulfide bound SDUF complex, 600 µM $Fe(NH_4)_2(SO_4)_2$, 160 µM L-cysteine, and 1 mM DTT after a 1 hour incubation on the 1 mL Nickel column. The absorbance at 405 nm is shown in blue and the 5-500 mM imidiazole gradient used to elute the SDUF complex from the column is shown in pink. The fractions collected are numbered 1-15. (B) 6.5% non-reducing coomassie stained Native-PAGE gel. The first four lanes are standards composed of SD, ISCU2, FXN, and the SDU complex. Lanes labeled 1 and 2 correspond to the ^{35}S-persulfide bound SDUF complex before building an Fe-S cluster and lanes labeled 3 and 4 correspond to Fe-S bound SDUF complex collected and concentrated from the nickel column fractions 11, 12, and 13. (C) Phosphor image obtained after a 12-hour exposure of the Native-PAGE gel shown in B.

and verifying the presence of a [Fe-S] cluster with a 405 nm filter (Figure 7-4A). Native PAGE revealed the cluster bound SDUF retained the ^{35}S-label (Figure 7-4B and Figure 7-4C). Next, Fe-S cluster incorporation of the ^{35}S-label was verified by incubation of the isolated [Fe-S] cluster bound SDUF complex with apo-FDX. After incubation, cluster bound FDX (verified using a 405 nm filter) was purified away from the complex using the nickel affinity column (Figure 7-5A). In this case, Native PAGE revealed the cluster bound FDX had acquired the ^{35}S-label (Figure 7-5B and Figure 7-5C).

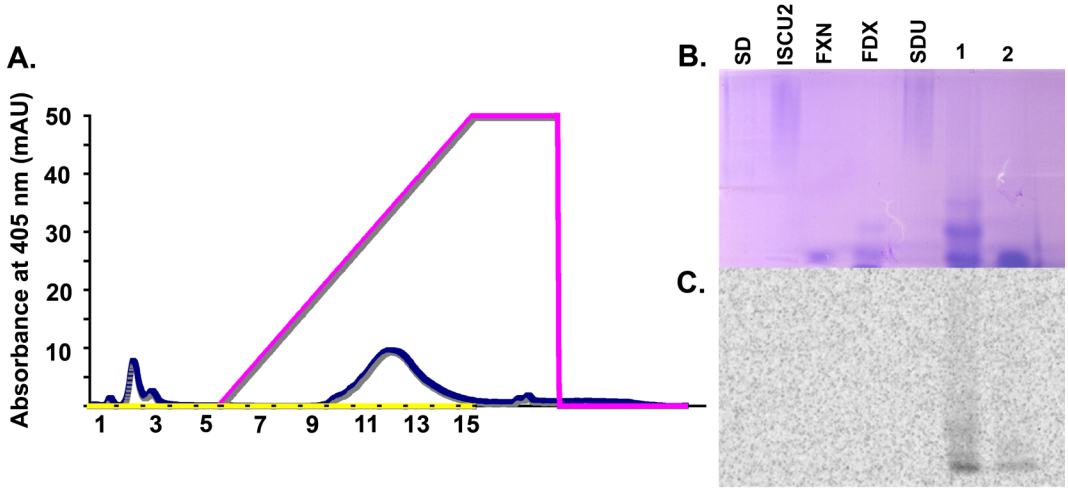

Figure 7-5. Isolation of the Fe-S bound Ferredoxin (FDX) from a 1 mL Nickel column. (A). Chromatogram generated from loading the reaction mixture containing Fe-S bound SDUF complex and apo FDX after a 1 hour incubation on the 1 mL Nickel column. The absorbance at 405 nm is shown in blue and the 5-500 mM imidiazole gradient used to elute the SDUF complex from the column is shown in pink. The fractions collected are numbered 1-15. (B) 6.5% non-reducing coomassie stained Native-PAGE gel. The first five lanes are standards composed of SD, ISCU2, FXN, FDX, and the SDU complex. Lanes labeled 1 and 2 correspond to the Fe-S bound FDX protein collected and concentrated from the nickel column fractions 2 and 3. (C) Phosphor image obtained after a 12-hour exposure of the Native-PAGE gel shown in B.

DISCUSSION

FXN has previously been called an allosteric activator of the Fe-S cluster biosynthetic complex [96]. This conclusion was based on kinetic results that showed FXN binding to the SDU complex stimulated the cysteine desulfurase activity from 25 to 7900 M^{-1} s^{-1} [96]. It was further hypothesized that FXN binding resulted in a conformational switch in ISCU2 that facilitated the sulfur transfer reaction [96]. Subsequent kinetic studies to better define the role of FXN in Fe-S cluster biosynthesis revealed the FRDA variants; N146K, Q148R, I154F, W155R, and R165C were compromised in their binding affinity for the SDU complex and/or their ability to activate both the cysteine desulfurase reaction and Fe-S cluster assembly on ISCU2 [189, 198]. The lower rates of the cysteine desulfurase reaction and Fe-S cluster assembly reactions were hypothesized to be a result of decreased ability of FRDA variants to facilitate sulfur transfer from NFS1 to ISCU2 [189, 198].

Here we directly tested the ability of native FXN and FRDA clinical variants N146K, Q148R, I154F, W155R, and R165C to affect the sulfur transfer reaction. In comparison of the SDU and SDUF protein complexes, there were consistently higher levels of radiolabel incorporated on both NFS1 and ISCU2 in the presence of FXN. This result is consistent with the previously proposed role of FXN stimulating the sulfur transfer reaction between NFS1 and ISCU2. As well, in comparison of the ability of native FXN to stimulate the rate of sulfur incorporation on ISCU2 to the FRDA variants, each of the mutants were diminished in their ability to facilitate the reaction. The clinical mutant W155R had the lowest level of radio-label incorporated on ISCU2 and

this can be correlated to previously measured kinetics in which the cysteine desulfurase activity measured in the presence of ISCU2 and 3 equivalents of W155R was on the order of the SDU complex. While we have shown that frataxin directly affects the sulfur transfer reaction and the rate of sulfur incorporation on ISCU2 to build Fe-S clusters, it has yet to be shown that the persulfide species formed on ISCU2 in the absence of iron is viable in downstream reactions.

To determine the viability of the persulfide species on ISCU2, a radio-labeled substrate was used and its progression was traced to decipher the mechanism of Fe-S cluster assembly. First, the ^{35}S-labeled SDUF complex was isolated and then analyzed for label retention after the addition of cysteine, ferrous iron, and DTT for cluster generation. After the Fe-S cluster was built and the Fe-S cluster containing complex was purified away from excess substrate, native PAGE revealed retention of the label. To clarify the presence of this label in either the cluster or a sub-population of SDUF complex that was ^{35}S-labeled with persulfide, a cluster transfer reaction from the SDUF

complex to apo FDX was conducted. Again, native PAGE revealed that the label had been incorporated in FDX and corroborated that the labeled persulfide species initially formed on ISCU2 was incorporated into Fe-S clusters on the SDUF complex, and then these Fe-S clusters could be transferred to FDX.

Previous data from the Vickery lab has shown that the *E. coli* IscS and IscU proteins form a high affinity complex capable of catalyzing the desulfurization of alanine and then capable of transferring a ^{35}S-labeled persulfide to IscU [183]. These studies on the human system for Fe-S cluster assembly have also revealed complex formation between the NFS1-ISD11 complex with ISCU2, that NFS1 can also transfer a ^{35}S-labeled persulfide to ISCU2, and that FXN can attenuate the rate of this transfer. Further studies show that this persulfide formed on ISCU2 is viable in cluster formation. Lastly, as the persulfide formation on ISCU2 happens in the absence of iron; sulfur transfer is the first step in Fe-S cluster assembly and thus consistent with the previously proposed sulfur first mechanism.

CHAPTER VIII

EFFECTOR ROLE REVERSAL DURING EVOLUTION: THE CASE OF FRATAXIN IN FE-S CLUSTER BIOSYNTHESIS*

INTRODUCTION

Iron-sulfur (Fe-S) clusters are protein cofactors that are essential for most living organisms. Fe-S clusters primarily function in electron transfer, but also participate in substrate binding and activation, protein stabilization, regulation of gene expression or enzyme activity, radical generation, and as a sulfur donor [2, 7, 39, 204]. These biological functions require the Fe-S cluster to vary from solvent accessible to completely buried, and to be accommodated in a diverse set of protein scaffolds [13]. Despite this diversity, conserved metallochaperone proteins recognize and insert Fe-S clusters into apo metalloproteins through mechanisms that remain poorly understood. This assembly system must also control the reactivity of the building blocks for Fe-S clusters, ferrous iron and sulfide, to reduce toxicity and cell death. Ferrous iron is prone to undergo Fenton chemistry: reaction with hydrogen peroxide to generate highly reactive hydroxyl radicals that damage proteins, lipids, [3]and DNA, whereas sulfide is more toxic than cyanide, is a potent inhibitor of cytochrome c oxidase, and targets olfactory nerves, the eyes, and the brain [205]. Defects in these metallochaperone

systems have profound effects on iron metabolism, and result in mitochondrial dysfunction and human disease [18, 119, 193].

In prokaryotes, three different Fe-S assembly systems have been characterized: the nitrogen fixation (NIF), iron-sulfur cluster assembly (ISC), and mobilization of sulfur (SUF) pathways [19-21, 99, 206]. *Escherichia coli* contains both ISC and SUF systems and appears to use the ISC pathway under 'normal' growth conditions and the SUF system under conditions of iron limitation or oxidative stress [35]. The ISC operon is controlled by IscR, a Fe-S cluster binding transcriptional repressor, and contains genes for a cysteine desulfurase (IscS), scaffold protein (IscU), ferredoxin (Fdx), IscA, and molecular chaperones (hscA and hscB). The scaffold protein IscU (in this manuscript the *E. coli* homolog is referred to as $IscU_{ec}$, or U_{ec}) is the central protein in Fe-S cluster biosynthesis and is responsible for the assembly of [2Fe-2S] and [4Fe-4S] clusters [147]. IscS (*E. coli* homolog referred to as $IscS_{ec}$ or S_{ec}) catalyzes the PLP-dependent breakdown of cysteine to alanine and provides the inorganic sulfur for Fe-S clusters [124, 207]. Fdx likely provides electrons for cluster assembly and IscA may be an iron donor or alternate scaffold [32, 100, 208]. Once the cluster is formed, the chaperones hscA and hscB facilitate the transfer of the intact Fe-S cluster to apo target proteins [37, 125, 209]. A homolog of human frataxin (*E. coli* homolog referred to as CyaY or as C_{ec} in protein complexes in this manuscript) is not part of the ISC operon, but has been shown to bind to a $IscS_{ec}$-$IscU_{ec}$ ($S_{ec}U_{ec}$) complex [33, 75, 89] and inhibit Fe-S cluster assembly [60].

A similar ISC Fe-S cluster assembly pathway functions in the matrix space of eukaryotic mitochondria [8, 119]. The Fe-S assembly proteins are encoded by nuclear DNA and often contain a targeting sequence that is cleaved upon import into mitochondria. For the human pathway, the cysteine desulfurase NFS1 (59% identical to $IscS_{ec}$), which forms a eukaryotic-specific functional complex with ISD11 [121-123], the scaffold protein ISCU2 (also known as Isu2; 70% identical to $IscU_{ec}$), and FXN (20% identical to CyaY) form a NFS1-ISD11-ISCU2-FXN (SDUF) complex [82, 96] that is analogous to the $IscS_{ec}$ $IscU_{ec}$-CyaY ($S_{ec}U_{ec}C_{ec}$) complex. Recent *in vitro* studies indicate that FXN is an allosteric activator of Fe-S cluster assembly that increases the catalytic efficiency (k_{cat}/K_M) for the cysteine desulfurase and the rate of Fe-S cluster biosynthesis [96]. Intriguingly, *in vitro* data also indicates *E. coli* CyaY and human FXN have opposing regulator functions in Fe-S cluster biosynthesis [60, 96]. Different physiological functions may also be supported by the dramatically different *in vivo* phenotypes for *E. coli* and mouse model systems lacking frataxin [92, 210]. However, both CyaY and FXN can at least partially complement strains of yeast lacking the frataxin homolog Yfh1 [211, 212], which implies similar functions.

To resolve this discrepancy and better understand the role of frataxin in Fe-S cluster biosynthesis, enzyme kinetic experiments were performed for the human and *E. coli* systems in which analogous components were interchanged. Surprisingly, our results reveal that the cysteine desulfurase component, $IscS_{ec}$/NFS1-ISD11, rather than CyaY/FXN or $IscU_{ec}$/ISCU2 dictated the functional differences in how the frataxin homologs modulate Fe-S cluster assembly.

EXPERIMENTAL PROCEDURES

Preparation of human recombinant proteins. Human NFS1 (Δ1-55) and ISD11 were coexpressed in *Escherichia coli* strain BL21(DE3) as previously described [135, 213]. Cells were lysed by French press in 50 mM Tris pH 8.0, 500 mM NaCl, and 5 mM imidiazole. The NFS1-ISD11 (SD) complex was purified as previously described [213] except that a cation exchange column was added between the Ni-NTA and S300 gel filtration chromatography steps. The yellow SD fractions from the Ni-NTA column were combined with 100 μM pyridoxal 5'-phosphate (PLP), 5 mM dithiothreitol (DTT), and 2 mM ethylenediaminetetracetic acid (EDTA), diluted 3-fold with 50 mM Tris pH 8.0, loaded onto a cation exchange column (16/14, POROS 50HS), and eluted with a linear gradient from 0-1000 mM NaCl. Human ISCU2 (D1-35) was purified as previously described [213] except the fractions for the cation exchange column were eluted with a linear gradient from 0 – 1000 mM NaCl in 50 mM Tris, pH 7.5 buffer and a S100 rather than a S300 gel filtration column was used. Human FXN (D1-55) was purified as previously described [213] except a S100 rather than a S300 column was used. The Bradford method [214] or extinction coefficients of 42670, 8250, and 26030 $M^{-1}cm^{-1}$ at 280 nm [170] were used to estimate the protein concentration of SD, ISCU2, and FXN, respectively.

Preparation of E. coli recombinant proteins. A plasmid containing the $IscS_{ec}$ gene [60] was transformed into BL21(DE3) *E. coli* cells and grown at 37 ºC. Protein expression was induced with 0.5 mM IPTG when the OD_{600} was ~0.6. Cells were harvested 5 hours later and lysed by sonication in 50 mM Tris pH 8.0, 500 mM NaCl, 5

mM imidiazole, and 100 mM PLP. After centrifugation, the supernatant was loaded on a Ni-NTA column (16/13, GBiosciences) and eluted with a linear gradient from 5 to 250 mM imidazole. Yellow fractions were concentrated and further purified on a Sephacryl S300 column (26/60, GE Healthcare) equilibrated in 50 mM HEPES pH 8.0, 250 mM NaCl. Plasmids that contained either $IscU_{ec}$ or CyaY genes [60] were transformed into BL21(DE3) cells and grown at 37 ºC. Protein expression was induced with 0.5 mM IPTG when the OD_{600} was ~0.6. Cells were harvested 3.5 hours later and lysed by sonication in 50 mM Tris pH 7.4, 150 mM NaCl, 1 mM EDTA, and 1 mM DTT. The supernatant was loaded onto a GST column and eluted with a linear gradient from 0-7 mM glutathione. The fractions that bound the column were concentrated and dialyzed into 50 mM Tris pH 8.0, 0.5 mM EDTA, and 1 mM DTT and then incubated at room temperature overnight with TEV protease. The tag cleavage product was loaded onto the GST column and the flow through was further purified on a S100 gel filtration column equilibrated in 50 mM HEPES pH 7.5, 150 mM NaCl. The Bradford method [214] or extinction coefficients of 41370, 11460, and 28990 $M^{-1}cm^{-1}$ at 280 nm [170] were used to estimate the protein concentration of $IscS_{ec}$, $IscU_{ec}$, and CyaY, respectively.

Titrations to determine protein complex stoichiometries. Cysteine desulfurase assays were used to determine reaction stoichiometries to favor protein complexes for different combinations of human and *E. coli* proteins. Cysteine desulfurase assays (see below for details) were initiated with 100 mM L-cysteine and included 0.5 μM of the cysteine desulfurase (SD or $IscS_{ec}$) and increasing amounts of the scaffold protein (ISCU2 or $IscU_{ec}$). Once the saturating number of equivalents of the scaffold protein

were determined (Table 8-1), additional titrations were performed with increasing amounts of frataxin (FXN or CyaY).

Table 8-1: Protein complexes and Reaction Stoichiometries.

Name	Components	Protein ratios
SDU	human NFS1/ISD11 and ISCU2	1:3
SDU_{ec}	human NFS1/ISD11; *E. coli* $IscU_{ec}$	1:3
SDUF	human NFS1/ISD11, ISCU2, and FXN	1:3:3
$SDU_{ec}F$	human NFS1/ISD11; *E. coli* $IscU_{ec}$; human FXN	1:3:200
$SDUC_{ec}$	human NFS1/ISD11 and ISCU2; *E. coli* CyaY	1:3:80
$SDU_{ec}C_{ec}$	human NFS1/ISD11; *E. coli* $IscU_{ec}$ and CyaY	1:3:30
$S_{ec}U_{ec}$	*E. coli* IscS and $IscU_{ec}$	1:5
$S_{ec}U$	*E. coli* IscS; human ISCU2	1:5
$S_{ec}U_{ec}C_{ec}$	*E. coli* IscS, $IscU_{ec}$, and CyaY	1:5:10
$S_{ec}UC_{ec}$	*E.coli* IscS; human ISCU2; *E. coli* CyaY	1:5:10
$S_{ec}U_{ec}F$	*E. coli* IscS and $IscU_{ec}$; human FXN	1:5:15
$S_{ec}UF$	*E. coli* IscS; human ISCU2 and FXN	1:5:15

Cysteine desulfurase activity measurements. Assay mixtures (800 μL) contained 0.5 μM cysteine desulfurase (SD or $IscS_{ec}$), 10 μM PLP, 2 mM DTT, 5 μM $Fe(NH_4)_2(SO_4)_2$, and increasing or saturating amounts (Table 8-1) of the scaffold protein (ISCU2 or $IscU_{ec}$) and frataxin (FXN or CyaY) in 50 mM Tris pH 8.0, and 250 mM NaCl [135, 136, 213]. Samples were incubated in an anaerobic glovebox (10~14 ^{o}C) for 30 minutes. The cysteine desulfurase reactions were initiated by addition of (0.01 to 1 mM) L-cysteine at 37 °C and quenched after 10 minutes by the addition of 100 ml of 20 mM *N,N*-dimethyl-*p*-phenylenediamine in 7.2 N HCl and 100 ml of 30 mM $FeCl_3$ in 1.2

N HCl, which also initiated the conversion of sulfide to methylene blue. After a twenty-minute incubation at 37 ^{o}C, the absorption at 670 nm due to methylene blue formation was measured and compared with a Na_2S standard curve to quantitate sulfide production. Cysteine desulfurase reactions were also performed for mixed species Fe-S assembly complexes with 0 to 80 equivalents of $Fe(NH_4)_2(SO_4)_2$ and 100 mM L-cysteine. Units are defined as mmol sulfide/mmol cysteine desulfurase per minute at 37 ^{o}C. Rates were fit to the Michaelis-Menten equation using KaleidaGraph (Synergy Software).

Fe-S Cluster Formation. Assay mixtures contained 8 μM of the cysteine desulfurase (SD or $IscS_{ec}$), 5 mM DTT, 200 μM $Fe(NH_4)_2(SO_4)_2$, 100 μM L-cysteine, 50 mM Tris pH 8.0, and 250 mM NaCl in a total volume of 0.2 mL. In addition, the number of equivalents (relative to the cysteine desulfurase) for the scaffold protein (ISCU2 or $IscU_{ec}$) and frataxin (FXN or CyaY) required to saturate the activity (above; Table 8-1) were included in the assay mixture. The scaffold protein was incubated with 5 mM DTT in 50 mM Tris pH 8, 250 mM NaCl in an anaerobic glovebox for 30 minutes prior to mixing with the remaining assay components in an anaerobic cuvette and then incubated at 10 °C for 30 minutes in the cuvette holder. The reaction was initiated by injecting L-cysteine to a final concentration of 100 μM with a gas-tight syringe. Fe-S cluster formation was monitored at 456 nm at 10 °C and then the first 3000 seconds were fit as first-order kinetics using KaleidaGraph. The rate was converted to the activity using an extinction coefficient of 5.8 $mM^{-1}cm^{-1}$ at 456 nm for [2Fe-2S] cluster absorbance [147]. Units are defined as the μmol of [2Fe-2S] cluster / mmol cysteine desulfurase per minute at 10 ^{o}C.

RESULTS

Protein complex stoichiometries for activity measurements. The objectives of this study were to provide insight into functional differences in frataxin-mediated regulation of Fe-S cluster biosynthesis for prokaryotes and eukaryotes by measuring cysteine desulfurase and Fe-S formation activities of mixed species protein complexes. The sulfur generated by the cysteine desulfurase reaction can be directed measured or can be used as a component of the Fe-S formation reaction. Previous experiments revealed that adding 3 equiv of ISCU2 minimized the cysteine desulfurase activity of the NFS1-ISD11 (SD) complex (Table 8-1), likely through formation of a NFS1-ISD11-ISCU2 (SDU) species [213]. Likewise, adding 3 equiv of FXN to SDU maximized the cysteine desulfurase activity by forming a NFS1-ISD11-ISCU2-FXN (SDUF) complex [213]. A similar strategy was used here to determine and then compensate for weaker binding of *E. coli* proteins to the human assembly complex and human proteins to the *E. coli* assembly complex.

First, protein reaction stoichiometries were determined for the human SD complexes by measuring cysteine desulfurase activities with increasing amounts of the scaffold protein, either ISCU2 or $IscU_{ec}$, and frataxin, either FXN or CyaY. The cysteine desulfurase activity of SD decreased with addition of either ISCU2 or $IscU_{ec}$ and minimized after the addition of ~2 equiv/SD (Figure 8-1A). Three equiv of ISCU2 or $IscU_{ec}$ were therefore included with SD for kinetic experiments of the SDU or NFS1-ISD11-$IscU_{ec}$ (SDU_{ec}) complexes (Table 8-1). The binding of frataxin homologs to the SDU complex increased the cysteine desulfurase activity that maximized after the

addition of either 3 equiv of FXN or 80 equiv of CyaY (Figure 8-1B). Similarly, the binding of frataxin homologs to the SDU_{ec} complex increased the cysteine desulfurase activity that maximized after either 200 equiv of FXN or 30 equiv of CyaY (Figure 8-1C).

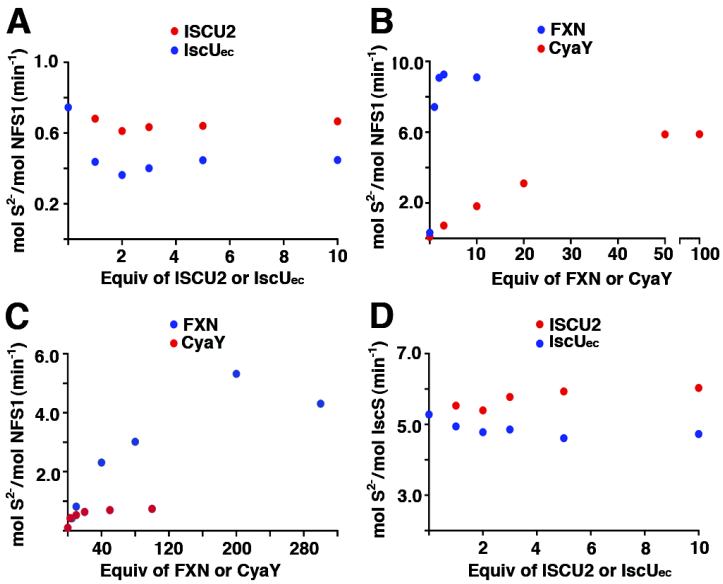

Figure 8-1. Determination of protein ratios that favor complex formation. Cysteine desulfurase activities were measured for (A) the human SD complex with increasing amounts of ISCU2 or $IscU_{ec}$, and for (B) the SDU and (C) SDU_{ec} complexes with increasing amounts of FXN or CyaY. (D) The cysteine desulfurase activity was measured for *E. coli* IscS with increasing amounts of ISCU2 or $IscU_{ec}$.

Second, protein reaction stoichiometries were determined for $IscS_{ec}$ using similar titrations. The cysteine desulfurase activity of $IscS_{ec}$ slightly decreased with addition of $IscU_{ec}$ and slightly increased with addition of ISCU2 (Figure 8-1D). This perturbation in $IscS_{ec}$ activity maximized after the addition of 3-5 equiv of $IscU_{ec}$ or ISCU2. To favor complex formation, five equiv of $IscU_{ec}$ or ISCU2 were therefore added to $IscS_{ec}$ (Table 8-1) for all kinetic experiments of $IscS_{ec}$-$IscU_{ec}$ ($S_{ec}U_{ec}$) and $IscS_{ec}$-ISCU2 ($S_{ec}U$) complexes, respectively. Titrations of up to 50 equiv of CyaY or FXN did not significantly change the cysteine desulfurase activity of either the $S_{ec}U_{ec}$ or $S_{ec}U$ complex (data not shown). Therefore, protein complex stoichiometries of 1:5:10 were used for the $S_{ec}U_{ec}C_{ec}$ and $S_{ec}UC_{ec}$ complexes based on the number of equivalents of CyaY previously determined to inhibit Fe-S cluster formation [60]. Similarly, protein complex stoichiometries of 1:5:15 were arbitrarily chosen for the Michaelis-Menten kinetics (below) of the $S_{ec}U_{ec}F$ and $S_{ec}UF$ complexes (Table 8-1).

$IscU_{ec}$ and CyaY stimulate the cysteine desulfurase activity of the human SD complex. Saturating amounts of ISCU2 or $IscU_{ec}$ and FXN or CyaY determined above were added to the SD complex and the rates of the cysteine desulfurase reaction were measured as a function of the L-cysteine concentration. The human SD complex exhibited a k_{cat}/K_M of 660 $M^{-1}s^{-1}$ for the cysteine desulfurase reaction (Table 8-2), which is slightly higher (primarily due to a lower K_M for L-cysteine) than previously reported values of ~100 $M^{-1}s^{-1}$ [135, 213]. The addition of ISCU2 or $IscU_{ec}$ and formation of the SDU or SDU_{ec} complex slightly decreased the k_{cat} (Figure 8-2 and Table 8-2). The binding of FXN to form the SDUF and $SDU_{ec}F$ complexes stimulated the k_{cat} for the cysteine desulfurase reaction by ~7-fold relative to the SDU and SDU_{ec} complexes (Figure 8-2). Similarly, CyaY binding and formation of the $SDUC_{ec}$ and $SDU_{ec}C_{ec}$ complexes resulted in a 4-6 fold increase in the k_{cat} relative to SDU and SDU_{ec} (Figure 8-2). These experiments show that $IscU_{ec}$ can functionally substitute for ISCU2 and that CyaY can replace FXN as an activator of the cysteine desulfurase reaction for the human Fe-S assembly complex.

Table 8-2: Kinetic data for Fe-S assembly complexes.

Name	k_{cat} (min^{-1})	K_M (mM)	k_{cat}/K_M ($M^{-1}sec^{-1}$)	Fe-S cluster assembly activity (min^{-1})
SD	1.5 ± 0.1	0.038 ± 0.012	660 ± 200	
SDU	1.0 ± 0.1	0.028 ± 0.008	600 ± 180	0.26 ± 0.22
SDUF	6.7 ± 0.4	0.011 ± 0.004	9700 ± 3900	
SDUF + Fe	15.4 ± 1.1	0.015 ± 0.006	16800 ± 6300	30.39 ± 1.18
$SDUC_{ec}$	5.7 ± 0.4	0.027 ± 0.01	3500 ± 1300	
$SDUC_{ec}$ + Fe	6.7 ± 0.2	0.016 ± 0.003	7100 ± 1400	3.94 ± 0.48
SDU_{ec}	0.59 ± 0.02	0.018 ± 0.003	550 ± 120	1.30 ± 0.32
$SDU_{ec}F$	4.2 ± 0.1	0.009 ± 0.002	7900 ± 2000	
$SDU_{ec}F$ + Fe	6.1 ± 0.3	0.012 ± 0.003	8300 ± 2300	25.54 ± 1.17
$SDU_{ec}C_{ec}$	2.1 ± 0.1	0.012 ± 0.003	2900 ± 840	
$SDU_{ec}C_{ec}$ + Fe	1.9 ± 0.1	0.011 ± 0.002	2800 ± 480	1.21 ± 0.19
S_{ec}	7.5 ± 0.1	0.017 ± 0.002	7300 ± 860	
$S_{ec}U_{ec}$	4.7 ± 0.3	0.019 ± 0.006	4100 ± 1400	12.23 ± 0.59
$S_{ec}U_{ec}C_{ec}$	5.8 ± 0.2	0.025 ± 0.003	3800 ± 440	
$S_{ec}U_{ec}C_{ec}$ + Fe	4.2 ± 0.1	0.020 ± 0.004	3500 ± 680	0.79 ± 1.76
$S_{ec}U_{ec}F$	5.2 ± 0.1	0.017 ± 0.002	5100 ± 870	
$S_{ec}U_{ec}F$ + Fe	4.5 ± 0.2	0.024 ± 0.004	3200 ± 940	4.56 ± 0.40
$S_{ec}U$	6.5 ± 0.2	0.019 ± 0.003	5800 ± 1000	14.63 ± 0.95
$S_{ec}UC_{ec}$	7.4 ± 0.1	0.016 ± 0.002	7600 ± 900	
$S_{ec}UC_{ec}$ + Fe	7.3 ± 0.3	0.017 ± 0.004	7100 ± 1600	0.88 ± 0.64
$S_{ec}UF$	7.6 ± 0.3	0.020 ± 0.006	6300 ± 1600	
$S_{ec}UF$ + Fe	6.9 ± 0.1	0.016 ± 0.002	7200 ± 890	3.62 ± 0.24

Iron-dependent stimulation of SD complexes. Cysteine desulfurase activities were determined for SD complexes as a function of added iron. From 0 to 80 equiv of

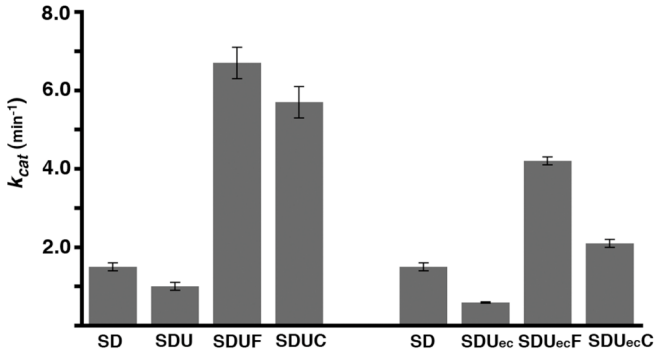

Figure 8-2. Stimulation of cysteine desulfurase reaction by addition of frataxin homologs. The k_{cat} for the cysteine desulfurase reaction was plotted for complexes of human SD with the scaffold protein (ISCU2 or IscU_{ec}) and frataxin (FXN or CyaY).

iron were added to the SDUF, SDUC_{ec}, SDU$_{ec}$F, and SDU$_{ec}C_{ec}$ complexes and the cysteine desulfurase activity was measured (Figure 8-3A). The activity maximized after about 1, 1, and 5 equiv for the SDUF, SDUC_{ec}, and SDU$_{ec}$F complexes, respectively. In contrast, the SDU$_{ec}C_{ec}$ complex did not exhibit a significant Fe-based activation. In addition, the SD complexes were incubated with 10 equiv of ferrous iron and the Michaelis-Menten parameters for the cysteine desulfurase activity were determined (Table 8-2). Iron had a large effect on the k_{cat} for the SDUF complex, as previously reported [213], a moderate effect for the SDUC_{ec} and SDU$_{ec}$F complexes, and no effect for the SDU$_{ec}C_{ec}$ complex (Figure 8-3B).

CyaY can substitute for FXN in the human SD complexes. The rate of Fe-S cluster assembly for the SDU, SDU$_{ec}$, SDUF, SDUC_{ec}, SDU$_{ec}$F, and SDU$_{ec}C_{ec}$

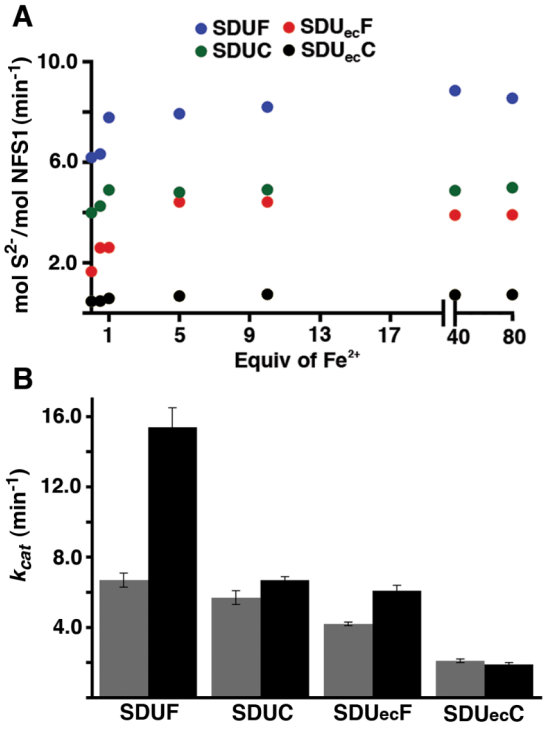

Figure 8-3. Iron-dependent perturbation of cysteine desulfurase activity for SD complexes. (A) Cysteine desulfurase activity plotted as a function of added ferrous iron. (B) Plot of k_{cat} values for the cysteine desulfurase reaction of SD complexes with (black) and without (gray) 10 equiv of ferrous iron.

complexes were determined by monitoring the increase in absorbance at 456 nm [147] at 10 °C and converting this change in absorbance to an activity measurement (mmol [2Fe-2S] / mmol of complex per minute). In the absence of FXN or CyaY, the SDU and SDU_{ec} complexes exhibited very low or no activity and were similar to a control reaction in which sulfide was substituted for cysteine (Table 8-2 and Figure 8-4). The addition of

FXN greatly stimulated the Fe-S assembly activity of SDU and SDU_{ec}. In contrast, addition of CyaY resulted in a very modest or no increase in Fe-S assembly activity of the SDU and SDU_{ec} complexes, respectively. A CyaY-based stimulation was more readily observed when the Fe-S cluster assembly assays were repeated at room temperature (Figure 8-4A inset). Thus, *E. coli* CyaY can substitute for human FXN in for the human Fe-S assembly complex and strongly stimulate the cysteine desulfurase activity and also weakly stimulate the Fe-S cluster formation reaction.

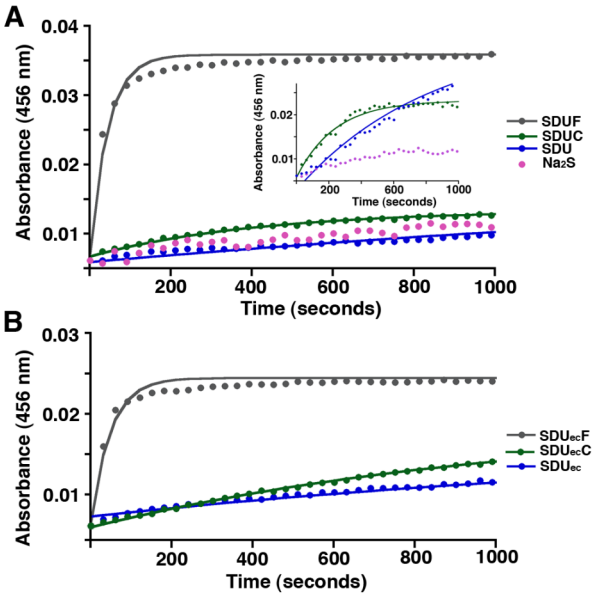

Figure 8-4. Stimulation of Fe-S cluster assembly activity by frataxin homologs. (A) The Fe-S assembly activities were measured at 10 °C for the Na_2S control and SDU, $SDUC_{ec}$, and SDUF complexes. The inset shows the activities of the SDU, $SDUC_{ec}$, and Na_2S control at 25 °C. (B) The Fe-S assembly activities were measured at 10 °C for the Na_2S control and SDU_{ec}, $SDU_{ec}C_{ec}$, and $SDU_{ec}F$ complexes.

CyaY and FXN have minor effects on the cysteine desulfurase activity for E. coli IscS complexes. Purified recombinant $IscS_{ec}$ exhibited a k_{cat} of 7.5 min^{-1} (Figure 8-5A and Table 8-2), which is similar to the previously reported value of 8.5 min^{-1} [183]. Addition of $IscU_{ec}$ diminished the k_{cat} for the cysteine desulfurase reaction by a factor of 1.6, whereas a more moderate decrease in k_{cat} was observed upon ISCU2 addition (Figure 8-5A). Previously, $IscU_{ec}$ was shown to either have no effect on the activity of $IscS_{ec}$ [187] or stimulate the activity 6-fold [109] using different experimental conditions and assays. The k_{cat} for $S_{ec}U_{ec}$ and $S_{ec}U$ were increased slightly upon addition of either

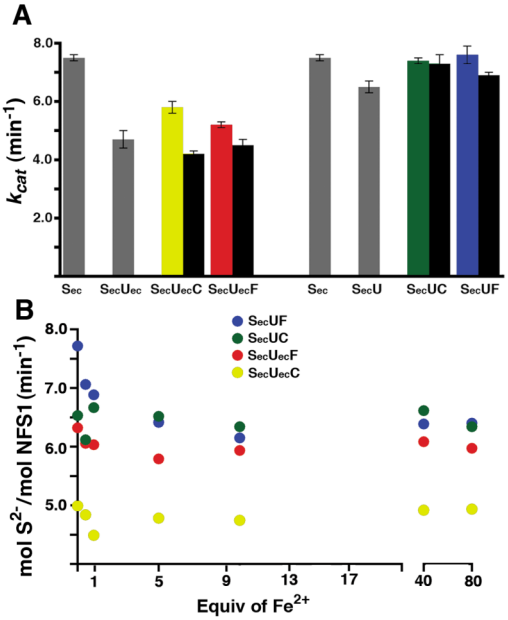

Figure 8-5. Cysteine desulfurase activities for IscS complexes with and without iron. (A) The k_{cat} for the cysteine desulfurase was plotted for complexes of *E. coli* IscS (S_{ec}) without (gray or colored) and with (black) 10 equiv of ferrous iron. (B) The cysteine desulfurase activities for IscS complexes were measured with 100 mM L-cysteine and increasing amounts of ferrous iron.

CyaY or FXN (Figure 8-5A and Table 8-2). The cysteine desulfurase activity was slightly decreased by added ferrous iron that appeared to occur within the first equiv of added iron for the $S_{ec}U_{ec}F$ and $S_{ec}U_{ec}C_{ec}$ complexes and 10 equiv of iron for the $S_{ec}UF$ complex (Figure 8-5B). Steady state kinetics also revealed the k_{cat} slightly decreased upon addition of 10 equiv of ferrous iron (Figure 8-5A). The slight decrease in cysteine desulfurase activity upon addition of iron (Figure 8-5) is opposite of the general Fe-based activation observed for SD complexes (Figure 8-3). Overall, these results indicate that binding of frataxin homologs and ferrous iron have minor effects on the cysteine desulfurase activity of IscS complexes.

CyaY and FXN inhibit Fe-S assembly by E. coli IscS complexes. The Fe-S cluster assembly rate for the $S_{ec}U_{ec}$ and $S_{ec}U$ complexes were similar and significantly higher than analogous complexes with NFS1-ISD11 (SDU_{ec} and SDU). Notably, the rate of Fe-S cluster formation for the FXN-activated SD complexes are 3 fold higher (Figure 8-4 and Table 8-2) than any $IscS_{ec}$ complex. Addition of 10 equiv of CyaY to the $S_{ec}U_{ec}$ and $S_{ec}U$ complexes completely inhibited Fe-S cluster formation (Figure 8-6A and 8-6B), consistent with previous results [60]. CyaY at 2 equiv inhibited the native $S_{ec}U_{ec}$ complex more effectively than the mixed species $S_{ec}U$ complex. Similarly, addition of FXN to the $S_{ec}U_{ec}$ and $S_{ec}U$ complexes (Figure 8-6C and 8-6D) lowered the rate and possibly the amount of cluster bound; however, FXN but did not completely eliminate Fe-S cluster formation.

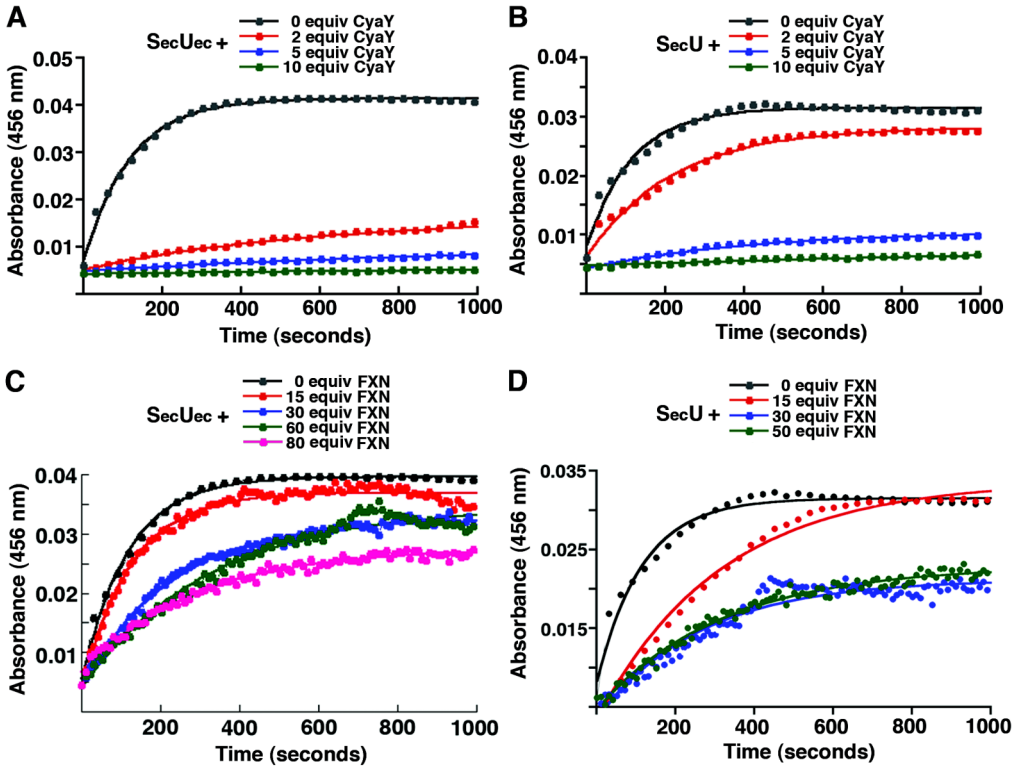

Figure 8-6. Frataxin-based inhibition of Fe-S cluster formation for IscS complexes. The rate of Fe-S cluster formation were measured for the $S_{ec}U_{ec}$ complex with increasing amounts of (A) CyaY and (C) FXN, and for the $S_{ec}U$ complex with increasing amounts of (B) CyaY and (D) FXN.

DISCUSSION

The physiological function of frataxin has been intensively investigated since it was associated with the neurodegenerative disease Friedreich's ataxia (FRDA; reviewed in [56, 113]). A decrease in FXN levels in yeast and mouse model systems results in a phenotype that include loss of Fe-S cluster enzyme activity, accumulation of iron in the mitochondria, and susceptibility to oxidative stress [56, 57, 157]. In addition, FXN levels are correlated with the age of disease onset for FRDA patients [115, 116], and FXN missense mutations were identified that show FRDA-like phenotypes in mouse [157] and yeast [78] model systems. A role for frataxin as an iron chaperone and/or donor in Fe-S cluster biosynthesis is often cited due to the frataxin depletion phenotype [56, 57, 157], the ability of frataxin to bind iron [48, 53, 68, 73, 80], and the acceleration of Fe-S cluster formation by Fe-bound FXN *in vitro* [53]. Recent *in vitro* data as well as data presented here reveals that human FXN binds to the SDU complex and activates both the cysteine desulfurase and Fe-S formation reactions [96]. Moreover, assays using FXN missense mutations exhibit defects in binding and activation that appear to correlate with the severity of clinical progression for FRDA patients [189, 198]. The physiological function of CyaY is less clear. In contrast to FXN in eukaryotes, deletion or overexpression of CyaY does not affect cellular growth, iron content, and survival after exposure to H_2O_2 [92, 93]. Part of the complication for these types of studies is the presence of both the ISC and SUF Fe-S assembly systems in *E. coli*. If the physiological role of CyaY were to inhibit Fe-S cluster formation by the ISC system, then one would expect overexpression of CyaY in the absence of the SUF system to give a loss of Fe-S

cluster phenotype. To the best of our knowledge this experiment has not been reported. Unfortunately, the complicated phenotype for human FXN depletion, the lack of a phenotype for CyaY depletion, and the opposing *in vitro* functions in Fe-S cluster assembly have contributed to the general confusion over the physiological role of this protein.

Here we used a function replacement approach to understand the factors that mediate the dramatically different *in vitro* responses to frataxin homolog binding. More specifically, *in vitro* cysteine desulfurase and Fe-S cluster assembly activities were evaluated for protein complexes in which components from the recombinant human Fe-S assembly system: the NFS1-ISD11 cysteine desulfurase complex, the scaffold protein ISCU2, and FXN, and the recombinant *E. coli* system composed of the IscS cysteine desulfurase, the scaffold protein $IscU_{ec}$, and CyaY, were interchanged. Surprisingly, our results reveal that activation or inhibition by the frataxin homolog is not controlled by the frataxin homolog but rather dictated by the cysteine desulfurase.

Interestingly, even though $IscS_{ec}$ and NFS1 are almost 60% identical, $IscS_{ec}$ exhibited a k_{cat}/K_M for the cysteine desulfurase activity that was 10-70 fold higher than the SD complex and was largely unchanged by the addition of $IscU_{ec}$ and $CyaY_{ec}$ [135, 213]. In contrast, the low activity of the SD complex could be rescued by the addition of ISCU2 and FXN; the SDUF complex had a k_{cat}/K_M that is about double that of $IscS_{ec}$ alone or as a $S_{ec}U_{ec}$ or $S_{ec}U_{ec}C_{ec}$ complex. The $S_{ec}U_{ec}$ and SDU complexes also exhibit striking differences in their ability to facilitate Fe-S cluster formation. The $S_{ec}U_{ec}$ complex is highly active in the Fe-S cluster assembly assay, whereas the SDU complex

exhibits little ability to mediate this reaction. These difference were not due to the identity of the scaffold protein; interchanging the $IscU_{ec}$ and ISCU2 proteins did not substantially alter the higher rate of the complexes containing S_{ec} or the substantially inhibited rates of complexes containing SD (Figures 8-4, 8-6). Moreover, addition of CyaY or FXN to these reactions inhibited Fe-S assembly by S_{ec}-containing complexes and activated Fe-S assembly by SD-containing complexes (Figures 8-4, 8-6), albeit inhibition of the *E. coli* complex by CyaY was more efficient than by FXN and activation of the human complex by FXN was more efficient than by CyaY.

Our data therefore suggest that intrinsic features of $IscS_{ec}$ and human SD cysteine desulfurase components control both the basal activity as well as the effect of binding the frataxin homologs CyaY and FXN. In both cases, binding of the effector molecule switches the activity the molecule, either from "off" to "on" or from "on" to "off". In this sense, NFS1 behaves less like its ortholog IscS and more like its paralogs, such as SufS, which are characterized by modest activity and the ability to be activated by accessory proteins [178, 215, 216]. Evolutionary innovations in cysteine desulfurases from eukaryotes that control the basal activity and intrinsic features of frataxin homolog regulation are not known; binding of ISD11 and conserved amino acid changes in eukaryotes near the active site could play important roles in this process. Precise features of these proteins that regulate these features are currently under investigation.

Our data are consistent with FXN and CyaY binding playing a role in modulating Fe-S cluster formation by trapping an "on" conformation of SDU or an "off" conformation of $S_{ec}U_{ec}$ (Figure 8-7). This model would be consistent with the fact that SDU forms a stable complex with FXN [213] and $S_{ec}U_{ec}$ forms a stable complex with CyaY that has been characterized by small angle X-ray scattering [33, 75, 89]. The fact that FXN and CyaY can functionally replace each other *in vitro*, albeit at lowered efficiencies, is consistent with the formation of a complex with a common structure and with the ability of both of these proteins to suppress defects caused by deletion of *YFH1*, which encodes the *S. cerevisiae* frataxin homolog [211, 212]. These modifications to the cysteine desulfurase may function as part of a protein-level regulatory mechanism. Future experiments will be aimed at providing additional mechanistic insight into the differences between the human SD complex and $IscS_{ec}$ and how these differences control Fe-S cluster assembly.

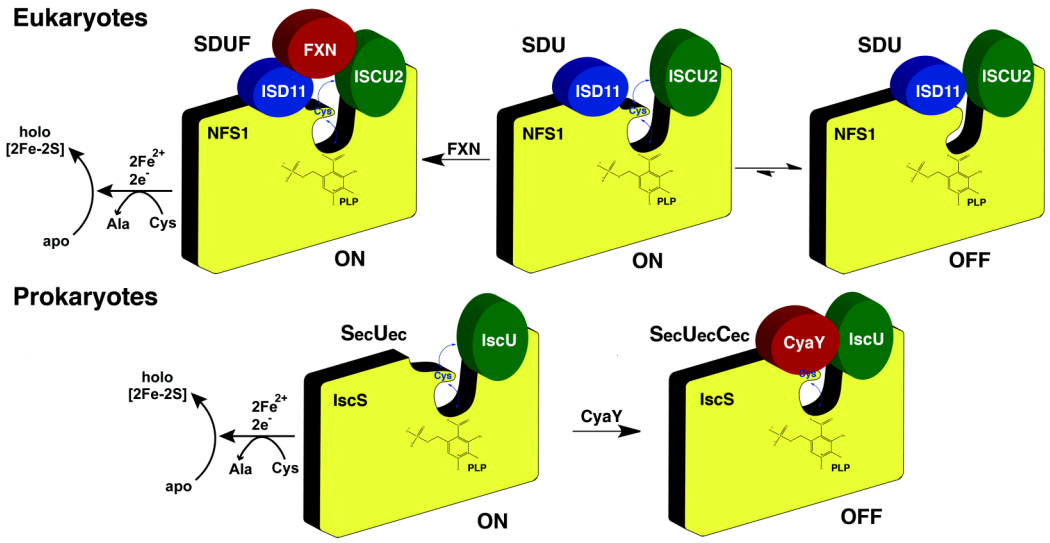

Figure 8-7. Working model for frataxin regulation of Fe-S cluster biosynthesis. In eukaryotes, a pre-equilibrium model is proposed in the absence of FXN in which a cysteine desulfurase and Fe-S cluster assembly deficient form is favored over a functional form of the SDU complex. FXN binding stabilizes the functional form and promotes sulfur transfer from NFS1 to ISCU2 and Fe-S cluster synthesis activities. In contrast, the prokaryotic $S_{ec}U_{ec}$ complex that lacks CyaY exhibits cysteine desulfurase and Fe-S assembly activities. CyaY binding may induce a conformational change in the $S_{ec}U_{ec}$ complex that does not significantly affect the cysteine desulfurase activity, but abolishes Fe-S cluster synthesis. The "ON" and "OFF" labels indicate the Fe-S assembly activity of the respective complexes, the blue arrows from the PLP to the mobile Cys loop indicate the presence of cysteine desulfurase activity, and the blue arrows from the Cys loop to the scaffold protein (shown in green) indicate interprotein sulfur transfer. The displayed model represents half of the expected dimeric Fe-S assembly complexes.

CHAPTER IX

CONCLUSION

Here we have further defined the role of FXN as an allosteric activator of the human Fe-S cluster biosynthetic machinery. Direct evidence has been provided that FXN is involved in stimulating the rate of sulfur transfer from NFS1 to ISCU2 and that FRDA clinical mutants are deficient in facilitating this reaction. Enzyme kinetic studies were used to understand how FRDA and related variants affect FXN binding to the SDUF complex and the ability of FXN to function as an allosteric activator of both the sulfur transfer and Fe-S cluster assembly reactions. Based on these biochemical experiments, four different classes of FXN variants have been established; class I variants (Q153A and W155R) displayed weak binding (at least 25-fold weaker than that of FXN) and substantially reduced cysteine desulfurase activity (k_{cat} less than 30% of that of FXN). Class II variants (R165C, N146K, and W155A) displayed weak binding but possessed a level of catalysis that was only mildly reduced (k_{cat} more than 45% of that of FXN). Class III variants (Q148R) had only modest defects in binding (3−10-fold weaker than that of FXN) but a substantially reduced level of catalysis (k_{cat} less than 25% of that of FXN). Class IV variants (W155F, N146A, Q148G, and I154F) had only modest defects in both binding and activation of the SDU complex. Crystal structures of the class II and IV variants with the highest k_{cat} values (W155F and R165C) position the aromatic rings of W155 or F155 into a solvent filled surface cavity and provide our working model: upon binding, W155 rotates to occupy the surface pocket on FXN and

interact with the SDU complex through π -π interactions or cation-π interactions. Coupling these classes to high resolution crystal structures, the guanidinium group of R165 was found to be imperative for FXN interaction with the SDU complex and that introduction of a positive charge in the solvent filled pocket that accommodates the rotated W155 rotamer will decrease FXN binding affinity. Overall the studies on the FRDA clinical mutants and related variants revealed the necessary components for Fxn binding and activation of the Fe-S cluster biosynthetic complex and has implications for understanding the molecular basis of Friedreich's ataxia. Future studies will focus on the FRDA clinical variant D122Y and related acidic patch FXN variants. Currently, we have shown the D122Y FRDA variant to be uncompromised in binding the SDU complex and in stimulating the activity of both the cysteine desulfurase reaction and Fe-S cluster assembly. Initial studies suggest the one difference between D122Y FXN and native FXN is that D122Y lacks the ferrous iron stimulation of the cysteine desulfurase reaction and thus may be an iron ligand.

Using enzyme kinetic studies and radio-labeled substrate, we have determined that after desulfurization of alanine by the catalytic cysteine on NFS1, the persulfide formed is directly transferred to C104 on ISCU2. As C104 is buried on an α–helix, this persulfide transfer event must be coupled to a helix to coil transition in order to expose C104 on ISCU2 to accept the persulfide sulfur. Based on our findings that a single point mutation, M106I on ISCU2 is able to bypass the need for FXN activation of the sulfur transfer reaction *in vitro*, a model was developed in which FXN binding to the SDU complex stabilizes the coiled conformation of ISCU2. Further studies on ISCU2 point

mutants and FXN variants identified residue H103 on ISCU2 as being critical for frataxin binding affinity and suggested that the rotation of FXN residue W155 into a solvent filled pocket on the surface of the protein is accompanied by ISCU2 residue H103 insertion into the native W155 position and formation of a cation-π interaction with FXN residue R165. This cation- π interaction formed at the interface of the SDUF protein complex likely imposes specificity and stability on the complex.

Additionally, evidence has been provided that the persulfide species transferred from NFS1 to ISCU2 is viable in Fe-S cluster assembly. Specifically, using a radio-labeled cysteine substrate, the ^{35}S label was traced from NFS1 to incorporation on ISCU2 as a persulfide, followed by incorporation into an Fe-S cluster on the scaffold protein, and lastly as a component of an Fe-S cluster transferred to ferredoxin. These studies are consistent with the mechanism of Fe-S cluster biosynthesis being sulfur first; ISCU2 can accept the persulfide sulfur in the absence of iron, following transpersulfuration of cysteine residues on ISCU2, ferrous iron can bind, and lastly, the sequential 2-electron reduction of each sulfane sulfur atom is required to complete cluster formation. Future studies will be aimed at tracing ^{55}Fe from its incorporation in the SDUF complex through Fe-S cluster assembly reaction and transfer to an apo target protein. These studies will be aimed at determining whether the stimulatory iron that binds to the SDUF complex is incorporated into Fe-S clusters and refine our mechanistic understanding of cluster assembly.

The concluding studies on the *E. coli* system for Fe-S cluster biosynthesis reveal that FXN and the FXN homolog in *E. coli,* CyaY*,* can functionally replace one another

in vitro. These studies confirm that FXN in the human system functions as an activator of both the cysteine desulfurase and Fe-S cluster reactions while CyaY is an inhibitor of Fe-S cluster assembly in *E. coli*. In a series of inter-species reactions, we have concluded that modifications to the cysteine desulfurase dictate the activator or inhibitor regulatory role of FXN in Fe-S cluster biosynthesis. Future studies will be aimed at deciphering the differences between the *E. coli* and human cysteine desulfurase enzymes and what modifications govern the intrinsic activity of the enzymes. As well, the mode of CyaY inhibition of Fe-S cluster assembly will also be investigated. Initial data using the ^{35}S-cysteine substrate and enzyme kinetics suggest that CyaY inhibition does not occur at the level of sulfur transfer from IscS to IscU. Other modes of inhibition will be investigated including whether CyaY stabilizes an off conformation that is incapable of cluster formation or whether CyaY inhibits iron incorporation.

REFERENCES

1. Huber, C. and Wachtershauser, G. (1998) Peptides by activation of amino acids with CO on (Ni,Fe)S surfaces: implications for the origin of life. *Science* 281(5377), 670-672.
2. Johnson, D.C., Dean, D.R., Smith, A.D., and Johnson, M.K. (2005) Structure, function, and formation of biological iron-sulfur clusters. *Annu. Rev. Biochem.* 74, 247-281.
3. Bandyopadhyay, S., K. Chandramouli, and Johnson, M.K. (2006) Iron-sulfur cluster biosynthesis. *Biochem. Soc. Trans.* 36(Pt 6), 1112-1119.
4. Henderson, R.A. (2005) Mechanistic studies on synthetic Fe-S-based clusters and their relevance to the action of nitrogenases. *Chem. Rev.* 105(6), 2365-437.
5. Johnson, M.K. (1998) Iron-sulfur proteins: new roles for old clusters. *Curr. Opin. Chem. Biol.* 2(2), 173-181.
6. Fontecave, M. (2006) Iron-sulfur clusters: ever-expanding roles. *Nat. Chem. Biol.* 2(4), 171-174.
7. Brzóska, K., S. Meczyńska, and Kruszewski, M. (2006) Iron-sulfur cluster proteins: electron transfer and beyond. *Acta Biochi.m Pol.* 53(4), 685-691.
8. Lill, R. (2009) Function and biogenesis of iron-sulphur proteins. *Nature* 460(7257), 831-838.
9. Dos Santos, P.C. and Dean, D.R. (2008) A newly discovered role for iron-sulfur clusters. *Proc. Natl. Acad. Sci. U. S. A.* 105(33), 11589-11590.

10. Rudolf, J., Makrantoni, V., Ingledew, W.J., Stark, M.J., and White, M.F. (2006) The DNA repair helicases XPD and FancJ have essential iron-sulfur domains. *Mol. Cell* 23(6), 801-808.

11. Beinert, H., Holm, R.H., and Munck, E. (1997) Iron-sulfur clusters: nature's modular, multipurpose structures. *Science* 277(5326), 653-659.

12. Frey, P.A., Hegeman, A.D., and Ruzicka, F.J. (2008) The Radical SAM Superfamily. *Crit. Rev. Biochem. Mol. Biol.* 43(1), 63-88.

13. Meyer, J. (2008) Iron-sulfur protein folds, iron-sulfur chemistry, and evolution. *J. Biol. Inorg. Chem.* 13(2), 157-170.

14. Crane, B.R., Siegel, L.M., and Getzoff, E.D. (1995) Sulfite reductase structure at 1.6 A: evolution and catalysis for reduction of inorganic anions. *Science*, 270(5233), 59-67.

15. Ragsdale, S.W. and Kumar, M., (1996) Nickel-Containing Carbon Monoxide Dehydrogenase/Acetyl-CoA Synthase. *Chem. Rev.* 96(7), 2515-2540.

16. Georgiadis, M.M., Komliya, H., Chakrabarti, P., Woo, D., Kornuc, J.J., and Rees, D.C. (1992) Crystallographic structure of the nitrogenase iron protein from Azotobacter vinelandii. *Science* 257(5077), 1653-1659.

17. Kim, J. and Rees, D.C. (1992) Structural models for the metal centers in the nitrogenase molybdenum-iron protein. *Science* 257(5077), 1677-1682.

18. Sheftel, A.D. and Lill, R. (2009) The power plant of the cell is also a smithy: the emerging role of mitochondria in cellular iron homeostasis. *Ann. Med.* 41(2), 82-99.

19. Jacobson, M.R., Cash, V.L, Weiss, M.C., Laird, N.F., Newton, W.E., and Dean, D.R. (1989) Biochemical and genetic analysis of the nifUSVWZM cluster from Azotobacter vinelandii. *Mol. Gen. Genet.* 219(1-2), 49-57.

20. Zheng, L., Flint, D.H., and Dean, D.R. (1998) Assembly of iron-sulfur clusters. Identification of an iscSUA-hscBA-fdx gene cluster from Azotobacter vinelandii. *J. Biol. Chem.* 273(21),. 13264-13272.

21. Takahashi, Y. and Tokumoto, U. (2002) A third bacterial system for the assembly of iron-sulfur clusters with homologs in archaea and plastids. *J. Biol. Chem.* 277(32), 28380-28383.

22. Xu, X.M. and Moller, S.G. (2008) Iron-sulfur cluster biogenesis systems and their crosstalk. *Chembiochem* **9**(15), 2355-2362.

23. Ayala-Castro, C., Saini, A., and Outten, F.W. (2008) Fe-S cluster assembly pathways in bacteria. *Microbiol. Mol. Biol. Re.v* 72(1), 110-25.

24. Fontecave, M. and Ollagnier-de-Choudens, S. (2008) Iron-sulfur cluster biosynthesis in bacteria: Mechanisms of cluster assembly and transfer. *Arch. Biochem. Biophy.s* 474(2), 226-237.

25. Tokumoto, U., Kitamura, S., Fukuyama, K., and Takhashi, Y. (2004) Interchangeability and distinct properties of bacterial Fe-S cluster assembly systems: functional replacement of the isc and suf operons in Escherichia coli with the nifSU-like operon from Helicobacter pylori. *J. Biochem.* 136(2), 199-209.

26. Jang, S. and Imlay, J.A. (2010) Hydrogen peroxide inactivates the Escherichia coli Isc iron-sulphur assembly system, and OxyR induces the Suf system to compensate. *Mol. Microbiol.* 78(6),. 1448-1467.

27. Imlay, J.A. (2003) Pathways of oxidative damage. *Annu Rev Microbiol.* **57**, 395-418.

28. Ott, M., Gogvadze, F., Orrenius, S., and Zhivotovsky, B. (2007) Mitochondria, oxidative stress and cell death. *Apoptosis* 12(5), 913-922.

29. Turrens, J.F. (2003) Mitochondrial formation of reactive oxygen species. *J. Physiol*. 552(Pt 2),. 335-344.

30. Zheng, L., White, R.H., Cash, V.L., and Dean, D.R. (1994) Mechanism for the desulfurization of L-cysteine catalyzed by the nifS gene product. *Biochemistry* 33(15),. 4714-4720.

31. Lill, R. and Muhlenhoff, U. (2006) Iron-sulfur protein biogenesis in eukaryotes: components and mechanisms. *Annu. Rev. Cell Dev. Biol.*, 22, 457-486.

32. Krebs, C., Smith, A.D., Frazzon, J., Dean, D.R., Huynh, B.H., and Johnson, M.K. (2001) IscA, an alternate scaffold for Fe-S cluster biosynthesis. *Biochemistry* 40(46), 14069-14080.

33. Shi, R., Villarroya, M., Moukadiri, I., Zhang, L., Trempe, J.F., Matte, A., Armengod, M.E., and Cygler, M. (2010) Structural basis for Fe-S cluster assembly and tRNA thiolation mediated by IscS protein-protein interactions. *PLoS. Biol.* 8(4), e1000354.

34. Frazzon, J. and Dean, D.R. (2001) Feedback regulation of iron-sulfur cluster biosynthesis. *Proc. Natl. Acad. Sci. U. S. A.* 98(26), 14751-14753.

35. Outten, F.W., Jaman, O.D., and Storz, G. (2004) A suf operon requirement for Fe-S cluster assembly during iron starvation in Escherichia coli. *Mol. Microbiol.* 52(3), 861-782.

36. Hentze, M.W., Muckenthaler, M.U., and Andrews, N.C. (2004) Balancing acts: molecular control of mammalian iron metabolism. *Cell* **117**(3), 285-297.

37. Vickery, L. and Cupp-Vickery, J. (2007) Molecular chaperones HscA/Ssq1 and HscB/Jac1 and their roles in iron-sulfur protein maturation. *Crit. Rev. Biochem. Mol. Biol.* 42(2), 95-111.

38. Santos, R., Silwa, D., Seguin, A., Camdro, J.M., and Lesuisse, E. (2010) Friedreich ataxia: molecular mechanisms, redox considerations, and therapeutic opportunities. *Antioxid Redox Signal* 13, 651-690.

39. Campuzano, V., Montermini, L., Molto, M.D., Pianese, L., Cossee, M., Cavalcanti, F., Monros, E., Rodius, P., Duclos, F., Monticelli, A., Zara, F., Canizares, J., Koutnikova, H., Bidichandani, S., Gellera, C., Brice, A., Trouillas, P., DeMichele, F., Filla, A., DeFrutos, R., Palau, F., Patel, P.I., DiDonato, S., Mandel, J.L., Cocozza, S., and Koenig, M. (1996) Friedreich's ataxia: autosomal recessive disease caused by an intronic GAA triplet repeat expansion. *Scienc* 271(5254), 1423-1427.

40. De Biase, I., Rasmussen, A., Monticelli, A., Al-Mahdawi, S., Pook, M., Cocozza, S. and Bidichandani, S.I. (2007) Somatic instability of the expanded GAA triplet-

repeat sequence in Friedreich ataxia progresses throughout life. *Genomics* 90(1), 1-5.

41. Harding, A.E. (1981) Friedreich's ataxia: a clinical and genetic study of 90 families with an analysis of early diagnostic criteria and intrafamilial clustering of clinical features. *Brain* 104(3), 589-620.

42. Babcock, M., Silva, D., Oaks, R., Davis-Kaplan, S., Jiralerspong, S., Monermini, L., Pandolfo, M., and Kaplan, J. (1997) Regulation of mitochondrial iron accumulation by Yfh1p, a putative homolog of frataxin. *Science* 276(5319), 1709-1712.

43. Bradley, J.L., Blake, J.C., Chamerlain, S., Thomas, P.K., Cooper, J.M., and Schapira, A.H. (2000) Clinical, biochemical and molecular genetic correlations in Friedreich's ataxia. *Hum. Mol. Genet*. 9(2), 275-282.

44. Rotig, A., deLonlay, P., Chretiaen, D., Foury, F., Koenig, M., Sidi, D., Munnich, A., and Rustin, P. (1997) Aconitase and mitochondrial iron-sulphur protein deficiency in Friedreich ataxia. *Nat. Genet.* 17(2), 215-217.

45. Ristow, M., Pfister, M.F., Yee, A.J., Schubert, M., Michael, L., Zhang, C.Y., Ueki, K., Michael, M.D., Lowell, B.B., and Kahn, C.R. (2000) Frataxin activates mitochondrial energy conversion and oxidative phosphorylation. *Proc. Natl. Acad. Sci. U. S. A*. 97(22), 12239-12243.

46. Jiralerspong, S., Ge, B., Hudson, T.J., and Pandofo, M. (2001) Manganese superoxide dismutase induction by iron is impaired in Friedreich ataxia cells. *FEBS Lett*. 509(1), 101-105.

47. Park, S., Gakh, O., Mooney, S.M., and Isaya, G. (2002) The ferroxidase activity of yeast frataxin. *J. Biol. Chem*. 277(41), 38589-38595.

48. Cavadini, P., O'Neill, H.A., Benada, O., and Isaya, G. (2002) Assembly and iron-binding properties of human frataxin, the protein deficient in Friedreich ataxia. *Hum. Mol. Genet*. 11(3), 217-227.

49. Gakh, O., D.Y.T. Smith, and Isaya, G. (2008) Assembly of the iron-binding protein frataxin in Saccharomyces cerevisiae responds to dynamic changes in mitochondrial iron influx and stress level. *J. Biol. Chem*. 283(46),. 31500-31510.

50. Schagerlof, U., Elmlund, H., Gakh, O., Nordlund, G., Hebert, H., Lindahl, M., Isaya, G., and Al-Karadaghi, S. (2008) Structural basis of the iron storage function of frataxin from single-particle reconstruction of the iron-loaded oligomer. *Biochemistry* 47(17), 4948-4954.

51. Karlberg, T., Gakh, O., Park, S., Ryde, U., Lindahl, M., Leath, K., Garman, E., Isaya, G., and Al-Karadaghi, S. (2006) The structures of frataxin oligomers reveal the mechanism for the delivery and detoxification of iron. *Structure* 14(10), 1535-1546.

52. Gakh, O., Park, S., Liu, G., Macomber, L., Imlay, J.A., Ferreira, G.C., and Isaya, G. (2006) Mitochondrial iron detoxification is a primary function of frataxin that limits oxidative damage and preserves cell longevity. *Hum. Mol. Genet*. 15(3), 467-479.

53. Yoon, T. and Cowan, J. (2003) Iron-sulfur cluster biosynthesis. Characterization of frataxin as an iron donor for assembly of [2Fe-2S] clusters in ISU-type proteins. *J. Am. Chem. Soc.* 125(20), 6078-6084.

54. Gerber, J., U. Muhlenhoff, and Lill, R. (2003) An interaction between frataxin and Isu1/Nfs1 that is crucial for Fe/S cluster synthesis on Isu1. *EMBO Rep.* 24(9), 906-911.

55. Huynen, M.A., Snel, B., Bork, P., and Gibson, T.J. (2001) The phylogenetic distribution of frataxin indicates a role in iron-sulfur cluster protein assembly. *Hum. Mol. Genet.* 10(21),. 2463-2468.

56. Muhlenhoff, U., Richhardt, N., Ristow, M., Kispal, G., and Lill, R. (2002) The yeast frataxin homolog Yfh1p plays a specific role in the maturation of cellular Fe/S proteins. *Hum. Mol. Genet*. 11(17), 2025-2036.

57. Stehling, O., Elsasser, H.P., Bruckel, B., Muhlenhoff, U., and Lill, R. (2004) Iron-sulfur protein maturation in human cells: evidence for a function of frataxin. *Hum. Mol. Genet*. 13(23), 3007-3015.

58. Lesuisse, E., Santos, R., Matzanke, B.F., Knight, S.A., Camadro, J.M., and Dancis, A. (2003) Iron use for haeme synthesis is under control of the yeast frataxin homologue (Yfh1). *Hum. Mol. Genet*. 12(8), 879-889.

59. Becker, E.M., Greer, J.M., Ponka, P., and Richardson, D.R. (2002) Erythroid differentiation and protoporphyrin IX down-regulate frataxin expression in Friend cells: characterization of frataxin expression compared to molecules involved in iron metabolism and hemoglobinization. *Blood* 99(10), 3813-3822.

60. Adinolfi, S., Iannuzzi, C., Prischi, F., Pastore, C., Iametti, S., Martin, S.R., Bonomi, F., and Pastore, A. (2009) Bacterial frataxin CyaY is the gatekeeper of iron-sulfur cluster formation catalyzed by IscS. *Nat. Struct. Mol. Biol*. 16(4), 390-396.

61. Delatycki, M.B., Williamson, R., and Forrest, S.M. (2000) Friedreich ataxia: an overview. *J. Med. Genet.* 37(1), 1-8.

62. Wong, A., Yang, J., Cavadini, P., Gellera, C., Lonnerdal, B., Taroni, F., and Cortopassi, G. (1999) The Friedreich's ataxia mutation confers cellular sensitivity to oxidant stress which is rescued by chelators of iron and calcium and inhibitors of apoptosis. *Hum. Mol. Genet*. 8(3), 425-430.

63. Radisky, D.C., M.C. Babcock, and Kaplan, J. (1999) The yeast frataxin homologue mediates mitochondrial iron efflux. Evidence for a mitochondrial iron cycle. *J. Biol. Chem.* 274(8), 4497-4499.

64. Foury, F. and Talibi, D. (2001) Mitochondrial control of iron homeostasis. A genome wide analysis of gene expression in a yeast frataxin-deficient strain. *J. Biol. Chem.* 276(11), 7762-7768.

65. Gakh, O., Bedekoviccs, T., Duncan, S.F., Smith, D.Y., Berkholz, D.S., and Isaya, G. (2010) Normal and Friedreich ataxia cells express different isoforms of frataxin with complementary roles in iron-sulfur cluster assembly. *J. Biol. Chem*. 285(49), 38486-38501.

66. Nichol, H., Gakh, O., O'Neill, H.A., Pickering, I.J., Isaya, G., and George, G.N. (2003) Structure of frataxin iron cores: an X-ray absorption spectroscopic study. *Biochemistry* 42(20), 5971-5976.

67. Park, S., Gakh, O., O'Neill, H.A., Magravita, A., Nichol, H., Ferreira, G.C., and Isaya, G. (2003) Yeast frataxin sequentially chaperones and stores iron by coupling protein assembly with iron oxidation. *J. Biol. Chem*. 278(33), 31340-31351.

68. Adinolfi, S., Trifuoggi, M., Politou, A.S., Martin, S., and Pastore, A. (2002) A structural approach to understanding the iron-binding properties of phylogenetically different frataxins. *Hum. Mol. Genet*. 11(16), 1865-1877.

69. Aloria, K., Schilke, B., Andre, A., and Craig, E.A. (2004) Iron-induced oligomerization of yeast frataxin homologue Yfh1 is dispensable in vivo. *EMBO Rep*. **5**(11), 1096-1101.

70. Seguin, A., Sutak, R., Bulteau, A.L., Garcia-Serres, R., Oddou, J.L., Lefevre, S., Santos, R., Dancis, A., Camadro, J.M., Latour, J.M., and Lesuisse, E. (2010) Evidence that yeast frataxin is not an iron storage protein in vivo. *Biochim. Biophys. Acta* 1802(6), 531-538.

71. Pandolfo, M. and Pastore, A. (2009) The pathogenesis of Friedreich ataxia and the structure and function of frataxin. *J. Neurol.* 256 Suppl 1,. 9-17.

72. Bou-Abdallah, F., Adinolfi, S., Pastore, A., Laue, T.M., and Dennis-Chasteen, N. (2004) Iron binding and oxidation kinetics in frataxin CyaY of Escherichia coli. *J. Mol. Biol*. 341(2), 605-615.

73. Cook, J.D., Bencze, K.Z., Jankovic, A.D., Crater, A.K., Busch, C.N., Bradley, P.B., Stemmler, A.J., Spaller, M.R., and Stemmler, T.L. (2006) Monomeric yeast frataxin is an iron-binding protein. *Biochemistry* 45(25), 7767-7777.

74. Foury, F., A. Pastore, and Trincal, M. (2007) Acidic residues of yeast frataxin have an essential role in Fe-S cluster assembly. *EMBO Rep*. 8(2), 194-199.

75. Layer, G., Sanakis, Y., and Fontecave, M. (2006) Iron-sulfur cluster biosynthesis: characterization of Escherichia coli CYaY as an iron donor for the assembly of [2Fe-2S] clusters in the scaffold IscU. *J. Biol. Chem*. 281(24), 16256-16263.

76. Ramazzotti, A., Vanmansart, V., and Foury, F. (2004) Mitochondrial functional interactions between frataxin and Isu1p, the iron-sulfur cluster scaffold protein, in Saccharomyces cerevisiae. *FEBS Lett*. **557**(1-3), 215-220.

77. Correia, A.R., Ow, S.Y., Wright, P.C., and Gomes, C.M. (2009) The conserved Trp155 in human frataxin as a hotspot for oxidative stress related chemical modifications. *Biochem. Biophys. Res. Commun*. 390(3), 1007-1011.

78. Leidgens, S., De Smet, S., and Foury, F. (2010) Frataxin interacts with Isu1 through a conserved tryptophan in its beta-sheet. *Hum. Mol. Genet.* 19(2), 276-86.

79. Wang, T. and. Craig, E.A. (2008) *Bi*nding of yeast frataxin to the scaffold for Fe-S cluster biogenesis, Isu. *J. Biol. Chem*. 283(18), 12674-12679.

80. Correia, A.R., Ow, S.Y., Wright, P.C., and Gomes, C.M. (2009) Dynamics, stability and iron-binding activity of frataxin clinical mutants. *FEBS J*. 275(14), 3680-36890.

81. Cook, J.D., Kondapalli, K.C., Rawat, S., Childs, W.C., Murgesan, Y., Dancis, A., and Stemmler, T.L. (2010) Molecular details of the yeast frataxin-Isu1 interaction during mitochondrial Fe-S cluster assembly. *Biochemistry* 49, 8756-8765.

82. Schmucker, S. (2011) Mammalian Frataxin: An Essential Function for Cellular Viability through an Interaction with a Preformed ISCU/NFS1/ISD11 Iron-Sulfur Assembly Complex. *PLoS ONE* **6**(1), e16199.

83. Leidgens, S., De Smet, S., and Foury, F. (2010) Frataxin interacts with Isu1 through a conserved tryptophan in its beta-sheet. *Hum. Mol. Genet*. 19, 276-286.

84. Wang, T. and Craig, E.A. (2008) Binding of yeast frataxin to the scaffold for Fe-S cluster biogenesis, Isu. *J. Biol. Chem*. 283(18), 12674-12679.

85. Shan, Y., Napoli, E., and Cortopassi, G.A. (2007) Mitochondrial frataxin interacts with ISD11 of the NFS1/ISCU complex and multiple mitochondrial chaperones. *Hum. Mol. Genet*. 16(8), 929-941.

86. Cupp-Vickery, J.R., Urbina, H., and Vickery, L.E. (2003) Crystal structure of IscS, a cysteine desulfurase from Escherichia coli. *J. Mol. Biol*. 330(5), 1049-1059.

87. Martin, R.G. and Rosner, J.L. (2001) The AraC transcriptional activators. *Curr. Opin. Microbiol*. 4(2), 132-137.

88. Schwartz, C.J., Giel, J.L., Patschkowski, T., Luther, C., Ruzicka, F.J., Beinert, H., and Kiley, P.J. (2001) IscR, an Fe-S cluster-containing transcription factor, represses expression of Escherichia coli genes encoding Fe-S cluster assembly proteins. *Proc. Natl. Acad. Sci .U. S. A.* 98(26), 14895-14900.

89. Prischi, F., Konarev, P.V., Iannuzzi, C., Pastore, C., Adinolfi, S., Martin, S.R., Svergun, D.I., and Pastore, A. (2010) Structural bases for the interaction of frataxin with the central components of iron-sulphur cluster assembly. *Nat. Commun.* 1(7), 95.

90. Adinolfi, S., Iannuzzi, F., Prischi, F., Pastore, C., Iametti, S., Martin, S.R., Bonomi, F., and Pastore, A. (2009) Bacterial frataxin CyaY is the gatekeeper of iron-sulfur cluster formation catalyzed by IscS. *Nat. Struct. Mol. Biol.* 16(4), 390-396.

91. Iannuzzi, C., Adinolfi, S., Howes, B.D., Garcia-Serres, R., Clemancey, M., Latour, J.M., Smulevich, G., and Pastore, A. (2011) The Role of CyaY in Iron Sulfur Cluster Assembly on the E. coli IscU Scaffold Protein. *PLoS One* 6(7), e21992.

92. Li, D., Ohshima, K., Jiralerspong, S., Bojanowski, M.R., and Pandolfo, M. (1999) Knock-out of the cyaY gene in Escherichia coli does not affect cellular iron content and sensitivity to oxidants. *FEBS Lett*. ***456***(1), 13-16.

93. Vivas, E., Skovran, E., and Downs, D.M. (2006) Salmonella enterica strains lacking the frataxin homolog CyaY show defects in Fe-S cluster metabolism in vivo. *J. Bacteriol*. 188(3), 1175-1179.

94. Marelja, Z., Stockein, W., Nimtz, M., and Leimkuhler, S. (2008) A novel role for human Nfs1 in the cytoplasm: Nfs1 acts as a sulfur donor for MOCS3, a protein involved in molybdenum cofactor biosynthesis. *J. Biol. Chem*. 283(37), 25178-25185.

95. Wiedemann, N., Urzica, E., Guiard, B., Muller, H., Lohaus, C., Meyer, H.E., Ruan, M.T., Meisinger, C., Muhlenhoff, U., Lill, R., and Pfanner, N. (2005) Essential role of Isd11 in mitochondrial iron-sulfur cluster synthesis on Isu scaffold proteins. *EMBO J*. 25(1), 184-195.

96. Tsai, C.-L. and Barondeau, D.P. (2010) Human frataxin is an allosteric switch that activates the Fe-S cluster biosynthetic complex. *Biochemistry* 49(43), 9132-9139.

97. Uhrigshardt, H., Singh, A., Kovtunovych, G., Ghosh, M., and Rouault, T.A. (2010) Characterization of the human HSC20, an unusual DnaJ type III protein, involved in iron-sulfur cluster biogenesis. Hum. Mol. Genet. 19(19), 3816-3834.

98. Bitto, E., Ingman, C.A., Bittova, L., Kondrahov, D.A., Bannen, R.M., Fox, B.G., Markley, J.L., and Phillips, G.N. (2008) Structure of human J-type co-chaperone HscB reveals a tetracysteine metal-binding domain. *J. Biol. Chem.* 283(44), 30184-30192.

99. Fontecave, M., Choudens, S.L., Py, B., and Barras, F. (2005) Mechanisms of iron-sulfur cluster assembly: the SUF machinery. *J. Biol. Inorg. Chem*. 10(7), 713-721.

100. Ollagnier de Choudens, S., Mattioli, T., Takhashi, Y., and Fontecave, M. (2001) Iron-sulfur cluster assembly: characterization of IscA and evidence for a specific and functional complex with ferredoxin. *J. Biol. Chem*. 276(25), 22604-22607.

101. Mansy, S.S., Wu, G., Surerus, K.K., and Cowan, J.A. (2002) Iron-sulfur cluster biosynthesis. Thermatoga maritima IscU is a structured iron-sulfur cluster assembly protein. *J. Biol. Chem*. 277(24), 21397-21404.

102. Urbina, H.D., Silbeg, J.J., Hoff, K.G., and Vickery, L.E. (2001) Transfer of sulfur from IscS to IscU during Fe/S cluster assembly. *J. Biol. Chem*. 276(48), 44521-44526.

103. Smith, A.D., Agar, J.N., Johnson, K.A., Frazzon, J., Amster, I.J., Dean, D.R., and Johnson, M.K. (2001) Sulfur transfer from IscS to IscU: the first step in iron-sulfur cluster biosynthesis. *J. Am. Chem. Soc*. 123(44), 11103-11104.

104. Sendra, M., Ollagnier de Choudens, S., Lascouz, D., Sanakis, Y., and Fontecave, M. (2007) The SUF iron-sulfur cluster biosynthetic machinery: sulfur transfer from the SUFS-SUFE complex to SUFA. *FEBS Lett*. 581(7), 1362-1368.

105. Huang, J. and Cowan, J.A. (2009) Iron-sulfur cluster biosynthesis: role of a semi-conserved histidine. *Chem. Commun. (Camb)* 21, 3071-3073.

106. Shimomura, Y., Wada, K., Fukuyama, K., and Takahashi, Y. (2008) The asymmetric trimeric architecture of [2Fe-2S] IscU: implications for its scaffolding during iron-sulfur cluster biosynthesis. *J. Mol. Biol.* 383(1), 133-143.

107. Foster, M.W.,Hwang, J., Pnner-Hahn, J.E., and Surerus, K.K. (2000) A mutant human IscU protein contains a stable [2Fe-2S](2+) center of possible functional significance. *JACS* 122(28),. 6805-6806.

108. Agar, J.N., Krebs, C., Huynh, B.H., Dean, D.R., and Johnson, M.K. (2000) IscU as a scaffold for iron-sulfur cluster biosynthesis: sequential assembly of [2Fe-2S] and [4Fe-4S] clusters in IscU. *Biochemistry* 39(27), 7856-7862.

109. Kato, S.-I., Kurihara, T., Takhashi, Y., Tokumoto, U., Yoshimura, T., and Esaki, N. (2002) Cys-328 of IscS and Cys-63 of IscU are the sites of disulfide bridge formation in a covalently bound IscS/IscU complex: implications for the mechanism of iron-sulfur cluster assembly. *Proc. Natl. Acad. Sci. U.S.A*. 99(9), 5948-5952.

110. Smith, A.D., Frazzon, J., Dean, D.R., and Johnson, M.K. (2005) Role of conserved cysteines in mediating sulfur transfer from IscS to IscU. *FEBS Lett*. 579(23), 5236-5240.

111. Bonomi, F., Iametti, S., Morleo, A., Ta, D., and Vickery, L.E. (2011) Facilitated Transfer of IscU-[2Fe2S] Clusters by Chaperone-Mediated Ligand Exchange. *Biochemistry* 50(44),. 9641-9650.

112. Schmucker, S. and Puccio, H. (2010) Understanding the molecular mechanisms of Friedreich Ataxia to develop therapeutic approaches. *Hum. Mol. Genet*. 19, R103-R110.

113. Santos, R., Lefevre, S., Silwa, D., Seguin, A., Cadro, J.M., and Lesuisse, E. (2010) Friedreich's Ataxia: Molecular Mechanisms, Redox Considerations and Therapeutic Opportunities. *Antioxid Redox Signal* 13(5), 651-690.

114. Schöls, L., Amoridis, G., Przuntek, H., Frank, G., Epplen, J.T., and Epplen, C. (1997) Friedreich's ataxia. Revision of the phenotype according to molecular genetics. *Brain* 120 (Pt 12), 2131-2140.

115. Dürr, A., Cossee, M., Agis, Y., Campuzano, V., Mignard, C., Penet, C., Manel, J., Brice, A., and Koenig, M. (1996) *C*linical and genetic abnormalities in patients with Friedreich's ataxia. *N. Engl. J. Med*. 335(16), 1169-1175.

116. Filla, A., DeMichele, G., Cavalcanti, F., Pianese, L., Monticelli, A., Campanella, G., and Cocozza, S. (1996) The relationship between trinucleotide (GAA) repeat length and clinical features in Friedreich ataxia. *Am. J. Hum. Genet*. 59(3), 554-560.

117. Cossee, M., Durr, A., Allinson, P., Kostrzewa, M., Nivelon-Chevallier, A., Gustavson, K.H., Kohlschutter, A., Muller, U., Mandel, J.L., Brice, A., Koenig, M., Cavalcanti, F., Tammaro, A., DeMichele, G., Fila, A., Cocozza, S., Labuda, M., Mantermini, L., Poirier, J., and Pandolfo, M. (1999) Friedreich's ataxia: point mutations and clinical presentation of compound heterozygotes. *Ann. Neurol*. 45(2), 200-206.

118. Deutsch, E.C., Santani, A.B., Perlman, S.L., Farmer, J.M., Stolle, C.A., Marusich, M.F., and Lynch, D.R. (2010) A rapid, noninvasive immunoassay for

frataxin: Utility in assessment of Friedreich ataxia. *Mol. Genet. Metab*. 101, 238-245.

119. Rouault, T.A. and. Tong, W.H. (2008) Iron-sulfur cluster biogenesis and human disease. *Trends Genet*. 24(8), 398-407.

120. Foster, M.W., Manxy, S.S., Hwang, J., Penner-Hahn, J.E., Surerus, K.K., and Cowan, J.A. (2000) A Mutant Human IscU Protein Contains a Stable [2Fe2S]2+ Center of Possible Functional Significance. *J. Am. Chem. Soc*. 122, 6805-6806.

121. Adam, A.C., Bornhovd, C., Prokisch, H., Neupert, W., and Hell, K. (2006) The Nfs1 interacting protein Isd11 has an essential role in Fe/S cluster biogenesis in mitochondria. *EMBO J.* 25(1), 174-183.

122. Shi, Y., Ghosh, M.C., Tong, W.H., and Rouault, T.A. (2009) Human ISD11 is essential for both iron-sulfur cluster assembly and maintenance of normal cellular iron homeostasis. *Hum. Mol. Genet.* 18(16), 3014-3025.

123. Wiedemann, N., Guiard, B., Muller, H., Lohaus, C., Meyer, H.E., Ryan, M.T., Mesinger, C., Muhlenhoff, U., Lill, R., and Pfanner, N. (2005) Essential role of Isd11 in mitochondrial iron-sulfur cluster synthesis on Isu scaffold proteins. *EMBO J*. **25**(1),. 184-195.

124. Zheng, L., White, R.H., Cash, V.L., Jack, R.F., and Dean, D.R. (1993) Cysteine desulfurase activity indicates a role for NIFS in metallocluster biosynthesis. Proc. Natl. Acad. Sci. U.SA. 90(7), 2754-2758.

125. Hoff, K.G., J.J. Silberg, and Vickery, L. (2000) Interaction of the iron-sulfur cluster assembly protein IscU with the Hsc66/Hsc20 molecular chaperone system of Escherichia coli. *Proc. Natl. Acad. Sci. U.S.A*. **97**(14), 7790-7795.

126. Fuzéry, A., Tonelli, M., Cornilescu, G., Vickery, L.E., and Markley, J.L. (2008) Solution Structure of the Iron-Sulfur Cluster Cochaperone HscB and Its Binding Surface for the Iron-Sulfur Assembly Scaffold Protein IscU. *Biochemistry* 47, 9394-9404.

127. Cavadini, P., Adamec, J., Taroni, F., Gakh, O., and Isaya, G. (2000) Two-step processing of human frataxin by mitochondrial processing peptidase. Precursor and intermediate forms are cleaved at different rates. *J. Biol. Chem*. 275(52), 41469-41475.

128. Schmucker, S., Argentini, M., Carelle-Calmels, N., Martelli, A., and Puccio, H. (2008) The in vivo mitochondrial two-step maturation of human frataxin. *Hum. Mol. Genet*. 17(22), 3521-3531.

129. Long, S., Jirku, M., Ayalo, F.J., and Lukes, J. (2008) Mitochondrial localization of human frataxin is necessary but processing is not for rescuing frataxin deficiency in Trypanosoma brucei. *Proc. Natl. Acad. Sci. U.SA*. 105(36), 13468-13473.

130. Koutnikova, H., V. Campuzano, and Koenig, M. (1998) Maturation of wild-type and mutated frataxin by the mitochondrial processing peptidase. *Hum. Mol. Genet*. **7**(9), 1485-1489.

131. Branda, S.S., Cavadini, P., Adamec, J., Kalousek, F., Taroni, F., and Isaya, G. (1999) Yeast and human frataxin are processed to mature form in two sequential steps by the mitochondrial processing peptidase. *J. Biol. Chem*. 274(32), 22763-22769.

132. Condo, I., Ventura, N., Malisan, F., Rufini, A., Tomassini, B., and Testi, R. (2007) In vivo maturation of human frataxin. *Hum. Mol. Genet.* 16(13), 1534-1540.

133. Yoon, T., Dizin, E., and Cowan, J.A. (2007) N-terminal iron-mediated self-cleavage of human frataxin: regulation of iron binding and complex formation with target proteins. *J. Biol. Inorg. Chem*. 12(4), 535-542.

134. Stemmler, T.L., Lesuisse, E., Pain, D., and Dancis, A. (2010) Frataxin and mitochondrial Fe-S cluster biogenesis. *J. Biol. Chem*. 285(35), 26737-26743.

135. Marelja, Z., Stocklein, W., Nimtz, M., and Leimkuhler, S. (2008) A novel role for human Nfs1 in the cytoplasm: Nfs1 acts as a sulfur donor for MOCS3, a protein involved in molybdenum cofactor biosynthesis. *J. Biol. Chem*. 283(37), 25178-25185.

136. Siegel, L.M. (1965) A direct microdetermination for sulfide. *Anal. Biochem*. 11, 126-132.

137. Huang, J. and Cowan, J.A. (2009) Iron-sulfur cluster biosynthesis: role of a semi-conserved histidine. *Chem. Commun. (Camb)*, 21(21), 3071-3073.

138. Di Cera, E. (2009) Kinetics of Allosteric Activation. *Methods in Enzymology, Vol 466: Biothermodynamics, Pt B* 466, 259-271.

139. Leslie, A.G.W. (1992) Recent changes to the MOSFLM package for processing film and image plate data *Joint CCP4 + ESF-EAMCB Newsletter on Protein Crystallography*, 26.

140. The CCP4 suite: programs for protein crystallography. (1994) *Acta Crystallogr D Biol Crystallogr*. 50(Pt 5), 760-763.

141. McCoy, A.J.(2007) Phaser crystallographic softwar*e. J. Appl. Crystallogr*. 40(Pt 4), 658-674.

142. Dhe-Paganon, S., Shigeta, R., Chi, Y.I., Ristow, M., and Shoelson, S.E. (2000) Crystal structure of human frataxin*. J. Biol. Chem*. 275(40), 30753-30756.

143. McRee, D.E. (1999) XtalView/Xfit A Versatile Program for Manipulating Atomic Coordinates and Electron Density. *J. of Struct.l Biol.* 125, 156-165.

144. Winn, M.D., G.N. Murshudov, and Papiz, M.Z. (2003) Macromolecular TLS refinement in REFMAC at moderate resolutions. *Methods Enzymol*. 374, 300-321.

145. Brunger, A.T. (1992) The Free R value: a Novel Statistical Quantity for Assessing the Accuracy of Crystal Structures*. Nature* 355, 472-474.

146. Furne, J., A. Saeed, and Levitt, M.D. (2008) Whole tissue hydrogen sulfide concentrations are orders of magnitude lower than presently accepted values*. Am. J. Physiol. Regul. Integr. Comp.Physiol*. 295(5),. R1479-R1485.

147. Agar, J.N., Krebs, C., Huynh, B.H., Dean, D.R., and Johnson, M.K. (2000) IscU as a scaffold for iron-sulfur cluster biosynthesis: sequential assembly of [2Fe-2S] and [4Fe-4S] clusters in IscU. *Biochemistry* 39(27), 7856-7862.

148. Musco, G. (2000) Towards a structural understanding of Friedreich's ataxia: the solution structure of frataxin. *Structure*, **8**(7), 695-707.

149. Pavone, V., Gaeta, G., Lonbardi, A., Nastri, F., Maglio, O., Isernia, C., and Saviano, M. (1996) Discovering protein secondary structures: classification and description of isolated alpha-turns. *Biopolymers* 38(6), 705-721.

150. Campuzano, C., Montermini, L., Molto, M.D., Pianese, L., Cossee, M., Cavalcanti, F., Monros, E.., Rodius, P., Duclos, F., Monticelli, A., Zara, F., Canizares, J., Koutnikova, H., Bidichandani, S., Gellera, C., Brice, A., Trouillas, P., DeMichele, F., Filla, A., DeFrutos, R., Palau, F., Patel, P.I., DiDonato, S., Mandel, J.L., Cocozza, S., and Koenig, M. (1996) Friedreich's ataxia: autosomal recessive disease caused by an intronic GAA triplet repeat expansion. *Scienc* 271(5254), 1423-1427.

152. Saccà, F., Puorro, G., Antenora, A., Marsili, A., Denaro, A., Piro, R., Sorrentino, P., Pane, C., Tessa, A., Morra, B., Cocozza, S., DeMichele, G., Sanorelli, F.M., and Filla, A. (2011) A combined nucleic Acid and protein analysis in friedreich ataxia: implications for diagnosis, pathogenesis and clinical trial design. *PLoS ONE* 6(3), e17627.

153. Correia, A.R., Adinolfi, S., Pastore, A., and Gomes, C.M. (2006) Conformational stability of human frataxin and effect of Friedreich's ataxia-related mutations on protein folding. *Biochem. J.* 398(3), 605-611.

154. Correia, A.R., Ow, S.Y., Wright, P.C., and Gomes, C.M. (2009) Dynamics, stability and iron-binding activity of frataxin clinical mutants. *FEBS J*. 275(14), 3680-36890.

155. Gordon, D.M., Shi, Q., Dancis, A., and Pain, D. (1999) Maturation of frataxin within mammalian and yeast mitochondria: one-step processing by matrix processing peptidase. *Hum. Mol. Genet.* 8(12), 2255-2262.

156. Rufini, A., Fortuni, S., Arcuri, G., Condo, I., Serio, D., Incani, O., Malisan, F., Ventura, N., and Testi, R. (2011) Preventing the ubiquitin/proteasome-dependent degradation of frataxin, the protein defective in Friedreich's Ataxia. *Hum. Mol. Genet.* 20(7), 1253-1261

157. Calmels, N., Schmucker, S., Wattenhofer-Donze, M., Martelli, A., Vaucamps, N., Reutenauer, L., Messaddeq, N., Bouton, C., and Puccio, H. (2009) The first cellular models based on frataxin missense mutations that reproduce spontaneously the defects associated with Friedreich ataxia. *PLoS ONE* **4**(7), e6379.

158. Boehm, T., Scheiber-Mojdehkar B., Kluge B., Goldenberg H., Laccone F., and Sturm B. (2011) Variations of frataxin protein levels in normal individuals. *Neurol. Sci*. 32, 327-330.

159. Steinkellner, H., Scheiber-Mojdehkar B., Goldenberg H., Sturm B. (2009) A high throughput electrochemiluminescence assay for the quantification of frataxin protein levels. *Anal. Chim. Acta* 659(1-2), 129-132.

160. Hudder, B., Morales J.G., Stubna A., Münck E., Hendrich M.P., and Lindahl P.A. (2007) Electron paramagnetic resonance and Mössbauer spectroscopy of intact mitochondria from respiring Saccharomyces cerevisiae. *J. Biol. Inorg. Chem.* 12, 1029-1053.

161. Ghaemmaghami, S., Huh W.K., Bower K., Howson R.W., Belle A., Dephoure N., O'Shea E.K., and Weissman J.S. (2003) Global analysis of protein expression in yeast. *Nature* 425(6959), 737-41.

162. Campuzano, V., Montermini L., Lutz Y., Cova L., Hindelang C., Jiralerspong S., Trottier Y., Kish S.J., Faucheux B., Trouillas P., Authier F.J., Dürr A., Mandel J.L., Vescovi A., Pandolfo M., and Koenig M. (1997) Frataxin is reduced in Friedreich ataxia patients and is associated with mitochondrial membranes. *Hum. Mol. Genet*. **6**(11), 1771-1780.

163. Willis, J., Isaya G., Gakh O., Capaldi R.A., and Marusich M.F. (2008) Lateral-flow immunoassay for the frataxin protein in Friedreich's ataxia patients and carriers. *Mol. Genet. Metab*. 94,. 491-497.

164. Ma, B., Elkayam T., Wolfson H., and Nussinov R. (2003) Protein-protein interactions: structurally conserved residues distinguish between binding sites and exposed protein surfaces. *Proc. Natl. Acad. Sci. U. S. A.* 100(10),. 5772-5777.

165. Gallivan, J.P. and Dougherty, D.A. (1999) Cation-pi interactions in structural biology. *Proc. Natl. Acad. Sci. U.S.A*. 96(17), 9459-9464.

166. Lane, D.J.R. and Richardson, D.R. (2010) Frataxin, a molecule of mystery: trading stability for function in its iron-binding site. *Biochem. J.* 426(2), e1-3.

167. Bulteau, A.-L., O'Neliss, H.A., Kennedy, M.C., Ikeda-Saito, M., Isaya, G., and Szweda, L.I. (2004) Frataxin acts as an iron chaperone protein to modulate mitochondrial aconitase activity. *Science* 305(5681), 242-245.

168. Cho, S., Lee, M.G., Yang, J.K., Lee, J.Y., and Suh, S.W. (2000) Crystal structure of Escherichia coli CyaY protein reveals a previously unidentified fold for the evolutionarily conserved frataxin family. *Proc. Natl. Acad. Sci. U.S.A*. 97(16), 8932-8937.

169. Tsai, C.L., Bridwell-Rabb, J., and Barondeau, D.P. (2011) Friedreich's ataxia variants I154F and W155R diminish frataxin-based activation of the iron-sulfur cluster assembly complex. *Biochemistry* 50(29), 6478-6487.

170. Gill, S.C. and Von Hippel, P.H. (1989) Calculation of protein extinction coefficients from amino acid sequence data. *Anal. Biochem*. 182(2), 319-326.

171. Tsai, C.L. and Barondeau, D.P. (2010) Human frataxin is an allosteric switch that activates the Fe-S cluster biosynthetic complex. *Biochemistry* 49(43), 9132-9139.

172. Tanaka, F., Fuller, R., Shim, H., Lerner, R.A., and Barbas, C.F. (2004) Evolution of aldolase antibodies in vitro: correlation of catalytic activity and reaction-based selection. *J. Mol. Biol*. 335(4), 1007-1018.

173. Gong, X.M., M.L. Paddock, and Okamura, M.Y. (2003) Interactions between cytochrome c2 and photosynthetic reaction center from Rhodobacter sphaeroides: changes in binding affinity and electron transfer rate due to

mutation of interfacial hydrophobic residues are strongly correlated. *Biochemistry* 42(49), 14492-14500.

174. Schwarz, A., F.M. Pierfederici, and Nidetzky, B. (2005) Catalytic mechanism of alpha-retaining glucosyl transfer by Corynebacterium callunae starch phosphorylase: the role of histidine-334 examined through kinetic characterization of site-directed mutants. *Biochem. J.* 387(Pt 2), 437-445.

175. Kessler, D. (2006) Enzymatic activation of sulfur for incorporation into biomolecules in prokaryotes. *FEMS Microbiol. R*ev. 30(6), 825-840.

176. Mueller, E.G. (2006) Trafficking in persulfides: delivering sulfur in biosynthetic pathways. *Nat. Chem. Biol*. 2(4), 185-194.

177. Behshad, E., S.E. Parkin, and Bollinger, J.M. (2004) Mechanism of cysteine desulfurase Slr0387 from Synechocystis sp. PCC 6803: kinetic analysis of cleavage of the persulfide intermediate by chemical reductants. *Biochemistry* 43(38), 12220-12226.

178. Outten, F.W., Wood, M.J., Munoz, F.M., and Storz, G. (2003) The SufE protein and the SufBCD complex enhance SufS cysteine desulfurase activity as part of a sulfur transfer pathway for Fe-S cluster assembly in Escherichia coli. *J. Biol. Chem.* 278(46), 45713-45719.

179. Ollagnier-de-Choudens, S., Lascoux, D., Loiseau, L., Barras, F., Forest, E., and Fontecave, M. (2003) Mechanistic studies of the SufS-SufE cysteine desulfurase: evidence for sulfur transfer from SufS to SufE. *FEBS Lett*. 555(2), 263-267.

180. Layer, G., Gaddam S.A., Ayala-Castro C.N., Ollagnier-de Choudens S., Lascoux D., Fontecave M., and Outten F.W. (2007) SufE transfers sulfur from SufS to SufB for iron-sulfur cluster assembly. *J. Biol. Chem*. 282(18), 13342-13350.

181. Riboldi, G.P., J.S. de Oliveira, and Frazzon, J. (2011) Enterococcus faecalis SufU scaffold protein enhances SufS desulfurase activity by acquiring sulfur from its cysteine-153. *Biochim. Biophys. Acta* 1814(12), 1910-1918.

182. Smith, A.D., Agar, J.N., Frazzon, J., Amster, I.J., Dean, D.R., and Johnson, M.K. (2001) Sulfur transfer from IscS to IscU: the first step in iron-sulfur cluster biosynthesis. *J. Am. Chem. Soc.* 123(44), 11103-11104.

183. Urbina, H.D., Silberg, J.J., Hoff, K.G., and Vickery, L.E. (2001) *T*ransfer of sulfur from IscS to IscU during Fe/S cluster assembly. *J. Biol. Chem.* 276(48), 44521-44526.

184. Cupp-Vickery, J., H.D. Urbina, and Vickery, L.E. (2003) Crystal structure of IscS, a cysteine desulfurase from Escherichia coli. *J. Mol. Biol.* 330(5), 1049-1059.

185. Smith, A.D., Frazzon, J., Dean, D.R., and Johnson, M.K. (2005) Role of conserved cysteines in mediating sulfur transfer from IscS to IscU. *FEBS Lett.* 579(23), 5236-5240.

186. Bonomi, F., Iametti, S., Morleo, A., Ta, D., and Vickery, L.E. (2011) Facilitated Transfer of IscU-[2Fe2S] Clusters by Chaperone-Mediated Ligand Exchange. *Biochemistry* 50(44),. 9641-9650.

187. Iannuzzi, C., Adinolfi, S., Howes, B.D., Garcia-Serres, R., Clemancey, M., Latour, J.M., Smulevich, G., and Pastore, A. (2011) The Role of CyaY in Iron Sulfur Cluster Assembly on the E. coli IscU Scaffold Protein. *PLoS One* 6(7), e21992.

188. Albrecht, A.G., Peuckert F., Landmann H., Miethke M., Seubert A., and Marahiel M.A. (2011) Mechanistic characterization of sulfur transfer from cysteine desulfurase SufS to the iron-sulfur scaffold SufU in Bacillus subtilis. *FEBS Lett*. 585(3), 465-470.

189. Tsai, C.L., Bridwell-Rabb, J., and Barondeau, D.P. (2011) Friedreich's ataxia variants I154F and W155R diminish frataxin-based activation of the iron-sulfur cluster assembly complex. *Biochemistry* 50(29), 6478-6487.

190. Shimomura, Y., Wada, K., Fukuyama, K., and Takahashi, Y. (2008), The Asymmetric Trimeric Architecture of [2Fe-2S] IscU: Implications for Its Scaffolding during Iron-Sulfur Cluster Biosynthesis. *J. Mol. Biol.* 383(1), 133-143.

191. Kim, J., Fuzery A.K., Tonelli, M., Ta, D.T., Westler, W.M., Vickery, L.E., and Markley, J.L. (2009) Structure and Dynamics of the Iron-Sulfur Cluster Assembly Scaffold Protein IscU and its Interaction with the Cochaperone HscB. *Biochemistry* 48(26), 6062-6071.

192. Kim, J.H., M. Tonelli, and Markley, J.L. (2011) Disordered form of the scaffold protein IscU is the substrate for iron-sulfur cluster assembly on cysteine desulfurase. *Proc. Natl. Acad. Sci. U .S. A.* 109(2), 454-459.

193. Ye, H. and Rouault, T.A. (2010) Human iron-sulfur cluster assembly, cellular iron homeostasis and disease. *Biochemistry* 49, 4945-4956.

194. Yoon, H., Golla R., Lesuisse E., Pain J., Donald J.E., Lyver E.R., Pain D., and Dancis, A. (2012) Mutation in Fe-S scaffold Isu bypasses frataxin deletion. *Biochem J.* 441(1), 473-480.

195. Andrew, A.J., Song, J.Y., Schilke, B., and Craig, E.A. (2008) Posttranslational regulation of the scaffold for Fe-S cluster biogenesis, Isu. *Mol .Biol. Cell.* 19(12), 5259-5266.

196. Kim, J., Fuzery A.K., Tonelli, M., Ta, D.T., Westler, W.M., Vickery, L.E., and Markley, J.L. (2009) Structure and Dynamics of the Iron-Sulfur Cluster Assembly Scaffold Protein IscU and its Interaction with the Cochaperone HscB. *Biochemistry* 48(26), 6062-6071.

197. Blaber, M., X.J. Zhang, and Matthews, B.M. (1993) Structural basis of amino acid alpha helix propensity. *Science* 260(5114), 1637-1640.

198. Bridwell-Rabb, J., Winn, A.M., and Barondeau, D.P. (2011) Structure-function analysis of Friedreich's ataxia mutants reveals determinants of frataxin binding and activation of the Fe-S assembly complex. *Biochemistry* 50(33), 7265-7274.

199. Crowley, P.B. and Golovin, A. (2005) Cation-pi interactions in protein-protein interfaces. *Proteins* 59(2), 231-239.

200. Gallivan, J.P. and Dougherty, D.A. (2000) A computational study of cation-pi interactions vs salt bridges in aqueous media: Implications for protein engineering. *J. Am. Chem. Soc.* 122(5), 870-874.

201. Qi, W. and Cowan, J.A. (2010) A structural and functional homolog supports a general role for frataxin in cellular iron chemistry. *Chem. Commun. (Camb)* 46(5), 719-721.

202. Albrecht, A.G., Landmann H., Nette D., Burghaus O., Peuckert F., Seubert A., Miethke M., and Marahiel M.A. (2011) The frataxin homologue Fra plays a key role in intracellular iron channeling in Bacillus subtilis. *Chembiochem*. 12(13), 2052-2061.

203. Bonomi, F., Iametti, S., Ta, D., and Vickery, L.E. (2005) Multiple turnover transfer of [2Fe2S] clusters by the iron-sulfur cluster assembly scaffold proteins IscU and IscA. *J. Biol. Chem*. 280(33), 29513-29518.

204. Py, B. and Barras, F. (2010) Building Fe-S proteins: bacterial strategies. *Nat. Rev. Microbiol*. 8(6), 436-446.

205. Hughes, M.N., Centelles, M.N., and Moore, K.P. (2009) Making and working with hydrogen sulfide: The chemistry and generation of hydrogen sulfide in vitro and its measurement in vivo: a review. *Free Radic. Biol. Med*. 47(10), 1346-1353.

206. Takahashi, Y. and Nakamura, M. (1999) Functional assignment of the ORF2-iscS-iscU-iscA-hscB-hscA-fdx-ORF3 gene cluster involved in the assembly of Fe-S clusters in Escherichia coli. *J. Biochem*. 126(5), 917-926.

207. Schwartz, C., Djaman, O., Imlay, J.A., and Kiley, P.J. (2000) The cysteine desulfurase, IscS, has a major role in in vivo Fe-S cluster formation in Escherichia coli. *Proc. Natl. Acad. Sci. U.S.A*. 97(16), 9009-9014.

208. Ding, H. and Clark, R.J. (2004) Characterization of iron binding in IscA, an ancient iron-sulphur cluster assembly protein. *Biochem. J*. 379(Pt 2), 433-440.

209. Chandramouli, K. and Johnson, M. (2006) HscA and HscB stimulate [2Fe-2S] cluster transfer from IscU to apoferredoxin in an ATP-dependent reaction. *Biochemistry* 45(37), 11087-11095.

210. Cossee, M., Puccio, H., Gansmuller, A., Koutnikova, H., Dierich, A., LeMeur, M., Fischbeck, K., Dollé, P., and Koenig, M. (2000) Inactivation of the Friedreich ataxia mouse gene leads to early embryonic lethality without iron accumulation. *Hum. Mol. Genet.* **9**(8), 1219-1226.

211. Bedekovics, Gajdos, G., Kispal, G., and Isaya, G. (2007) Partial conservation of functions between eukaryotic frataxin and the Escherichia coli frataxin homolog CyaY. *FEMS Yeast Res*. 7, 1276-1284.

212. Cavadini, P., Gellara, C., and Isaya, G. (2007) Human frataxin maintains mitochondrial iron homeostasis in Saccharomyces cerevisiae. *Hum. Mol. Genet*. 9(17), 2523-2530.

213. Tsai, C.-L. and Barondeau, D.P. (2010) Human frataxin is an allosteric switch that activates the Fe-S cluster biosynthetic complex. *Biochemistry* 49(43), 9132-9139.

214. Bradford, M.M. (1976) A rapid and sensitive method for the quantitation of microgram quantities of protein utilizing the principle of protein-dye binding. *Anal. Biochem.* 72, 248-254.

215. Tirupati, B., Vey, J.L., Drennan, C.L., and Bollinger, J.M. (2004) Kinetic and structural characterization of Slr0077/SufS, the essential cysteine desulfurase from Synechocystis sp. PCC 6803. *Biochemistry* 43(38), 12210-12219.

216. Loiseau, L., Ollagnier-de-Choudens, S., Nachin, L., Fontecave, M., and Barras, F. (2003) Biogenesis of Fe-S cluster by the bacterial Suf system: SufS and SufE form a new type of cysteine desulfurase. *J. Biol. Chem*. 278(40), 38352-38359.

APPENDIX A

THE KAIA PROTEIN OF THE CYANOBACTERIAL CIRCADIAN OSCILLATOR IS MODULATED BY A REDOX ACTIVE COFACTOR*

ABSTRACT

The circadian rhythms exhibited in the cyanobacterium *Synechococcus elongatus* are generated by an oscillator [4]comprised of the proteins KaiA, KaiB, and KaiC. An external signal that commonly affects the circadian clock is light. Previously, we reported that the bacteriophytochrome-like protein CikA passes environmental signals to the oscillator by directly binding a quinone and using cellular redox state as a measure of light in this photosynthetic organism. Here, we report that KaiA also binds the quinone analog 2,5-dibromo-3-methyl-6-isopropyl-p-benzoquinone (DBMIB), and the oxidized form of DBMIB, but not its reduced form, decreases the stability of KaiA in vivo, causes multimerization in vitro, and blocks KaiA stimulation of KaiC phosphorylation, which is central to circadian oscillation. Our data suggest that KaiA directly senses environmental signals as changes in redox state and modulates the circadian clock.

*Reprinted with permission from "The KaiA Protein of the Cyanobacterial Circadian Oscillator is Modulated by a Redox Active Cofactor" by Wood, T.L., Bridwell-Rabb, J., Kim, Y.I., Gao, T., Chang. Y.G., LiWang, A., Barondeau, D.P., and Golden, S.S. 2010. *PNAS*, 107, 5804-5809. Copyright 2010 by the Proceedings of the National Academy of Sciences.

INTRODUCTION

Circadian rhythms of physiological processes occur in diverse prokaryotes and eukaryotes from cyanobacteria to humans (1, 2). The biochemical nature of the endogenous clock that drives these rhythms has been described in rich detail for the cyanobacterium *Synechococcus elongatus*, which uses a circadian oscillator that is evolutionarily and mechanistically distinct from those of eukaryotic organisms. Three proteins that comprise an oscillator, KaiA, KaiB, and KaiC, are sufficient to establish a circadian rhythm of KaiC phosphorylation in vitro when incubated in appropriate ratios in the presence of ATP (3). KaiC has both autophosphorylation and autodephosphorylation activity (4, 5), as well as a temperature-compensated ATPase activity (6). KaiA stimulates KaiC phosphorylation (7, 8), whereas KaiB attenuates the effects of KaiA (8, 9). These interactions result in a cycle of specific phosphorylation events, and presumably different conformational states, that comprise a basic circadian oscillation (10, 11). In vivo, additional components of the clock, such as the KaiC interacting kinase SasA (12, 13), serve as output pathways to deliver temporal information to downstream cellular processes including gene expression (14) and chromosome compaction (15); input pathways transmit environmental cues to the oscillator and synchronize it with local time.

Known members of the input pathways include the redox active members LdpA, an FeS protein (16, 17), and CikA, a histidine protein kinase (18, 19). LdpA fine-tunes the period of circadian rhythms in the cyanobacterium; in an ldpA null mutant, the circadian period is locked into the shorter end of a range of periods between 24 and 26 h that normally varies with incident light intensity, such that the period is shorter under higher light and longer under lower light (16). The bacteriophytochrome-like protein CikA is required to reset the timing of circadian peaks—the relative phasing of the rhythm—in response to a dark pulse (18). CikA mutants also have a shortened circadian period, a reduction in amplitude of gene expression rhythms, and an altered circadian pattern of KaiC phosphorylation. CikA abundance varies inversely with light intensity, with the highest levels in the dark; in an ldpA mutant, CikA abundance is locked at its lowest level independent of light intensity, and KaiA, whose levels are not light dependent, is elevated (17, 20).

We previously used the photosynthetic electron transport inhibitor 2,5-dibromo-3-methyl-6-isopropyl-p-benzoquinone (DBMIB), a water-soluble halogenated analog of native plastoquinone (PQ) (21), in experiments designed to manipulate the redox state of the PQ pool in cyanobacterial cells (21). An unexpected finding was that DBMIB decreases the stability of LdpA, CikA, and, to a lesser degree, KaiA (17). The pseudoreceiver (PsR) domain of CikA was shown to bind to DBMIB and other quinone analogs directly (20, 22). The data suggest that the cyanobacterial clock obtains information regarding the light environment indirectly, through redox changes in a CikA-bound quinone (20).

Like CikA, KaiA has a PsR domain and is destabilized in vivo in the presence of DBMIB. Here, we show that oxidized, but not reduced, DBMIB binds directly to the PsR domain of KaiA and affects the oligomeric state of KaiA and its ability to stimulate the phosphorylation of KaiC. The data suggest that KaiA itself is a redox sensor and a key component of the circadian input pathway in *S. elongatus*.

RESULTS

The Oxidized Form of the PQ Analog DBMIB Affects the Stability of KaiA and CikA in Vivo. We showed previously that DBMIB decreases the abundance of LdpA, CikA, and, to a lesser degree, KaiA in vivo, but has no impact on levels of D1 (a key photosystem II protein) or PsaC (a photosystem I iron-sulfur-containing protein) (17). To investigate which redox state of DBMIB [Em 1/4 90 mV (23)] affects the stability of KaiA and CikA, immunoblot analysis was performed using DBMIB (oxidized) and DBMIB reduced with sodium dithionite (24). Treatment of cells with oxidized DBMIB decreased the levels of KaiA and CikA, but neither protein was affected by addition of reduced DBMIB (Fig. 1A) or by the ethanol and dithionite added with DBMIB (Fig. 1A). KaiB, an internal control, was not affected by either the oxidized or reduced form of DBMIB. Although these protein levels were not affected by dithionite, this reducing agent may have other effects in the cell that were not detected by this assay.

DBMIB Causes Aggregation of KaiA in Vitro That Is Dependent on the PsR Domain and DBMIB Oxidation State. To examine the effect of DBMIB on KaiA in vitro, we performed reactions using purified KaiA incubated for 20 min with either oxidized or reduced DBMIB and subjected the samples to native polyacrylamide gel electrophoresis (PAGE). Most of the KaiA band was shifted after incubation with oxidized DBMIB, but very little was shifted when the DBMIB was reduced with dithionite (Fig. 1B). Additional experiments showed that the KaiA aggregation is noncovalent (Fig. S1) and irreversible (Fig. S2). Because quinone binding by CikA occurs in the PsR domain, we tested KaiA140C, a dimeric protein variant that is missing

that domain (Fig. 1C). The migration of KaiA140C was not shifted after incubation with either oxidized or reduced

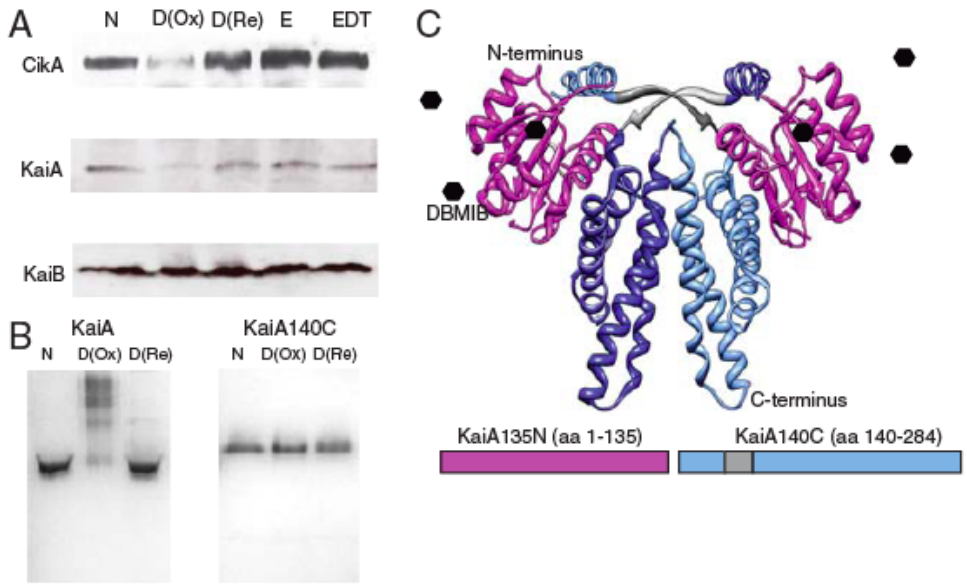

Figure 1. Interaction of oxidized DBMIB with the N-terminal domain of KaiA. (A) Effects of oxidized and reduced DBMIB on the stability of CikA, KaiA, and KaiB in vivo. Cyanobacterial cells were treated for 20 min with oxidized [D(Ox)] or reduced [D(Re)] DBMIB, or with ethanol and dithionite (EDT) or ethanol (E) as controls. Soluble protein extracts were separated by SDS-PAGE and subjected to immunoblot analysis with antisera to detect CikA, KaiA, and KaiB as indicated. (B) The PsR domain of KaiA is responsible for DBMIB sensitivity. Oxidized [D(Ox)], but not reduced [D(Re)] DBMIB reduced the mobility of KaiA, but not KaiA140C, on native gels. N, no addition. (C) Structure of KaiA showing the relative positions and relevant endpoints of the N-terminal (KaiA135N) and C-terminal (KaiA140C) domains used in this study. DBMIB is depicted as a black hexagon, interacting with the N-terminal domain.

DBMIB (Fig. 1B). The N-terminal PsR can be purified as a monomeric folded domain

comprising the first 135 aa residues of KaiA (KaiA135N) (8). This domain also showed noncovalent aggregation upon DBMIB treatment (Fig. S1 C and D). An oxidized analog of ubiquinone (not native to *Synechococcus*), Q0, also caused aggregation of KaiA in vitro (Fig. S3) with some reversibility (Fig. S2). Thus, an oxidized quinone interacts with the PsR domain of KaiA and affects its migration in vitro, consistent with previous findings that the effect of DBMIB on KaiA levels in vivo is posttranslational (20).

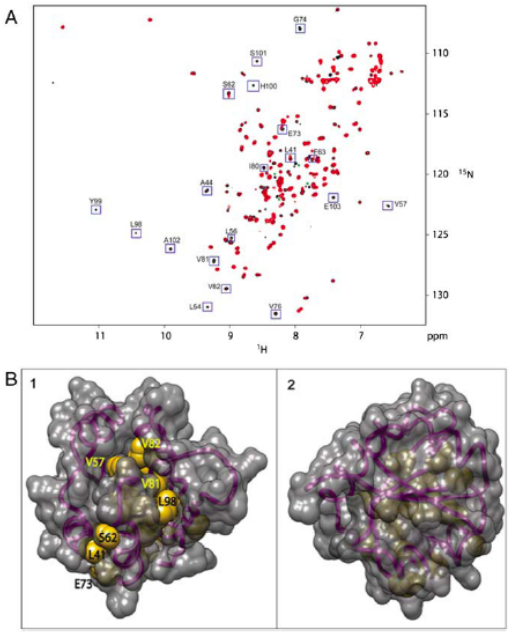

Figure 2. Interaction of DBMIB with KaiA135N in solution. (A) 15N, 1H HSQC spectra of KaiA135N (black contours) and KaiA135N ? DBMIB (red contours). The concentration of KaiA135N in both samples was 100 μM. DBMIB was added to one sample to a final concentration of 50 μM and the untreated sample was normalized with respect to ethanol concentration. Assignable peaks showing significant perturbation upon the addition of DBMIB are boxed and labeled. Asterisks denote small contaminating peaks in the spectrum. (B) Structure of KaiA135N showing the side chains of assignable residues most affected by DBMIB. (1) The surface of KaiA135N showing affected residues (labeled) not blocked from view. (2) The side of KaiA135N directly opposite to that shown in (A).

DBMIB Binds Directly to the PsR Domain of KaiA. We collected two dimensional 1H, 15N, heteronuclear single quantum correlation (HSQC) NMR spectra in the presence and absence of DBMIB to detect binding of the quinone analog to KaiA135N, controlling for small perturbations that might be induced by the ethanol solvent (0.6% vol/vol). At a 2:1 molar ratio of KaiA135N to DBMIB significant perturbations were seen for the peaks of L41, A44, L54, L56, V57, S62, F63 E73, G74, V76, I80, V81, V82, L98- E103 and others near the crowded center of the spectrum (Fg. 2A). Mapping the perturbed residues that were assignable from the HSQC spectrum onto the NMR structure of KaiA135N revealed that the spectral perturbations are clustered together (Fig. 2B), involving sections of α2, α3, β3, β4, and preceding β5. DBMIB-induced chemical shift perturbations do not map identically onto the structures of KaiA135N and CikAPsR, suggesting that there are differences in the way DBMIB binds to these PsRs (20, 22). In contrast, a 10-fold higher concentration of DBMIB caused no changes in the peaks of CheY, Fig. S4, a canonical receiver domain (25), which was tested as a control to determine whether quinone interaction was an accidental consequence of the receiver fold. Reduced DBMIB did not affect the spectrum of KaiA135N (Fig. S5). The NMR titration results are consistent with the specific interaction of DBMIB with the PsR

domain of KaiA.

The dissociation constant for DBMIB binding to KaiA was calculated by quenching of KaiA tryptophan fluorescence at 338 nm (Fig. 3A). Nonlinear fitting of the quenching data to Eq. 2 (see Materials and Methods) indicated a Kd of oxidized DBMIB

binding to KaiA of 1.8 ± 0.3 μM at a stoichiometry of approximately 1 quinone per monomer. For reduced quinone binding measurements, there was no change in the corrected fluorescence as calculated by Eq. 1 (Fig. S6). The absence of quenching suggests that reduced quinone does not bind to KaiA.

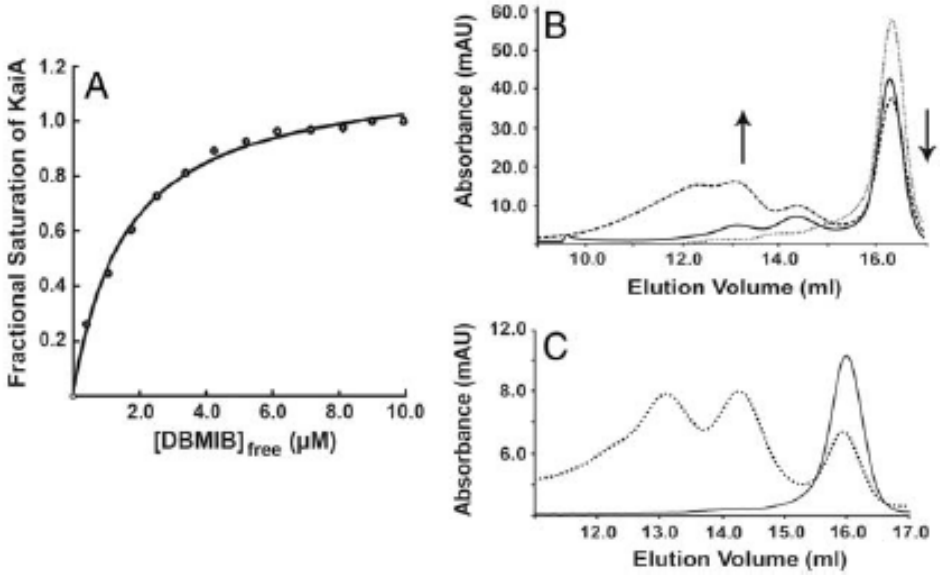

Figure 3. Quinone binding and KaiA aggregation state. (A) One of three equivalent trials of KaiA fluorescence quenching by titration of DBMIB. x axis, concentration of free DBMIB in solution as calculated by Eq. 4; y axis, fractional saturation of KaiA as calculated by equation. (B) Chromatogram from gel filtration analysis of KaiA135N with 0, 3, and 5 molar equivalents of oxidized DBMIB. Arrows indicate the increase in oligomeric species and the concomitant decrease in monomeric KaiA135N with increasing quinone concentration. (C) Chromatogram from gel filtration analysis of KaiA135N with 5 M equivalents of oxidized DBMIB (dotted line) and 5 M equivalents of DBMIB and sodium dithionite (solid line).

To examine the specificity of aggregation, oxidized DBMIB was added in 3 and 5M equivalents to KaiA135N and the sample was analyzed by gel filtration. The result was an increase in the aggregation state of KaiA135N with increasing quinone concentration and a concomitant decrease in the amount of KaiA135N monomer (Fig. 3B). The aggregated material is a complex mixture with molecular weights that correspond to a trimer, a hexamer, and a nonamer for this normally monomeric domain. Reduced DBMIB added to KaiA135N at 5 M equivalents did not change the oligomeric state of KaiA135N (Fig. 3C). Thus, the PsR domain of KaiA aggregates specifically in the presence of oxidized, but not reduced quinone, suggesting a direct regulatory role for redox sensing by the circadian oscillator.

KaiC Phosphorylation Is Influenced by Oxidized Quinone. KaiC isolated from Escherichia coli is approximately 50% phosphorylated (26); over the course of 6–10 h it dephosphorylates extensively when incubated alone and phosphorylates extensively in the presence of KaiA (26). Unphosphorylated and phosphorylated forms are separable in SDS-PAGE gels, where phospho-KaiC migrates more slowly (Fig. 4). We examined the effect of oxidized and reduced DBMIB on the ability of KaiA to stimulate KaiC phosphorylation over a 24 h time course (Fig. 4). KaiC in the presence of KaiA and DBMIB increased in phosphorylation state during the first 4 h, and then KaiC started to dephosphorylate (Fig. 4). At approximately the same time, KaiC incubated with untreated KaiA, or with KaiA in the presence of both DBMIB and sodium dithionite, became increasingly phosphorylated. In the absence of DBMIB, no effect was seen on KaiC phosphorylation by addition of sodium dithionite and ethanol, which was the

solvent added in trace amounts for the quinone (Fig. 4). Thus, the oxidized form of DBMIB affects KaiA stimulation of KaiC, but the reduced form of DBMIB does not. These results support the regulation of KaiC phosphorylation by redox signals through KaiA. Addition of dithionite after 12 h did not restore KaiC phosphorylation, consistent with irreversibility of aggregation (Fig. S2).

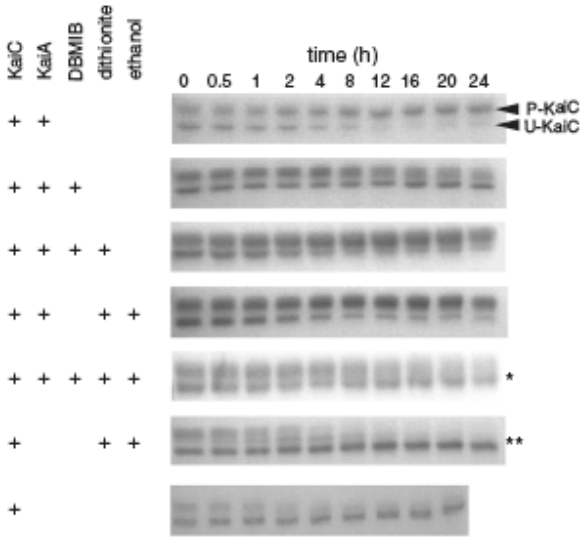

Figure 4. KaiC phosphorylation with KaiA in the presence of oxidized or reduced DBMIB as a function of time. KaiC was incubated with the additions indicated by a plus sign and samples were taken at the times shown across the top. SDS-PAGE was used to separate the slower migrating phosphorylated forms of KaiC (P-KaiC) from the unphosphorylated form (U-KaiC). Ethanol, used as the solvent for DBMIB, was included as a control in some reactions that lack DBMIB. *Dithionite was added after 12 h. **There was no KaiA in the reaction.

DISCUSSION

The biological clock is typically viewed as the combined activities of a central oscillator, behavior-controlling output pathways, and synchronizing input pathways. The N-terminal PsR domain of KaiA belongs to a class of signal transduction proteins, suggesting that information impinges on the oscillator through KaiA (8). However, it was assumed that the direct sensing of light, or redox, or any other cue that acts through a cofactor, would be transmitted from an upstream partner such as LdpA and CikA. Here, we show that KaiA can sense redox signals directly. However, these data do not discount the potential roles of partner interactions in the entrainment of the clock in vivo.

Quinones are used widely as redox-active cofactors. As shown for KaiA and CikA, the ArcB (27) and RegB (28) sensor kinases from *E. coli* and Rhodobacter capsulatus, respectively, are inhibited by the oxidized form of exogenously added soluble quinone analogs, but not by their reduced forms. Both ArcB and RegB are integral membrane proteins. CikA and KaiA are not integral membrane proteins, yet they bind quinones, which are generally lipid-soluble electron carriers. The prospect of protein interactions at the periphery of a cellular membrane could explain this dilemma. CikA localizes to a pole of the cell, dependent on the PsR domain, consistent with peripheral membrane association (19). Soluble truncated variants of the kinases BvgS and EvgS of *Bordetella pertussis* and *E. coli*, respectively, which are missing their transmembrane spans, are inhibited specifically by oxidized Q0, a soluble analog mimic of the native ubiquinone-8 (29). Yan et al. recently showed that the crystal structure of the cytochrome b6f complex from the cyanobacterium *Mastigocladus laminosus* carries

DBMIB (crystallized in place of PQ) in a peripheral binding site, accessible to both aqueous and membrane lipid phases, from which it likely shuttles into the Qp binding site through an intraprotein channel (30). Quinones in this interface may be accessible to hydrophobic pockets in peripheral membrane proteins.

What is the quinone that serves as a cofactor for KaiA and CikA in vivo? Photosynthetic electron transport inhibitors that modify the redox state of the PQ pool linking photosystem II and cytochrome b6f affect CikA and KaiA stability; thus, it was initially assumed that this bulk PQ pool serves as a signal (20). However, the data presented here suggest that the cofactor does not exchange with the PQ pool. Oxidized DBMIB affects KaiA stability and oligomerization, but it causes overall reduction of the PQ pool (21). Moreover, oxidation of the PQ pool by addition of the photosystem II inhibitor 3-(3,4-dichlorophenyl)-1,1-dimethylurea (21) does not cause changes in KaiA or CikA (17, 20). Thus, it is unlikely that PQ from the bulk pool is the cofactor of these clock proteins. A tightly bound PQ is a candidate, and *S. elongatus* also contains a polar naphthoquinone (31). We propose that the KaiA quinone undergoes redox changes with a specific partner. CikA and LdpA, which copurify with KaiA, are good candidates for specific electron transfer partners.

KaiA is responsible for switching KaiC from an autophosphatase to an autokinase. Fig. 4 shows that oxidized DBMIB, which causes KaiA aggregation, also attenuates KaiA-mediated stimulation of KaiC kinase activity. These data support a role for a redox-active KaiA as an input mechanism (8) to synchronize the circadian oscillator with daily external cycles that affect cellular physiology.

EXPERIMENTAL PROCEDURES

Bacterial Strains and Culture Conditions. *S. elongatus* PCC 7942 strain AMC 1239 (17) was grown in 100 ml BG-11M medium (32) with 2 μg⁄ml of spectinomycin. The strain was cultured as described previously (33) at 30 °C under 150 μE⁄m^{2}s. *E. coli* strain BL21(DE3) was used for KaiA and KaiB expression, and it was grown in LB medium with 200 μg⁄ml ampicillin at 37 °C. *E. coli* strain DH5α was used for KaiC expression, and it was grown in LB medium with 200 μg⁄ml ampicillin at 30 °C as described previously (26, 34).

Construction of the KaiA Truncation Variant and DNA Manipulation. The gene encoding KaiA140C was amplified by PCR with Pfu polymerase and primers to create the flanking restriction sites for NcoI (forward primer) in front of the codon for KaiA residue L140 and a BamHI restriction site and the stop codon (reverse primer). After double digestion of the PCR product, the fragment was cloned into the pET32a+ vector (Novagen) and introduced into *E. coli* BL21(DE3) competent cells. Basic DNA manipulations were performed using standard procedures (34). Plasmid DNA was isolated using a Mini Kit (Qiagen, Inc., Chatsworth, CA) and digested by restriction enzymes from New England Biolabs, Inc. (Beverly, MA). DNA sequencing was performed by the Gene Technologies Laboratory (Texas A&M University).

Protein Expression and Purification. Purification of polyhistidine tagged KaiA, KaiA135N, and KaiA140C from *E. coli* BL21 DE3⁄pET32a+ (kaiA), BL21DE3⁄pET32a+ (kaiA135N), and BL21 DE3⁄pET32a+ (kaiA140C), respectively, and of glutathione-S-transferase tagged KaiC from *E. coli* DH5α/pGEX-6P-2(kaiC), was

performed as described previously (26).

NMR Experiments. ^{1}H, ^{15}N HSQC spectra of KaiA135N - DBMIB were acquired with eight scans in 39.5 min at 600 MHz. The acquisition times in both dimensions were 66(t_1) And 67(t_2) ms, consisting of 128 and 640 complex points, respectively, and processed such that the final digital resolutions were 4.2(F_1) and 6.2(F_2) Hz/pt.

Gel Filtration Analysis of Quinone Binding to KaiA135N. Gel filtration analysis was performed using an Akta FPLC and a Superdex 200 gel filtration column from GE Healthcare. Reduced quinone gel filtration studies were performed in an M-Braun glovebox with an atmosphere that contains less than 1 ppm oxygen as monitored continuously by a Teledyne oxygen analyzer. The Superdex 200 was run with 20 mM Tris, 150 mM NaCl, 0.5 mM EDTA, and 5 mM $MgCl_2$ buffer at pH = 8. Samples were fit to a standard curve generated from the gel filtration standard (Bio-Rad) chromatogramfor molecular weight determination. Aerobic samples were prepared to contain 60 μM KaiA135N alone and with 3 and 5 M equivalents of DBMIB. For gel filtration analysis of the effects of reduced quinone binding to KaiA135N, samples contained KaiA135N with 5 M equivalents of DBMIB, with and without sodium dithionite.

Fluorescence Determination of KaiA-DBMIB Dissociation Constant (Kd). Tryptophan quenching in KaiA by titration with DBMIB was used to determine the Kd for the complex of DBMIB-KaiA at 25 °C (35). DBMIB was mixed with KaiA for 2 min and immediately measured for fluorescence intensity at 338 nm with excitation at 280 nm. Fluorescence [FluoroMax-4 (HORIBA Jobin Yvon)] was corrected for inner filter

effect using Eq. A-1 and the absorbance (Agilent UV-Visible ChemStation) of the DBMIB-KaiA complex at 280(A_{ex}) and 338(A_{em}) nm (35),

$$F_{corrected} = F_{observed} \times anti\log\left(\frac{A_{ex} + A_{em}}{2}\right) \qquad \text{(A-1)}$$

The Kd for DBMIB binding was determined by nonlinear fitting (Kaleidagraph) to Eq. 2 (35),

$$\chi = \frac{n[DBMIB]_{free}}{K_d + [DBMIB]_{free}} \qquad \text{(A-2)}$$

Fractional saturation χ of KaiA was calculated using Eq. 3, which included corrected fluorescence with (F), without ($F_{[DBMIB]0}$),and saturating ($F_{[DBMIB]\ max}$) DBMIB concentrations (35),

$$\chi = \frac{F_{[DBMIB]0} - F}{F_{[DBMIB]0} - F_{[DBMIB]\max}} \qquad \text{(A-3)}$$

Unbound DBMIB ($[DBMIB]_{free}$) was determined by Eq. 4, where $[DBMIB]_{total}$ and $[KaiA]_{total}$ are the total concentrations of quinone and KaiA, corrected for dilution (35),

$$[DBMIB]_{free} = [DBMIB]_{total} - \chi[KaiA]_{total} \qquad \text{(A-4)}$$

KaiC Phosphorylation Reaction. Purified KaiA (1.5 μM) was added to a 1.5 ml

centrifuge tube containing 50 μM DBMIB (Sigma-Aldrich, St. Louis, MO), autophosphorylation assay buffer (20 mM Tris-HCl, 150 mM NaCl, 0.5 mM EDTA, 5 mM $MgCl_2$, 5 mM ATP, pH 8.0), and/or 1 mM sodium dithionite. An equivalent volume of ethanol, the solvent for the DBMIB stock, was used instead of DBMIB as a control. After the sampleswere incubated at room temperature for 15 min, 3.5 μMKaiC was added into the sample. The total volume of each sample was 500 μl, and the sample was sterilized by filtration using 0.2 μm Acrodisc syringe filters (Pall, Ann Arbor, MI). The samples were incubated at 30 °C, and 40 μl aliquots were collected at each 4-h time point (0–24 h) and added to centrifuge tubes containing 6 μl of 5X loading dye. The "zero" time point sample was collected immediately after KaiC was added. The samples were analyzed using sodium dodecyl sulfate- SDS-PAGE (26).

DBMIB Treatment and Immunoblot Analysis. To induce the expression of His-tagged LdpA in AMC 1239 strain prior to the treatment with DBMIB, 100 μM of IPTG was added to cultures for 24 h (17). DBMIB was added to cyanobacterial cultures to a final concentration of 10 μM. For the reduced DBMIB sample, excess sodium dithionite (100 μM) was added into the reaction. Since DBMIB was dissolved in ethanol, the same amount of ethanol was added to control samples. The 50 ml cyanobacterial cultures (OD_{750} = 0.7) were treated for 20 min, and the cells were pelleted at 1,500 x g for 10 min at 4 °C. The cell pellets were resuspended in 50 μl chilled IA lysis buffer (17). The resuspended cells were lysed by vigorous vortex mixing in the presence of glass beads in cycles of 30 s mixing and 30 s cooling on ice for 5 min. The 50 μl chilled IA buffer was added into the lysate samples. Beads were removed by a brief spin at 1,000 x g and the

total sample was analyzed using SDS-PAGE.

Immunoblot analysis was performed as previously described (17, 36) except that proteins were incubated at room temperature for 1 h. Antisera were diluted with Tris buffered saline buffer with addition of 0.1% Tween 20 and 2% milk. After washing, the blots were incubated with peroxidase-conjugated goat antirabbit IgG (Calbiochem, San Diego, CA) at 1:5; 000 dilution. SuperSignal West Pico chemiluminescent substrate (Pierce, Rockford, IL) was used for signal visualization, and the blots were exposed to X-ray film.

Native Polyacrylamide Gel Electrophoresis. To prepare samples for native polyacrylamide gel electrophoresis, 10 μM of KaiA or KaiA140C was incubated with 100 μM DBMIB in buffer (20 mM Tris-HCl, 150 mM NaCl, 0.5 mM EDTA, 5 mM $MgCl_2$, pH 8.0) for 20 min at room temperature, and then 5X loading dye was added to the samples. For the reduced DBMIB sample, 1 mM sodium dithionite was added into the reaction to keep DBMIB in the reduced form. The samples were analyzed using native PAGE (37).

SUPPLEMENTAL METHODS

SDS polyacrylamide gel electrophoresis. To prepare samples for SDS polyacrylamide gel electrophoresis shown in Fig. S1 B, D, F, and H, and Fig. S3B, 10 μM samples of KaiA variants were incubated with DBMIB or Q0 at the indicated concentrations (μM) in buffer (20 mM Tris-HCl, 150 mM NaCl, 0.5 mM EDTA, 5 mM MgCl2, pH 8.0) for 20 min at room tem- perature, and then 2x gel loading buffer (100 mM Tris-HCl, 4% SDS, 0.2% Bromophenol Blue, 30% Glycerol, pH 7.5) was added to the samples. When indicated on the figure, the gel loading buffer also included 200 mM DTT. The samples were boiled for 10 min at 100 °C before loading the lanes.

N-Ethylmaleimide (NEM) modification of KaiA. N-Ethylmaleimide (Pierce) modification of KaiA was performed for Fig. S1 G and H by following the manufacturer's instructions. To calcu- late modified Cys residues in KaiA and NEM-modified KaiA (KaiA-NEM), an Ellman's reagent (Pierce) reaction was per- formed by the manufacturer's instruction.

Briefly, three different concentrations (10, 20, and 30 μM) of KaiA or KaiA-NEM were made in reaction buffer (100 mM sodium phosphate, 1 mM EDTA, pH 1⁄4 8.0). These protein solutions were incubated with 10 mM Ellman's reagent for 1 h. The numbers of free Cys resi- dues available to react with the modifier were calculated by mea- suring absorbance at 412 nm. For wild-type KaiA, 2.1 ` 0.6 Cys residues per monomer reacted with Ellman's reagent. For KaiA- NEM, no free Cys residue was detected (0.32 ` 0.13).

Recovery of aggregation by adding reducing agent. For Fig. S2, dithionite was added before or after addition of DBMIB as indicated on the figure. For the control group, 1,000 μM (final concentration) dithionite was added before KaiA to generate re- duced DBMIB or Q0 which was added at the indicated concen- tration (μM). Dithionite or buffer was added after KaiA to check recovery or aggregation, respectively. There were 20 min waiting periods for aggregation and recovery. All samples were analyzed using native PAGE (36).

SUPPLEMENTAL FIGURES

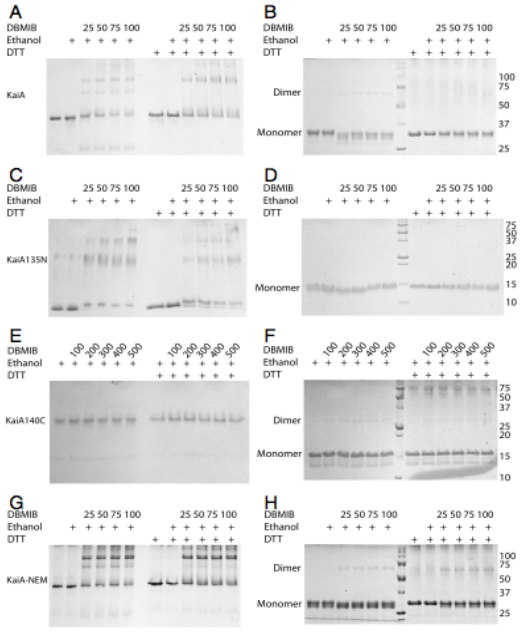

Figure S1. The aggregation of the KaiA PsR by DBMIB is not due to intermolecular disulfide bond formation. To examine intermolecular disulfide bond for- mation in the KaiA aggregates, we compared the migration of bands on native gels (A, C, E, and G) with that on SDS-PAGE with and without DTT in the gel loading buffer (B, D, F, and H). Plus symbols indicate the presence in some samples of DBMIB at the indicated concentration (μM), ethanol at the concentration present in DBMIB-containing samples, and DTT at 100 mM. Molecular markers (center lane) for the SDS-PAGE gels are labeled on the right side (kDa). In the native gel (A), KaiA bands were shifted after incubation with DBMIB and the shifts were not affected by the presence of DTT. It should be noted that thiols convert DBMIB to a monobromothymoquinone but do not fully reduce it (1). Notably, KaiA ran primarily as a monomer, even in the presence of DBMIB, on nonreducing SDS-PAGE. Under these conditions a small portion of KaiA migrates as a dimer that is likely to be due to an intermolecular disulfide bond because the band density was decreased by adding DTT to generate reducing conditions (B). This low level of dimerization appears to occur in the C-terminal domain and is not related to DBMIB-induced aggregation of the N-terminal PsR; the KaiA135N variant does not show any evidence of dimerization on nonreducing SDS-PAGE (D) although it aggregates significantly in the presence of DBMIB under native gel conditions (C). The C-terminal domain (KaiA140C) does not exhibit DBMIB-induced aggregation (E), but it does show the low level of dimer formation (F). To further exclude the action of disulfide bond formation in the quinone-induced aggregation of KaiA, the modifying agent N-ethylmaleimide (NEM) was used to render exposed sulfhydryls unreactive. KaiA has 5 N-terminal and 1 C-terminal domain Cys residues. If KaiA aggregation results from disulfide bond formation, the NEM treatment will block the effect of DBMIB on aggregation. We treated full-length KaiA with NEM and confirmed effective modification of exposed Cys residues (see SI Methods). As shown in G, NEM treatment of KaiA did not affect KaiA aggregation (compare G and H with A and B). We conclude that KaiA with oxidized quinone aggregates through noncovalent interactions.

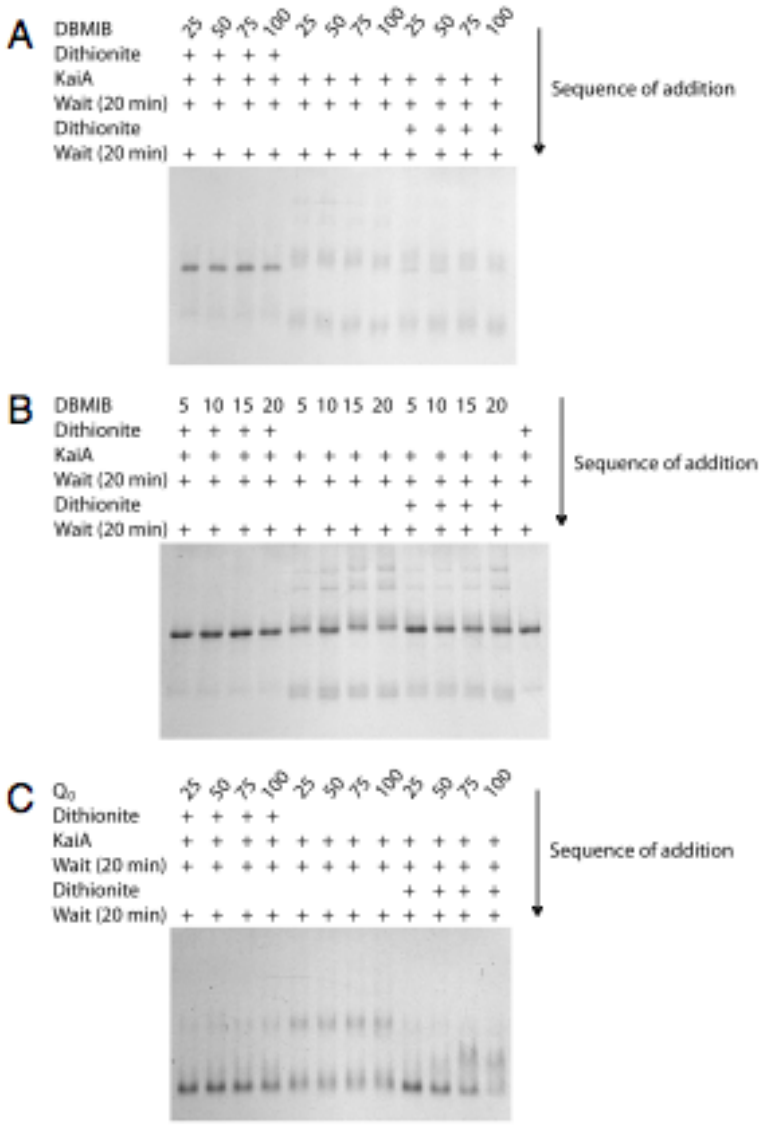

Figure S2. The KaiA aggregates induced by DBMIB cannot be reversed by adding dithionite. Oxidized DBMIB binds to the KaiA PsR domain and causes ag- gregation but reduced DBMIB does not bind KaiA. To check whether the KaiA aggregates that are induced by DBMIB addition can be reversed under reducing conditions, we performed a KaiA recovery experiment. Dithionite (1 mM) was added to DBMIB-containing solutions either prior to addition of KaiA or after a 20 min incubation of KaiA with oxidized DBMIB. All panels are native electrophoretic gels. A and B differ in the range of DBMIB used in the samples. Substantial aggregation occurred when DBMIB was not reduced prior to addition of KaiA. Recovery of unaggregated KaiA was very low even with the low concentrations of DBMIB present in B. In contrast, greater disaggregation occured when protein aggregated by addition of oxidized Q0 was subsequently treated with dithionite (C). Additional information on use of Q0 is shown in Fig. S3.

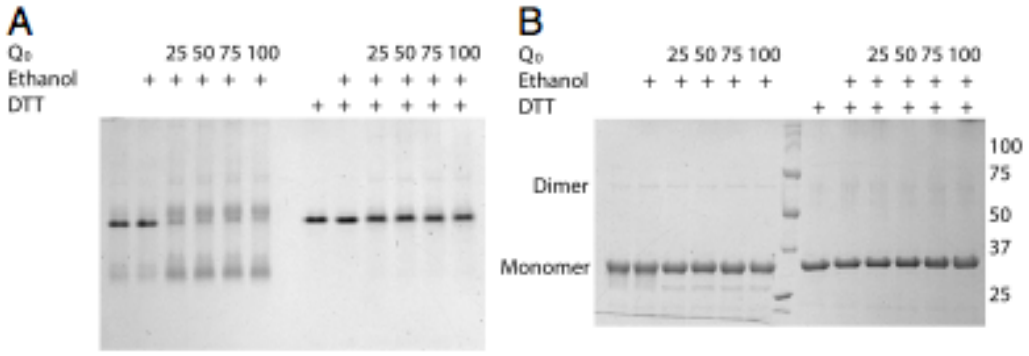

Figure S3. The quinone analog Q0 also causes aggregation of KaiA in vitro. Because we do not know what the native quinone is that would interact with KaiA in vivo, we tested interaction of KaiA with another quinone analog that is used for studies in proteobacteria and mitochondria, Q0. (2, 3) Although the native quinone it mimics, ubiquinone, is not known to be present in Synechococcus elongatus, Q0 is not halogenated and helps to rule out the possibility that DBMIB causes aggregation by halogen reaction with exposed sulfhydryls. Conditions are as described for Fig. S1, with a native gel shown in A and SDS-PAGE in B. KaiA aggregated in the presence of Q0; however, DTT treatment recovered most of the aggregates to the KaiA dimer (Fig. S2).

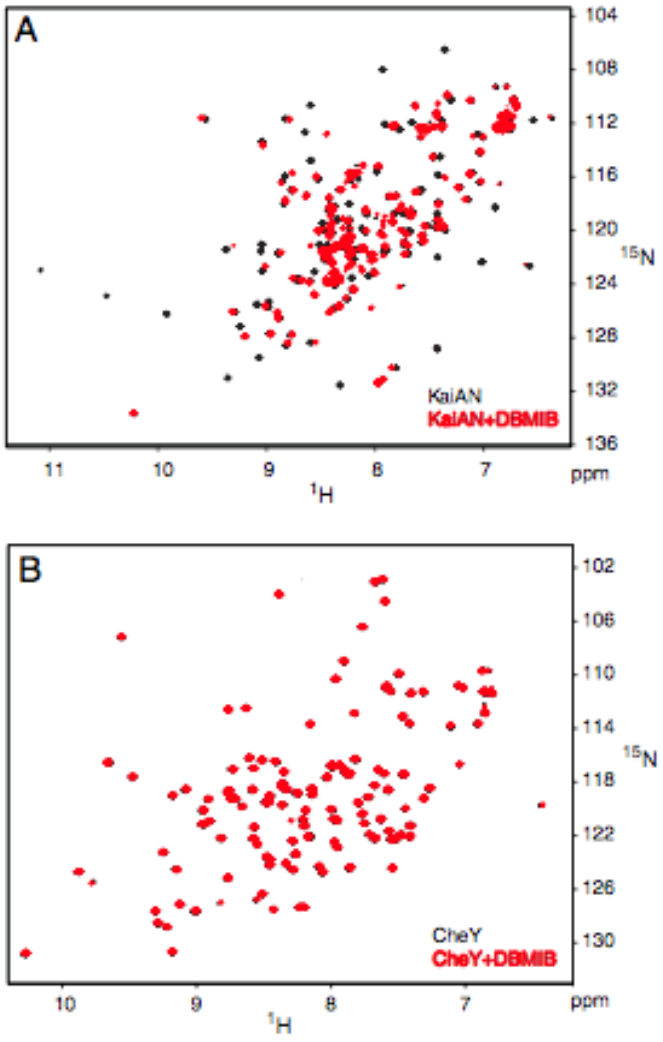

Figure S4. DBMIB does not interact with the receiver domain protein CheY. Two dimensional 15N, 1H HSQC NMR spectra were collected at 600MHz forKaiA135N (A) and CheY (B) in the presence (red) and absence (black) of 5 M equivalents of DBMIB. Samples were dissolved in 50 mM NaCl, 20 mM sodium phosphate at pH 7.0, 0.1 mM DSS, 95% H2O⁄5% D2O; equivalent ethanol concentrations were present in all samples.

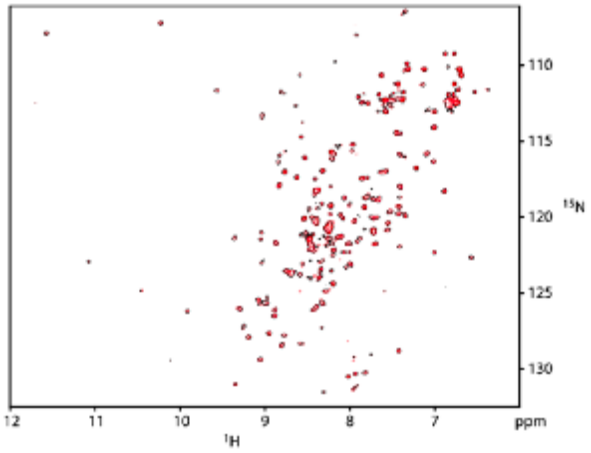

Figure S5. Reduced DBMIB does not interact with KaiA135N as measured by two-dimensional 15 N, 1 H HSQC NMR. A spectrum for KaiA135N only (black) is shown superimposed with a spectrum containing a 1:2 ratio of KaiA135N:DBMIB reduced by dithionite (red). All other conditions were as for Fig. 2.

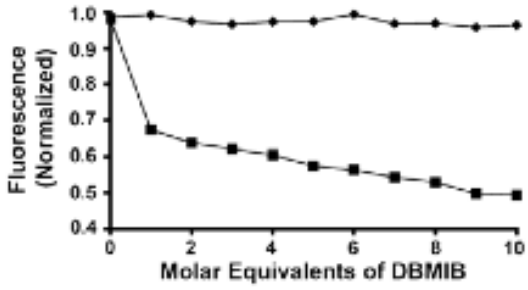

Figure S6. Reduced DBMIB does not interact with KaiA135N as measured by two-dimensional 15 N, 1 H HSQC NMR. A spectrum for KaiA135N only (black) is shown superimposed with a spectrum containing a 1:2 ratio of KaiA135N:DBMIB reduced by dithionite (red). All other conditions were as for Fig. 2.

REFERENCES

1. Dunlap JC, Loros JJ, and DeCoursey PJ (2004) *Chronobiology: Biological Timekeeping* (Sinauer Associates, Inc., Sunderland, MA).
2. McClung CR (2007) The cyanobacterial circadian clock is based on the intrinsic ATPase activity of KaiC. *Proc Natl Acad Sci U S A* 104(43):16727-16728.
3. Nakajima M, Imai K, Ito H, NIshiwaki T, Murayama T, Iwasaki H, Oyama T, and Kondo T (2005) Reconstitution of circadian oscillation of cyanobacterial KaiC phosphorylation in vitro. *Science* 308(5720):414-415.
4. Xu Y, Mori T, and Johnson CH (2003) Cyanobacterial circadian clockwork: roles of KaiA, KaiB and the *kaiBC* promoter in regulating KaiC. *EMBO J.* 22(9):2117-2126.
5. Nishiwaki T, Iwasaki H, Ishiura M, and Kondo T (2000) Nucleotide binding and autophosphorylation of the clock protein KaiC as a circadian timing process of cyanobacteria. *Proc Natl Acad Sci U S A* 97(1):495-499.
6. Terauchi K, Kitayama Y, Nishiwaki T, Miwa K, Murayama Y, Oyama T, and Kondo T (2007) ATPase activity of KaiC determines the basic timing for circadian clock of cyanobacteria. *Proc Natl Acad Sci U S A* 104(41):16377-16381.

7. Iwasaki H, Nishiwaki T, Kitayama Y, Nakajima M, and Kondo T (2002) KaiA-stimulated KaiC phosphorylation in circadian timing loops in cyanobacteria. *Proc Natl Acad Sci U S A* 99(24):15788-15793.

8. Williams SB, Vakonakis I, Golden SS, and LiWang AC (2002) Structure and function from the circadian clock protein KaiA of *Synechococcus elongatus*: a potential clock input mechanism. *Proc. Natl. Acad. Sci. U S A* 99(24):15357-15362.

9. Kitayama Y, Iwasaki H, Nishiwaki T, and Kondo T (2003) KaiB functions as an attenuator of KaiC phosphorylation in the cyanobacterial circadian clock system. *EMBO J* 22(9):2127-2134.

10. Nishiwaki T, Satomi Y, Kitayama Y, Terauchi K, Kiyohara R, Takao T, and Kondo T (2007) A sequential program of dual phosphorylation of KaiC as a basis for circadian rhythm in cyanobacteria. *EMBO J* 26(17):4029-4037.

11. Rust MJ, Markson JS, Lane WS, Fisher DS, and O'Shea EK (2007) Ordered phosphorylation governs oscillation of a three-protein circadian clock. *Science* 318(5851):809-812.

12. Vakonakis I, Klewer DA, Williams SB, Golden SS, and LiWang AC (2004) Structure of the N-terminal domain of the circadian clock-associated histidine kinase SasA. *J Mol Biol* 342(1):9-17.

13. Iwasaki H, Williams SB, Kitayama Y, Ishiura M, Golden SS, and Kondo T (2000) A kaiC-interacting sensory histidine kinase, SasA, necessary to sustain robust circadian oscillation in cyanobacteria. *Cell* 101(2):223-233.

14. Mackey SR and Golden SS (2007) Winding up the cyanobacterial circadian clock. *Trends Microbiol* 15(9):381-388.

15. Smith RM and Williams SB (2006) Circadian rhythms in gene transcription imparted by chromosome compaction in the cyanobacterium Synechococcus elongatus. *Proc Natl Acad Sci U S A* 103(22):8564-8569.

16. Katayama M, Kondo T, Xiong J, and Golden SS (2003) LdpA encodes an iron-sulfur protein involved in light-dependent modulation of the circadian period in the cyanobacterium *Synechococcus elongatus* PCC 7942. *J. Bacteriol.* 185(4):1415-1422.

17. Ivleva NB, Bramlett MR, Lindahl PA, and Golden SS (2005) LdpA: a component of the circadian clock senses redox state of the cell. *EMBO J* 24(6):1202-1210.

18. Schmitz O, Katayama M, Williams SB, Kondo T, and Golden SS (2000) CikA, a bacteriophytochrome that resets the cyanobacterial circadian clock. *Science* 289(5480):765-768.

19. Zhang X, Dong G, and Golden SS (2006) The pseudo-receiver domain of CikA regulates the cyanobacterial circadian input pathway. *Mol Microbiol* 60(3):658-668.

20. Ivleva NB, Gao T, LiWang AC, and Golden SS (2006) Quinone sensing by the circadian input kinase of the cyanobacterial circadian clock. *Proc Natl Acad Sci U S A* 103(46):17468-17473.

21. Trebst A (1980) Inhibitors in electron flow: tools for the functional and structural localization of carriers and energy conservation sites. *Methods Enzymol.* 69:675-715.

22. Gao T, Zhang X, Ivleva NB, Golden SS, and LiWang A (2007) NMR structure of the *pseudo*-receiver domain of CikA. *Protein Sci.* 16(3):465-475.

23. Prince RC, Linkletter SJG, and Dutton PL (1981) The Thermodynamic Properties of Some Commonly Used Oxidation Reduction Mediators Inhibitors and Dyes as Determined by Polarography. *Biochimica et Biophysica Acta* 635(1):132-148.

24. Stidham MA and Siedow JN (1983) Photochemical reactions of di bromothymoquinone structure and inhibitory properties of the photoproduct. *Photochem. Photobiol.* 38(5):537-540.

25. Baker MD, Wolanin PM, and Stock JB (2006) Signal transduction in bacterial chemotaxis. *Bioessays* 28(1):9-22.

26. Kim Y-I, Dong G, Carruthers CW, Jr., Golden SS, and LiWang A (2008) The day/night switch in KaiC, a central oscillator component of the circadian clock of cyanobacteria. *Proc. Natl. Acad. Sci. U S A* 105(35):12825-12830.

27. Georgellis D, Kwon O, and Lin EC (2001) Quinones as the redox signal for the arc two-component system of bacteria. *Science* 292(5525):2314-2316.

28. Swem LR, Gong X, Yu CA, and Bauer CE (2006) Identification of a ubiquinone-binding site that affects autophosphorylation of the sensor kinase RegB. *J Biol Chem* 281(10):6768-6775.

29. Bock A and Gross R (2002) The unorthodox histidine kinases BvgS and EvgS are responsive to the oxidation status of a quinone electron carrier. *Eur J Biochem* 269(14):3479-3484.

30. Yan J, Kurisu G, and Cramer WA (2006) Intraprotein transfer of the quinone analogue inhibitor 2,5-dibromo-3-methyl-6-isopropyl-p-benzoquinone in the cytochrome b6f complex. *Proc Natl Acad Sci U S A* 103(1):69-74.

31. Law A, Thomas G, and Threlfall DR (1973) 5'-Monohydroxyphylloquinone from *Anacystis* and *Euglena*. *Phytochemistry* 12:1999-2004.

32. Bustos SA and Golden SS (1991) Expression of the *psbDII* gene in *Synechococcus* sp. strain PCC 7942 requires sequences downstream of the transcription start site. *J. Bacteriol.* 173(23):7525-7533.

33. Mutsuda M, Michel KP, Zhang X, Montgomery BL, and Golden SS (2003) Biochemical properties of CikA, an unusual phytochrome-like histidine protein kinase that resets the circadian clock in *Synechococcus elongatus* PCC 7942. *J Biol Chem* 278(21):19102-19110.

34. Sambrook J, Fritsch EF, and Maniatis T (1989) *Molecular Cloning: A Laboratory Manual* (Cold spring Harbor Laboratory Press, Cold Spring Harbor, NY).

35. Simkovic M and Frerman FE (2004) Alternative quinone substrates and inhibitors of human electron-transfer flavoprotein-ubiquinone oxidoreductase. *Biochem J* 378(Pt 2):633-640.

36. Ivleva NB and Golden SS (2007) *Methods in Molecular Biology* (Humana Press, Totowa).

37. Walker JM (1994) *Methods in Molecular Biology* (Humana Press, Totowa).